

**3D TECTONOSTRATIGRAPHIC
ANALYSIS OF THE MESSINIAN
EVAPORITES IN THE LEVANT BASIN,
EASTERN MEDITERRANEAN**

CLAUDIA BERTONI

**Submitted in partial fulfilment of the requirements for the
degree of Ph.D.**

Cardiff University

February 2006

UMI Number: U584786

All rights reserved

INFORMATION TO ALL USERS

The quality of this reproduction is dependent upon the quality of the copy submitted.

In the unlikely event that the author did not send a complete manuscript and there are missing pages, these will be noted. Also, if material had to be removed, a note will indicate the deletion.



UMI U584786

Published by ProQuest LLC 2013. Copyright in the Dissertation held by the Author.
Microform Edition © ProQuest LLC.

All rights reserved. This work is protected against
unauthorized copying under Title 17, United States Code.



ProQuest LLC
789 East Eisenhower Parkway
P.O. Box 1346
Ann Arbor, MI 48106-1346

SUMMARY

This thesis uses industry seismic (3D and 2D) and well data to investigate the depositional and deformational processes of the Messinian evaporites in the Levant Basin, Eastern Mediterranean. Detailed interpretation of the geometry, structural and stratigraphic context of the evaporites has been undertaken in order to improve our understanding of the events occurring during the Messinian Salinity Crisis in the region.

The Messinian evaporites form a wedge up to 1.8km thick that pinches out towards the continental margin, where they pass laterally to a prominent erosional surface. The 3D seismic data have allowed the complete basinal evaporitic series to be imaged in three dimensions for the first time. Investigations showed that clastic bodies and focused incisional pattern developed at their base. The internal part of the evaporites is composed of parallel and continuous seismic reflections, alternating with transparent seismic facies. These internal reflections are truncated at the top of the Messinian evaporites, against a widespread erosional unconformity.

The analysis of the 2D seismic data permitted the connection of these morphological features with a regional system of canyons, developed on the Levant continental margin since the Oligocene. The canyons acted during the Messinian Salinity Crisis as clastic fairways, erosional loci and depocentres for the evaporites. The morpho-structural observations collected have been compared to the pre- and post-evaporitic setting, in order to infer the depositional environment and post-depositional behaviour of the evaporites. Relative sea-level changes in the basin have been interpreted in relation with two major erosional events developed at the base and at the top of the evaporites. Finally, the three-dimensional analysis also allowed an early (Messinian) stage of deformation of the evaporites to be identified, and the discovery of the occurrence of evaporite dissolution during the Pliocene.

AUTHOR'S NOTE

Chapters Two, Three, Four and Five of the present Thesis have been submitted as papers for four different international publications. The content of these papers is the result of the first author's own research, being the role of the co-authors limited to supervision throughout the PhD research. The present status of these publications is summarised as follows:

- **Chapter Two** has been published as: *Controls on the basinwide architecture of late Miocene (Messinian) evaporites on the Levant margin (Eastern Mediterranean)*, C. Bertoni & J. A. Cartwright, *Sedimentary Geology*, in press.
- **Chapter Three** has been published as: *Clastic depositional systems at the base of the Messinian (late Miocene) evaporitic series of the Eastern Mediterranean: Evidence from 3D seismic data*, Special Publications, Geological Society of London, in press.
- **Chapter Four** has been submitted to Basin Research as: *Origin of the unconformity at the top of the basinwide late Miocene evaporites in the Eastern Mediterranean*, C. Bertoni & J. A. Cartwright.
- **Chapter Five** has been published as: *3D seismic analysis of circular evaporite dissolution structures, Eastern Mediterranean*, C. Bertoni & J. A. Cartwright, *Journal of the Geological Society of London*, 162, (2005) 909-926.

ACKNOWLEDGEMENTS

I would like to express all my gratitude to my supervisor Joe Cartwright, for making this research project possible and for excellent supervision throughout the time of my graduate studies in Cardiff. His enthusiasm and passion for geology have been a constant source of inspiration for me, as were his amazing geological sketches that filled my notebook. I shall also thank him for his invaluable teaching on how to write scientific papers, while reviewing the many drafts of my manuscripts. My second supervisor Richard Davies is greatly thanked for his advice, help on seismic interpretation, suggestions and feedback on my manuscripts. Special thanks go to Mads Huuse for many long discussions on seismic and sequence stratigraphy, and for always having an open door for help and supplying good papers to read.

Thanks are due to BG-Group for providing the seismic and well data upon which this work is based, and for their permission to publish the results. In particular, I would like to express my gratitude to I. Campbell for his help in obtaining permission to publish most of the papers that comprise this thesis. Schlumberger Ltd is acknowledged for the use of Geoquest seismic interpretation software. I am grateful to the managers of the 3D Lab through the years, Neil Ferguson and Gwen Pettigrew, for providing continuous technical support and for sorting out all those computer problems. I also give particular thanks to all the editors and reviewers of my papers, which greatly helped improve the quality of my work at various stages of its development: Ian Alsop, Ian Davison, Marco Roveri, James Clark, Dave Griffin, Jean Mascle, Jean-Marie Rouchy, Charlotte Schreiber and John Warren. I am grateful to all the people that provided very helpful informal reviews of my manuscripts: Jose Frey-Martinez, Mads Huuse, Richard Davies, Mairi Nelson and Mike Hohbein. Charlotte is also thanked for her continuous support and encouragement.

The Geological Society Garwood Fund and Cardiff University Charles Cole Scholarship are acknowledged for financially supporting my fieldtrip to Almeria. In Cardiff University, I am particularly grateful to Wes Gibbons and Teresa Moreno, with whom I was lucky enough to go on two fieldtrip seasons to Almeria, and for their subsequent help in the organization of my fieldwork. Thanks also to Robert Riding for discussions on the Messinian and for providing useful information for my fieldtrip, and to Neil Mitchell for his advice and for numerous chats on canyons.

I would also like to acknowledge all the people that I have met in the conferences attended during my PhD: Stefano Lugli, Rocco Dominici, Mirko Barone, Johanna Lofi, Maria Bianca Cita, Julio Aguirre, Juan Carlos Braga. I have considerably benefited from talking to them about seismic, sequence stratigraphy and Messinian issues. Domenico (Mimmo) Ridente is also gratefully acknowledged for numerous discussion on canyons, sequence and seismic stratigraphy, and for the good time spent together in Florence during the 32 IGC. I would like to thank Bridget Wade for sharing the experience of a conference in Corsica during a very hot summer. Thanks are also due to Carlo Doglioni and Goffredo Mariotti, for planting the seeds of my move to Cardiff University.

Thanks to all my office, lab and university mates, Andy (the seismic king), Valente, Mairi, Gordon, Mike, Valeria and many others for all advice, help and chats throughout the years. Particular thanks go to Mairi (Scottish Power) for our long discussions on almost any aspect of doing a PhD, for extra-help with the English, and for providing - together with Cat - feedback on the structural part of my project.

Dorthe is thanked for lots of tips and for being a super-efficient field assistant in Almeria.

A special mention goes to all the friends that supported me throughout this PhD experience. First of all, my old friends in Italy: Lilli, for being a true friend when it mattered most, and for being my 'memoria storica', Chiara and Cristina Basci, Daniela, Alessia, Francesco, Pako, Paola ... and many others – thank you all! In Cardiff, I would like to thank for their friendship Francesca, Uli, Natasha for the good time spent in Shirley Road, Rich for continuous encouragement and for supplying tons of excellent music, and to Bénédicte for the nice walks in the Welsh countryside. Angela is particularly thanked for our squash matches and for inviting me to visit her in Gabon. Our fantastic trip through forests, turtles and beaches literally broadened my horizons. Thanks to all the friendly people met there and especially to Josh, for sharing his passion for Gabonese music.

I wish to thank particularly all the people that provided me with a bed in Cardiff in the final 'homeless' writing-up year: Fabrizio, Mads, Rob and Suzie, Valente, Ana Laura and lovely little Cecilia - I really enjoyed the additional time spent with them. I am particularly grateful to Francesca and Uli, for their endless generosity and for always making me feel at home. Thank you also to all the friends that offered hospitality, Rich, Mike, Elisenda, Maira, Thierry, Andy amongst the others. I wish all of them a bright future. A mention goes to Oxford, where I lived for one year. The walks on the street of this beautiful city, through colleges, bookshops and parks made my final writing-up year a more bearable one. Here I had the chance to meet Mariella, who introduced me to the practise of Astanga Yoga, and to know Henry's pub, where the best ever fish pie and bitter shandy are served. They both helped keep my balance in these difficult times!

My parents Alida and Enzo are greatly thanked for personal and financial support in all my decisions, for visiting me in Cardiff and Oxford, and patiently listening to my stories about geology and the UK. I also would like to thank my brother Nicola for his support. I admire him for his brave daily fight against heavy odds – my thoughts have been with him every day of my PhD, and I wish I could have spent more time with him. And finally, I thank Jose, for his immense amistad y amor, his continuous help and support throughout this long adventure. I am deeply grateful to him for his patience and invaluable encouragement, especially during my final writing-up year. He greatly cheered me up and motivated me, cooking for me some of the best tortilla and hand-baked bread I have ever eaten. Now I appreciate his engineer's theory that a PhD thesis is like a block of granite, that has to be destroyed bit by bit every day. I finally made it!

TABLE OF CONTENTS

Summary	I
Author's note	II
Acknowledgements.....	III
Table of Contents.....	V
List of Figures.....	IX
List of Tables	XVIII
List of Abbreviations	XIX

Chapter One

1. Introduction.....	1 - 1
1.1 Project rationale	1 - 1
1.2 Aims of study	1 - 2
1.3 Geographic, structural and stratigraphic setting	1 - 4
1.4 Synthesis of the Messinian Salinity Crisis.....	1 - 9
1.4.1 Onset and termination of the MSC	1 - 11
1.4.2 Depositional setting	1 - 13
1.5 Database.....	1 - 20
1.6 Geophysical interpretation methods	1 - 25
1.6.1 Seismic interpretation	1 - 25
1.6.2 Imaging problems	1 - 30
1.7 Thesis layout	1 - 32

Chapter Two

2. Controls on the architecture of the Messinian evaporites	2 - 1
2.1 Abstract	2 - 1
2.2 Introduction.....	2 - 2
2.3 Geological setting	2 - 5
2.4 Methodology	2 - 8
2.5 Seismic stratigraphy.....	2 - 6
2.5.1 Unit 1 (Late Cretaceous – late Miocene)	2 - 10
2.5.2 Unit 2 (Messinian evaporites).....	2 - 10
2.5.3 Unit 3 (Pliocene to Recent).....	2 - 13
2.6 Interpretation of tectonic and topographic controls	2 - 13
2.6.1 Time-thickness of Unit 2	2 - 15
2.6.2 Morpho-structural analysis	2 - 20
2.6.2.1 Tectonic structures	2 - 20
2.6.2.2 Geomorphological features	2 - 25
2.7 Discussion.....	2 - 29
2.7.1 Summary of the main observations.....	2 - 29
2.7.2 Linear edge of evaporites.....	2 - 30
2.7.3 Salients and embayments.....	2 - 31

2.7.4 Implications for the MSC.....	2 - 32
2.8 Summary and conclusions	2 - 35

Chapter Three

3. Clastic systems in the Messinian evaporites	3 - 1
3.1 Abstract	3 - 1
3.2 Introduction.....	3 - 2
3.3 Geological setting	3 - 4
3.4 Seismic analysis.....	3 - 4
3.4.1 Detailed 3D seismic description of HABI.....	3 - 6
3.5 Interpretation	3 - 19
3.6 Discussion	3 - 21
3.6.1 Distribution of clastic sediments within the Messinian evaporites.....	3 - 21
3.6.2 Depositional environment - submarine or subaerial?	3 - 22
3.6.3 Sea-level position.....	3 - 25
3.7 Conclusions.....	3 - 26

Chapter Four

4. Unconformity at the top of the Messinian evaporites.....	4 - 1
4.1 Abstract	4 - 1
4.2 Introduction.....	4 - 2
4.3 Geological background.....	4 - 3
4.4 Dataset and methodology.....	4 - 5
4.5 Seismic stratigraphy of the Messinian evaporites.....	4 - 6
4.6 Geometry of the evaporitic unit	4 - 11
4.6.1 Geometry of the intra-evaporitic horizons	4 - 11
4.6.2 Intra-evaporitic seismic packages	4 - 18
4.6.3 Structural deformation of the intra-evaporitic horizons.....	4 - 20
4.7 Interpretation.....	4 - 21
4.7.1 Intra-evaporitic deformation	4 - 21
4.7.2 Structural deformation of the intra-evaporitic horizons.....	4 - 22
4.8 Discussion.....	4 - 25
4.8.1 Depositional geometry of the Messinian evaporites.....	4 - 25
4.8.2 Mechanism of structural deformation.....	4 - 28
4.8.3 Implications for the Messinian erosional events in the Mediterranean Basin.....	4 - 29
4.9 Conclusions.....	4 - 31

Chapter Five

5. Dissolution structures in the Messinian evaporites.....	5 - 1
5.1 Abstract	5 - 1
5.2 Introduction.....	5 - 2
5.3 Regional framework.....	5 - 3
5.4 Dataset and methodology.....	5 - 5
5.5 Seismic stratigraphic framework	5 - 7

5.5.1 Unit 1	5 - 7
5.5.2 Unit 2	5 - 11
5.5.2.1 Well calibration of Unit 2	5 - 11
5.5.3 Unit 3	5 - 13
5.6 Description of the circular structures	5 - 13
5.6.1 General features	5 - 13
5.6.2 Circular structure CS-1: detailed 3D seismic interpretation	5 - 18
5.6.2.1 Morphology.....	5 - 18
5.6.2.2 Stratigraphic architecture	5 - 19
5.6.2.3 Structural analysis.....	5 - 20
5.6.2.4 Faults.....	5 - 20
5.6.2.5 Onset and timing.....	5 - 22
5.6.3 Circular structure CS-2 to CS-10: detailed 3D seismic interpretation.....	5 - 26
5.7 Discussion	5 - 27
5.7.1 Observations and identification	5 - 27
5.7.2 Genesis.....	5 - 29
5.7.2.1 Mechanism of dissolution.....	5 - 29
5.7.2.2 Origin of fluid flow.....	5 - 29
5.8 Conclusions.....	2 - 35

Chapter Six

6. Summary and discussion	6 - 1
6.1 Introduction.....	6 - 1
6.2 Summary of results	6 - 1
6.2.1 Results on the controls for the architecture of the Messinian evaporites in the Levant region (Chapter 2).....	6 - 1
6.2.2 Results from the analysis of clastic deposits at the base of the Messinian evaporitic system (Chapter 3).....	6 - 2
6.2.3 Results on the central and upper part of the Messinian evaporites (Chapter 4)....	6 - 2
6.2.4 Results on post-depositional evaporite deformation (Chapter 5)	6 - 3
6.3 Basinal evolution of the Messinian evaporitic system.....	6 - 4
6.3.1 Observations on the architecture of the Levant margin	6 - 4
6.3.2 Sea-level at the base of the Messinian evaporites.....	6 - 12
6.3.3 Sea-level during the deposition of the Messinian evaporites.....	6 - 16
6.3.4 Sea-level at the top of the Messinian evaporites.....	6 - 21
6.3.5 Remarks on the formation of the marginal Messinian erosional surface.....	6 - 26
6.3.6 Summary of relative sea-level changes during the MSC.....	6 - 28
6.4 Comparison with previous models and other evaporitic basins.....	6 - 31
6.5 Limitations and future research	6 - 35

Chapter Seven

7. Conclusions.....	7 - 1
7.1 General conclusions.....	7 - 1
7.2 Controls on the architecture of the Messinian evaporites.....	7 - 2
7.3 Clastic deposits at the base of the Messinian evaporites	7 - 3
7.4 Nature of the top of the Messinian evaporites	7 - 3

7.5 Evaporite deformation: dissolution and salt tectonics7 - 4

8. References8 - 1

Appendices

- Publications.
- CD: Thesis in digital format.

LIST OF FIGURES

Chapter One: Introduction

Figure No.	Figure Caption	PAGE No.
1.1	Regional structural map of the Eastern Mediterranean area, modified after Bardawy & Horvath (1999), showing the location of the study area (black box). The box highlighted by the black dotted line indicates the location of Fig. 1.2.	1-5
1.2	Location map showing the main structural elements of the Levant-Nile region (after Neev & Ben-Avraham, 1977; Tibor et al., 1992; Robertson, 1998; Abdel Aal et al., 2000; Vidal et al., 2000) with indication of the study area. The location of the 2D seismic dataset is highlighted by the light blue box, while the location of the 3D seismic dataset is highlighted by the dark blue box.	1-6
1.3	Stratigraphic context of the Levant region. a) Regional geological profile crossing the study region in a NW-SE direction (location in Fig. 1.8), showing the main stratigraphic groups in the Cretaceous-Recent interval, and the hydrogeological context (after Hargreaves et al., 2004). b) Table summarizing the main lithostratigraphic units of the Levant continental margin (after Sneh et al., 2000).	1-7
1.4	Distribution of Messinian evaporitic deposits in the Mediterranean Basin (after Rouchy, 1980; Reading, 1996; Warren, 1999). The Rifian Corridor' in Morocco and the 'Betic Strait' in Spain mark the approximate locations of the waterways that connected the Mediterranean Sea and the Atlantic Ocean prior to the Messinian Salinity Crisis (after Muller & Hsu, 1987; Benson et al., 1991; Kastens, 1992). The light-blue colour highlights the distribution of Paratethys deposits during the Messinian (from Steininger & Rogl, 1984). The red box indicates the location of the study area. The background is composed by the map of the seismic hazard in the European-Mediterranean area (Giardini et al., 2003), which highlights the main tectonic lineaments active at the present day.	1-10
1.5	Main basinwide evaporitic settings (from Warren, 1989; Kendall, 1992; Warren, 1999). See text for explanation.	1-14
1.6	Diagram summarizing the stratigraphic context of the different depositional models developed for the Messinian Salinity Crisis in the Mediterranean area (modified from Warren, 1999). The main diachronous and synchronous models explained in the text and illustrated in Fig. 1.7 are compared and their different phases plotted against global stratigraphic and climatic curves.	1-16
1.7	Schematic diagrams illustrating the main models for the evolution of the Messinian Salinity Crisis in the Mediterranean Basin. a) Model proposed by Krijgsman et al. (1999). b) Model proposed by Clauzon et al. (1996) c) Model proposed by Butler et al. (1995). d) Model proposed by Druckman et al. (1995) for the Levant continental shelf.	1-17/ 1-18
1.8	Location map of the study area showing the extent of the 2D and 3D seismic surveys and the position of the exploration well used in this study. Nomenclature for the exploration wells is: 1= Gaza Marine-1, 2= Gaza Marine-2, 3= Noa-1 South, 4= Noa-1, 5= Or South-1, 6= Or-1, 7= Yam West-2, 8= Yam West-1, 9= Nir-1.	1-21
1.9	Stratigraphy of the Messinian evaporites in the study area. a) Well correlation panel (location of wells in Fig. 1.9b). Acronyms of wells are explained in Fig. 1.9b. b) Isochron map of the Messinian evaporitic unit in the Levant 3D survey area. The thickness is expressed in milliseconds TWTT (two-way travel time).	1-23/ 1-24
1.10	Explanation of some key seismic characteristics of the main seismic units and horizons analysed in this research study. a) Schematic representation of the acoustic impedance (Z) and reflection coefficient (R) of seismic reflections, i.e. the main seismic parameters used for identifying the boundaries of the Messinian evaporitic unit in the study area (Horizons M and N). b) Dominant seismic frequencies observed within the three main seismic-stratigraphic units analysed in this study, as displayed on a representative seismic section across the 3D seismic dataset.	1-29
1.11	Examples of seismic effects affecting data interpretation in the study area. a) 2D seismic line displaying examples of simple and peg-leg multiples of Horizon M. b) 3D seismic line displaying examples of simple multiples of Horizon M. c) Interpreted seismic sections showing how the comparison of overlapping 2D and 3D seismic data can often be used to aid interpretation and distinguish multiple from real stratigraphic horizons. d) 2D and 3D seismic lines displaying examples of 'smile' effect nearby faults displacing the top of the evaporites.	1-33/ 1-34

1.12	Schematic diagram illustrating the comparison between resolution achieved in studies based on well and outcrop analysis (e.g. Druckman et al., 1995; Buchbinder et al., 1997) and on seismic data (this study). The two approaches differ in terms of areal and vertical coverage of the Messinian evaporites, resolving geological processes of variable scales (see discussion in the text).	1-35
------	--	------

Chapter Two: Controls on the architecture of the Messinian evaporites

Figure No.	Figure Caption	Page No.
2.1	Location map of the study area showing the main structural elements in the Levant-Nile region (after Neev & Ben-Avraham, 1977; Bartov, 1990; Abdel Aal et al., 2000) and the location of the 2D and 3D seismic surveys.	2-3
2.2	Composite 3D seismic section perpendicular to the Levant margin (location in Fig. 2.5b), showing the general seismic-stratigraphic context of the study area. On the vertical scale, TWT is two-way travel time expressed in seconds. T: localized truncation at the top of Unit 2 against Horizon N. B.S.: Base Senonian horizon. M: Horizon M. N: Horizon N. The deformation of the Base Senonian horizon and overlying reflections in Unit 1 is linked to the compressional structures of the Syrian arc foldbelt. Unit 2 is internally composed of an alternation of discernible seismic reflections (Horizons ME20-ME60) and transparent seismic facies. In the southeastern part of the section, Unit 3 is crossed by extensional faults (black dashed lines) detaching at the top of Unit 2.	2-7
2.3	3D seismic section parallel to the Levant margin (location in Fig. 2.5b), showing the seismic-stratigraphy of the proximal part of the study area. The stratigraphy is defined by correlation with nearby wells. The Oligo-Miocene Afq Canyon exhibits a major incisional phase cutting down to the Base Senonian horizon (B.S.), and a series of minor incisional phases (black dashed lines) evidenced by truncation of seismic reflections. B.M.: Base Miocene horizon; L.E.: Late Eocene horizon. Other acronyms are explained in Fig. 2.2.	2-8
2.4	3D seismic section parallel to the Levant margin, showing the seismic-stratigraphic context of the distal part of the study area (location in Fig. 2.5b). The localized erosional truncation of the reflections at the top of Unit 1 against Horizon N is highlighted by arrows. The other acronyms are explained in Fig. 2.2.	2-9
2.5	Time-structure maps generated in the 2D seismic dataset. The spectrum bar is indicated in milliseconds TWT. (a) Time-structure map of Horizon N, with contour line spacing of 50 ms. The morphology of Horizon N in the central and distal part of the area defines a surface gently sloping toward the northwest. The white dashed lines indicate the pattern of erosional truncation of the seismic reflections at the top of Unit 1 against Horizon N. (b) Time-structure map of Horizon M, with contour lines spacing of 100 ms. This surface appears irregular and nearly flat in its central part. The red dotted lines highlight the subcircular and composite elongated structural depressions described at the top of Unit 2.	2-11
2.6	(a) 3D seismic section across the Levant margin (location in Fig. 2.7b). The erosional truncation defining the floor of the El Arish Canyon (dotted line) is indicated by black arrows underneath the dotted line. The canyon floor is overlapped by the overlying canyon fill reflections (upper black arrows). The Messinian evaporites (Unit 2) pinch out toward the south-southeast and pass laterally to an erosional surface, truncating the underlying reflections at the top of Unit 1 (T, black arrows). The black dashed lines in Unit 3 indicate the main extensional faults and grabens related to thin-skinned gravitational tectonics. The apparent downwarping of seismic reflections underneath the main graben is interpreted as a seismic artefact, due to the seismic velocity contrast between the deep-water sediments of Unit 3 and the evaporites of Unit 2. The rectangular box highlights the interpreted geo-seismic section in Fig. 6b. Other acronyms are explained in Fig. 2.2. (b) Interpreted geo-seismic section corrected for the seismic artifacts. The black dashed line represents the projected elevation of the overall flat Horizon M along the undeformed top basinal evaporite datum, up to the proximal area east of the boundary. The point where this projected line meets Horizon M is interpreted as the possible locus of evaporite pinch-out before deformation (Fig. 2.6b). This gives an approximate indication of the amount of evaporite removal due to post-depositional deformation (dark grey area: removed evaporites).	2-14
2.7	(a) Time-thickness (isochron) map of Unit 2 generated in the 2D seismic dataset, between Horizon N and M, showing the regular thickening of Unit B toward the northwest. Time-thickness is expressed in milliseconds (ms), with isochron contours spacing of 50 ms. The white bold lines and arrows traces the localised thickening of the evaporites observed above or basinward of the thalwegs of the El Arish-Afiq and Ashdod Canyons. (b) Close-up of the isochron map of Unit 2 generated in the 3D seismic dataset. Canyon tributaries, suggested by the shorter wavelength embayments in the distal-proximal evaporite boundary, are marked with white dotted lines.	2-16

2.8	Seismic sections (location in Fig. 2.7) crossing the Oligo-Miocene submarine canyons, and showing the thickening of Unit 2 directly above the axis of the canyons. (a) 3D seismic section across the El Arish-Afiq Canyon. The black dotted line indicates the main incisional phase of the canyon. (b) 2D seismic section across the Ashdod Canyon, showing two main erosional episodes (black dashed line) and truncation of canyon fill against Horizon N (black arrows). P.F.: Palmahim fault. Other acronyms explained in Fig. 2.2.	2-17
2.9	Idealized geo-seismic section across the Levant margin, obtained overlapping two seismic sections located respectively inside and outside the embayment above the El Arish Afiq Canyon (section 1 and 2 in Fig. 2.7a). Note that the evaporite pinch-out in the section outside the canyon (p.o.1) is located significantly basinward of the pinch-out in the section along the canyon axis (p.o.2).	2-18
2.10	Synoptic diagram illustrating the main morphological and structural features observed in the study area, and their relation to the distribution of the Messinian evaporites.	2-21
2.11	Seismic sections across the Levant margin (location in Fig. 2.7). (a) 2D seismic section showing the Syrian Arc anticlines (S.A.), mostly evident at the Base Senonian horizon (B.S.). The crests of the hinge of successive anticlines deepen westwards, and Horizon M is generally concordant with them. The box highlights an area of concave upward erosional relief on Horizon M, directly above a major anticline of the Syrian Arc. This geometry is associated with onlap (black arrows) of the reflections at the base of Unit 3. m: multiple, other acronyms explained in Fig. 2.2. (b) 3D seismic section (location in Fig. 2.7) showing the detailed stratigraphy and deformation above one of the Syrian arc anticlines. B.S.: Base Senonian Horizon; L.E.: Late Eocene Horizon; B.M.: Base Miocene Horizon (stratigraphy calibrated with well data). The Base Senonian Base Miocene seismic package clearly thins, onlaps and is upwarped against the Syrian Arc anticline, suggesting protracted activity of the structure in this time-span. The morphology of Horizon M still reflects the influence of the anticline, and is associated with low-angle truncation (T, black arrows) of the reflections at the top of Unit 1 against Horizon M.	2-22
2.12	2D seismic section (location in Fig. 2.10) illustrating the cross-sectional geometry of the two zones of deformation in the southern part of the study area. The Palmahim fault zone (P) is imaged as two main vertical fractures marked by black dashed lines, nearby the Ashdod Canyon. These faults appear to displace the entire stratigraphic section from Unit 1 to Unit 3. The Gaza structure (G?) is tentatively correlated with a deformation zone displacing the Base Senonian horizon. This structure is mostly evident at the Syrian Arc anticline located below the Afiq Canyon. For explanation of the other acronyms see Figs. 2.2 and 2.11.	2-24
2.13	(a) 3D seismic section along the proximal part of the evaporitic system on the Levant margin, and (b) interpretation (location in Fig. 2.10). The black dashed line on the right side of the section shows the main incision of the El Arish Afiq Canyon, associated with erosional truncation pattern of the underlying seismic reflections. Erosional truncation is also observed on the reflections at the top of Unit 1 against Horizon N (shaded grey areas).	2-26
2.14	2D seismic cross section (location in Fig. 2.10) showing the geometry of Horizon M in the proximal part of the study area. A well-defined slope break (MS1) between a steeply sloping and a low-angle surface is associated with erosional truncation at the top of Unit 1 and downlap and onlap termination of reflections at the base of Unit 3 against Horizon M (black arrows). MS2 and MS3 present similar characteristics. The black dashed lines indicate faults within Unit 3. For explanation of other acronyms see Figs. 2.2 and 2.11. The area of concave upward erosional relief comprised between MS1 and MS2 occurs directly above a tributary of the Ashdod Canyon (see location in Fig. 2.10) and is interpreted as a valley incision.	2-27
2.15	Schematic cartoon illustrating the possible geometries of the base of the Messinian evaporites (Horizon N) and modality of infill in relation with the underlying canyon system. (a) Pre-evaporitic submarine canyon completely filled, successively re-excavated at the onset of the MSC; (b) Pre-evaporitic submarine canyon incompletely filled, Messinian evaporite filling the relict topography; (c) A combination of the two previous scenarios, which is the most likely geometry for the deposits in the study area; (d) the distal scenario, with unconfined pre-evaporitic deep-basin sediments excavated by the canyons at Horizon N, at the basinward prosecution of the Oligo-Miocene submarine canyons.	2-33

Chapter Three: Clastic systems in the Messinian evaporites

Figure No.	Figure Caption	Page No.
3.1	Location maps for the study area in the Eastern Mediterranean. The areas where 3D seismic data are available are indicated. The grey dashed line marks the locus of pinch-out of the buried Messinian evaporites (from Bertoni & Cartwright, in press).	3-3

3.2	Schematic geo-seismic section showing the seismic-stratigraphic context of the study area in the Levant Basin and continental margin (see text for detailed explanation). N= Horizon N; M= Horizon M; YSM= Yafo Sand Member (indicated by the dotted fill pattern). The marginal faults in the Plio-Pleistocene unit are marked by subvertical dashed lines. The crossover point of Fig. 3.3 is also indicated. On the vertical scale, TWT is the two-way travel time expressed in seconds.	3-5
3.3	Seismic section crossing the study area in a NE-SW direction (location in Fig. 3.1). The stratigraphy of the distal part of the Messinian evaporites is displayed. In this area the Messinian evaporites are seismically composed of transparent facies alternating with medium to low amplitude seismic reflections (Horizon ME20 to ME50).	3-7
3.4	Seismic section crossing the study area in a NW-SE direction (see location in Fig. 3.7) displaying the stratigraphy of the Messinian evaporites from their proximal (SE) to their distal (NW) part. Note that the Messinian evaporites form in the study area a wedge from 1.8 km thick in the distal part to a few tens of meters towards the SE, where Horizon N and M merge into a single seismic horizon.	3-8
3.5	Seismic section crossing the study area in a NW-SE direction, and b) interpretation (see location in Fig. 3.7). a) Close-up of the Messinian evaporites as displayed in the seismic section in Fig. 3.4. In the lower part of this unit, directly above Horizon N, the high-amplitude seismic reflections described in the text are indicated by the black arrows. b) Line-drawing of the seismic section, with interpretation of faults and terminations of seismic reflections (indicated by black arrows).	3-9
3.6	Seismic section crossing the study area in a NE-SW direction (see Figs. 3.5 and 3.7 for location). a) Seismic cross-section with indication of the main seismic horizons and reflection terminations. b) Line-drawing of the seismic section, with interpretation of faults and terminations of seismic reflections (indicated by black arrows) interpretation. In the lower part of this unit, the onlap termination of the high-amplitude seismic reflection against Horizon N (indicated by the black arrow) should be noted.	3-10
3.7	Maximum seismic amplitudes calculated over a 120 ms TWT (two-way travel time) window above Horizon N. The resulting image shows that the high-amplitude reflections shown on seismic sections in Figs. 3.4 to 3.6 correlate with a series of km-scale high-amplitude bodies (dark-grey coloured areas, marked with a white dotted line) named HAB1, HAB 2 and HAB 3. The bodies show an irregular and elongated ellipsoidal morphology. These bodies are located basinward of the pinch-out of the Messinian evaporites and thus fully confined within this unit.	3-11
3.8	Seismic sections across the main high-amplitude body HAB1. a) Seismic section oriented in a NE-SW direction (location in Fig. 3.10). b) Line-drawing of the seismic section displayed in Fig. 3.8a, with interpretation of the main seismic horizons and reflection terminations. HAB1 is bounded at the top by a high-amplitude negative seismic reflection (Horizon ME2, white dashed line). The base of HAB1 is represented by a low-amplitude seismic reflection lying closely over Horizon N (black dashed line). The erosional truncation of the Oligo-Miocene reflections against Horizon N is indicated by the black arrows. c) Seismic section oriented in a NW-SE direction (location in Fig. 3.10). d) Line-drawing of the seismic section displayed in Fig. 3.8c, with interpretation of the main seismic horizons and reflection terminations.	3-12
3.9	Seismic sections crossing the main high-amplitude body HAB1 (location in Fig. 3.10). a) Seismic section crossing the body HAB1 in a S-N/SW-NE direction. In this section, HAB1 presents an asymmetric geometry that is produced by the pinch-out of the body on a structurally elevated area to the SW and on a structurally depressed area to the NE. b) Seismic section crossing the body HAB1 in a NE-SW direction. On the north-eastern side of HAB1, Horizon ME2 is deformed by remobilization, hindering the interpretation of the nature of its original termination.	3-14
3.10	Morpho-structural maps of HAB1. a) Close-up of Fig. 3.7, showing details of the morphology of HAB1 with a different colour display. b) Isochron map calculated between the base and the top of HAB1. A synopsis of the nature and distribution of the lateral terminations of HAB1 is displayed in this map.	3-15
3.11	Seismic sections crossing HAB1 (location in Fig. 10a) a) Seismic section crossing in a NW-SE direction the two ribbon-shaped high-amplitude bodies attached to the main part of HAB1. The bodies are subtle, convex-upward features and appear as alternately confined and filling in the underlying lows or totally unconfined and showing a distinct constructional geometry. b) Seismic section crossing the two ribbon-shaped bodies in a NW-SE direction. The bodies appears to be laterally shifted with regard to the location of the underlying structural depressions. c) Seismic section crossing the thicker high amplitude body located landward and to the south of the main part of HAB1 (location in Fig. 10a). In cross-section this body does not present a clear internal geometry because it is highly disrupted by a subsequent deformational phase.	3-17
3.12	Three-dimensional perspective of HAB1 (as displayed in Fig. 3.10) draped over the time-structure map of Horizon N (location in Fig. 3.7). The maximum amplitude values are shown in red colour.	3-18

	This visualization illustrates the overall morphology and geometry of HABI: the thicker body to the south of the ribbon-shaped features is located on a structurally elevated area and the main part of HABI is confined to a structurally depressed area to the NW, within the floor of the El Arish-Afiq Canyon. The ribbon-shaped features are positioned on a sloping part of the time-structure map of Horizon N that links the structurally elevated area to the SE to the depressed area to the NW. Fault and ridges indicated represent post-evaporitic deformational structures.	
3.13	Map of the sector of the Eastern Mediterranean analysed, showing the regional setting of the basal discordance to the Messinian salt (and associated evaporite and clastic formations) and its marginal continuity with Horizon M (contour lines in seconds TWT; after Ryan, 1978). The landward limit of the Messinian salt in the region is also indicated (after Sage & Letouzey, 1990; Loncke, 2002; Bertoni & Cartwright in press). In the figure to the right, the distribution of the clastic sediments (in grey) is shown within the paleogeographic context of the base of the Messinian evaporites. Canyon incisions, erosional scarps and contour lines (in seconds TWT) of the base of the Messinian evaporites are after Bertoni & Cartwright (in press). The grey areas identify the location of the clastic deposits described in this study.	3-24

Chapter Four: Unconformity at the top of the Messinian evaporites

Figure No.	Figure Caption	Page No.
4.1	Location map showing the main structural elements of the Levant-Nile region (after Neev & Ben-Avraham, 1977; Tibor et al., 1992; Robertson, 1998; Abdel Aal et al., 2000; Vidal et al., 2000) with indication of the study area (2D and 3D seismic surveys).	4-4
4.2	Seismic section crossing the three 3D seismic datasets in a NW-SE direction (location in Fig. 4.6), showing the seismic stratigraphic context of the Messinian evaporites. On the vertical scale, TWTT is the two-way travel time expressed in milliseconds. In this section, the structures deforming Horizon M and the overlying Plio-Pleistocene reflections should be noted. These folds and faults and the associated syn-kinematic growth of the seismic packages are caused by thin-skinned gravitational gliding of the clastic wedge, detached above or within the Messinian evaporites (see text for explanation). In the lower part of the figure, two close-ups of the seismic section highlight the updip terminations of Horizon ME20 and ME50, as indicated by the black arrows.	4-7
4.3	3D seismic section crossing the study area in a NE-SW direction (location in Fig. 4.6), showing the seismic stratigraphic context of the Messinian evaporites. On the vertical scale, TWTT is the two-way travel time expressed in milliseconds. T1 to T4 are the transparent seismic packages and L1 to L2 are the layered seismic packages defined in this study within the unit of the Messinian evaporites. In the lower part of the figure, three close-ups of the seismic section show the waveform response of a single wavelet (highlighted over the seismic volume) across the seabed, Horizon M and Horizon N. Note that the seabed and Horizon M produce a positive wavelet (the main peak deviates to the right).	4-8
4.4	Seismic sections crossing the study area in a NW-SE direction (location in Fig.4.6). On the vertical scale, TWTT is the two-way travel time expressed in milliseconds. Note that Horizon M is overlain by the seismic reflections of the Plio-Pleistocene unit, which display a clinoformal geometry. These reflections onlap Horizon M in the marginal area to the SE (as indicated by black arrows), and downlap (as indicated by black arrows) or tangentially converge with it in the distal area to the NW. The occurrence of a prominent slump deposit within the Plio-Pleistocene Unit is highlighted with grey colour.	4-10
4.5	Seismic section crossing the Levant 3D seismic dataset in a NW-SE direction (location in Fig. 4.10) showing the geometrical relationship of the intra-evaporitic horizons ME20 to ME40 to the top of the Messinian evaporites (Horizon M). The discordance of the intra-evaporitic seismic horizons ME35 to ME40 with Horizon M should be noted. These horizons terminate updip against Horizon M basinwards (i.e. to the NW) of the pinch-out of the Messinian evaporites. On the vertical scale, TWTT is the two-way travel time expressed in milliseconds.	4-12
4.6	Time-structure map of Horizon M obtained in the 2D seismic dataset (colour bar expressed in milliseconds TWTT), showing the regional distribution of the updip termination of the intra-evaporitic horizons ME20, ME40 and ME60 on the top of the Messinian evaporites. The pinch-out of the Messinian evaporitic wedge is indicated by the black dashed line. The updip terminations are not clearly defined and therefore not mappable in areas where the Messinian evaporites are extensively deformed (e.g. located nearby structural depressions defined at the top of the Messinian evaporites, i.e. white shaded areas in the figure).	4-13
4.7	Schematic cartoon showing the thickness variations of the seismic packages bounded by Horizon M and each of the intra-evaporitic horizons ME20, ME35, ME40. The cartoon evidences how the	4-14

	thickness variation is strictly dependent on the angle subtended by Horizon M and each of the intra-evaporitic horizons (angle α).	
4.8	3D seismic sections crossing the study area in a NW-SE direction (location in Fig. 4.10), showing the general context of intra-evaporitic deformation. a) The top of the Messinian evaporites (Horizon M) is relatively unstructured in comparison with the intensely deformed intra-evaporitic horizons. T1 to T4 are the transparent seismic packages and L1 to L2 are the layered seismic packages defined in this study within the unit of the Messinian evaporites. The black arrows indicate truncation reflection terminations. b) Two types of structures deform the intra-evaporitic horizons: low amplitude weakly asymmetric folds, and thrust faults. The faults are marked with black dotted lines. The black arrows indicate truncated reflection termination.	4-15
4.9	3D seismic sections showing the details of the intra-evaporitic deformation. On the vertical scale, TWTT is the two-way travel time expressed in milliseconds. a) 3D seismic section crossing the study area in a NW-SE direction (location in Fig. 4.10), showing the folded structures deforming the intra-evaporitic layered package L1. In the right part of the figure, the hypothetical reconstruction of the eroded folds above Horizon M is indicated by the dotted lines. b) 3D seismic section crossing the study area in a SW-NE direction (location in Fig. 4.10), showing one of the faulted structures deforming the intra-evaporitic layered package L1. In the right part of the figure, the hypothetical reconstruction of the eroded fault above Horizon M is indicated by the dotted lines. c) 3D seismic section crossing the study area in a NW-SE direction (location in Fig. 4.10), showing the general context of the truncated folded structures deforming the intra-evaporitic layered package L1.	4-16
4.10	Maps showing the general structural deformation of Horizon ME40. a) Time-structure map of Horizon ME35 obtained in the 3D seismic dataset (location in Fig. 4.6). The colour bar is expressed in milliseconds TWTT. The interpretation of the folds and faults deforming Horizon ME40 is shown. The discordant structures appear to be laterally persistent for many kilometres. In plan view, the direction of these faults and folds is consistent, and is dominantly oriented to the NW-SE and N-S, while the vergence of the thrust sequences is to the E or NE. b) Horizon-based coherency amplitude extraction of Horizon ME35 (covering the same area of Fig. 4.10a), showing the detailed structural interpretation. The red dashed line indicates a superimposed strike-slip fault system post-dating the deposition of the Messinian evaporites. The area of Fig. 4.10b is marked with the black peripheral box for comparison.	4-17
4.11	Schematic cartoon showing the two possible geometry of updip termination of reflections against flat-lying overlying reflections. a) Geometry defining a nondepositional unconformity (Brown & Fisher, 1980). b) Geometry defining an erosional unconformity (Brown & Fisher, 1980).	4-23
4.12	Schematic cartoon illustrating the possible original geometry of Horizons ME20- ME60 preceding the completion of the unconformity expressed at Horizon M. The dotted lines indicate the eroded part of the horizons while the continuous lines indicate the preserved part of the horizons. The arrows mark the expected termination patterns. a) Original geometry of horizons as sigmoidal/oblique clinofolds. b) Original geometry of horizons as parallel onlap. c) Original geometry of horizons as divergent onlap.	4-27

Chapter Five: Dissolution structures in the Messinian evaporites

Figure No.	Figure Caption	Page No.
5.1	a) Schematic map of the Eastern Mediterranean, at the zone of interaction among the Anatolian, African and Arabian Plate. The main tectonic lineaments and the location of the Nile delta are indicated. The study area is highlighted by the dark grey box (3D and 2D seismic data). The contour lines represent the depth in metres of the Mediterranean seafloor. The position of the present day shelfbreak is approximately indicated by the 200 m contour line. Modified from Tibor et al. (1992); Robertson (1998); Vidal et al. (2000). b) Schematic regional cross-section through the Eastern Mediterranean basin (location shown in Fig. 5.1a; modified from Garfunkel 1998). C = Cretaceous; J - Jurassic.	5-4
5.2	Map showing the details of the seismic surveys used in this study, together with the location of selected exploration wells. The 3D seismic surveys (Levant A, Gal C and Med Ashdod) are outlined by the dashed rectangles. The 2D seismic lines are outlined by the black dotted lines. The location of	5-6

	the seismic sections presented in Fig. 5.4 is also indicated.	
5.3	a) Idealised circular collapse depression showing the parameters measured for quantitative analysis of the dissolution structures studied in this paper (modified from Branney, 1995). The E.I. is defined by Thorsen (1963) as the ratio between the thickness of deposits downthrown (b, directly above the collapse structure) and the thickness upthrown (a, i.e. undisturbed sediments laterally bounding the collapse structure) measured on successive discrete stratigraphic intervals. The vertical relief (ΔZ) is measured on a selected stratigraphic horizon, as the difference in elevation between the centre and the rim of the collapse structure. b) Schematic representation of the expected geometry resulting from pre-sedimentary growth versus syn-sedimentary growth of the circular collapse structure. Note the difference between concentric parallel onlap in the first case, and concentric onlap coupled with divergent strata configuration and thickness variation in the second case.	5-8
5.4	a) Composite seismic section across the Levant Basin and continental margin (see Fig. 5.2 for location). The three seismic-stratigraphic unit defined in this study (Unit 1, Unit 2 and Unit 3) are shown, together with the main interpreted horizons. Unit 2, the focus of this study, is represented by a thick wedge of evaporites pinching out towards the Levant continental margin. Marginal extensional faults within the Unit 3, detaching at Unit 2, are marked by dashed lines. The cross-over point of Figure 5.4b is indicated at the top and base of the section. YSM = Yafo Sand Member. B.S. = Base Senonian horizon; L.E. = Late Eocene horizon; M = Horizon M; N = Horizon N; B.P. = Base Pleistocene horizon. b) Seismic section along the direction of the Levant margin. Note the presence of the Oligo-Miocene Afiq submarine canyon, deeply incising within Unit 1. In Unit 3, interpretation of slump deposits is after Frey-Martinez et al. (2005). Localized downwarping of seismic reflections is observed within Unit 3 and highlighted by the black arrows. The cross-over point of Fig. 5.4a is indicated at the top and base of the section. CS-1 = circular structure CS-1; YSM = Yafo Sand Member.	5-9
5.5	Stratigraphic chart showing the main formations observed in the study area (after Garfunkel & Almagor, 1987; Druckman et al., 1995), their age and the correlation with the seismic-stratigraphic units described in this paper. The lithological data are derived from unpublished stratigraphic well reports. Fm = Formation; YSM = Yafo Sand Member.	5-10
5.6	Correlation scheme of the Messinian evaporites in the Levant A seismic survey. a) Seismic section nearby the Levant margin, crossing the wells (location of wells in Fig. 5.2), and showing the seismic-stratigraphic units and the interpretation of the main seismic horizons. b) Schematic representation of the lithology and stratigraphic relationship of the Messinian evaporites as described in unpublished well reports. The main seismic horizons have been tied where possible to the lithological and stratigraphic units of the Mavqim Formation.	5-12
5.7	Time-structure map of Horizon M in the Levant A seismic survey. The zoom shows the distribution of the circular structures analyzed, named progressively CS-1 to CS-10. Note the presence of the linear depression and the extensional faults nearby the pinch-out of the Messinian evaporites. The main deep structures of the study area are represented by the anticlines (axes highlighted on the map) related to the Syrian Arc foldbelt system (Neev & Ben-Avraham, 1977, Tibor & Ben-Avraham, 1992). The location of the seismic sections displayed in Fig. 5.8, 5.9 and 5.13 is indicated.	5-15
5.8	a) Seismic section perpendicular to the Levant margin, crossing the structure CS-1 through its centre (location in Fig. 5.6). The seismic package from the Base Pleistocene to Q60 shows thickness variation across the extensional faults, defining their phase of growth. b) Seismic section crossing CS-1 through its centre, and c) interpretation. The apparent downsag of Horizon N and the underlying seismic reflections below CS-1 is caused by a seismic 'push-down', due to the seismic velocity contrast between the Messinian evaporites (Unit 2) and the marine clastic sediments of Unit 3. This section shows the thickening of the stratigraphic package PL20-PL50 and onlap of reflections within the same interval above CS-1. Note the set of extensional and subvertical faults, steeply dipping toward the centre of CS-1 and deforming its overburden. YSM = Yafo Sand Member. d) 1:1 vertical to horizontal ratio of Fig. 5.8c.	5-16
5.9	a) Variance time slice (2512 ms) showing the circular appearance of CS-2, CS-9 and CS-10 in plan view. The location of the seismic cross section of Fig. 5.9b is indicated. b) Seismic section across CS-2 (see Fig. 5.7 for location). A minor push-down effect is present at the Horizon N beneath CS-2. c) Variance time slice (2256 ms) showing the circular appearance of CS-8 in plan view. The location of the seismic cross section of Fig. 9d is indicated. d) Seismic section across CS-8 (see Fig. 5.7 for location). e) Seismic section across CS-3, CS-6 and CS-7 (see Fig. 5.7 for location). f) Seismic section across CS-4 and CS-5 (see Fig. 5.7 for location). M = Horizon M, N = Horizon N. g) Salt outlier located in the northern area of the pinch-out of the Messinian evaporites (see Fig. 5.7 for location).	5-17
5.10	Three-dimensional visualization of the time-structure map of Horizon PL20, cutting at the top of a seismic section parallel to the Levant continental margin (see location in Fig. 5.7), and crossing the circular structure CS-1. Half of CS-1 is visualized on this map, showing the relationship with the underlying stratigraphy. In Unit 2 (Messinian evaporites) the interval between Horizon ME20 and Horizon M appears to thin-out toward the flanks of CS-1.	5-20
5.11	a) TWT-dip attribute map of Horizon PL20, and b) interpretation, showing the detailed morphology of this surface and the deformation associated with the circular structure CS-1. Note the pattern of	5-23

	concentric extensional and subvertical faults around CS-1. The dotted lines highlight the position of the seismic sections used for the measurements displayed in Fig. 5.12.	
5.12	Diagrams showing the vertical relief (ΔZ) and expansion index (E.I.) measured and calculated on random seismic sections across CS-1 (see location of sections in Fig. 5.10). See Fig. 5.3a for explanation of the parameters. The reference horizon for the measurements is taken at the seabed that represents a horizontal surface above CS-1. ΔZ (Fig. 5.11a to c) and E.I. (Fig. 5.11d to f) are plotted (x axis) in the diagrams against the depth of the reference horizon (y axis, in meters), and against the stratigraphic chart. The grey areas highlight the maximum observed variation of the vertical relief (Figure 5.11a to c) and the maximum values of the expansion index (Figure 5.11d to f), which are interpreted as related to the time of maximum syn-sedimentary growth of CS-1.	5-24
5.13	Schematic cartoon depicting the successive phases of formation of the circular dissolution structure CS-1. The dissolution process started in the early Piacenzian (B), when vertical focused fluid flow begun corroding the lower evaporitic unit and dissolving its upper and more soluble part, causing collapse of the overburden and successive onlap of sediments (B and C) at the coeval seabed. Note in this interval the formation of the concentric faults directly related to the collapse of the sediments above the depleted evaporitic unit. The process terminated by the late Piacenzian (D), with the deposition of Horizon PL50. N = Horizon N; M = Horizon M.	5-32
5.14	Seismic section crossing the Levant continental margin in a W-E direction, showing the deep structural setting of the study area (location of seismic section shown in Fig. 5.7). Note the relative position of the structure CS-3 above the Afq submarine canyon (dashed line) and the axis of the Syrian Arc anticline, and related fault system (dotted lines). B.S. = Base Senonian horizon; M = Horizon M; N = Horizon N. The interpretation of the faults post-dating the deposition of the Messinian evaporites, within Unit 3, is indicated with dotted lines.	5-34

Chapter Six: Summary and discussion

Figure No.	Figure Caption	PAGE No.
6.1	2D seismic sections crossing the Levant region in a NW-SE direction. The seismic sections are time-depth converted applying a simple layer-cake model of seismic velocity distribution to the seismic units analysed, as explained in the text. The black dotted line represents the projection of the regional top of the Messinian evaporites towards the margin. The coincidence of this projection with the marginal step in the erosional surface developed landward of the pinch-out of the evaporites should be noted in Fig. 6.1a, f and g. On the vertical scale, the numbers refer to seconds two-way travel time on the seismic sections, and to kilometres depth on the interpreted time-depth converted section. a) 2D seismic line em83-31 (location in Fig. 6.2). b) 2D seismic line em83-33 (location in Fig. 6.2). c) 2D seismic line em83-34 (location in Fig. 6.2). d) 2D seismic line em83-35 (location in Fig. 6.2). e) 2D seismic line em83-43 (location in Fig. 6.2). f) 2D seismic line em83-45 (location in Fig. 6.2). g) 2D seismic line em83-44 (location in Fig. 6.2).	6-6/ 6-9
6.2	Map of the time-depth converted Horizon M in the 2D seismic survey area. The continuous white lines indicate the location of the marginal scarps MS1, 2 and 3 described in the text. The location of the seismic sections displayed in Fig. 6.1 and 6.7 is indicated by the white dotted lines.	6-10
6.3	Synoptic diagram illustrating the distribution of clastic bodies (dark grey areas) throughout the study area. The location of the clastic bodies HAB1, 2 and 3 analysed in Chapter 3 is indicated. The map in the background shows the the main morphological and structural features overlain on the isochron lines of the base of the Messinian evaporites (Horizon N). For the explanation of the symbols, see Chapter 2, Fig. 2.10. The location of the seismic lines displayed in Fig. 6.4 is also indicated.	6-13
6.4	Seismic sections showing the distribution of clastic bodies at the base of the Messinian evaporites in the study area. a) 2D seismic section crossing the Levant region in a NW-SE direction (location in Fig. 6.3). The lower part of the figure displays a close-up of the seismic section, with the line-drawing and interpretation of the clastic body (dark grey colour) resting above the base of the Messinian evaporites (Horizon N). The black arrows mark the truncated termination of the pre-evaporitic reflection, directly related to the location of the Afq-EI Arish canyon flanks. b) 2D seismic section crossing the Levant region in a NW-SE direction (location in Fig. 6.3). The clastic body at the base of the Messinian evaporites is identified by the high-amplitude seismic event, by analogy with the procedure applied in Chapter 3.	6-14

6.5	<p>Basinal models proposed for the creation of the accommodation space necessary for the deposition of the ca. 1.8 km-thick Messinian evaporitic wedge in the Levant region.</p> <p>a) The first model implies the deposition of the distal part of the evaporites in a pre-existing very shallow sea (max. 200m deep), with accommodation space created only by tectonic subsidence and sediment load.</p> <p>b) The second model implies the deposition of the distal evaporites in a pre-existing shallow ramp-setting sea.</p> <p>c) The third model involves the deposition of the evaporitic wedge in an intermediate (ca. 1000m deep) sea characterised by a pre-existing shelf-slope-basin setting.</p> <p>The most likely basinal setting for the deposition of the Messinian evaporites is the third model (see discussion in the text).</p>	6-17
6.6	<p>Seismic sections showing the details of the morphology and truncation of seismic reflections associated with the Messinian marginal scarps identified at Horizon M, eastward of the pinch-out of the Messinian evaporites.</p> <p>a) 2D seismic section crossing the Levant margin in a NW-SE direction (location in Fig. 6.2). The location of the marginal scarp developed between MS2 and MS3 (cliff 2/3) is indicated.</p> <p>b) Close-up of the seismic section displayed in Fig. 6.6a (location in Fig. 6.6a and in Fig. 6.2), showing the detailed seismic stratigraphic context of the marginal scarp developed between MS2 and MS3 (cliff 2/3). The interpretation of the main reflections, faults and seismic effects is indicated. The seismic package highlighted in blue is of unknown origin and it might correspond to marginal Messinian deposits, whose internal architecture is beyond seismic resolution.</p> <p>c) 3D seismic section crossing the Levant margin in a NW-SE direction (location in Fig. 6.2). The onlap of the early Pliocene reflections on the scarp developed between MS2 and MS3 (cliff 2/3 of Fig. 6.6a) should be noted. It is significant to note also that the base of the cliff (MS3) is coincident with the projected top of the Messinian evaporites (horizontal black dashed line). The downward bending of the seismic reflections directly above MS2 is probably the product of post-depositional differential compaction of the Pliocene sediments above the morphological step defined at Horizon M.</p>	6-23/ 6-24
6.7	<p>Cartoon showing a simplified evolutionary reconstruction of the relative sea-level changes and of the depositional and erosional processes occurred in the study area during the MSC (see detailed discussion in the text).</p>	6-29
6.8	<p>Map showing the location and age of some of the major basinwide evaporite deposits. The basins are drawn for visual clarity, not to exact scale (Warren, 1999).</p>	6-32

LIST OF TABLES

Chapter One: Introduction

Table No.	Table Caption	PAGE NO.
1.1	Different nomenclature applied in the Mediterranean Basin to the lower and upper boundary of the Messinian evaporites and to the marginal (proximal) erosional surface on seismic data. In this PhD research, the terminology established by Ryan et al. (1973) and Ryan (1978) has been adopted.	1-26
1.2	Summary of the main physical properties of different sediments and of sea-water influencing their seismic response: v_p = velocity of compressional waves; ρ bulk= bulk density; Z = acoustic impedance. Data from Rider (1986), Keary et al. (2002) (density and velocity), Nurmi (1988) (density in brackets).	1-28

Chapter Six: Summary and discussion

Figure No.	Table Caption	PAGE NO.
6.1	Summary of maximum amplitude of sea-level fall and rise linked to the MSC in the Mediterranean Basin, as estimated in previous studies. The overall equivalence between the drawdown and reflooding amplitudes should be noted.	6-30

LIST OF ABBREVIATIONS

2D	Two-dimensional
3D	Three-dimensional
B.M.	Base Miocene horizon
B.S.	Base Senonian horizon
CS (1 to 10)	Circular (dissolution) structures
L.E.	Late Eocene horizon
m	Multiple
M	Horizon M (top of the Messinian evaporites)
MSC	Messinian Salinity Crisis
N	Horizon N (base of the Messinian evaporites)
OS	Offshore Structure (Syrian Arc)
S.A.	Syrian Arc
T	Truncation
TWTT/TWT	Two-way travel time
U1/U2/U3	Seismic stratigraphic Unit 1, 2 and 3
YSM	Yafo Sand Member

Chapter One: Introduction

1.1 Project rationale

The presence of evaporitic deposits of Messinian age under the Mediterranean Sea was discovered at the beginning of the '70s by the Deep Sea Drilling Project (DSDP) Cruise Leg 13 (Hsü et al., 1973). This first drilling campaign in the Mediterranean, complemented with the acquisition of 2D seismic data, revealed the existence of extensive late Miocene erosional surfaces developed over most of the continental margins, and of a thick (more than 2 km) sequence of evaporites in the deeper part of the present Mediterranean Basin (Ryan et al., 1973). The evaporites were found to be clearly linked to the well-known evaporitic succession of Messinian age, cropping out in the circum-Mediterranean areas (Selli, 1960; Decima & Wezel, 1973). Regional mapping of the evaporites in the marginal and distal domains showed that the Messinian basin extended across some 2400 x 600 km (Rouchy, 1982; Kendall & Harwood, 1996) determining its status among the largest of the ancient 'saline giants' in the world (Warren, 1999).

The geological event that led to the deposition of the late Miocene evaporites in the Mediterranean area is known as the 'Messinian Salinity Crisis' (MSC) (Selli, 1960). After the discovery of the basinwide extent of the evaporites, this term was used to indicate the isolation from the global ocean system and the deep desiccation of the Mediterranean Basin (e.g. Hsü et al., 1973). Normal marine sedimentation was interrupted and a dominant hypersaline environment became widespread across the basin. The MSC has been recognized as one of the most dramatic events on Earth during the Cenozoic era (Hsü et al., 1977). On a global scale, the event reduced world ocean salinity, altered evolutionary trends of marine organisms within and beyond the Mediterranean Sea, and temporarily modified global thermohaline circulation (Hsü et al., 1977; Kastens, 1992).

Although intense and durable interest from the international research community led to continuous advances in knowledge throughout the last 30 years, the MSC is still the subject of considerable scientific disputes. Amongst the main controversial issues, the causes and modality of the deposition of this saline giant still remain enigmatic.

The absence of modern analogues of a scale comparable to ancient ‘evaporite giants’ represents the main factor hindering the development of a depositional model for the Messinian evaporites. Furthermore, the lithology of the greatest part of the evaporites in the Mediterranean Basin is still unknown, because only the upper few tens of metres (i.e. ca. 10% of the total section) have been drilled (Hardie & Lowenstein, 2004). So far, basinwide depositional models have strongly relied on the 2D seismic record, which is, however, subject to limited resolution and spatial aliasing. The lack of 3D seismic data has strongly limited the identification and detailed analysis of depositional and deformational features within the evaporites, such as erosional and stream patterns, clastic bodies, carbonate reefs or internal tectonic structures.

Consequently, important questions remain that have not been answered by the methods used so far. These include the temporal and spatial relationship between the deposition of the marginal and basinal evaporitic series, the differences observed in the series deposited in the Eastern and Western Mediterranean, the events leading to the re-establishment of normal marine conditions after the crisis and their timing. Additionally, some of the implications of the presence of the evaporites on the evolution of the continental margins are still relatively unexplored. This is particularly the case of their impact on stability, erosion and fluid flow patterns. Therefore, there is clear scope for application of new analytical techniques to provide insights into these questions.

1.2 Aims of study

The main purpose of this research is to build an evolutionary model for the deposition and deformation of the Messinian evaporitic system in the Levant region (Eastern Mediterranean). The ultimate goal of this project is to improve our current understanding of the processes that occurred during the Messinian Salinity Crisis in the Mediterranean Basin. These main purposes are pursued by addressing a series of key aims, which are listed as follows:

- Define a detailed 3D stratigraphic analysis of the Messinian evaporitic unit on the Levant continental margin and deduce the factors controlling their distribution in the region.

- Evaluate the position of the sea-level prior, during and after the MSC, assessing relative sea-level changes in this time-span.
- Investigate the impact of local vs. regional factors in governing the events linked to the MSC in the region.
- Account for the areal erosional patterns and unconformities during the MSC.
- Determine the distribution of clastic sediments within the evaporites, and interpret clastic sediment fairways during the deposition of the Messinian evaporites.
- Develop means for identifying the erosional and depositional activity of a system of slope canyons (i.e. El Arish, Afiq and Ashdod Canyons) throughout the MSC.
- Define the basinwide depositional architecture of the evaporites.
- Assess the deformation of the evaporitic unit caused by dissolution and syn- and post-depositional salt tectonics, exploring their mechanism and impact on present-day evaporite stratigraphy.
- Analyse the relationship between evaporite deposition and creation of accommodation space.
- Assess the impact of evaporite deposition on local subsidence, slope stability, erosion and fluid flow at the continental margin.
- Compare the local evolutionary model of the evaporites with previous Messinian models for the region and with worldwide analogues.

To address the issues above, extensive interpretation of regional 2D seismic datasets and detailed interpretation of 3D seismic data in the Levant region, provided by the industry sponsor (BG-Group), was undertaken. Seismic interpretation was calibrated with local well data from the marginal part of the evaporitic system. 2D seismic data were used for regional correlation and stratigraphic analysis. Detailed interpretation of the 3D seismic data and well data were used to highlight the controls on smaller-scale structures such as depositional, erosional, dissolution and structural features. The combination of all data and results is summarized in the form of an evolutionary model of the Messinian evaporites in Chapter 6.

1.3 Geographic, structural and stratigraphic setting

The Levant continental margin is situated in the easternmost part of the Mediterranean Sea, at the zone of interaction among the Anatolian, African and Arabian plates (Figs. 1.1 and 1.2; Vidal et al., 2000). The Levant passive continental margin was formed due to the rifting of the Tethys Ocean during the Late Triassic to Early Jurassic (Garfunkel & Derin, 1984). The Tethys linked the area occupied by the present Mediterranean with the Indian Ocean (Buchbinder & Zilberman, 1997). Associated with the opening of the Tethys, the Dead Sea system formed as a transform fault. During rifting, the Eratosthenes Seamount (Fig. 1.2) detached as a block and drifted away from the Africa-Arabian continent (Vidal et al., 2000) which formed at that time a single plate block (Badawy & Horvath, 1999).

Throughout most of the Cretaceous, the Levant margin was marked by a distinct shelf edge, separating shallow platform carbonates in the east from deep-water carbonates on the slope and basin in the west (Bein & Gvirtzman, 1977; Druckman et al., 1995). In the Senonian (late Cretaceous), a change in plate motion caused the African-Arabian plate to converge with the Eurasian plate, closing the back-arc of the Tethys ocean (Badawy & Horvath, 1999). The main structure connected to this geodynamic event in the Levant Basin is the Cyprus arc or trench (Figs. 1.1 and 1.2). Significantly for the study region, the plate collision resulted in the formation of a series of NE-SW directed compressional structures i.e. the Syrian Arc fold belt (Figs. 1.2 and 1.3a, Garfunkel, 1998; Eyal, 1996, Buchbinder & Zilberman, 1997). At this time the platform of the Levant continental margin was drowned and pelagic chalk-rich sedimentation prevailed while in the slope area non-deposition and erosion dominantly occurred (Druckman et al., 1995). Between the Senonian and the Paleocene, the deposition of the Mount Scopus and Avedat Groups occurred, characterised mainly by sedimentation of carbonates and marls (Fig. 1.3b).

Since the upper Eocene, the most important stratigraphic unit for this research study was deposited, i.e. the Saqiye Group (Fig. 1.3b). Its stratigraphic relation to the older units and structural highs is displayed in the representative region profile of Fig. 1.3a. Starting in the Oligocene, the Levant continental margin was incised by several submarine canyons (Druckman et al., 1995). The most prominent of these erosional features is the Afiq Canyon (Druckman et al., 1995; or Gaza - Beer Sheva Canyon, Buchbinder & Zilberman, 1997).

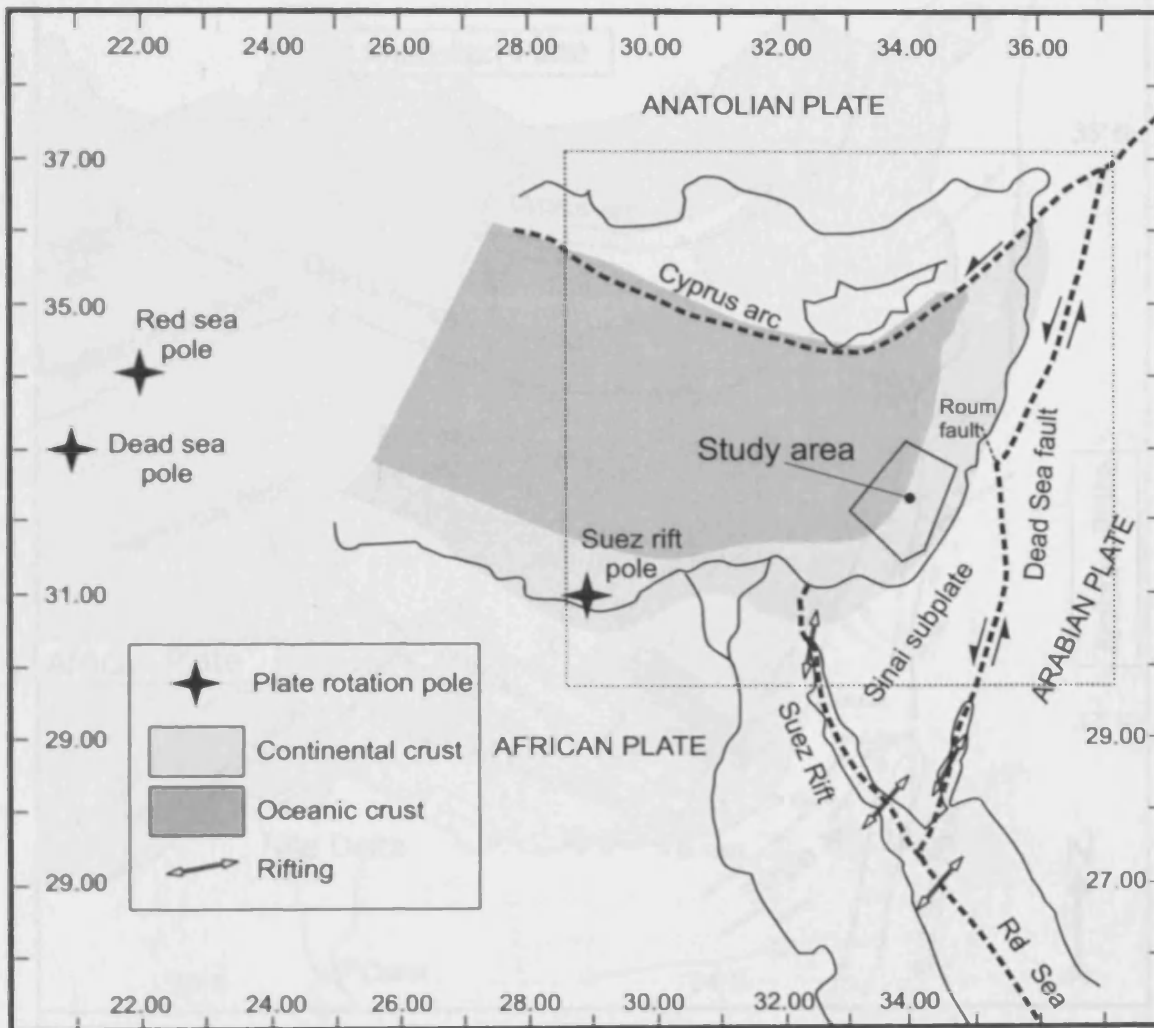


Figure 1.1 Regional structural map of the Eastern Mediterranean area, modified after Bardawy & Horvath (1999), showing the location of the study area (black box). The box highlighted by the black dotted line indicates the location of Fig. 1.2.

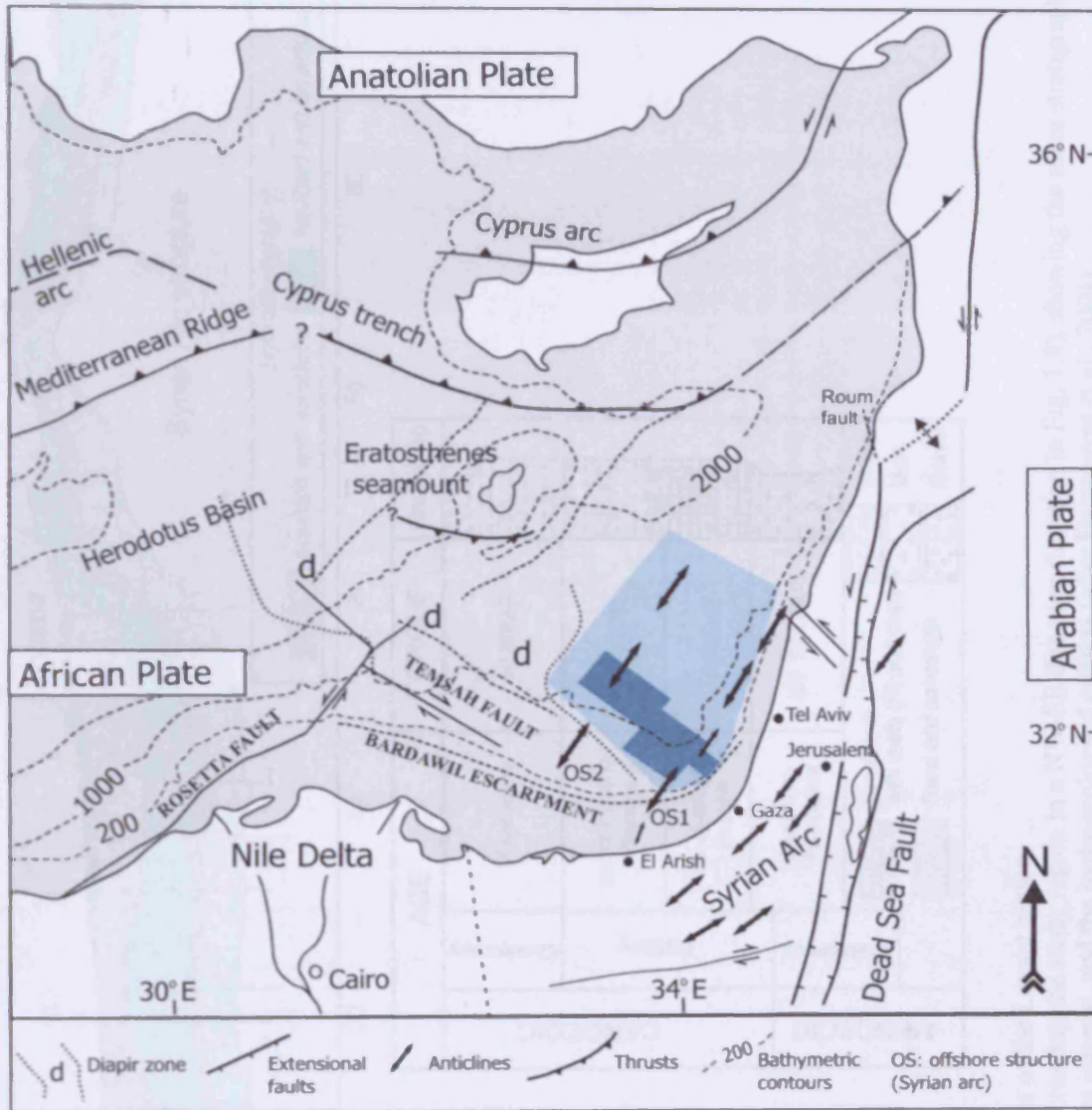
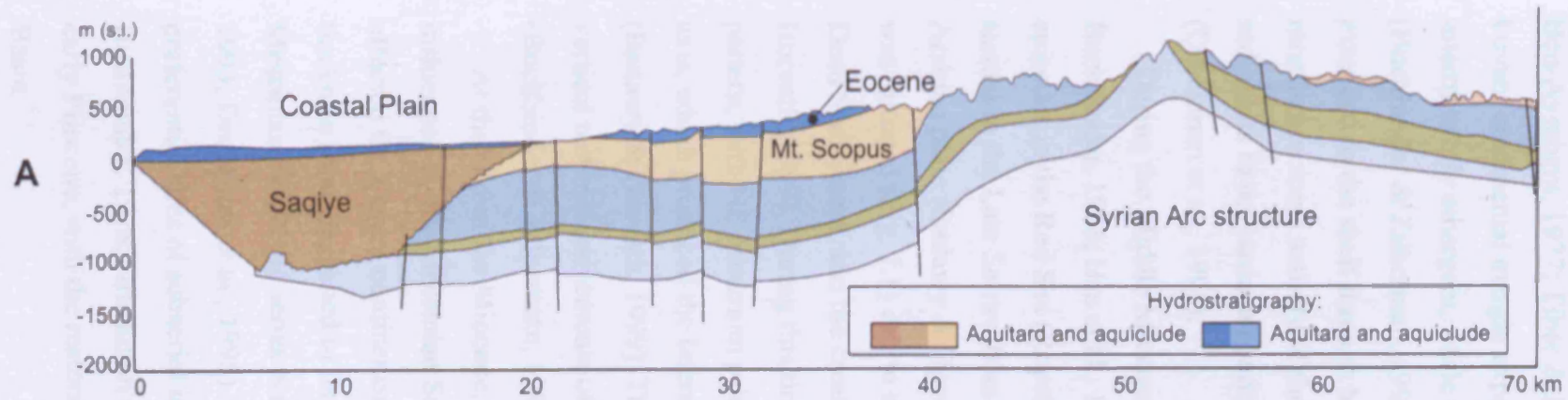


Figure 1.2 Location map showing the main structural elements of the Levant-Nile region (after Neev and Ben-Avraham, 1977; Tibor et al., 1992; Robertson, 1998; Abdel Aal et al., 2000; Vidal et al., 2000) with indication of the study area. The location of the 2D seismic dataset is highlighted by the light blue box, while the location of the 3D seismic dataset is highlighted by the dark blue box.



B

		AGE	GROUP	Graphic log
CENOZOIC	Quaternary	Pleistocene	KURKAR	[Graphic log symbol]
	Tertiary	upper Eocene-Pliocene	SAQIYE	[Graphic log symbol]
		lower-middle Eocene	AVEDAT	[Graphic log symbol]
MESOZOIC	Cretaceous	Senonian-Paleocene	MT. SCOPUS	[Graphic log symbol]

[Graphic log symbol]	Limestone with reefs (R) and chert	[Graphic log symbol]	Shale
[Graphic log symbol]	Sand and sandstone	[Graphic log symbol]	Marl
		[Graphic log symbol]	Gravel

Figure 1.3 Stratigraphic context of the Levant region.

a) Regional geological profile crossing the study region in a NW-SE direction (location in Fig. 1.8), showing the main stratigraphic groups in the Cretaceous-Recent interval, and the hydrogeological context (after Hargreaves et al., 2004).

b) Table summarizing the main lithostratigraphic units of the Levant continental margin (after Sneh et al., 2000).

In the early Miocene, the Syrian Arc began to emerge, with a series of NE-SW trending anticlines and synclines on the Levant margin (Figs. 1.2 and 1.3a; Neev & Ben-Avraham, 1977; Tibor & Ben-Avraham, 1992). Consequently, the shelf area of the Levant continental margin experienced localized tectonic uplift and became intermittently emergent, while the slope and basin areas continued to subside (Buchbinder & Zilberman, 1997). As a result, the Oligocene submarine canyons extended to the shelf through headward erosion (Buchbinder & Zilberman, 1997). The renewed tectonic activity of the Syrian Arc caused an increased supply of clastic sediments to the basin, a condition which has been continuing until the present day (Druckman et al., 1995).

During the Middle Miocene, the Indo-Pacific connections closed (Gvirtzman & Buchbinder, 1978; Hsu et al., 1978; Steininger & Rogl, 1984), causing evaporitic episodes in the Red Sea (Rouchy et al., 1995). Seafloor spreading in the Red Sea started in the Late Serravallian (12-13 My), caused by an increase of rotation of the Arabian plate (Badawy & Horvath, 1999). In this tectonic context, the Dead Sea Fault was initiated (Fig. 1.1) due to the shifting of the motion from the Gulf of Suez to the Dead Sea system, and the creation of the Sinai subplate (or microplate) (Badawy & Horvath, 1999). During this time the motion was associated with a strike-slip stress pattern, with NE minimum principle stress axis and NW maximum principle stress axis, which produced the lateral motion between the Arabian and Sinai subplates (Badawy & Horvath, 1999). The creation of this plate boundary strongly affected the vertical tectonic movements of the Miocene-Pliocene Levant margin and basin (Buchbinder & Zilberman, 1997).

At the end of the Miocene, the evolution of the Levant margin was greatly influenced by the Messinian Salinity Crisis. During this period, a major erosional phase affected the Levant continental margin while a thick evaporitic series (up to 2 km of thickness) was deposited in its central part (Tibor & Ben-Avraham, 1992). The Messinian evaporitic series is named Mavqi'im Formation in Israel (Cohen, 1988, 1993; Druckman et al., 1995). Simultaneously, the Oligo-Miocene canyons became preferential sites of subaerial incision along the continental margin (Gvirtzman & Buchbinder, 1978; Druckman et al., 1995). The Messinian Salinity Crisis ended in the early Pliocene, with the restoration of normal marine conditions in the Mediterranean Basin.

Since the Pliocene, a thick wedge of mainly Nile-derived, siliciclastic sediments, deposited on the Levant continental margin and basin (Yafo Formation) (Tibor & Ben-Avraham, 1992). The submarine canyons ceased their activity in the Pliocene and represent now buried features (Druckman et al., 1995). During the Pleistocene, a major episode of continental shelf construction occurred (Tibor & Ben-Avraham, 1992), due to an increase in the sediment supply to the basin. The youngest depositional unit on the Levant margin is represented by a wedge of Holocene siliciclastic sediments, overlying a subaerial unconformity of probable Würmian age, i.e. related to the last glacial lowstand (Neev & Ben-Avraham, 1977). The Pliocene to Recent sediments in large areas of the Levant margin and basin are affected by thin-skinned tectonics above the Messinian evaporites (Tibor & Ben-Avraham, 1992; Garfunkel, 1998). In the southern part of the margin, NE-SW directed shallow normal faulting represents the main deformation style. This type of deformation has been related to flow and migration of the Messinian evaporites, probably begun in the late Pliocene (Garfunkel and Almagor, 1985, 1987; Tibor & Ben-Avraham, 1992).

1.4 Synthesis of the Messinian Salinity Crisis

During the latest Miocene, the Mediterranean Sea became partially and gradually isolated from the global ocean system (Hsü et al., 1973, 1978; Clauzon et al., 1996). This condition was reached through a series of rapid and dramatic paleogeographic changes involving complex feedback among tectonics, eustasy and climate in the Mediterranean area (Roveri et al., 2001). At the Mediterranean continental margins, a relative sea level fall of 1 to 2 km is suggested by the incision of river canyons (Druckman et al., 1995, Clauzon et al., 1996). As a consequence, a dominantly hypersaline environment became widespread on the Mediterranean Basin, leading to the deposition of 2-3 km thick evaporite series in its central parts. The distribution of the evaporites in Fig. 1.4 shows the basinwide extent of this event. In the following sections, the previous studies regarding the onset and termination of the MSC, and the depositional model of the Messinian evaporites are introduced as a base for the main topics investigated in this research project.

1-10

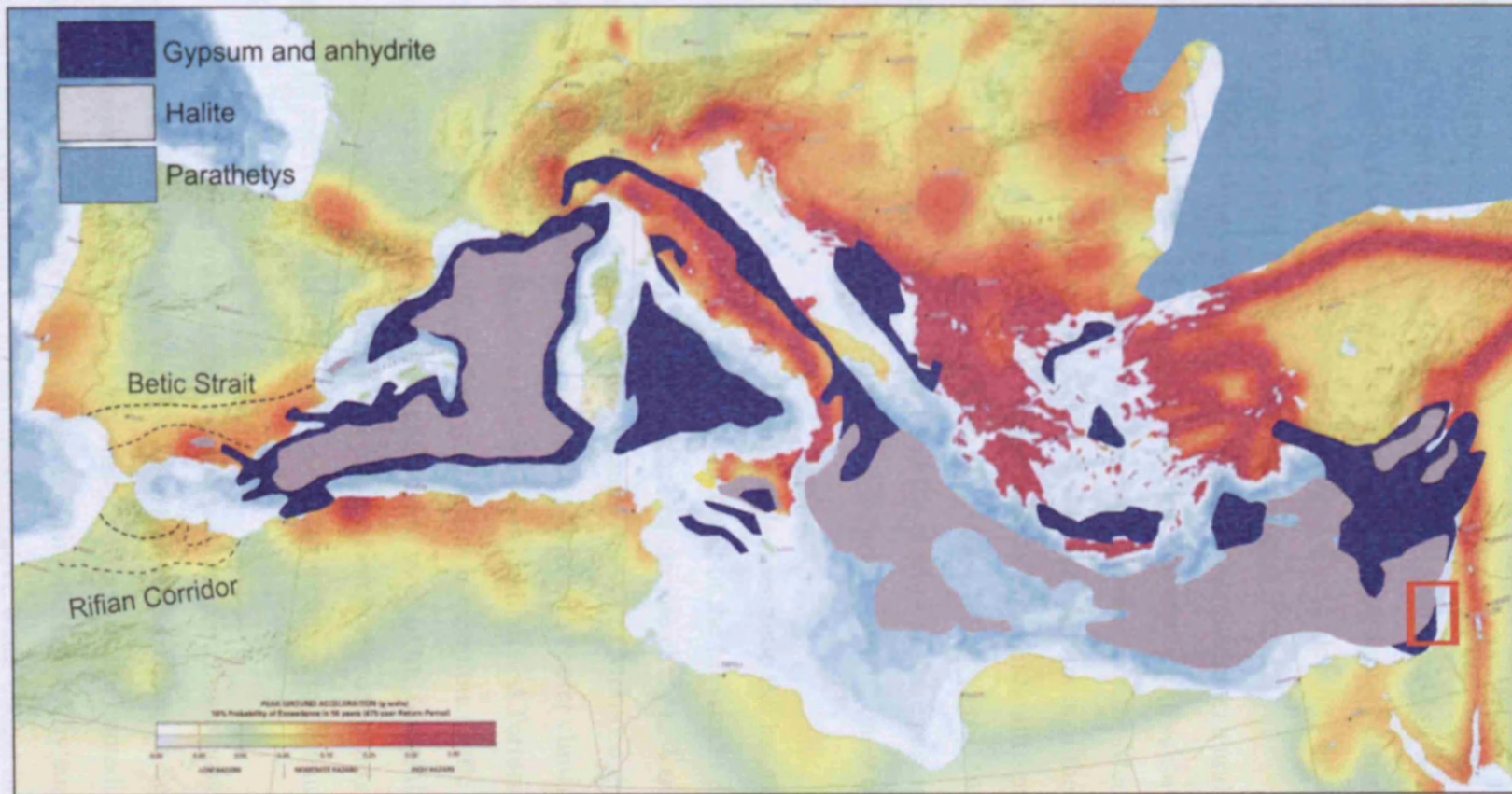


Figure 1.4 Distribution of Messinian evaporitic deposits in the Mediterranean Basin (after Rouchy, 1980; Reading, 1996; Warren, 1999). The Rifian Corridor' in Morocco and the 'Betic Strait' in Spain mark the approximate locations of the waterways that connected the Mediterranean Sea and the Atlantic Ocean prior to the Messinian Salinity Crisis (after Muller & Hsu, 1987; Benson et al., 1991; Kastens, 1992). The light-blue colour highlights the distribution of Parathetys deposits during the Messinian (from Steininger & Rogl, 1984). The red box indicates the location of the study area. The background is composed by the map of the seismic hazard in the European-Mediterranean area (Giardini et al., 2003), which highlights the main tectonic lineaments active at the present day.

1.4.1 Onset and termination of the MSC

The Mediterranean Sea is an enclosed basin which retains its only link with the Atlantic Ocean through the Gibraltar Strait. Before the Middle Miocene, the paleogeography of the Mediterranean area was considerably different to that of the present day: the basin was connected to the Atlantic Ocean to the west, and to the Indian Ocean and the Paratethys basin to the east (Fig. 1.4).

The final severance of the link between the Mediterranean and the Indian Ocean probably occurred ca. 14 My ago, during the Serravallian (Buchbinder and Gvirtzman, 1976). Almost simultaneously, the complete separation of the Mediterranean from the Paratethys lakes took place (Hsü et al., 1978). The last links of the Mediterranean with the world ocean before the MSC were the Betic Strait in South Spain and Rifian Corridor in Morocco (Fig. 1.4; Hsü et al., 1978; Muller & Hsu, 1987; Benson et al., 1991; Kastens, 1992). It is believed that the closure of these passages in the late Miocene caused the isolation of the Mediterranean and the onset of evaporite deposition.

Climate change, tectonic uplift and/or glacioeustatic fall have been traditionally considered as the primary controls on the onset of the Messinian Salinity Crisis (Warny et al., 2003). With respect to the influence of climate change, Warny et al. (2003) indicate a stable dry climate on the Atlantic margin of Morocco throughout the late Miocene. The most remarkable change to a drier and cooler climate took place before the Tortonian or at the transition between Serravallian and Tortonian, when the severance of the basin with the Indian Ocean was complete. Little or no variation occurred since the early Tortonian and during most of the Messinian (Hsü et al., 1978, Vidal et al., 2000). Consequently, the onset of evaporite deposition in the deep basin cannot be interpreted as a response to a dramatic change in climate (Warny et al., 2003).

Global sea-level lowering has also been often quoted as a possible cause of the onset of the MSC (Hodell et al., 1986; Kastens, 1992; Zhang & Scott, 1996). These studies emphasize the role of glacio-eustatic effects as the immediate trigger for the beginning of the salinity crisis. Albeit favouring the control by eustasy and glaciations preparing the conditions for an enhanced negative water budget in the Mediterranean

Basin, it is recognised that long-term tectonic movements must have established the necessary preconditions for the salinity crisis, creating the shallow-silled straits (Hodell et al., 1986; Kastens, 1992; Vidal et al. 2000).

Therefore, tectonic activity is generally envisaged as the major control on the final closure of the Betic Strait and Rifian Corridor and, consequently, on the isolation and hydrographic deficit of the Mediterranean Basin (Vidal et al., 2000; Duggen et al., 2003; Warny et al., 2003). The deep Betic strait shoaled after the end of the middle Miocene, as a result of the northward movement of the African Plate. Duggen et al. (2003) proposed roll-back of the Tethys oceanic lithosphere as the driving mechanism of the uplift of the northern African and the southern Iberian margins, and the closure of the Miocene gateways to the Atlantic Ocean.

Restriction of the Rifian Corridor, due to tectonic movements, began at ~7 Ma (Vidal et al., 2000; Warny et al., 2003). From 6.26 to 5.4 Ma shoaling had progressed to the degree that marine communication at the Rifian Corridor was controlled by small glacioeustatic fluctuations (Warny et al., 2003). Weak links, similar to the Gibraltar Strait of today, seem to have been competent enough to keep the Mediterranean waters as having normal marine salinity (Hsü et al., 1978). This argument is based on the consideration that the amount of evaporites deposited from a column of 1000 m of sea water does not exceed 14 m in thickness (Kendall & Harwood, 1996). Thus, the great (1-2 km) thickness of the Messinian evaporites implies a continuous supply of marine waters, and some residual communication between the Mediterranean and the global ocean during much of the salinity crisis (Hodell et al., 1986).

Throughout the Mediterranean, the early Pliocene is usually thought to mark the abrupt restoration of open marine conditions that, except for episodic marine influences, replaces the dominantly continental setting of the late Messinian basin (Cita et al., 1978; Pierre et al., 1998; Iaccarino & Bossio, 1999; Orszag-Sperber et al., 1989; Rouchy et al., 2001; Rouchy et al., 2003). Alternatively, other studies assumed that in some western and central parts of the Mediterranean Basin, the marine reflooding occurred during the late Messinian (Butler et al., 1995; Riding et al., 1998; Carnevale et al., 2006) or indeed, that the Mediterranean never desiccated completely during the MSC (e.g. Martinez del Olmo, 1996; Roveri et al., 2001; Manzi et al., 2005).

Nonetheless, it is generally agreed that opening of the Gibraltar Strait eventually led to the reflooding of the Mediterranean. The cause and modality of these events are

still debated. Traditionally, a catastrophic flooding of the basin after the breach of the Gibraltar strait has been envisaged by the first DSDP and ODP campaigns (see review in McKenzie, 1999). Notwithstanding different theories on the rapid or gradual refilling of the Mediterranean Basin, it is believed that the end of the MSC was linked to a tectonic cause, similar to that causing its onset (Duggen et al., 2003; Warny et al., 2003). 'Normal' marine conditions were fully re-established in the Mediterranean Basin 250,000 years after the reflooding (McKenzie & Sprovieri, 1990).

1.4.2 Depositional setting

During the MSC, two styles of evaporite deposition characterized the Mediterranean Basin. The first style comprised high level, marginward circum-Mediterranean deposits (Warren, 1999). The second was characterized by much larger, thicker basin-centre deposits (Warren, 1999). Basin-centre evaporites, with thickness up to 2 km, have been studied on 2D seismic data and well data since the early '70s. However, due to safety regulations, most of the DSDP and ODP drillcores recovered only the upper part of the evaporitic series, and little sampling is available from the lower part of these deep sections (Müller & Mueller, 1991). Therefore, the internal stratigraphy of the basinal evaporites is largely unsampled and uninterpreted (Warren, 1999) and their age is still strongly based on the correlation with the marginal Messinian series. Based on comparison of world analogues, basinwide evaporites are generally thought to be deposited in three main settings (Fig. 1.5; Warren, 1999):

- *Deep water-deep basin* evaporites have basin centers dominated by 'deep water' evaporites (5-300 m of water depth) composed mostly of finely laminated salts (e.g. basin centre of north and south Zechstein basins) (Fig. 1.5a; Warren, 1999).
- *Shallow water-shallow basin* evaporites are dominated by interfingering saltern and mudflat succession often crosscut by karstic erosional surfaces (e.g. African Rift) (Fig. 1.5b; Warren, 1999).
- *Shallow water-deep basin* evaporites are dominated by shallow water evaporites deposited as stacked saltern and mudflat cycles in a base level hundreds to thousands of meters below sea level (Fig. 1.5c; Warren, 1999).

Of these three settings, the shallow water-deep basin model (also known as the 'desiccated deep-basin model') is traditionally applied to the deposition of the

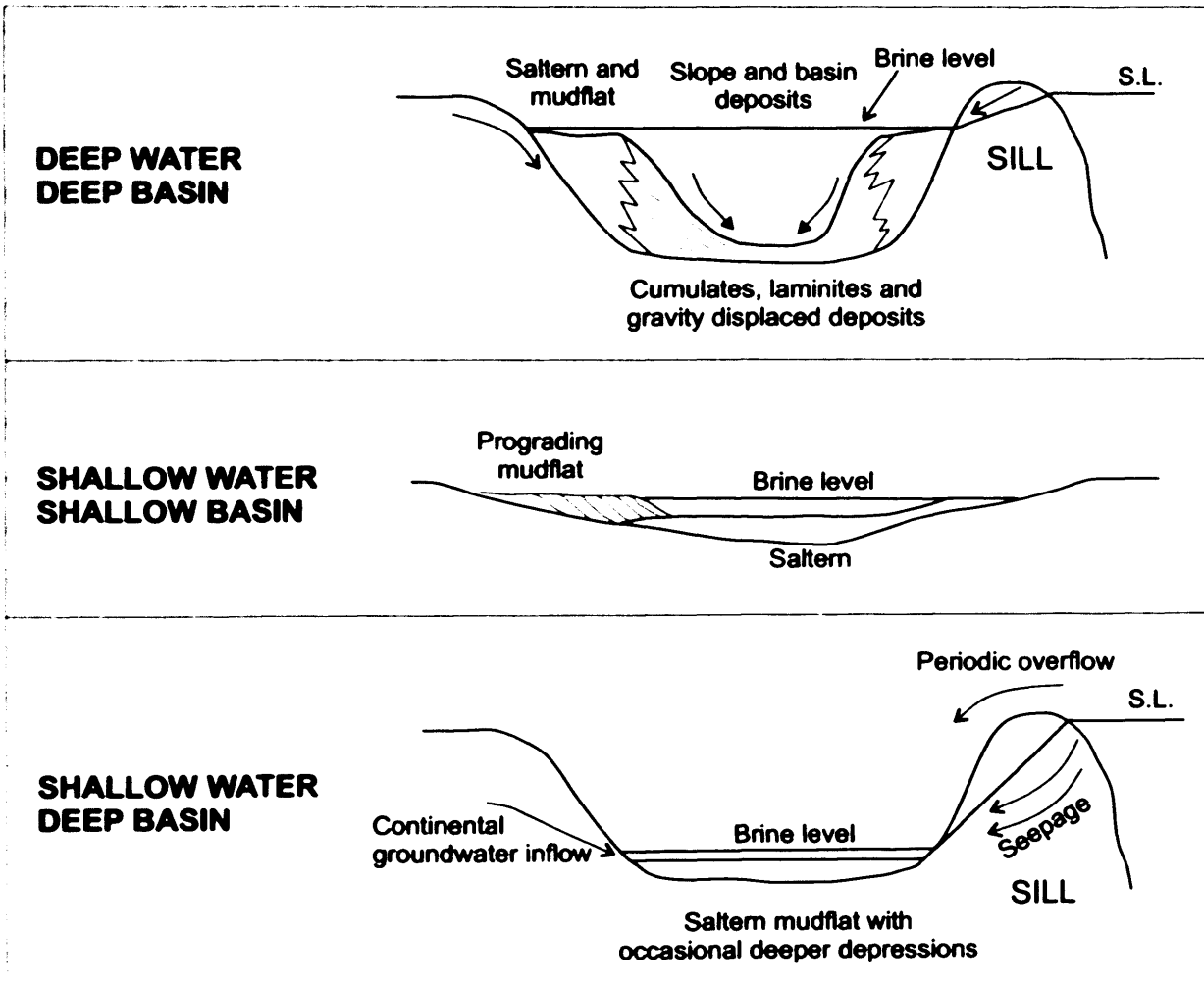


Figure 1.5 Main basinwide evaporitic settings (from Warren, 1989; Kendall, 1992; Warren, 1999). See text for explanation.

Messinian evaporites (Hsü et al., 1973). Although this model is widely accepted, alternative interpretations involving a shallow water-shallow basin setting have been put forward by other authors (Nesterhoff, 1973; Fabricius et al., 1978). Nevertheless, seismic data have shown that a deep Miocene basin indeed existed prior to evaporite deposition (Montadert et al., 1978), so that the shallow water – shallow basin model can be excluded for the deposition of the Messinian evaporites. Other studies have recently questioned that the Mediterranean basin had ever desiccated during the MSC (Martinez del Olmo, 1996; Manzi et al., 2005), proposing a deep water-deep basin model for the deposition of the Messinian evaporites.

A series of theoretical models for the deposition of the basinwide Messinian evaporites and the progression of the MSC have been proposed in previous studies (e.g. Butler et al., 1995; Clauzon et al., 1996; Krijgsman et al., 1999). The stratigraphic and chronological constraints of these models have been based mainly on the analysis of outcrops in Spain, Italy, Greece and North Africa, covering thus the marginal or transitional evaporites (Butler et al., 1995; Clauzon et al., 1996; Krijgsman et al., 1999; Rouchy et al., 2001, 2003; Warny et al., 2003). Evaporitic deposits are generally not directly datable (Kastens, 1992) and their age is usually bracketed by dating horizons below and above. This is due to the fact that evaporites deposit from waters of anomalous isotopic composition and their depositional environment tends to be inhabited by specialised organisms that have low biostratigraphic potential (Kastens, 1992).

In the last years, the use of new stratigraphic methods like magnetostratigraphy and astrochronology has attempted to overcome this problem (see e.g. Krijgsman et al., 1999). Nevertheless, controversies still exist over the development of the MSC. Indeed, various models ranging from the deposition of the evaporites as a synchronous event (i.e. the coeval onset of the MSC in marginal and basinal areas; Hsu et al., 1973, Krijgsman et al., 1999b) to a diachronous event (Butler et al., 1995; Druckman et al., 1995; Clauzon et al., 1996) have been proposed. The relative chronology of the MSC and the synchronous and diachronous hypotheses are summarized as follows (Figs. 1.6 and 1.7):

Synchronous model (Figs. 1.6 and 1.7a): According to Krijgsman et al. (1999) the onset of the MSC was synchronous over the entire Mediterranean basin. The evaporite series have been dated using astrochronology and cyclostratigraphy analysis of the

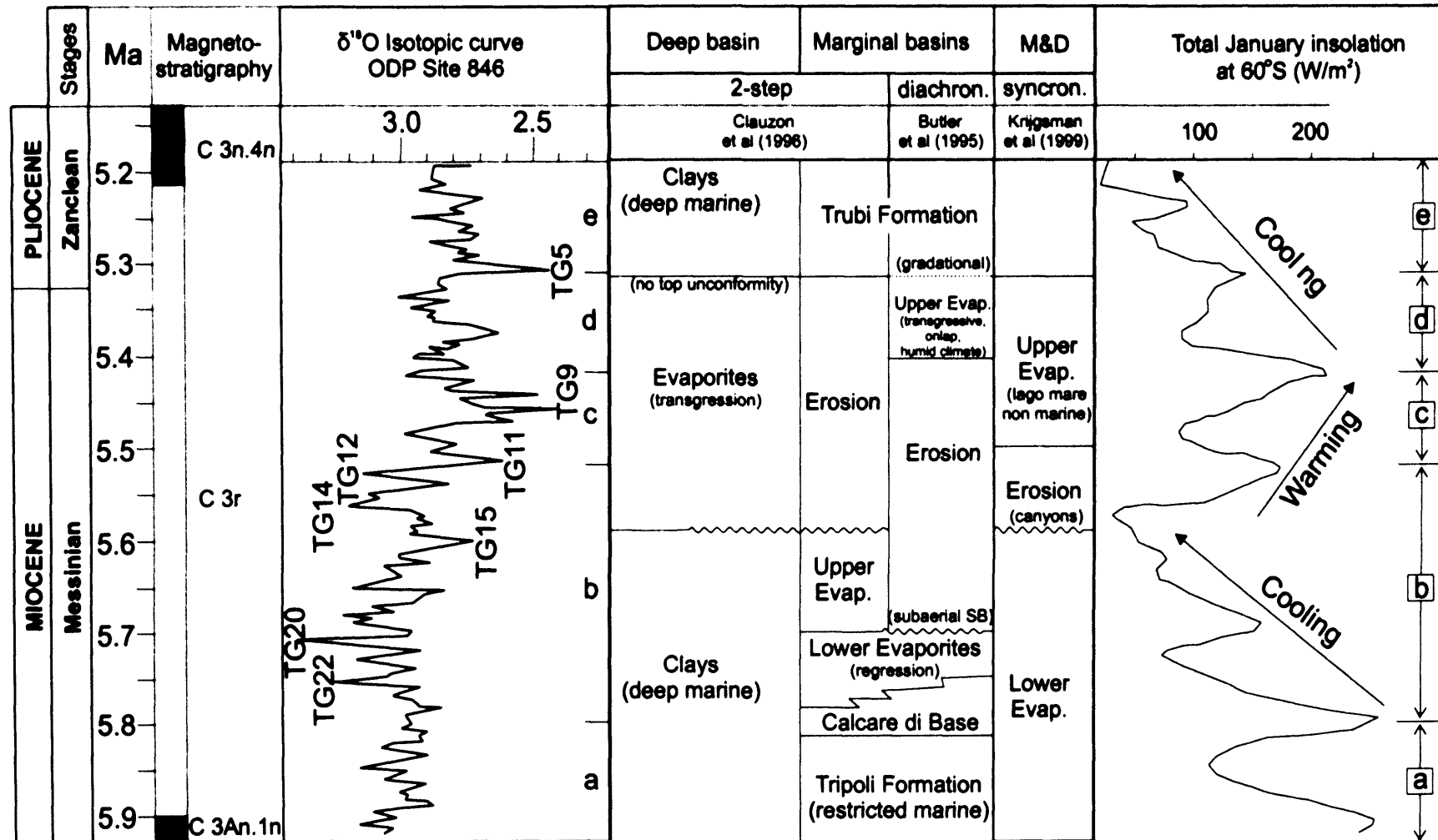
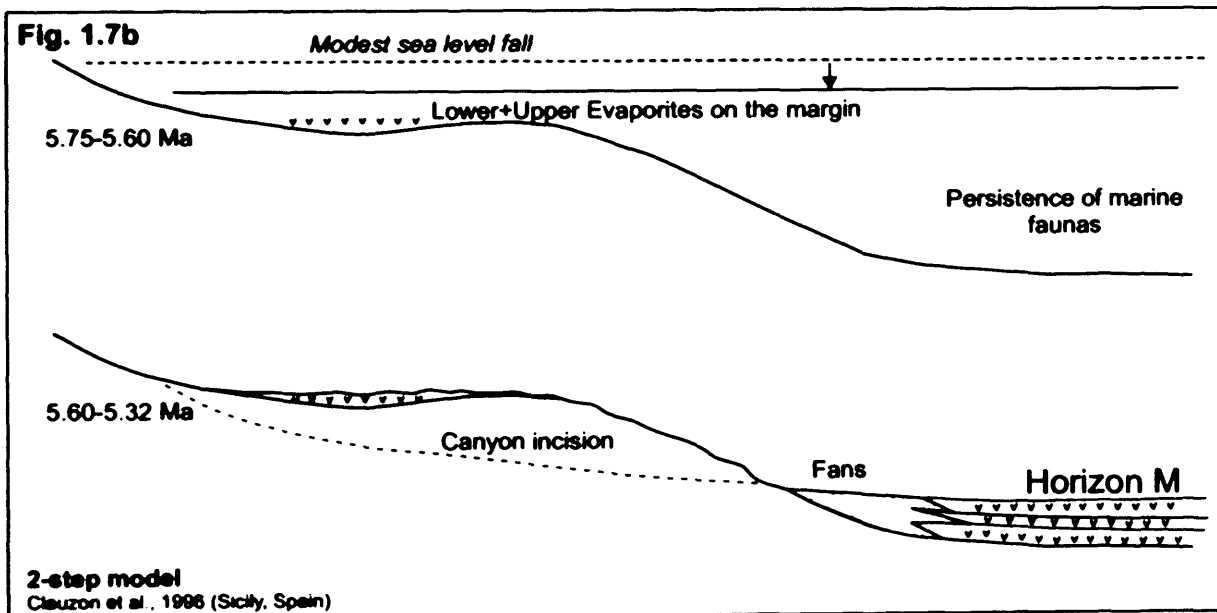
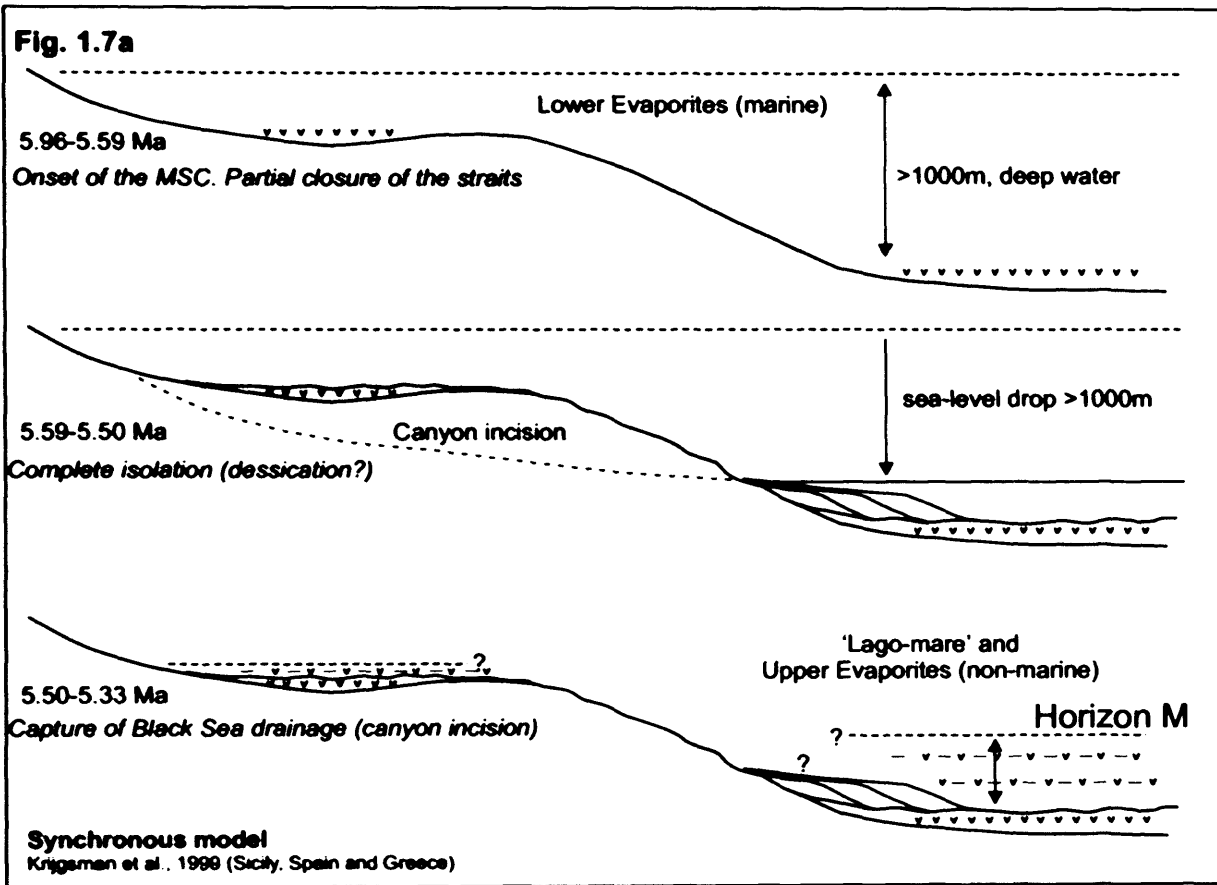


Figure 1.6 Diagram summarizing the stratigraphic context of the different depositional models developed for the Messinian Salinity Crisis in the Mediterranean area (modified from Warren, 1999). The main diachronous and synchronous models explained in the text and illustrated in Fig. 1.7 are compared and their different phases plotted against global stratigraphic and climatic curves.



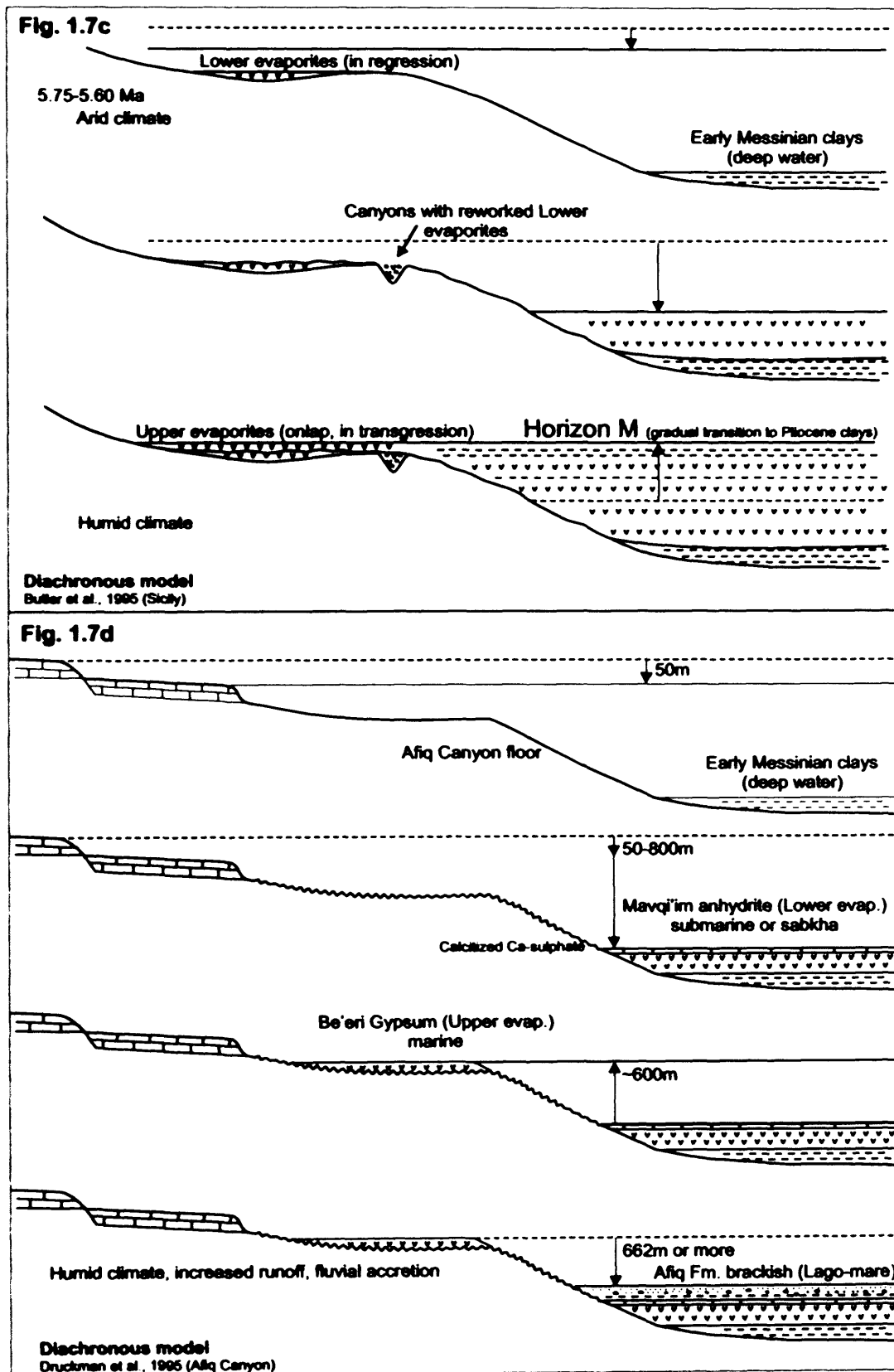


Figure 1.7 Schematic diagrams illustrating the main models for the evolution of the Messinian Salinity Crisis in the Mediterranean Basin.

- a) Model proposed by Krijgsman et al. (1999).
- b) Model proposed by Clauzon et al. (1996)
- c) Model proposed by Butler et al. (1995).
- d) Model proposed by Druckman et al. (1995) for the Levant continental shelf.

evaporitic series in Southern Spain (Sorbas Basin), Sicily (Caltanissetta Basin) and Greece (Gavdos Basin), and subsequently extrapolated to the entire Mediterranean Basin. Following this methodology, the beginning of the Salinity Crisis is dated back to 5.96 ± 0.02 Myr ago, and its duration is approximately calculated to be 640 ky (Krijgsman et al., 1999). At this time, the deposition of the Lower Evaporites took place in the marginal basins and in the basin-centre (>1000 m deep).

Complete isolation from the Atlantic Ocean and possible desiccation was established between 5.59 and 5.33 million years ago, when the Mediterranean water level dropped more than 1000 m, as indicated by incised canyons of the Rhone, Ebro, Po and Nile rivers on the Mediterranean margins (Krijgsman et al., 1999). This erosional phase lasted from 5.59 to 5.50 My. The deposition of the Upper Evaporite unit (5.50 – 5.33 My), overlying the erosional surface, took place in a non-marine Mediterranean basin forming a large ‘Lago-Mare’ (i.e. ‘lake-sea’) due to the dilution of the previous hyperhaline waters (McCullogh & De Deckker, 1989; Cipollari et al., 1999; Iaccarino & Bossio, 1999; Rouchy et al. 2001; Bassetti et al. 2003). Additionally, it is suggested that canyon incision in the Aegean region may have caused the transition to Lago-Mare conditions by capturing the Black Sea drainage.

Diachronous models (Figs. 1.6 and 1.7b,c and d): Clauzon et al. (1995) model (Figs. 1.6 and 1.7b) considers the deposition of evaporites in the marginal areas to be diachronous with the basin, based on their stratigraphic relationship with a major Messinian erosional surface. According to this model, the deposition of marginal evaporites took place from 5.75 to 5.60 My in response to a modest sea-level fall, during a global cooling period (Clauzon et al., 1996). In the second phase, from 5.60 to 5.32 My, the Mediterranean basin became isolated, and the deposition of basinal evaporites and the cutting of Mediterranean canyons occurred (Clauzon et al., 1996).

In contrast, Butler et al. (1995) (Figs. 1.6 and 1.7c) propose a completely diachronous deposition of the evaporites in the various sub-basin of Sicily. The evaporites are divided into two main cycles: the Lower and Upper evaporites, separated by a major sequence boundary. This boundary is associated with the drawdown of the Mediterranean Basin and the formation of a major regional unconformity. Subsequently, the Upper Evaporites deposited in isolated marginal seepage basins once the Mediterranean was flooded again by sea-water. On the Levant continental margin, a further diachronous model has been developed by Druckman et al. (1995) (Fig. 1.7d)

for the evaporitic deposits of the Mavqiim Formation. A first sea-level drop (50-800m) at the beginning of the MSC led to the deposition of the Lower evaporite (Mavqiim anhydrites). Subsequently, the sea-level rose more than 600m and the Upper evaporites (Be'eri Gypsum) deposited. Finally, a sea-level drop produced the deposition of brackish and continental deposits (the 'Lago-Mare facies) above the Lower evaporites (Fig. 1.7d, Druckman et al., 1995).

It should be stressed, however, that the models previously described are mainly derived from observations of the marginal outcropping evaporitic series. While this marginward series has been intensively studied, the basinwide architecture of the evaporites is still poorly known. Furthermore, the information available on the basin-centre part of the Messinian evaporites is focused on the Western Mediterranean area, where three main units are identified: the seismically layered 'Lower evaporites', a thick salt layer (0.5-1.5 km), and the layered 'Upper evaporites' (500-600 m thick) (Montadert et al., 1978). Such a subdivision is not applicable to the coeval evaporites in the Eastern Mediterranean, where the internal stratigraphy of the basinal deposits is considerably different (see e.g. seismic profiles published in Ryan, 1978; Garfunkel & Almagor, 1987; Polonia et al., 2002). It is therefore clear that further studies in this area are needed in order to compare the Eastern Mediterranean with the Western Mediterranean record, with the previously described models constituting the foundation for the interpretation of the evolution of the MSC in the study area.

1.5 Database

The database used in this research project consists of industry seismic data (3D and 2D) and a set of nine exploration wells. The location of the dataset is shown in Fig. 1.8. All data were obtained through BG-Group.

The 3D seismic coverage (Fig. 1.8) is represented by three seismic surveys acquired in 2000 by Geko-Prakla. The 3D seismic data cover a total area of approximately 6200 km², extending from the Levant Basin to the continental margin (Fig. 1.8). The seismic surveys were acquired with an in-line trace interval of 6.25 m, a line spacing of 25 m and a sampling interval of 4 ms. The final data for these two surveys were defined on a 12.5 by 12.5 m grid with 6400 bin cells per sq km after processing (BG-Group Report SA9029, 2000). The dataset was migrated with a single

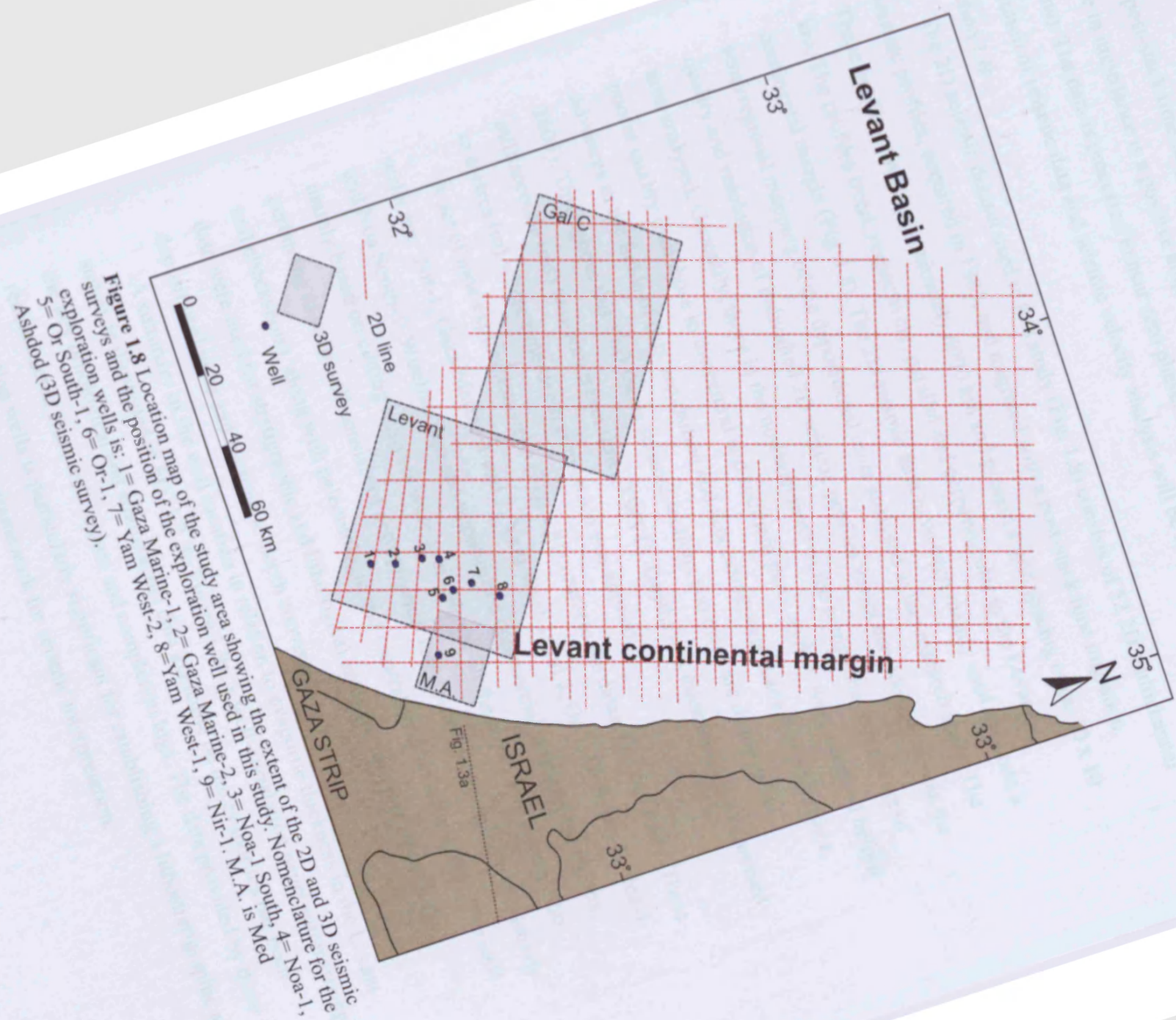


Figure 1.8 Location map of the study area showing the extent of the 2D and 3D seismic surveys and the position of the exploration well used in this study. Nomenclature for the exploration wells is: 1 = Gaza Marine-1, 2 = Gaza Marine-2, 3 = Noa-1 South, 4 = Noa-1, 5 = Or South-1, 6 = Or-1, 7 = Yam West-1, 8 = Yam West-2, 9 = Nir-1. M.A. is Med Ashdod (3D seismic survey).

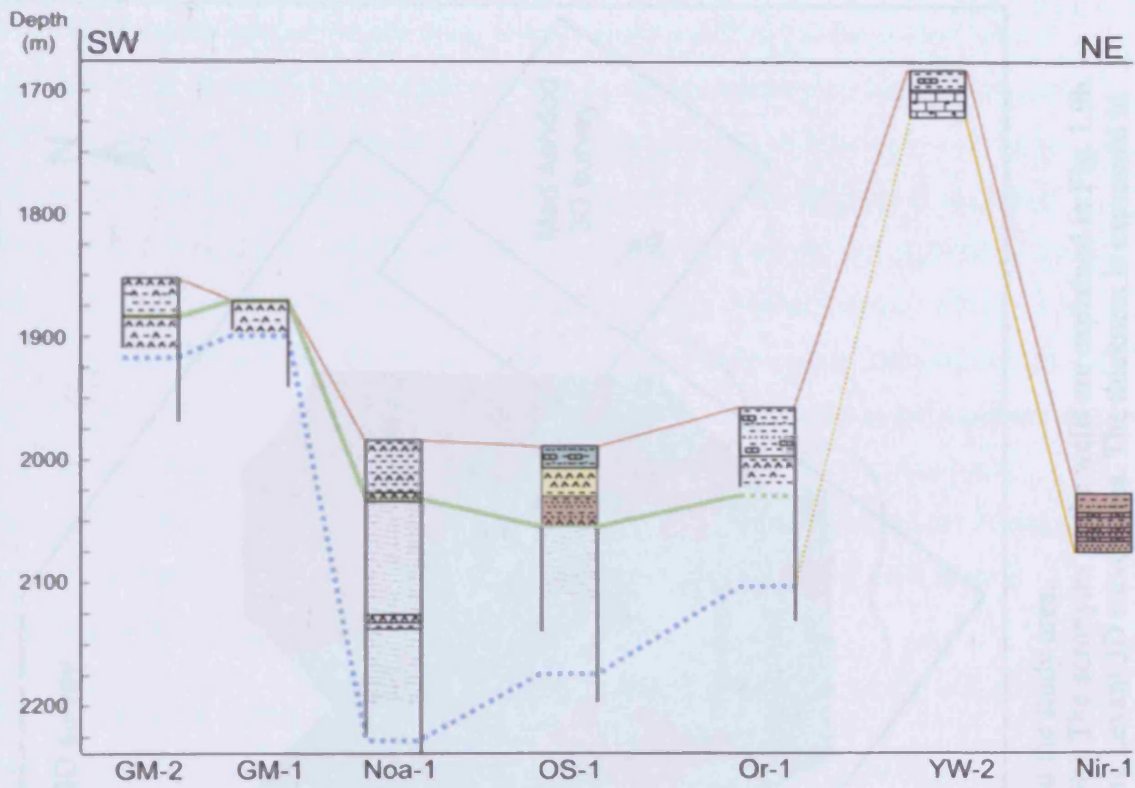
pass 3D post-stack time migration. Seismic data are SEG normal polarity, i.e. an increase in impedance is a positive amplitude (red colour in the original seismic sections). The data is processed to near zero phase. Further details on frequency, resolution of seismic data and seismic velocity analysis will be illustrated in detail in Section 1.6.





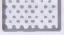


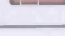
The 2D seismic dataset used in this study (Fig. 1.8) consists of 52 2D multichannel seismic profiles, acquired in 1983, and migrated with a post-stack time migration. These profiles cover approximately 6000 km and present a grid spacing of ca. 10 x 10 km. The profiles trend, respectively, parallel and perpendicular to the Levant continental margin (Fig. 1.8). The 2D seismic data have been mainly used to obtain a semi-regional mapping of the depositional units analysed in this research study. The quality and resolution of individual 2D seismic profiles varies considerably across the area analysed. Generally, those in the northern parts of the continental margin are of poorer quality than those in the central and southern parts, as they were acquired before advances in the fields of data acquisition and processing were made (Frey-Martinez, 2005). Throughout this PhD thesis seismic sections and maps are displayed in milliseconds (ms) two-way travel time (TWTT). Depths and thicknesses are expressed in metres (m) where time-depth conversion was applied.

A set of nine exploration wells (Fig. 1.8) complete the dataset of this study. These wells are: Nir-1, Gaza Marine-1 and 2, Yam West-1 and 2, Or-1, Or South-1, Noa-1 and Noa South-1. Wireline logs and unpublished commercial stratigraphic reports, mainly based on cutting analyses were available for all the wells. The information pertaining to each well consists of petrophysical logs (γ -ray, sonic, velocity, resistivity and checkshots), along with paleontologic and biostratigraphic information. The well data were used for stratigraphic and lithological analysis, for correlation of the depositional units and for time-to-depth conversion.

A summary of the well location in relation to evaporite thickness in the Levant survey is illustrated in Fig. 1.9. In Figure 1.9a, a well-correlation panel summarizing the key lithological and stratigraphic data available on the evaporites has been reconstructed from well reports and completion logs. The data provided by these exploration wells is particularly significant for establishing a lithostratigraphic and chronostratigraphic framework for seismic interpretation.

Fig. 1.9a



<ul style="list-style-type: none"> — Top Messinian (well data) — Horizon M and top Messinian (well data) Horizon M Horizon N — Base Mavqim Fm. 	<p>LITHOLOGY:</p> <ul style="list-style-type: none">  Limestone  Crypto- and microcrystalline anhydrite  Marl/Claystone  Halite (inferred from logs and increase in chloride content of muds)  Sand
<p>DEPOSITIONAL ENVIRONMENTS:</p> <ul style="list-style-type: none">  Brackish  Sabkha  Fluvialite, sabkha and shallow marine 	

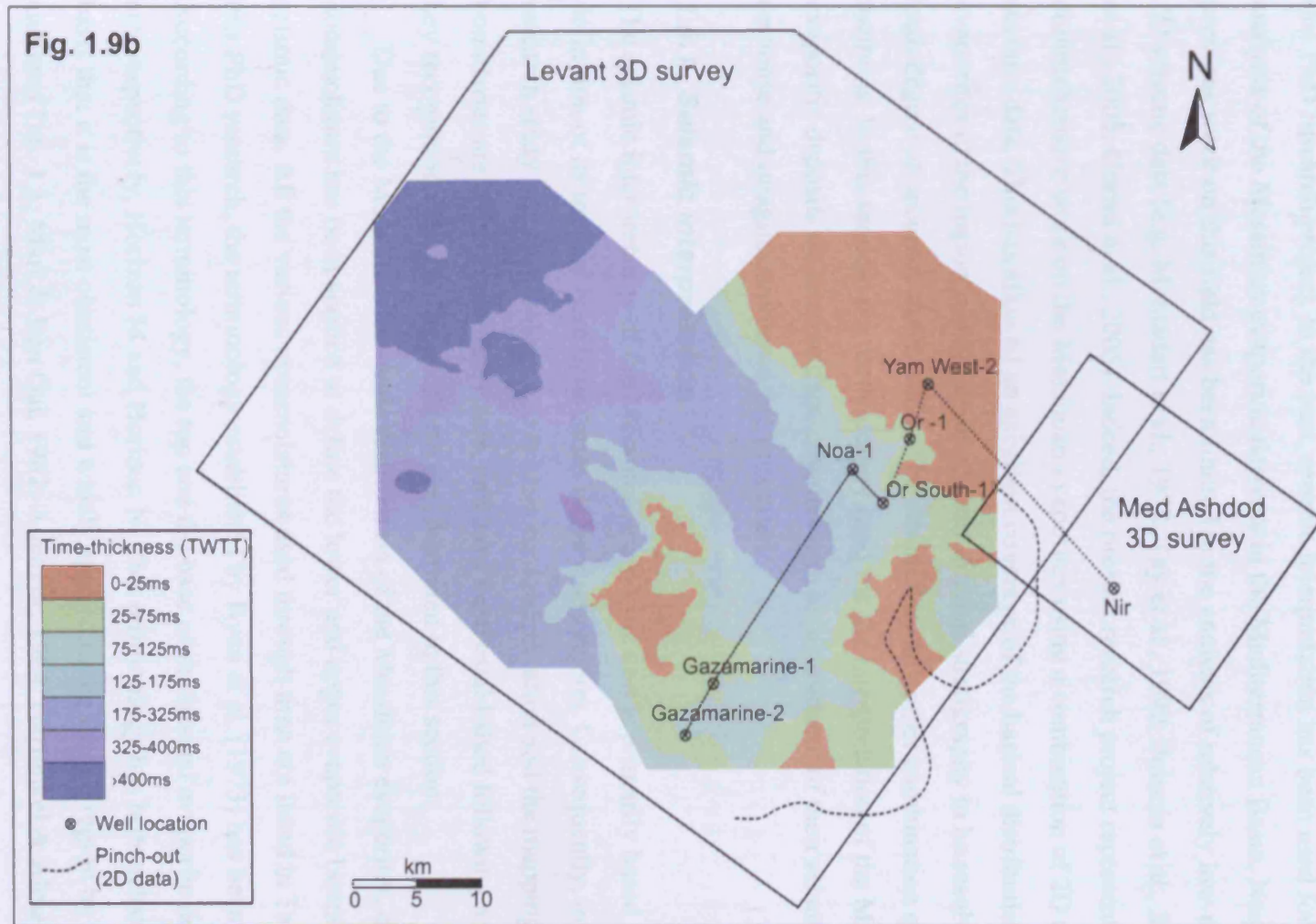


Figure 1.9 Stratigraphy of the Messinian evaporites in the study area.

- a) Well correlation panel (location of wells in Fig. 1.9b). The acronyms of the wells are explained in Fig. 1.9a.
 b) Isochron map of the Messinian evaporitic unit in the Levant 3D survey area. The thickness is expressed in milliseconds TWTT (two-way travel time).

1.6 Geophysical interpretation methods

The interpretation of 2D and 3D seismic data represents the core method used in this PhD research project. In the past, seismic interpretation has been used for the analysis of the Messinian evaporitic deposits in the Mediterranean Basin. Nonetheless, previous work on this field has been limited to the analysis of relatively low-resolution 2D seismic data (e.g. Montadert et al., 1978; Tay et al., 1999; Polonia et al., 2002; Lofi et al., 2005; Gorini et al., 2005). Indeed, the present research project represents the first comprehensive work on the Messinian evaporites using a combination of 2D and 3D seismic data. This has allowed an excellent coverage of the basinal distribution of the evaporites in the region and has enabled their internal stratigraphy to be resolved to a high degree of accuracy that could not be attained by any other combination of methods. In this section, the methodology used for the interpretation of the Messinian evaporitic deposits on seismic data, coupled with an assessment of their seismic response and imaging problems, are presented.

1.6.1 Seismic interpretation

The seismic interpretation of the Messinian evaporitic unit is primarily based on the definition of its top and base boundaries in the study region. Consequently, in this research study, the terminology and criteria for interpretation and the mapping of these boundaries are of particular relevance, and have been established following a series of key recognition criteria. These criteria are illustrated in this section.

Due to the Mediterranean-wide distribution of the Messinian evaporites, different nomenclature has been applied to define the lower and upper evaporitic boundaries on seismic data. All the various nomenclatures used through time are listed in Tab. 1.1. In this PhD research, the terminology established by Ryan et al. (1973) has been adopted. According to this terminology, the top and the base of the basinal evaporite deposits are, respectively, Horizon M and Horizon N. This terminology has been selected on the basis that it is the most consistent and widely applied to the Levant region by previous authors (Tab. 1.1; Mart & Ben Gai, 1982; Almagor, 1984; Garfunkel & Almagor, 1987; Tibor et al., 1992).

Author	Base distal evaporites	Top distal evaporites	Proximal surface
Hsu et al., 1973			M-reflector
Ross & Uchupi, 1977		Horizon M	
Ryan et al., 1971		M-Reflectors	
Ryan et al., 1973	N-Reflectors	M-Reflectors	
Finetti & Morelli, 1973		Horizon A	Horizon A?
Ryan, 1978	Basal discordance	Horizon 'M'	Horizon 'M'
Gvirtzman & Buchbinder, 1978			'M' horizon
Ryan & Cita, 1978	Messinian discordance?	Horizon M	Messinian discordance-Horizon M
Neev, 1979		'M' Reflector	
Barber, 1981			Messinian erosional surface
Mart & Ben Gai, 1982	'N' reflector	'M' reflector	'M' reflector
Almagor, 1984	reflector N	reflector M	
Garfunkel & Almagor, 1985		Horizon M	Reflector M
Garfunkel & Almagor, 1987	N (Ryan et al. 1970, 1973)	M (Ryan et al. 1970, 1973)	
Escutia & Maldonado, 1992	Reflector	Horizon M	Horizon M
Tibor et al., 1992	reflector N	reflector M	
Lofi et al., 2003			MD (Messinian Discordance)
Lofi et al., 2005	?Messinian erosional surface	'M' reflector	Messinian erosional surface

Table 1.1 Different nomenclature applied in the Mediterranean Basin to the lower and upper boundary of the Messinian evaporites and to the marginal (proximal) erosional surface on seismic data. In this PhD research, the terminology established by Ryan et al. (1973) and Ryan (1978) has been adopted.

In the area of study, Horizon M and N represent continuous high-amplitude seismic reflections generated by the high acoustic impedance contrast between the evaporites and their bounding deep-water clastic sediments. Acoustic impedance is defined as the product of the P-wave velocity and the density of a material (Keary et al., 2002). As listed in Tab. 1.2, evaporitic deposits typically have a higher P-wave velocity and density than the enclosing sedimentary series. Consequently, there is a significant increase in acoustic impedance at the interface between the evaporites and the enclosing medias, resulting in a high-amplitude seismic reflection at these interfaces (Badley, 1985). The strength of the reflection generated at the interface can be quantified in terms of the reflection coefficient (R), which is directly proportional to the contrast in acoustic impedance (Z) across the interface (Fig. 1.10a). This coefficient can be positive or negative depending upon whether 'softer' rocks overlie 'harder' rocks, or viceversa (Badley, 1985). These seismic characteristics (i.e. acoustic impedance, reflection coefficient) can be used as criteria for the identification of the top of the Messinian evaporites (Horizon M) in the study area.

In the Levant region, 'soft' clastic deposits of Plio-Pleistocene age overlie the Messinian evaporitic deposits. Consequently, there is a positive acoustic impedance contrast between the Plio-Pleistocene and the Messinian units. Horizon M is characterised by a positive ('hard') seismic event, displayed as a red colour on seismic sections (Fig. 1.10a). The polarity of this reflection is defined by analogy with the phase and polarity of the seabed horizon and with flat spots observed at a comparable stratigraphic level (see e.g. Chapter 5). Based on this primary criterion, mapping of Horizon M in the study area is relatively straightforward in the 2D and 3D datasets. Additionally, stratigraphic markers from well tie provides support the seismic interpretation, as displayed by the well correlation panel in Fig. 1.9a.

The base of the Messinian evaporites, i.e. Horizon N, represents the interface between the evaporites and underlying Oligo-Miocene siliciclastic sediments. This horizon is therefore marked by a distinct decrease in acoustic impedance, and characterised by a negative reflection coefficient (Fig. 1.10a). This horizon is displayed on seismic data as a negative high-amplitude reflection, i.e. a 'soft' seismic event (Fig. 1.10b). The seismic character of this prominent horizon has been used as the main criterion for the identification of the base of the Messinian evaporites in the study area. It should be stressed that none of the available wells drilled the base of the

LITHOLOGY	vp (km/s)	ρ bulk (Mg/m ³)	Z
shale	1.5 - 2.5	2.06 - 2.66	4.2 10 ³
sand	1.5 - 2.0 (water-saturated)		
anhydrite	4.5 - 6.5	2.06 - 2.66 (2.96)	9.9 10 ³
gypsum	2.0 - 3.5	(2.32)	
halite	(3.5) 4.5 - 5.0	2.10 - 2.40 (2.17)	9.9 10 ³
limestone	3 - 4 (bioclastic & oolites) 2 - 2.5 (chalk)	2.60 - 2.80 (2.71)	9.45-10.8 10 ³
dolomite	2.5 - 6.5	2.28 - 2.90 (2.87)	9.9 10 ³
water	1.5		2.25 10 ³

Table 1.2 Summary of the main physical properties of different sediments and of sea-water influencing their seismic response: vp= velocity of compressional waves; ρ bulk= bulk density; Z= acoustic impedance. Data from Rider (1986), Keary et al. (2002) (density and velocity), Nurmi (1988) (density in brackets).

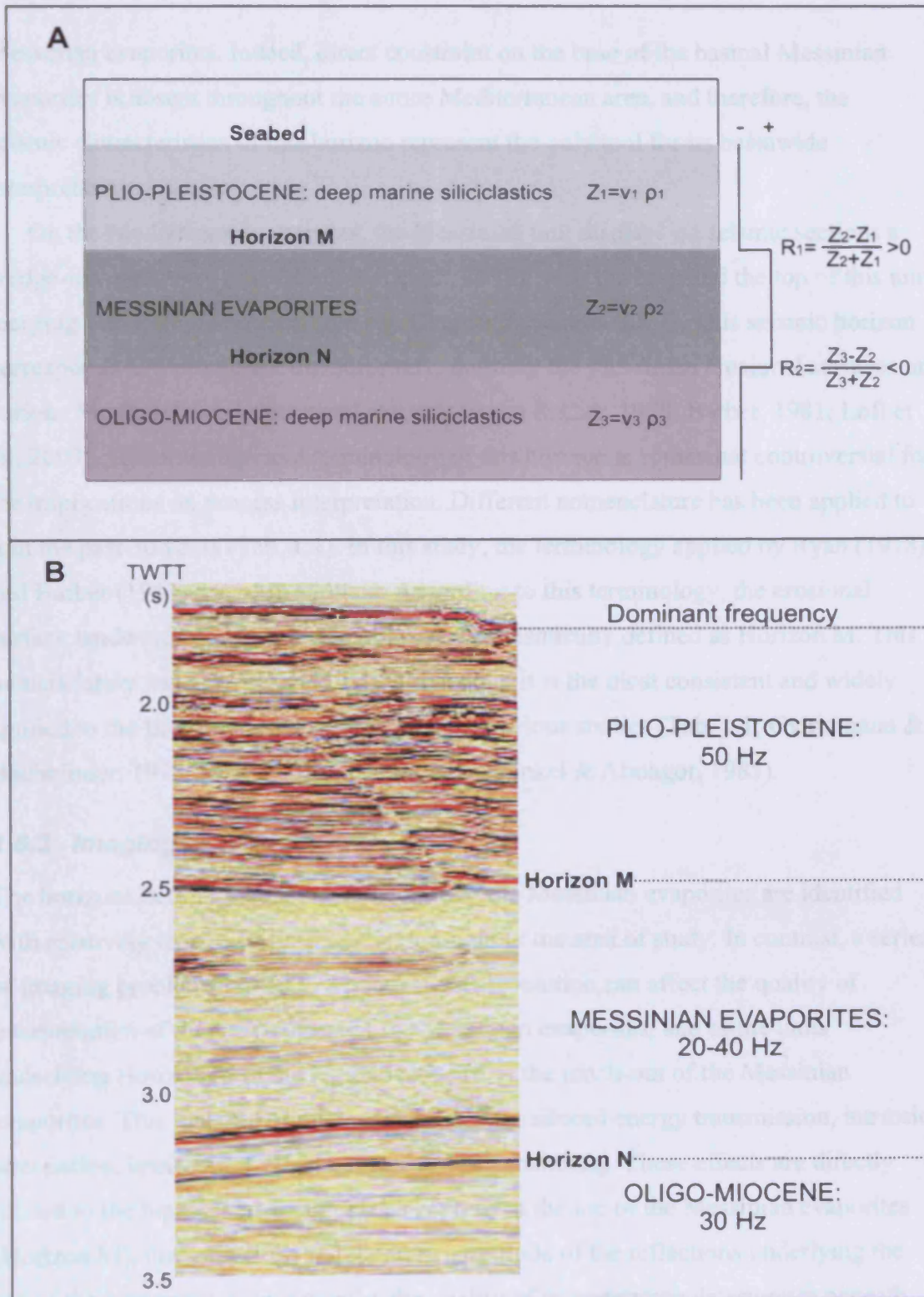


Figure 1.10 Explanation of some key seismic characteristics of the main seismic units and horizons analysed in this research study.

a) Schematic representation of the acoustic impedance (Z) and reflection coefficient (R) of seismic reflections, i.e. the main seismic parameters used for identifying the boundaries of the Messinian evaporitic unit in the study area (Horizons M and N).

b) Dominant seismic frequencies observed within the three main seismic-stratigraphic units analysed in this study, as displayed on a representative seismic section across the 3D seismic dataset.

Messinian evaporites. Indeed, direct constraint on the base of the basinal Messinian evaporites is absent throughout the entire Mediterranean area, and therefore, the seismic characteristics of this horizon represent the only tool for its basinwide interpretation.

On the Mediterranean margins, the Messinian unit displays on seismic sections a wedge-like geometry (e.g. Montadert et al., 1978), with the base and the top of this unit merging into a single horizon (see e.g. Chapter 2, Section 2.5.2). This seismic horizon corresponds to a prominent unconformity, defining the Messinian erosional surfaces on various Mediterranean continental margins (Ryan & Cita, 1978; Barber, 1981; Lofi et al., 2003). The definition and terminology of this horizon is somewhat controversial for the implications on process interpretation. Different nomenclature has been applied to it in the past 30 years (Tab. 1.1). In this study, the terminology applied by Ryan (1978) and Barber (1981) has been adopted. According to this terminology, the erosional surface landward of the evaporite pinch-out is seismically defined as Horizon M. This nomenclature has been selected on the basis that it is the most consistent and widely applied to the Eastern Mediterranean area in previous studies (Tab. 1.1; Gvirtzmann & Buchbinder, 1978; Mart & Ben Gai, 1982; Garfunkel & Almagor, 1985).

1.6.2 Imaging problems

The horizons defining the top and the base of the Messinian evaporites are identified with relatively ease in seismic section throughout the area of study. In contrast, a series of imaging problems linked to a poor seismic resolution can affect the quality of interpretation of the internal part of the Messinian evaporites, and of the units underlying Horizon M in the region landward of the pinch-out of the Messinian evaporites. This imaging problems are related to reduced energy transmission, intrinsic attenuation, interference effects, refraction and scattering. These effects are directly related to the high acoustic impedance contrast at the top of the Messinian evaporites (Horizon M), that causes the reduction in amplitude of the reflections underlying the top of the evaporites. Consequently, the quality of interpretation deteriorates beneath this high-amplitude reflection.

Seismic resolution is generally significantly lower in the Messinian evaporitic unit than in the bounding siliciclastic deposits. The resolving power of seismic data is generally measured in terms of the seismic wavelength, which is given by the quotient

of velocity and frequency (Brown, 1999). Seismic velocity increases with depth because the rocks are older and more compacted. The predominant frequency decreases with depth because the higher frequencies in the seismic signal are more quickly attenuated (Brown, 1999). As a result, the wavelength decreases significantly with depth, making resolution poorer (Brown, 1999).

In the case of the 3D seismic surveys analysed in this research study, the frequency is approximately 50 Hz in the Pliocene to recent section (Fig. 1.10b). The vertical resolution within a particular seismic interval is based on the limit of separability of the wavelets from adjacent reflecting interfaces, and equals to one-quarter of the wavelength (Brown, 1999). The vertical resolution for the Pliocene interval is estimated to be 10 m, using an average velocity value of 2000 m/s (TWTT), as derived from checkshot of the Gaza Marine-1 exploration well. For this well, a maximum error of 7-12% is estimated for the time-to-depth conversions (Frey-Martinez et al., in press).

Because the evaporites have higher interval velocities than the bounding sediments, it can be expected that the vertical resolution within this lithological unit would be poorer than an equivalent deep-marine clastic section. Within the Messinian evaporitic unit, the vertical resolution can change significantly due to the high variability in the frequency content (Fig. 1.10b) and in the seismic velocity. The dominant frequency of the evaporitic unit has been estimated on a series of seismic sections using the IESX interpretation software for well synthetics, and it is on average 30 Hz (Fig. 1.10b).

The estimation of the seismic velocity within the evaporitic unit is more complex, and it has been based on the integrated analysis of checkshots and sonic logs in the wells Gaza Marine-1 and 2, Or-1 and Or-South-1 and on the comparison with data from previous studies (e.g. Garfunkel & Almagor, 1987; Polonia et al., 2002). Seismic velocity within the Messinian evaporites is highly variable due to lithological differences, and a dominant velocity of $4000 \text{ m/s} \pm 500 \text{ m/s}$ is the estimated average value. Therefore, the resulting minimum vertical resolution in the evaporitic unit is ranging between 22.5 m and 50 m.

The interpretation of the intra or sub-evaporite section can be additionally affected by the presence of multiple reflections of Horizon M, like e.g. simple and peg-leg multiples (Badley, 1985). Simple multiples from the seafloor and other sedimentary strata are easily identified as they are often parallel to each other at a predictable TWTT separation, and they tend to cross-cut stratigraphy. Examples of simple multiples of

Horizon M are clearly displayed in Figs. 1.11a and b. Peg-leg multiples of Horizon M are recognised by the presence of highly repetitive forms that mimic this horizon, and can interfere to create zones of incoherent noise. This type of multiple is observed particularly in the 2D seismic dataset (Fig. 1.11a). The comparison of overlapping 2D and 3D seismic data can often be used to aid interpretation and distinguish multiple from real stratigraphic horizons (Fig. 1.11c).

Over-migration can affect seismic interpretation, due to the inaccurate derivation of migration velocities in a particular dataset. Indeed, the seismic data used during this research project were processed and migrated to obtain the best imaging for the post-Messinian interval. This was due to the fact that the main exploration targets are located within the Pliocene section. Over-migration produces a 'smile' effect where the diffraction from the sharp edge of a flat horizon is pulled up (Badley, 1985). In the 3D seismic dataset, this 'smile' effect is particularly evident near faults displacing the top of the evaporites (Fig. 1.11d).

The scale of the geological processes addressed in the present research study is mainly dependent on the available resolution of the seismic data. As previously discussed, the maximum resolution provided by 3D seismic is in the order of a few tens of metres. This, compared to the centimetre-scale resolution achieved by previous outcrop and well-based analysis, is obviously limited in detail. However, the remarkable areal coverage and 3D spatial resolution of the seismic data permit to define both the full extent and the morphology (external and internal) of the evaporitic deposits. This allows a better understanding of their basinal distribution, internal configuration and evolution through time in those parts of the continental margin and basin that were previously excluded by outcrop and well-based analyses. This is schematically illustrated in Fig. 1.12. The combination of the results presented in this study with those of previous works (e.g. Druckman et al., 1995; Buchbinder et al., 1997) thus allows an integrated understanding of the geological processes governing the deposition of the Messinian evaporites on both a local and a regional scale.

1.7 Thesis layout

The main part of this thesis is subdivided into four submitted papers (Chapters 2, 3, 4 and 5) addressing the most important topics analysed during this research project. The

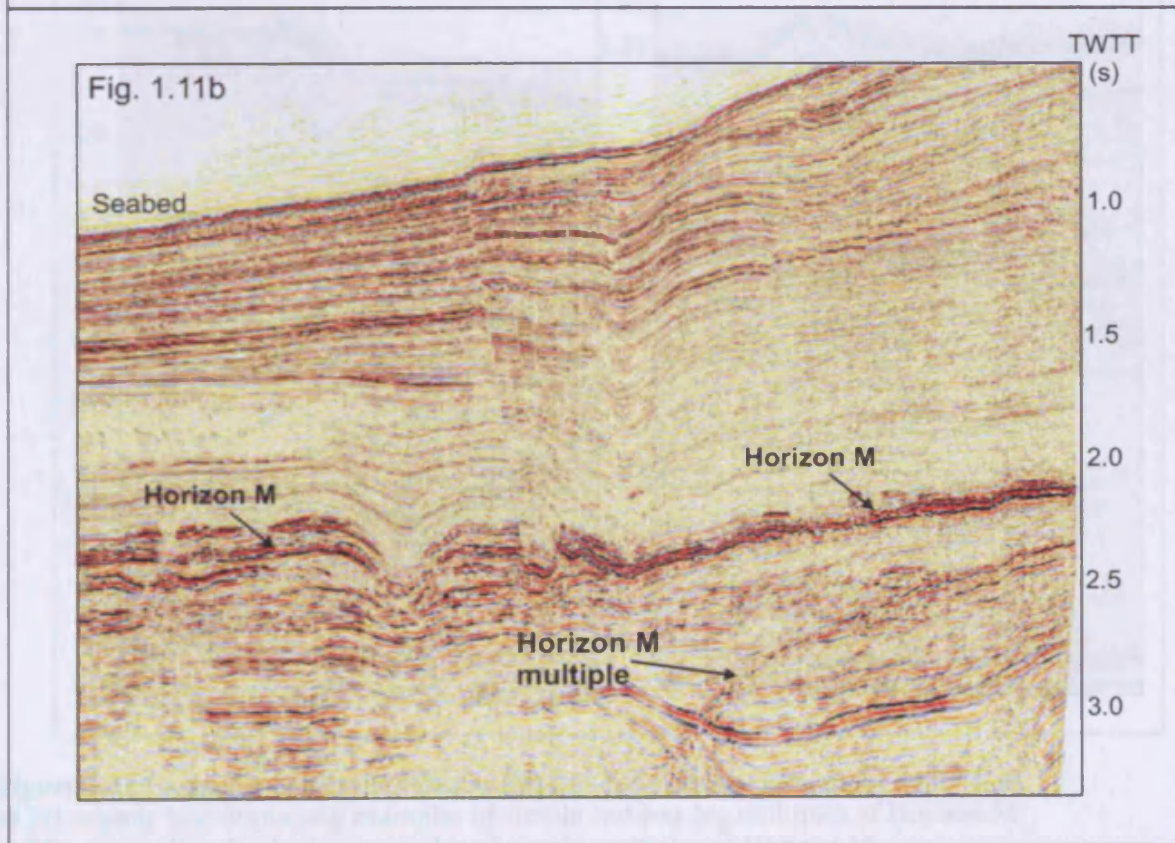
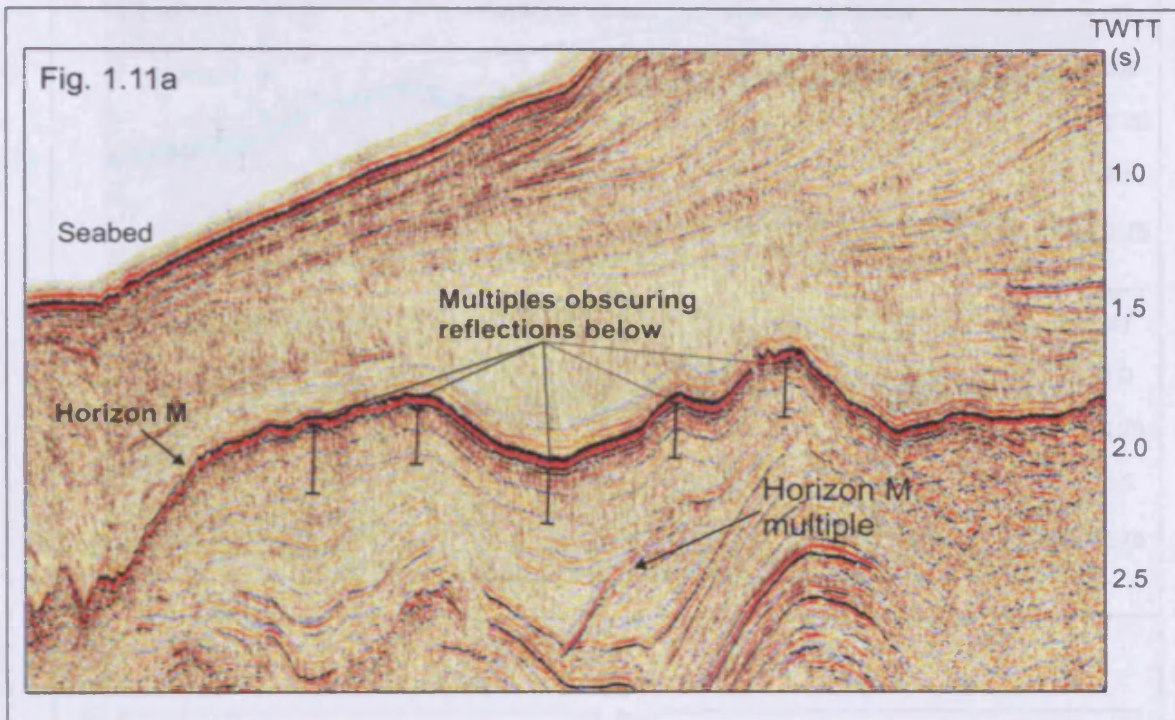


Fig. 1.11a and Fig. 1.11b are interpreted seismic sections showing how the acquisition of overlapping 2D and 3D seismic data (Fig. 1.11a) can be used to aid interpretation and distinguish multiple from real stratigraphic features. Fig. 1.11b and 3D seismic lines (not shown) are examples of 'wide' offset nearby faults displacing the top of the sequence.

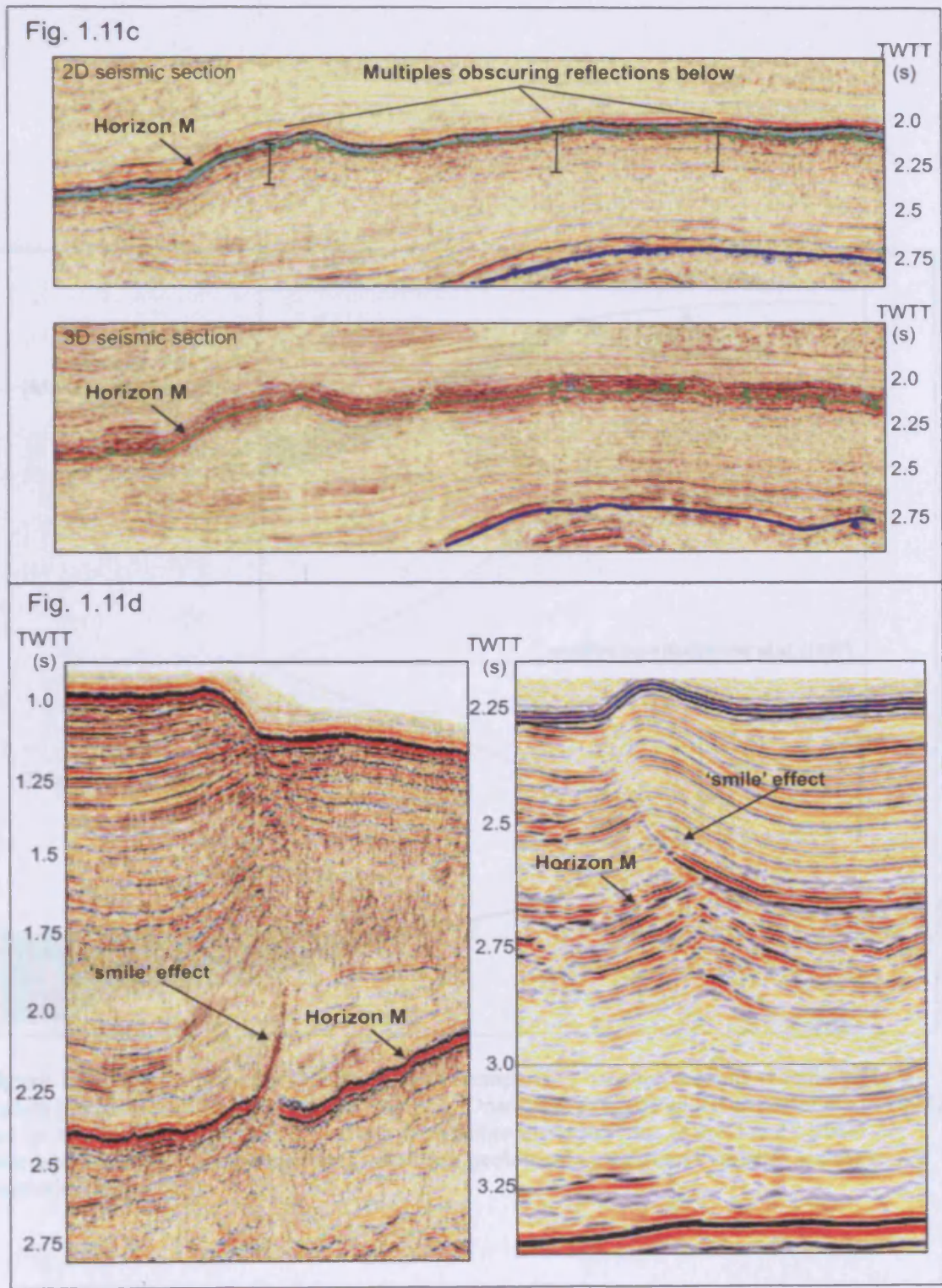


Figure 1.11 Examples of seismic effects affecting data interpretation in the study area.
 a) 2D seismic line displaying examples of simple and peg-leg multiples of Horizon M.
 b) 3D seismic line displaying examples of simple multiples of Horizon M.
 c) Interpreted seismic sections showing how the comparison of overlapping 2D and 3D seismic data can often be used to aid interpretation and distinguish multiple from real stratigraphic horizons.
 d) 2D and 3D seismic lines displaying examples of 'smile' effect nearby faults displacing the top of the evaporites.

last two chapters (Chapters 6 and 7) details and concludes, respectively, the main scientific results of this investigation.

Chapter 2 is a study of the factors controlling the lateral distribution of the Messinian evaporites in the Levant region. In this chapter, the combination of 2D and 3D seismic data is used to produce a cross-section, each of the synorogenic

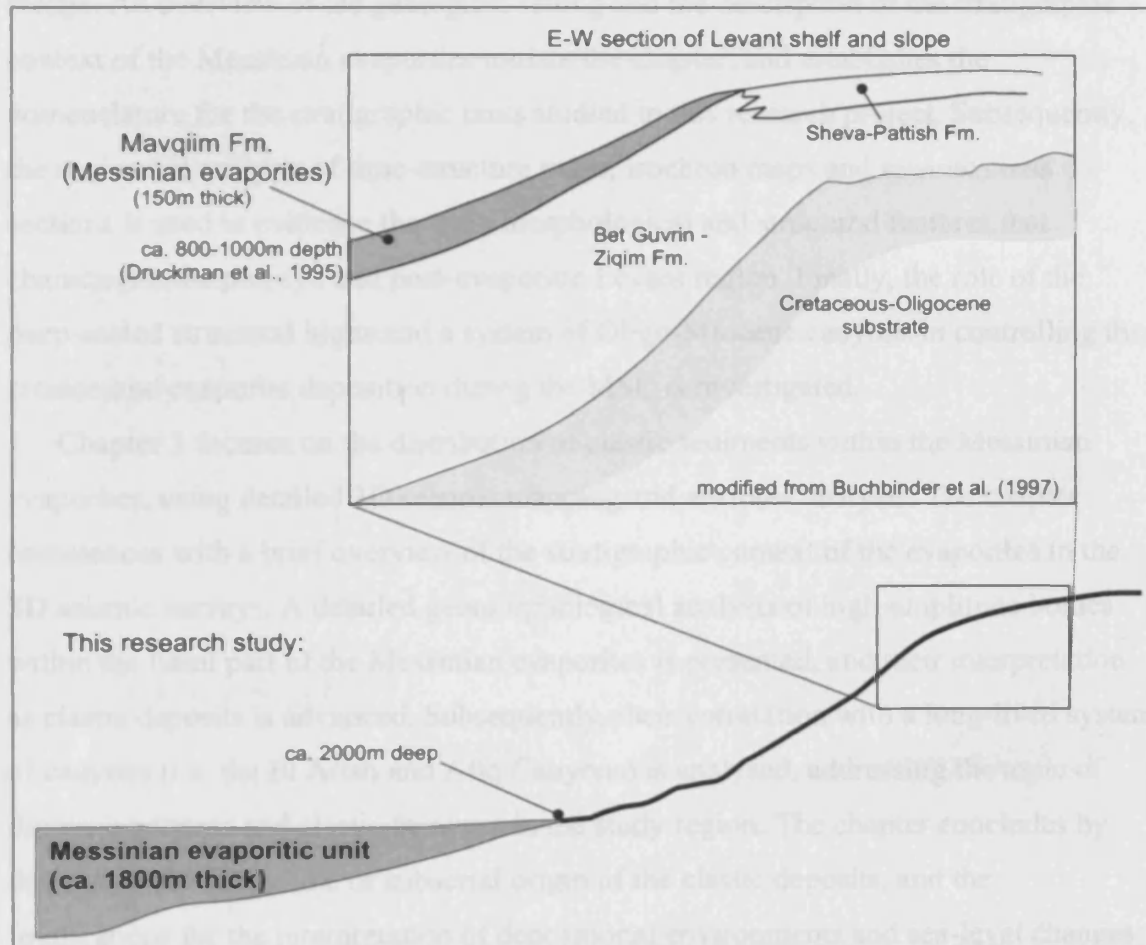


Figure 1.12 Schematic diagram illustrating the comparison between resolution achieved in studies based on well and outcrop analysis (e.g. Druckman et al., 1995; Buchbinder et al., 1997) and on seismic data (this study). The two approaches differ in terms of areal and vertical coverage of the Messinian evaporites, resolving geological processes of variable scales (see discussion in the text).

processes going along the NW margin of the MSC. A description of the regional stratigraphic context of the top of the Messinian evaporites is provided. This led to mapping of the pre-evaporitic tectonics in cross-section, in order to explore their relationship to Horst 04, and to produce a structural analysis of these horizons. This permits the description of an early phase of Messinian syn-depositional fault reactivation, and the identification of a regional erosional unconformity at the top of the Messinian evaporites. This chapter concludes with the discussion of the submarine

last two chapters (Chapters 6 and 7) discuss and conclude, respectively, the main scientific results of this investigation.

Chapter 2 is a study of the factors controlling the basinal architecture of the Messinian evaporitic unit in the Levant region. In this chapter, the combination of 2D and 3D seismic data is used to produce a semi-regional analysis of the evaporitic wedge. An overview of the geological setting and the description of the stratigraphic context of the Messinian evaporites initiate the chapter, and establishes the nomenclature for the stratigraphic units studied in this research project. Subsequently, the sequential analysis of time-structure maps, isochron maps and seismic cross sections is used to evidence the main morphological and structural features that characterise the pre, syn and post-evaporitic Levant region. Finally, the role of the deep-seated structural highs and a system of Oligo-Miocene canyons in controlling the erosion and evaporite deposition during the MSC is investigated.

Chapter 3 focuses on the distribution of clastic sediments within the Messinian evaporites, using detailed 3D seismic mapping and attribute analysis. The chapter commences with a brief overview of the stratigraphic context of the evaporites in the 3D seismic surveys. A detailed geomorphological analysis of high-amplitude bodies within the basal part of the Messinian evaporites is presented, and their interpretation as clastic deposits is advanced. Subsequently, their correlation with a long-lived system of canyons (i.e. the El Arish and Afq Canyons) is analysed, addressing the topic of drainage patterns and clastic fairways in the study region. The chapter concludes by discussing the submarine or subaerial origin of the clastic deposits, and the implications for the interpretation of depositional environments and sea-level changes during the MSC.

Chapter 4 addresses the origin of the surface defining the top of the Messinian evaporites (Horizon M), and discusses its significance for the understanding of the processes acting during the last stages of the MSC. A description of the seismic stratigraphic context of the top of the Messinian evaporites is produced. Detailed mapping of the intra-evaporitic horizons is consequently undertaken, in order to analyse their relationship to Horizon M, and to produce a structural analysis of these horizons. This permits the description of an early phase of Messinian syn-depositional salt tectonics, and the identification of a regional erosional unconformity at the top of the Messinian evaporites. This chapter concludes with the discussion of the submarine

or subaerial context of this erosional surface, and of the possible mechanism of intra-evaporite deformation during the last stages of the MSC.

Chapter 5 is a study of evaporite dissolution in the Levant region. Detailed analysis of 3D seismic data is here used to describe a series of km-scale circular collapse structures rooted at the top of the Messinian evaporites. The focus is on the description of the associated deformation of the evaporites and of the overburden to these structures. A structural analysis of the overburden is used to date the dissolution event and to estimate its duration. The chapter concludes by analysing the possible mechanism of evaporite dissolution and proposing a model for the formation of the collapse structures, based on the interaction between the evaporites and deep vertical fluid flow at the Levant continental margin.

Chapter 6 draws together the key scientific results of the research, comparing the observations and deductions from Chapters 2 to 5 with previous studies in the Levant and Mediterranean region. During this discussion, the evolutionary model for the deposition of the Messinian evaporites in the Levant region will be proposed. A review of the possible worldwide analogues for the deposits studied in this thesis is also undertaken, demonstrating the global implications and applicability of the results obtained. A brief synopsis of the limitations and uncertainties associated with this study and proposals for future work concludes the chapter.

Finally, Chapter 7 summarizes the main conclusions of this research.

Chapter Two: Controls on the architecture of the Messinian evaporites¹

2.1 Abstract

Interpretation of 2D and 3D seismic data from the Levant margin (Eastern Mediterranean) has revealed the complex depositional and structural setting of the basinwide late Miocene (Messinian) evaporites. The dataset covers a total area of 20,000 km², permitting a semi-regional investigation of the thick (up to 1.8km) evaporitic wedge. The sequential analysis of time-structure maps, isochron maps and seismic cross sections highlighted the main morphological and structural features characterizing the pre-, syn- and post-evaporitic Levant margin. This approach allowed for the recognition of the factors controlling evaporite distribution, and provided insights on the impact of local vs. regional factors in governing the events linked to the Messinian Salinity Crisis in the region.

Two regional features have been recognized as the most significant controlling factors for the architecture of the Messinian evaporites. Firstly, a series of anticlines of the Syrian Arc foldbelt acted as a structural barrier indirectly governing the overall landward extension of the evaporites. Secondly, submarine canyons active in the area at least since the Oligocene (Afiq, El Arish and Ashdod Canyons) represented preferential sites of erosion and deposition of evaporites. Our results document therefore the importance of the deep-seated structures and relict drainage for the architecture of the Messinian evaporites on the Levant margin. The new insights provided can be additionally used to infer the original depositional geometry of the evaporites in the study area and as an analogue in other Mediterranean areas where 3D seismic is not available yet and sub-salt imaging is limited.

¹ *Published as:*

C. Bertoni & J. A. Cartwright, Controls on the basinwide architecture of late Miocene (Messinian) evaporites on the Levant margin (Eastern Mediterranean). Sedimentary Geology, in press.

2.2 Introduction

Understanding the controls on the architecture of the late Miocene (Messinian) evaporites in the Mediterranean basin is fundamental for developing a depositional model for this giant saline system. The Messinian evaporites are analogous in many respects to other extensively studied evaporitic systems worldwide, e.g. the Zechstein Basin (Upper Permian) of the North Sea and Gulf Coast Basin (Callovian) of Gulf of Mexico (see Warren, 1999 for synthesis). The interest in these salt-bearing basins has been traditionally related to their applications to hydrocarbon exploration (Taylor, 1998). Even though their structural setting is now well understood, the depositional context of giant evaporitic systems and in particular, of the Messinian evaporites, remains highly controversial (Kendall & Harwood, 1996; Warren, 1999; Hardie & Lowenstein, 2004).

The Messinian evaporites represent an unusual case amongst saline giants, as their deposition took place in a variety of tectonic settings but during the same, very short time interval. Previous regional studies based on outcrop, well and 2D seismic data have demonstrated that the Messinian evaporites were deposited in settings ranging from passive margins (Montadert et al., 1978) to foredeep systems (Roveri et al., 2001). Therefore their stratigraphic architecture is particularly complex, as it depends upon a number of different geological factors. The evaporites cropping out in the Mediterranean marginal basins have been extensively studied in the field and are well documented (see e.g. Schreiber et al., 1976; Rouchy, 1982; Butler et al., 1995; Clauzon et al., 1996; Riding et al., 1998; Krijgsman et al., 1999). Conversely, the knowledge of the correlative multi-kilometer thick offshore evaporites has so far been hampered by the paucity of coverage and resolution of 2D seismic data.

The Messinian evaporites in the Nile Cone and Levant areas (Fig. 2.1) have been the subject of a number of previous studies focused on the post-evaporitic structural deformation (Garfunkel & Almagor, 1987; Abdel Aal et al., 2000; Loncke, 2002). Other investigations in the area have dealt with the morphological and structural features influencing the depositional context of the evaporites (Mart, 1982; Garfunkel & Almagor, 1987; Druckman et al., 1995; Buchbinder and Zilberman, 1997). Nevertheless, the precise manner by which these features interacted to control the original thickness and facies distribution of the Messinian evaporites has not yet been

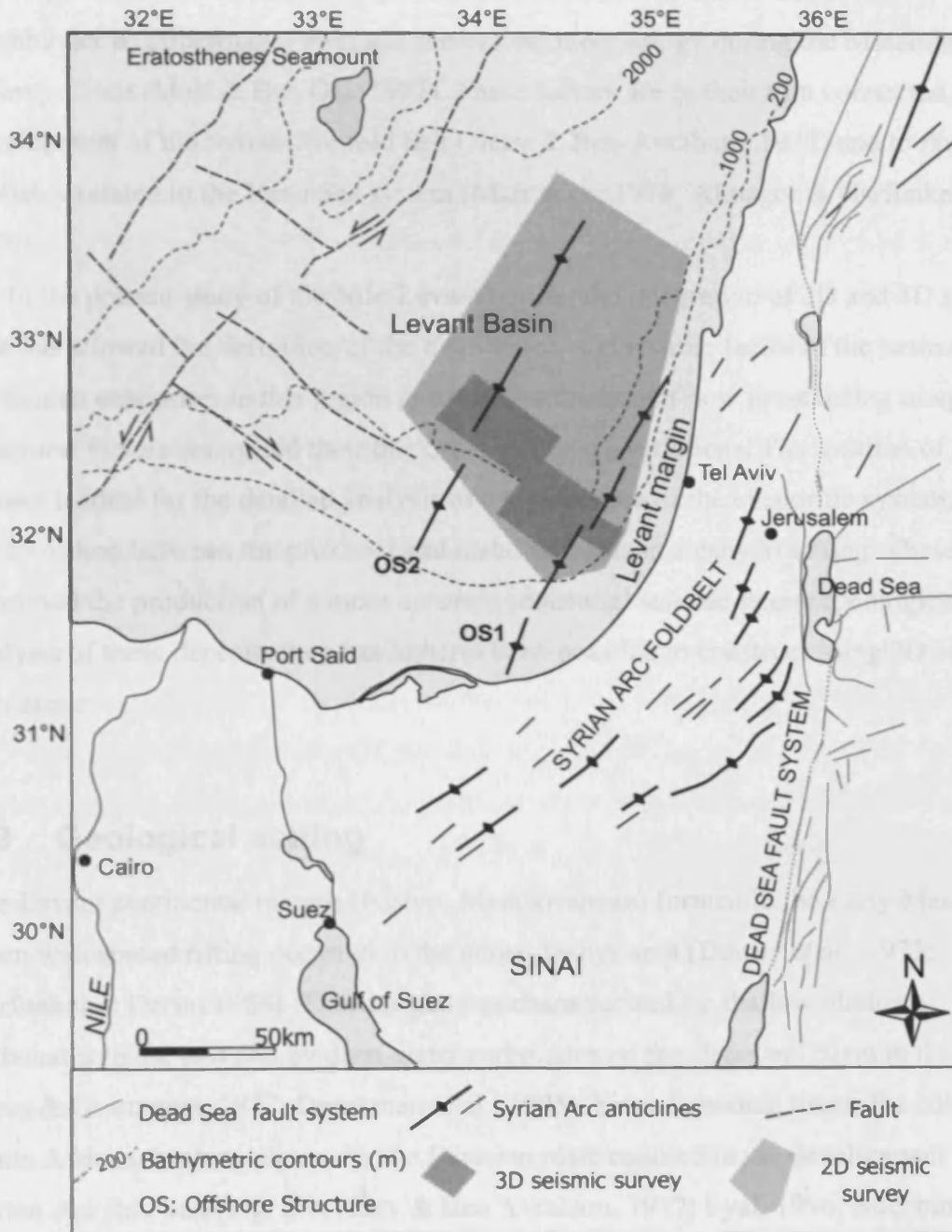


Figure 2.1 Location map of the study area showing the main structural elements in the Levant-Nile region (after Neev & Ben-Avraham, 1977; Bartov, 1990; Abdel Aal et al., 2000) and the location of the 2D and 3D seismic surveys.

clarified. In the study area, a series of possible interconnected factors controlling the distribution of the evaporites are identified. These factors are primarily represented by the Oligo-Miocene submarine canyons (Neev, 1979; Druckman et al., 1995; Buchbinder & Zilberman, 1997) and the basinal morphology during the Messinian Salinity Crisis (Mart & Ben Gai, 1982). These factors are in their turn connected to the development of the Syrian Arc fold belt (Neev & Ben-Avraham, 1977) and to faults probably related to the Dead Sea system (Mart et al., 1978; Almagor & Garfunkel, 1979).

In the present study of the Nile-Levant region, the integration of 2D and 3D seismic data has allowed the definition of the distribution and seismic facies of the basinwide Messinian evaporites in this region and the examination of how pre-existing morpho-structural factors controlled their thickness and facies variations. The location of the dataset is ideal for the detailed analysis of a critical area of the evaporitic system, i.e. the transition between the proximal and distal domains in a canyon setting. These data permitted the production of a more accurate sequential seismic-geomorphological analysis of these deposits than has hitherto been possible to construct using 2D seismic data alone.

2.3 Geological setting

The Levant continental margin (Eastern Mediterranean) formed in the Early Mesozoic, when widespread rifting occurred in the entire Tethys area (Dewey et al., 1973; Garfunkel & Derin, 1984). This margin was characterized by shallow platform carbonates in the east and by deep-water carbonates on the slope and basin in the west (Bein & Gvirtzman, 1977; Druckman et al., 1995). Since Senonian times, the collision of the African-Arabian plate with the Eurasian plate resulted in the development of the Syrian Arc fold belt (Fig. 2.1; Neev & Ben Avraham, 1977; Eyal, 1996; Buchbinder & Zilberman, 1997; Garfunkel, 1998). The Syrian Arc folding continued at least until the end of the early Miocene (Tibor et al., 1992; Druckman et al., 1995; Eyal, 1996). In the slope area, the Senonian to Eocene represented a period of non-deposition and erosion, and submarine canyons developed after the Oligocene, namely the Afiq (Beer-Sheva), El Arish and Ashdod (Palmahim) Canyons (Druckman et al., 1995; Buchbinder & Zilberman, 1997). During the early Miocene the Syrian Arc began to emerge on the

Levant margin (Buchbinder & Zilberman, 1997). The shelf area underwent localized tectonic uplift and became intermittently emergent (Buchbinder & Zilberman, 1997). As a result, the entire basin experienced an increase in clastic sediment supply (Druckman et al., 1995) and the submarine canyons were extended to the shelf area through headward erosion (Buchbinder & Zilberman, 1997).

At the end of the Miocene, the reduced connection of the Mediterranean basin from the world oceans led to the onset of the Messinian Salinity Crisis (MSC) (Hsü et al., 1978). At this time, the Levant continental margin underwent extensive erosion and evaporite deposition (Gvirtzman & Buchbinder, 1978; Druckman et al., 1995), a pattern common to most of the Mediterranean basin (Hsü et al., 1978). Thick evaporites (up to > 2 km) were deposited on the seafloor, while the continental margin was affected by erosion producing deeply incised valleys (Cita & Ryan, 1978; Garfunkel & Almagor, 1987). The Messinian evaporites do not crop out onland and have been studied solely on 2D seismic data on the continental slope and basin (e.g. Mart & Ben Gai, 1982; Garfunkel & Almagor, 1987), and in boreholes in the coastal plain and continental shelf area (e.g. Cohen, 1988; 1993; Druckman et al., 1995).

Since the beginning of the Pliocene, the end of the MSC led to the re-establishment of normal marine conditions in the Mediterranean basin (Hsü et al., 1978). In the Levant region, a thick progradational-aggradational wedge of mainly Nile-derived siliciclastic sediments was deposited on the margin and in the basin (Tibor & Ben-Avraham, 1992; Druckman et al., 1995). The submarine canyons ceased their activity in the Pliocene and are now infilled and buried (Druckman et al., 1995; Buchbinder & Zilberman, 1997). The Pliocene to Recent sediments in large areas of the Levant margin and adjacent basin are affected by thin-skinned deformation, due to salt mobilization and shelf loading that caused the collapse and landward tilt of these deposits above the Messinian evaporites (Tibor & Ben-Avraham, 1992).

2.4 Methodology

The 2D seismic dataset used in this study (Fig. 2.1) consists of 52 2D multichannel seismic profiles acquired in 1983, covering ca. 6,200 km. The seismic profiles are spaced approximately 10 by 10 km and trend parallel and perpendicular to the Levant margin. These data have been used for a semi-regional mapping of the depositional

units analysed herein. The 3D seismic coverage (Fig. 2.1) is represented by three seismic surveys acquired in 2000. The dataset was migrated with a single pass 3D post-stack time migration generating a seismic grid with grid cells of 12.5 by 12.5 m, with a sampling interval of 4 ms. Seismic data are SEG normal polarity, i.e. an increase in impedance is a positive amplitude (red colour in the original seismic sections). The data is processed to near zero phase.

The stratigraphic interval of study represents the upper 2.5-3.5 s of the seismic data. The dominant frequency content of the data varies with depth but it is approximately 50 Hz in the uppermost 2.5 seconds. The vertical and lateral resolution for this interval is estimated to be respectively 10 m and 40 m, using an average velocity value of 2000 m/s, which is derived from velocity checkshot data in the available wells. Velocity of seismic waves within the Messinian evaporites is highly variable due to lithological differences, therefore an average velocity value of 4000 m/s \pm 500 m/s has been calculated here, based on well checkshot and petrophysical data. The dominant frequency in the Messinian evaporites is 30 Hz, giving a minimum resolution of 50 m and maximum resolution of 22.5 m. Wireline logs along with unpublished commercial stratigraphic reports for a set of exploration wells (Fig. 2.1) have been used for stratigraphic and lithological analysis, correlation of the depositional units and time to depth conversion. Throughout this paper seismic sections and maps are displayed in milliseconds (ms) two-way travel time (TWT). Depths and thicknesses are expressed in metres (m) where time-depth conversion was possible.

2.5 Seismic stratigraphy

The seismic-stratigraphic context of the study area on the Levant margin has been divided into three informal seismic-stratigraphic units: Unit 1, Unit 2 and Unit 3 which have been defined on the basis of their seismic character and well calibration (Bertoni & Cartwright, 2005). Three seismic profiles (Figs. 2.2-2.4) oriented perpendicular and parallel to the continental margin in its proximal and distal parts illustrate the geometry of the seismic-stratigraphic units.

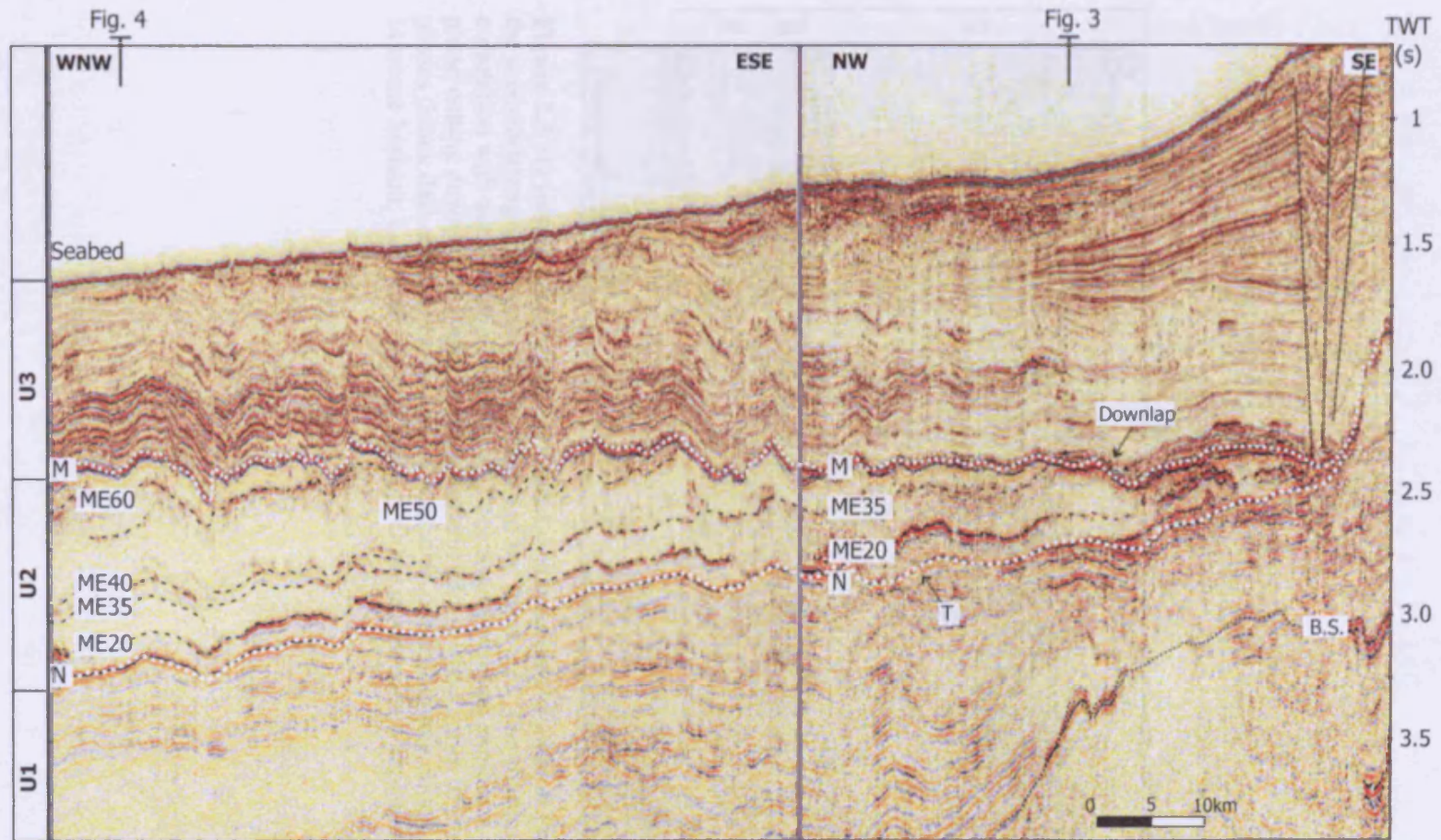


Figure 2.2 Composite 3D seismic section perpendicular to the Levant margin (location in Fig. 2.5b), showing the general seismic-stratigraphic context of the study area. On the vertical scale, TWT is two-way travel time expressed in seconds. T: localized truncation at the top of Unit 2 against Horizon N. B.S.: Base Senonian horizon. M: Horizon M. N: Horizon N. The deformation of the Base Senonian horizon and overlying reflections in Unit 1 is linked to the compressional structures of the Syrian arc foldbelt. Unit 2 is internally composed of an alternation of discernible seismic reflections (Horizons ME20-ME60) and transparent seismic facies. In the southeastern part of the section, Unit 3 is crossed by extensional faults (black dashed lines) detaching at the top of Unit 2.

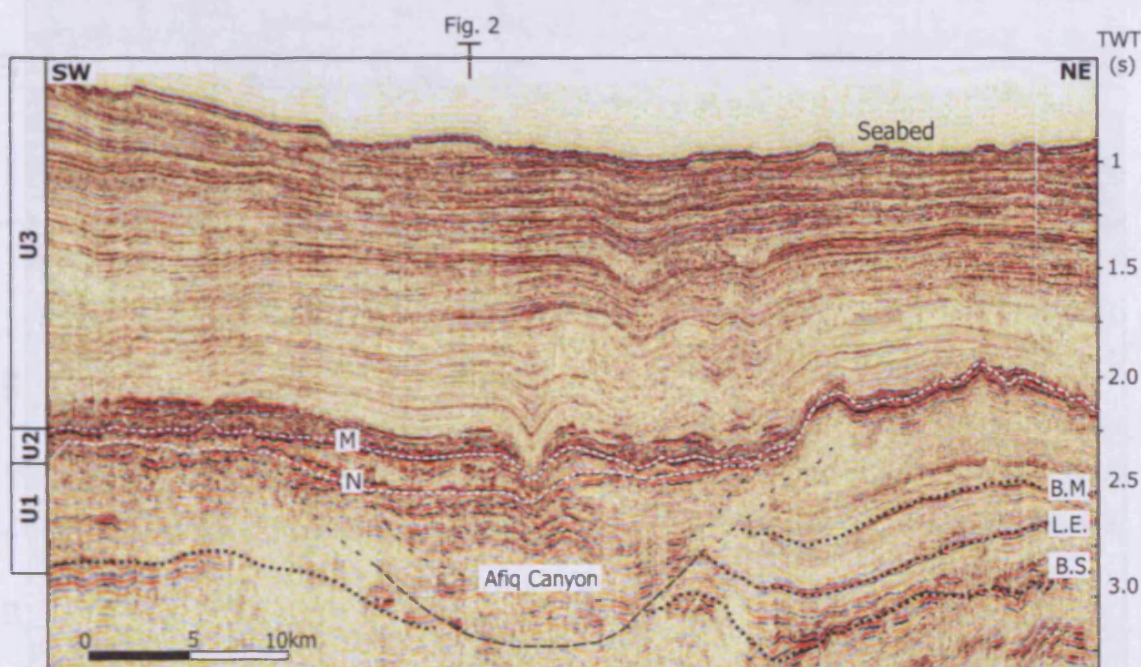


Figure 2.3 3D seismic section parallel to the Levant margin (location in Fig. 2.5b), showing the seismic-stratigraphy of the proximal part of the study area. The stratigraphy is defined by correlation with nearby wells. The Oligo-Miocene Afiq Canyon exhibits a major incisional phase cutting down to the Base Senonian horizon (B.S.), and a series of minor incisional phases (black dashed lines) evidenced by truncation of seismic reflections. B.M.: Base Miocene horizon; L.E.: Late Eocene horizon. Other acronyms are explained in Fig. 2.2.

2.5.3 Unit 3 (Late Greifengasse – late Miocene)

Unit 3 includes mainly deep-sea clastic sediments deposited from the East

Cenozoic is the high Miocene (Figs. 2.2 and 2.3), unpublished well reports. The base

of the unit, i.e. the base Seiridun terrace, and the overlying interval

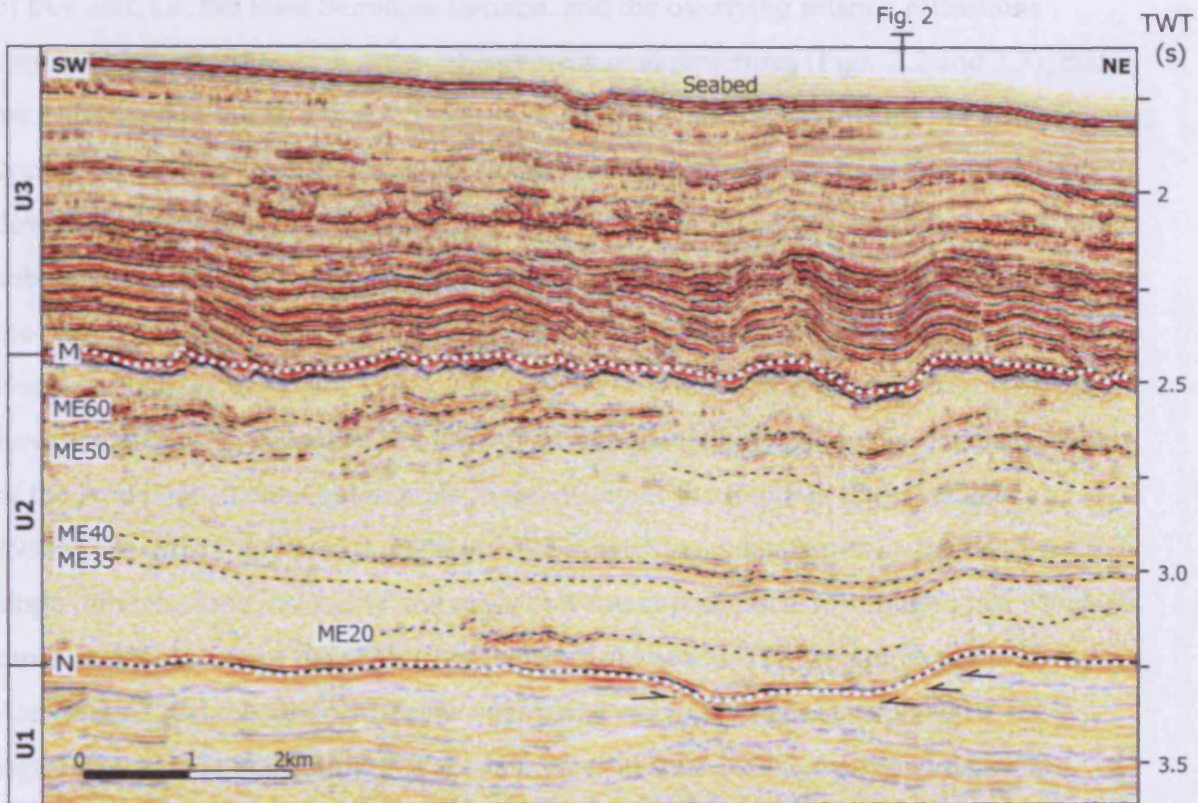


Figure 2.4 3D seismic section parallel to the Levant margin, showing the seismic-stratigraphic context of the distal part of the study area (location in Fig. 2.5b). The localized erosional truncation of the reflections at the top of Unit 1 against Horizon N is highlighted by arrows. The other acronyms are explained in Fig. 2.2.

Unit 2 represents the locus of frontal, seismic data collected with well data permit the correlation of this unit with the Mediterranean with Miocene evaporites and with the Messinian. Furthermore the Israeli published (Cohen, 1977) unpublished well reports). The base and top of Unit 2 (Figs. 2.2–2.4) are respectively identified as Horizons N and M, two regional seismic events traditionally defining the boundaries of the Messinian evaporites in the Mediterranean Basin (Ryan et al., 1973). In the study area, Horizons N and M are continuous and high amplitude seismic reflections generated by the high acoustic impedance contrast between the evaporites and their bounding deep-water clastic sediments. The time-slice map of Horizon N obtained on the 2D seismic dataset is displayed in Fig. 2.5a. The contour lines define a surface

2.5.1 Unit 1 (Late Cretaceous – late Miocene)

Unit 1 includes mainly deep-water clastic sediments deposited from the Late Cretaceous to the late Miocene (Figs. 2.2 and 2.3; unpublished well reports). The base of this unit, i.e. the Base Senonian horizon, and the overlying seismic reflections appear to be deformed by a series of compressional structures (Figs. 2.2 and 2.3), that are correlated to the Syrian Arc foldbelt (Fig.1; Neev & Ben Avraham, 1977). The upper part of Unit 1 is characterised by a series of prominent incisional features that cut down into the Cretaceous deposits (Fig. 2.3). These incisions are related to a system of submarine canyons (namely, the El Arish, Afiq and Ashdod Canyons) developed on the Levant margin since the Oligocene (Neev, 1960; Druckman et al., 1995; Buchbinder & Zilbermann, 1997). The Oligocene phase of submarine erosion on the Levant margin was linked to an increase in sediment supply caused by the emergence of the Arabian-African Craton prior to the rifting of the Red Sea (Druckman et al., 1995). The Afiq Canyon is thought to have initiated and developed on the continental slope through slope instability and mass movement processes, resulting in late Miocene times in the capture of the shelf (Druckman et al., 1995). The structures of the Syrian Arc foldbelt and the Oligo-Miocene submarine canyons might have played a significant role in controlling the accommodation space of the overlying deposits therefore they will be analysed in detail with respect to the distribution of the Messinian evaporites.

2.5.2 Unit 2 (Messinian evaporites)

Unit 2 represents the focus of this study. Seismic data calibrated with well data permit the correlation of this unit with the Mediterranean-wide Messinian evaporites and with the Mavqiiim Formation on the Israeli mainland (Cohen, 1988; unpublished well reports). The base and top of Unit 2 (Figs. 2.2-2.4) are correlatable respectively to Horizons N and M, two regional seismic events traditionally defining the boundaries of the Messinian evaporites in the Mediterranean basin (Ryan et al., 1973). In the study area, Horizons N and M are continuous and high amplitude seismic reflections generated by the high acoustic impedance contrast between the evaporites and their bounding deep-water clastic sediments. The time-structure map of Horizon N obtained on the 2D seismic dataset is displayed in Fig. 2.5a. The contour lines define a surface

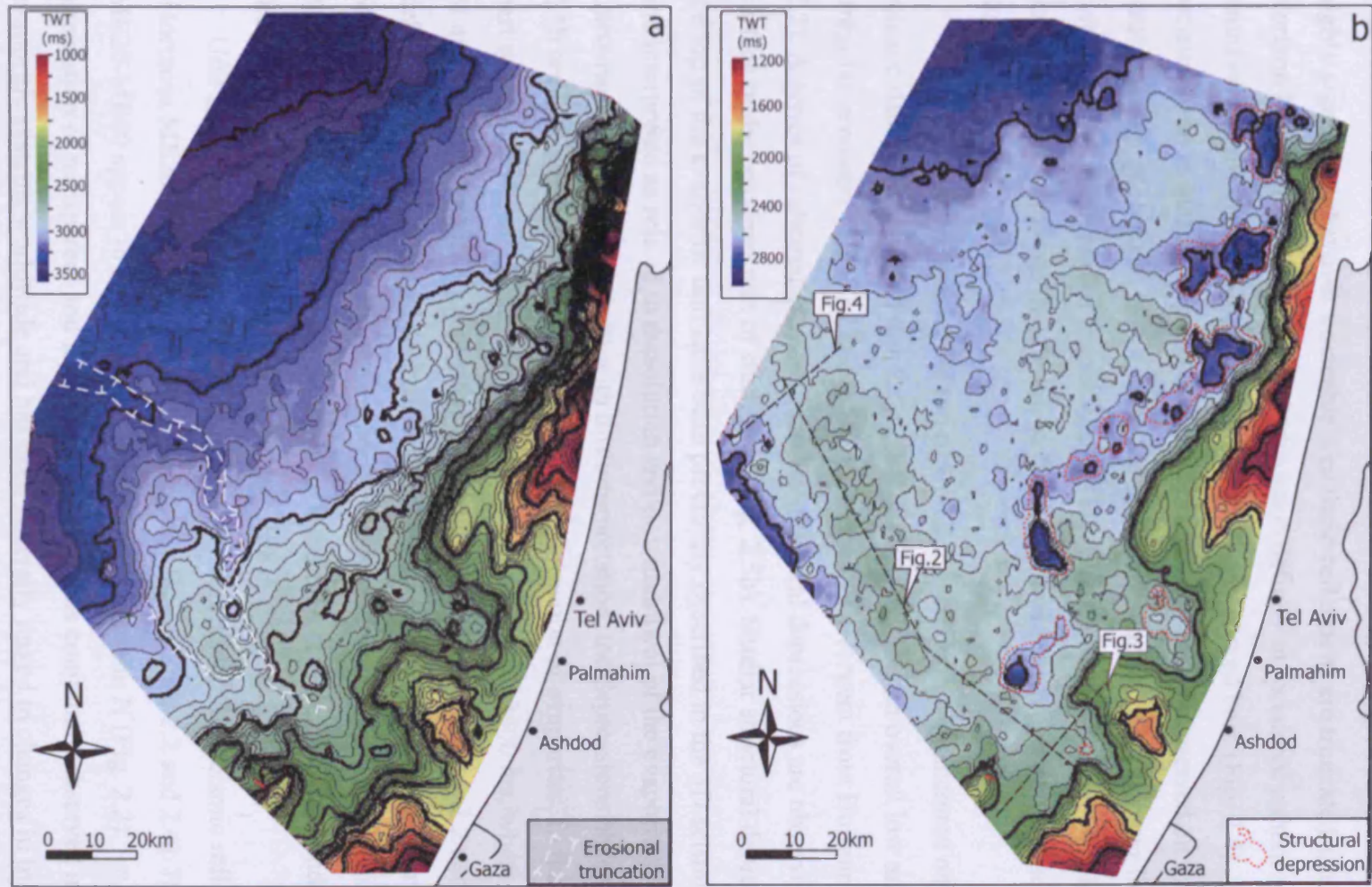


Figure 2.5 Time-structure maps generated in the 2D seismic dataset. The spectrum bar is indicated in milliseconds TWT. (a) Time-structure map of Horizon N, with contour line spacing of 50 ms. The morphology of Horizon N in the central and distal part of the area defines a surface gently sloping toward the northwest. The white dashed lines indicate the pattern of erosional truncation of the seismic reflections at the top of Unit 1 against Horizon N. (b) Time-structure map of Horizon M, with contour lines spacing of 100 ms. This surface appears irregular and nearly flat in its central part. The red dotted lines highlight the subcircular and composite elongated structural depressions described at the top of Unit 2.

gently dipping to the northwest (Fig. 2.5a) with a maximum dip of 1-2°, measured taking the top of Unit 2 as the regional reference datum. Horizon N is generally concordant with the seismic reflections at the top of Unit 1 (Fig. 2.2). However, it is highly significant that over a sizeable area these reflections are truncated against Horizon N (Fig. 2.4). This erosional truncation defines an incisional pattern with concave upward geometry, characterized by a flat or curved base (Fig. 2.4). The incision is up to 300 m deep and 2 km wide (Fig. 2.4), and is expressed on the time-structure map of Horizon N as a localized landward bending of the contour lines in the central and southern part of the study area (Fig. 2.5a). This bending can be clearly traced from the proximal (landward) to the distal (basinward) part of the time-structure map (Fig. 2.5a).

The time-structure map of the top of Unit 2, i.e. Horizon M, generated on 2D seismic data is displayed in Fig. 2.5b. This horizon exhibits an overall low angle and irregular geometry (Figs. 2.2 and 2.5b) and is clearly divergent from Horizon N (Fig. 2.2). A series of subcircular and composite structural depressions are observed at this surface in the proximal part of study area (Fig. 2.5b). Similar structural depressions at the top of the evaporitic unit have been previously described in the 3D seismic dataset, and interpreted as related to dissolution and/or withdrawal of the evaporites (Bertoni & Cartwright, 2005). By analogy with this interpretation, the depressions observed in Fig. 2.5b are here attributed to post-depositional deformation of evaporites. In the proximal part of the study area, Unit 2 pinches out at depth of 2200 to 2500 ms, where Horizons M and N merge into a single positive high amplitude reflection (Figs. 2.2 and 2.3). The definition of this correlative seismic horizon is somewhat controversial for implications on process interpretation. For the purposes of this study, we follow the seismic definition of Horizon M as representing the Messinian erosional surface landward of the evaporite pinch-out (Ryan, 1978; Barber, 1981).

Unit 2 is internally composed of an alternation of discernible seismic reflections (Horizons ME20-ME60) and transparent seismic facies (Figs. 2.2 and 2.4). Horizons ME20-ME60 appear to be broadly concordant with Horizon N (Fig. 2.2). An alternation of transparent and layered seismic facies is commonly observed in evaporitic systems worldwide and has been generally linked to changes in lithology, i.e. to the alternation of bitterns, dolomite, anhydrite, halite and/or siliciclastic sediments (e.g. Upper Permian basin of the North Sea: Taylor, 1998; Birrel & Courtier,

1999; Aptian evaporites of the Santos basin: Gamboa, 2004). By analogy with previous studies (Garfunkel & Almagor, 1987; Cohen, 1993) it is therefore suggested that the observed variation between transparent and layered seismic facies on the Levant margin is related to lithological and or diagenetic differences. A definitive interpretation of the seismic facies is not possible at this stage, and requires direct well calibration to resolve.

2.5.3 Unit 3 (Pliocene-Recent)

Unit 3 is bounded at the base by Horizon M and it is composed of a wedge of prograding and aggrading shelf to base-of-slope deposits, of Pliocene to recent age, divided in the Yafo (Plio-Pleistocene) and Herfer formations (Holocene) (unpublished well report; Frey-Martinez et al., 2005). This unit is composed mainly of sand in its basal part, and of hemipelagic turbiditic claystones, alternating with sandstones, siltstones and marls of outer neritic/middle bathyal environment in its upper part (Frey-Martinez et al., 2005). The reflections at the base of Unit 3 onlap and downlap against Horizon M in the proximal part of the study area (Fig. 2.2), whilst they are concordant to it in its distal part (Figs. 2.2 and 2.4).

Unit 3 is extensively affected by deformation mainly observed at the continental margin and close to the pinch-out of Unit 2 (Fig. 2.6). On this seismic section, the proximal part of Unit 3, at the base of the continental slope, is evidently affected by a system of folds and extensional faults detaching above or within Unit 2 (Fig. 2.6). These tectonic structures positively correlate with the deformation pattern of Horizon M, and have been related to thin-skinned gravitational tectonics linked to salt withdrawal (Almagor, 1984; Garfunkel & Almagor, 1987). The localized downwarping of Unit 3 reflections above the updip withdrawal edge of the salt edge of the evaporites could be either generated by downdip salt migration or by preferential dissolution at the margin of the salt sheet as commonly observed in evaporitic basins (Warren, 1999).

2.6 Interpretation of tectonic and topographic controls

The mapping undertaken on the 2D and 3D seismic datasets allows the recognition of the main morphological and structural features present on Horizons N and M. Due to the complex interaction among these features, a synopsis is needed in order to unify

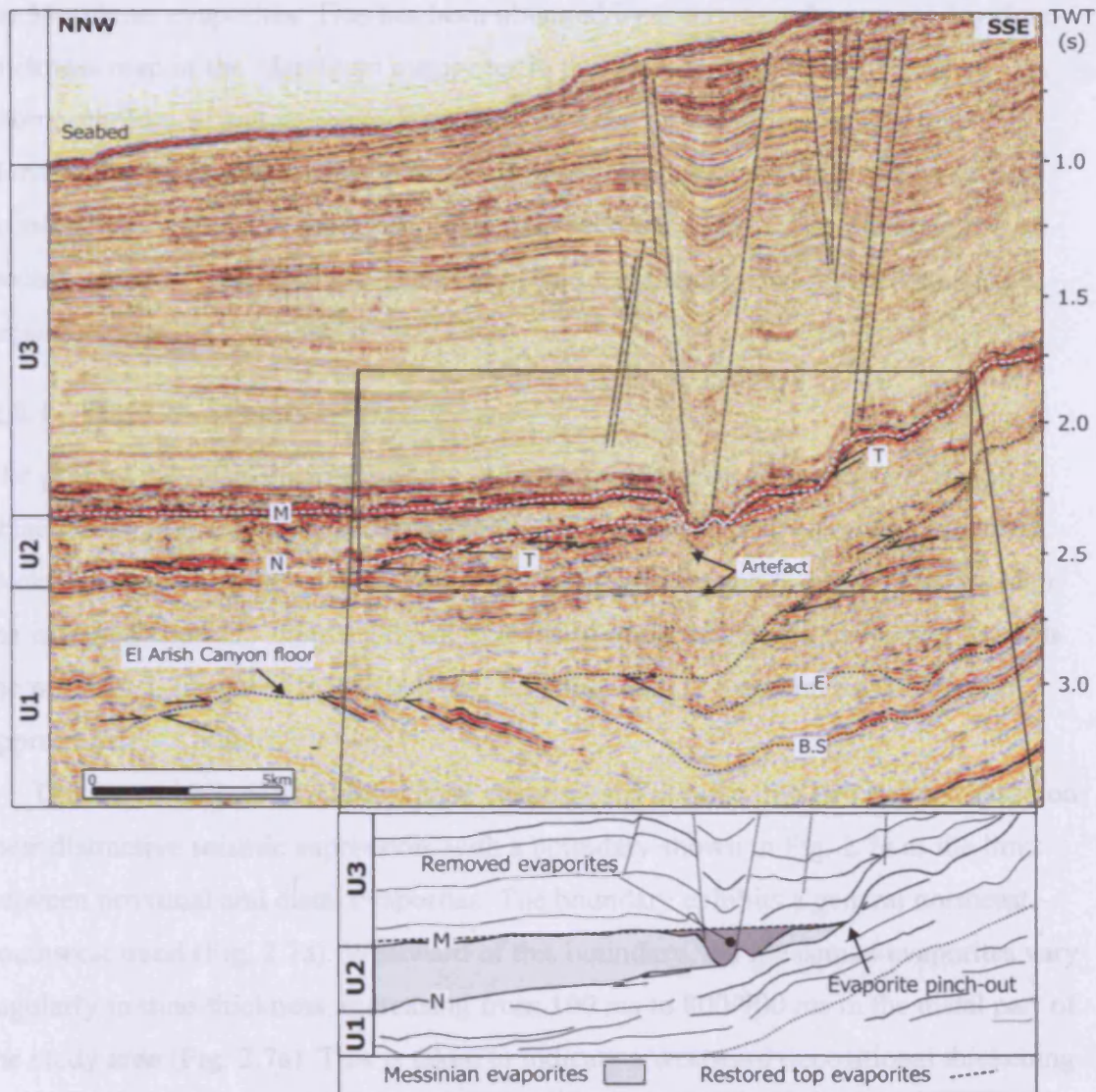


Figure 2.6 (a) 3D seismic section across the Levant margin (location in Fig. 2.7b). The erosional truncation defining the floor of the El Arish Canyon (dotted line) is indicated by black arrows underneath the dotted line. The canyon floor is overlapped by the overlying canyon fill reflections (upper black arrows). The Messinian evaporites (Unit 2) pinch out toward the south-southeast and pass laterally to an erosional surface, truncating the underlying reflections at the top of Unit 1 (T, black arrows). The black dashed lines in Unit 3 indicate the main extensional faults and grabens related to thin-skinned gravitational tectonics. The apparent downwarping of seismic reflections underneath the main graben is interpreted as a seismic artefact, due to the seismic velocity contrast between the deep-water sediments of Unit 3 and the evaporites of Unit 2. The rectangular box highlights the interpreted geo-seismic section in Fig. 6b. Other acronyms are explained in Fig. 2.2. (b) Interpreted geo-seismic section corrected for the seismic artifacts. The black dashed line represents the projected elevation of the overall flat Horizon M along the undeformed top basinal evaporite datum, up to the proximal area east of the boundary. The point where this projected line meets Horizon M is interpreted as the possible locus of evaporite pinch-out before deformation (Fig. 2.6b). This gives an approximate indication of the amount of evaporite removal due to post-depositional deformation (dark grey area: removed evaporites).

this record and, ultimately, to understand the controlling factors on the distribution of the Messinian evaporites. This has been obtained by computing the present day time-thickness map of the Messinian evaporites in the study area, relating it to the geomorphological and structural elements observed on the time-structure maps of Horizon N and M, and finally linking it to deep-seated features observed on seismic sections. The results are described in the next section and primarily illustrated by an isochron map of Unit 2 (Fig. 2.7) and by seismic and interpreted geo-seismic cross sections (Figs. 2.8 and 2.9).

2.6.1 Time-thickness of Unit 2

The present day time-thickness of the Messinian evaporites on the Levant margin is presented in Fig. 2.7. This isochron map has been generated by computing the time-thickness of the seismic package comprised between Horizon N and M. On this map, the isochron contours show a general thickening of the Messinian evaporites towards the northwest, from nearly 0 to 900 ms, corresponding to a maximum thickness of approximately 1800 m.

The area with preserved Messinian evaporites is divided into two regions based on their distinctive seismic expression, with a boundary shown in Fig. 2.7a as the limit between proximal and distal evaporites. The boundary exhibits a general northeast – southwest trend (Fig. 2.7a). Westward of this boundary, the Messinian evaporites vary regularly in time-thickness, increasing from 100 ms to 800/900 ms in the distal part of the study area (Fig. 2.7a). This is taken to indicate a westward depositional thickening of the evaporites. Eastward of the boundary, the evaporites display a constant time-thickness comprised between 0 and 100 ms (Fig. 2.7a). This geometric relationship is suggestive of a pinch-out of the thick distal wedge of the Messinian evaporites close to the position of the boundary. The regular variation in thickness and in seismic character observed west and east of this boundary suggest differences in the depositional and/or erosional processes operating in the two areas.

In most large evaporite basins, the original pinch-out of the evaporites is generally difficult to define on seismic data, as it represents a preferential site for the detachment of overlying faults (see e.g. Jenyon, 1986; Warren, 1999). Consequently, it is often difficult to quantify the amount of post-depositional deformation in the basin margin

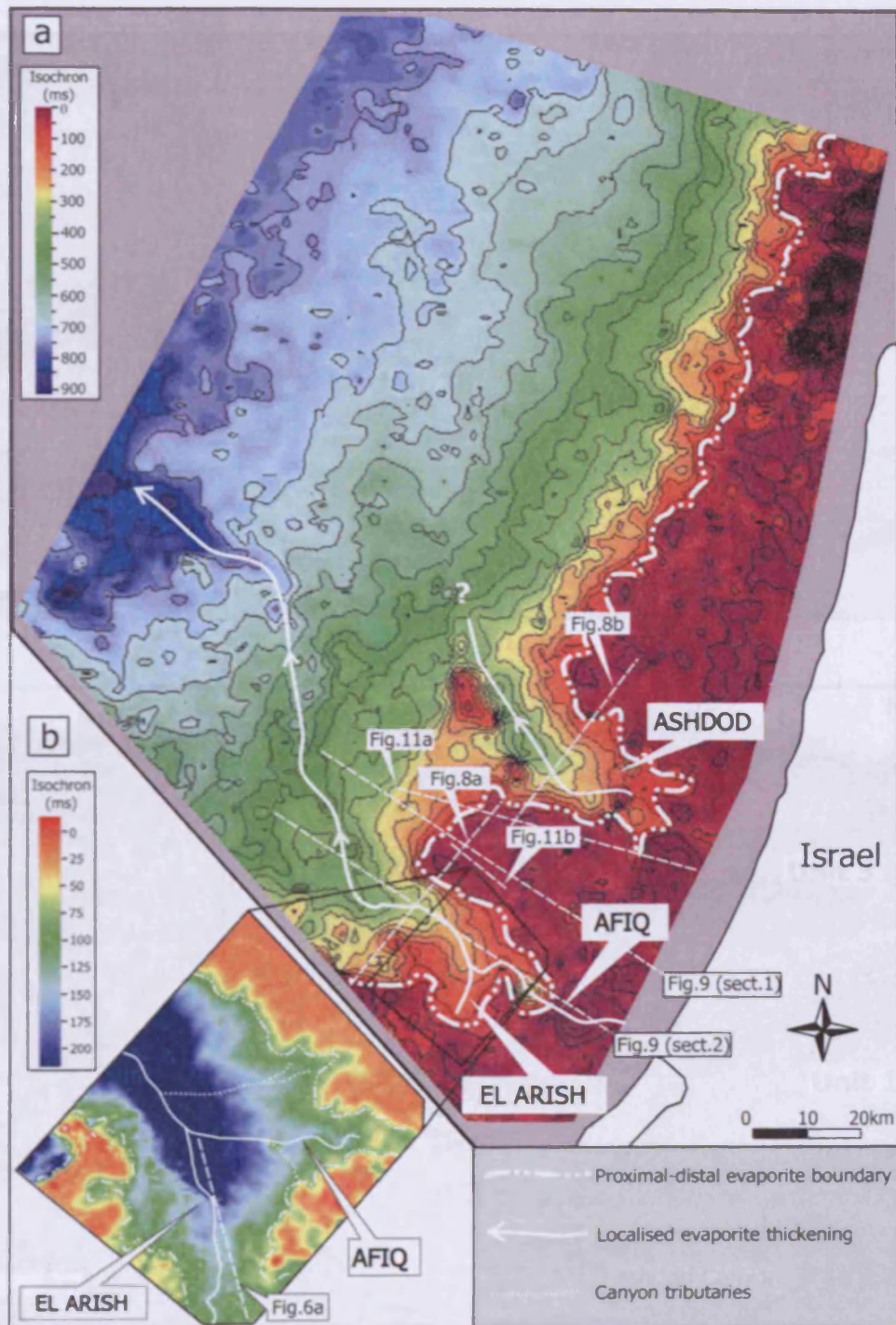


Figure 2.7 (a) Time-thickness (isochron) map of Unit 2 generated in the 2D seismic dataset, between Horizon N and M, showing the regular thickening of Unit B toward the northwest. Time-thickness is expressed in milliseconds (ms), with isochron contours spacing of 50 ms. The white bold lines and arrows trace the localised thickening of the evaporites observed above or basinward of the thalwegs of the El Arish-Afiq and Ashdod Canyons. (b) Close-up of the isochron map of Unit 2 generated in the 3D seismic dataset. Canyon tributaries, suggested by the shorter wavelength embayments in the distal-proximal evaporite boundary, are marked with white dotted lines.

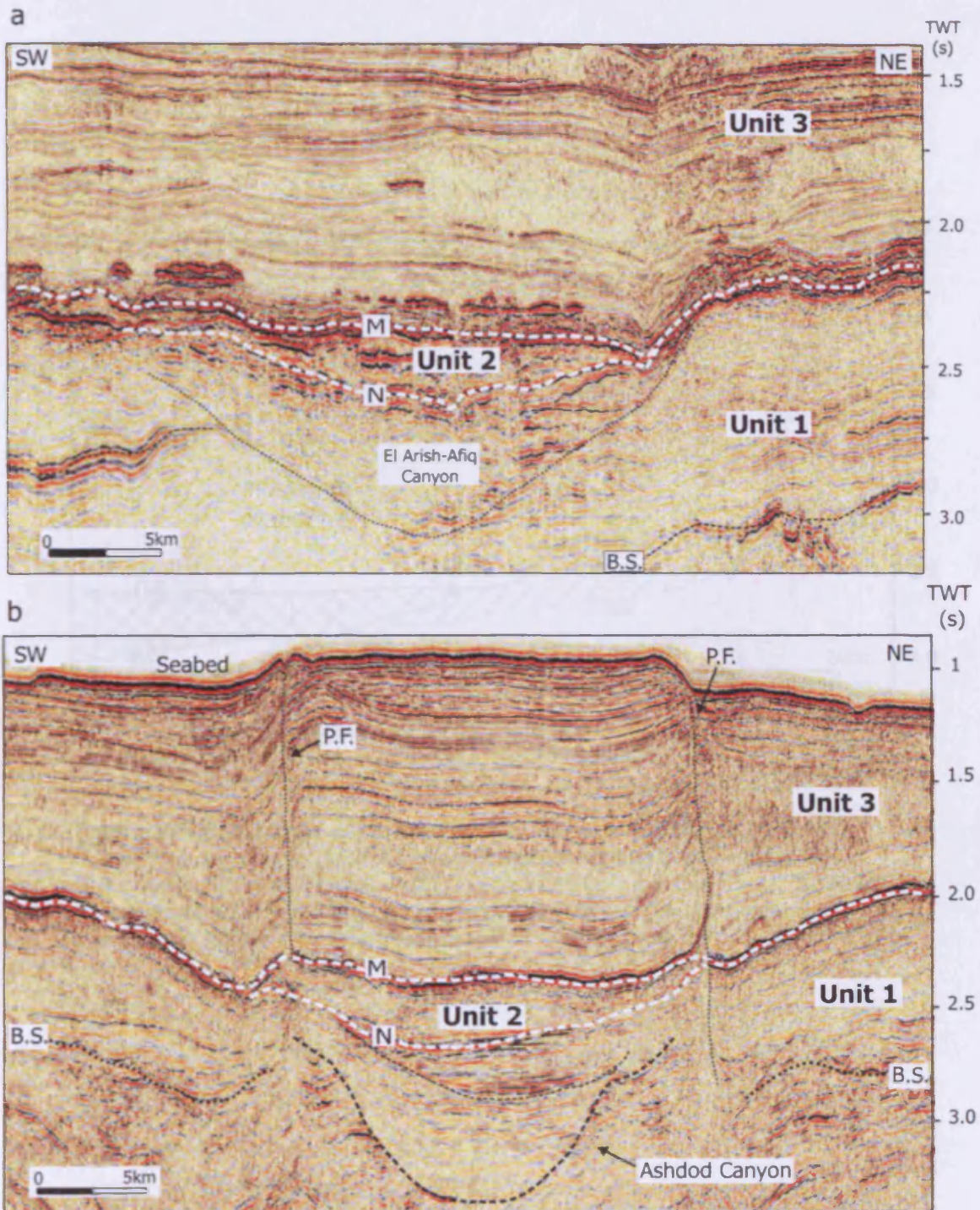


Figure 2.8 Seismic sections (location in Fig. 2.7) crossing the Oligo-Miocene submarine canyons, and showing the thickening of Unit 2 directly above the axis of the canyons. (a) 3D seismic section across the El Arish-Afiq Canyon. The black dotted line indicates the main incisional phase of the canyon. (b) 2D seismic section across the Ashdod Canyon, showing two main erosional episodes (black dashed line) and truncation of canyon fill against Horizon N (black arrows). P.F.: Palmahim fault. Other acronyms explained in Fig. 2.2.

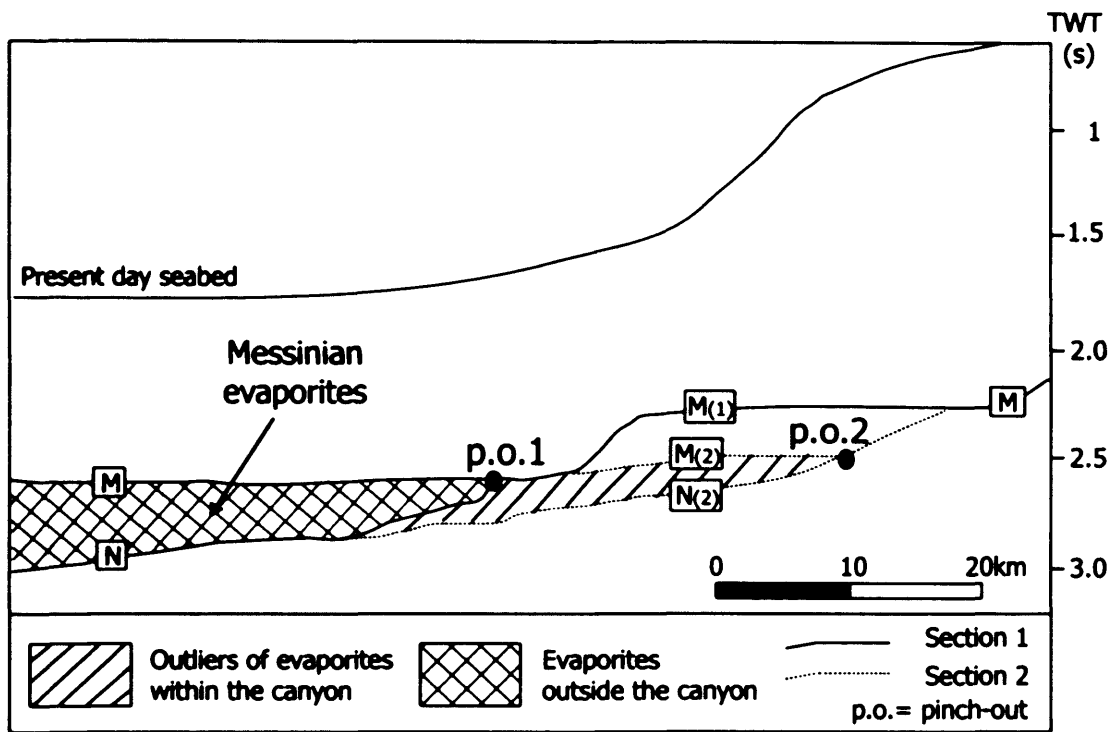


Figure 2.9 Idealized geo-seismic section across the Levant margin, obtained overlapping two seismic sections located respectively inside and outside the embayment above the El Arish Afq Canyon (section 1 and 2 in Fig. 2.7a). Note that the evaporite pinch-out in the section outside the canyon (p.o.1) is located significantly basinward of the pinch-out in the section along the canyon axis (p.o.2).

region. In order to overcome this problem we projected the elevation of Horizon M along the undeformed top basinal evaporite datum west of the present day boundary, to the proximal area east of the boundary, as shown on the seismic section displayed in Figs. 2.6a and 2.6b. The point where this projected line meets Horizon M is taken as the possible locus of evaporite pinch-out before deformation (Fig. 2.6b). This gives an approximate indication of the amount of evaporite removal due to post-depositional deformation (Fig. 2.6b) but it is of course subject to errors of projection, and assumes that the basinal evaporites have not lost volume. According to this analysis, the deformation observed at this boundary is localized and its impact on the original evaporite stratigraphy is clearly recognizable by the intense localization of extensional deformation of the post-evaporitic sequence (Fig. 2.6b).

Two major areas of focused landward bending of the boundary between proximal and distal evaporites are observed in the southern part of the time-thickness map (Fig. 2.7a). This trend is mostly evident on the isochron contours of value 0 to 400 ms (Fig. 2.7a). This pattern indicates two areas of thickening of the Messinian evaporites along a northwest-southeast directed axis (Fig. 2.7a). Importantly, as clearly illustrated in Figs. 2.8a and b, the embayments and the relative thickening of the Messinian evaporites occur directly above the axis of the Oligo-Miocene submarine canyons. The southernmost embayment can be correlated with the occurrence of the El Arish and Afq Canyons (Fig. 2.8a) while the embayment located ca. 30 km to the north is related to the Ashdod Canyon (Fig. 2.8b). A close-up of the isochron map of Unit 2 has been generated in the 3D seismic dataset (Fig. 2.7b). This map highlights the complexity and shorter wavelength embayments in the described boundary above the El Arish - Afq Canyons (Fig. 2.7b) suggesting the existence of a series of canyon tributaries.

The relationship between the localized thickening of the evaporites and the underlying canyons is schematically illustrated in Fig. 2.9. The areas of evaporite thickening above the El Arish, Afq and Ashdod Canyons (Fig. 2.8) can be defined as landward outliers of the evaporites. An idealized section across the Levant margin is here used to illustrate this geometry (Fig. 2.9). This section is obtained by overlapping two seismic sections located respectively inside and outside the embayment above the El Arish - Afq Canyon (location of the sections in Fig. 2.7a). It is significant that the pinch-out of the evaporites within the canyon (pinch-out 2 in Fig. 2.9) is located landward (>20 km) of the correlative evaporite pinch-out outside the canyon (pinch-out

1 in Fig. 2.9). The canyon therefore represents a depocentre for the most inland extension of the distal evaporites. The same embayments are observed on the time-thickness map up to an isochron value of 800 ms, where they exhibit a more confined and subdued morphology (Fig. 2.7a). Thickening of the Messinian evaporites is observed on the time-thickness map also above the Ashdod Canyon (Fig. 2.7a) although it appears less defined than above the El Arish – Afiq Canyon. In conclusion, the observed association between the embayments and the axes of the El Arish, Afiq and Ashdod Canyons points to a direct control of the canyon location on the erosional and depositional loci of the Messinian evaporites up to the more distal part of the study area.

2.6.2 Morpho-structural analysis

The observations made on the structural and morphological setting of the Messinian evaporites in the study area are summarized in a synoptic diagram (Fig. 2.10). This diagram facilitates the analysis of how the different features described herein may have controlled evaporite distribution. The morphological and structural features can be combined into two main groups:

- Tectonic structures: folds and faults (Fig. 2.10);
- Geomorphological features: canyons, marginal scarps, distal/proximal evaporite boundary (Fig. 2.10).

2.6.2.1 Tectonic structures

Folds. Offshore Israel, two main structures related to the Syrian Arc foldbelt have been previously described: Offshore Structure No. 1 and No. 2 (OS1 and OS2 in Fig. 2.1; Neev & Ben Avraham, 1977). The location of the Syrian Arc anticlines analysed in our study approximately corresponds to these offshore structures. However, an exact correlation with them has not been possible because of the lack of precise location of the fold axes in previous studies. The Syrian Arc anticlines are best illustrated at the Base Senonian level (Figs. 2.11a and b) although their activity is documented at least until the Miocene (Eyal, 1996; Fig. 2.11). The axes of the anticlines have been mapped across the seismic dataset and are highlighted on the synoptic diagram of Fig. 2.10, where they exhibit a northeast-southwest trend. They are spaced approximately 10-20 km in the eastern and central part of the study area.

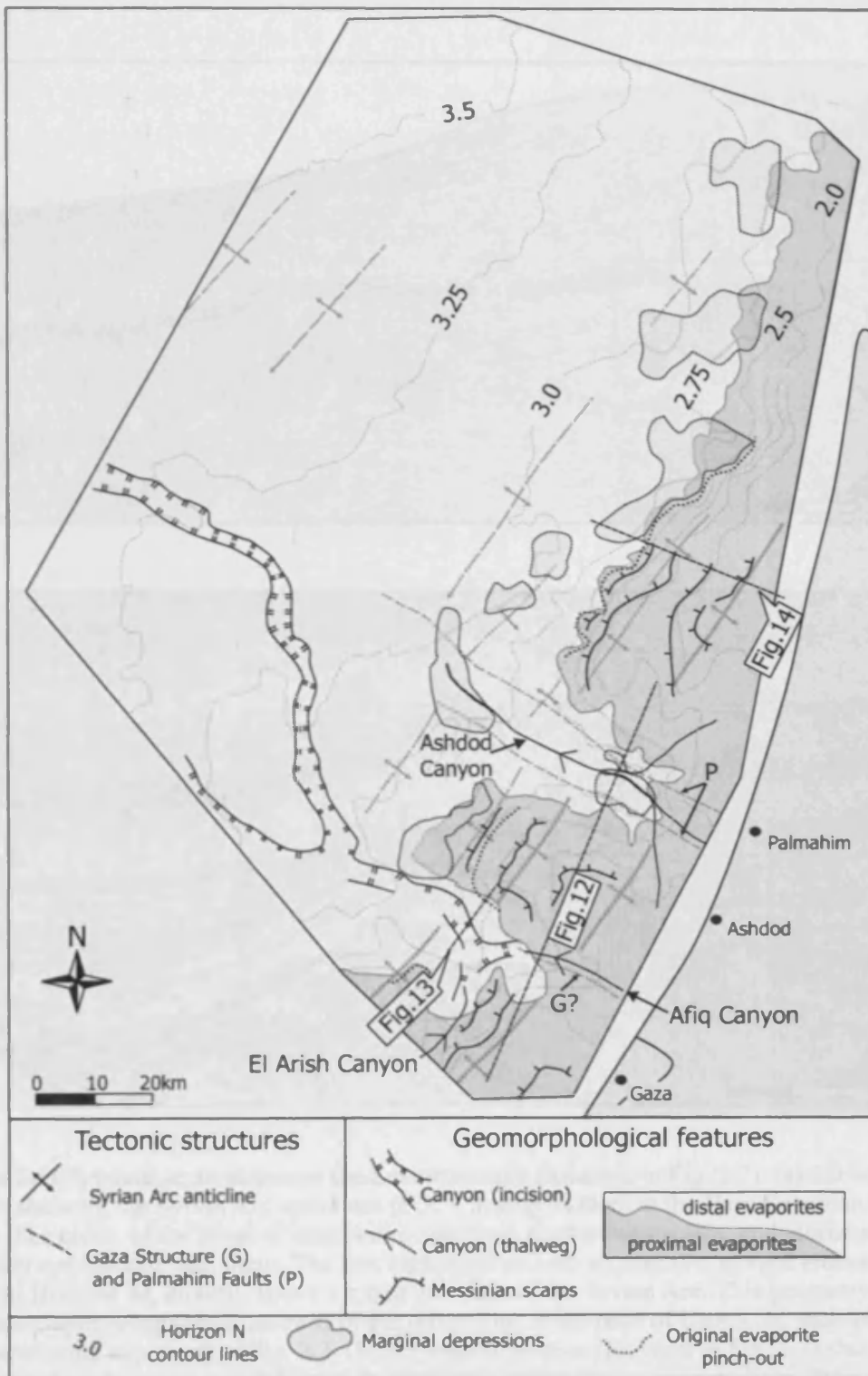


Figure 2.10 Synoptic diagram illustrating the main morphological and structural features observed in the study area, and their relation to the distribution of the Messinian evaporites.

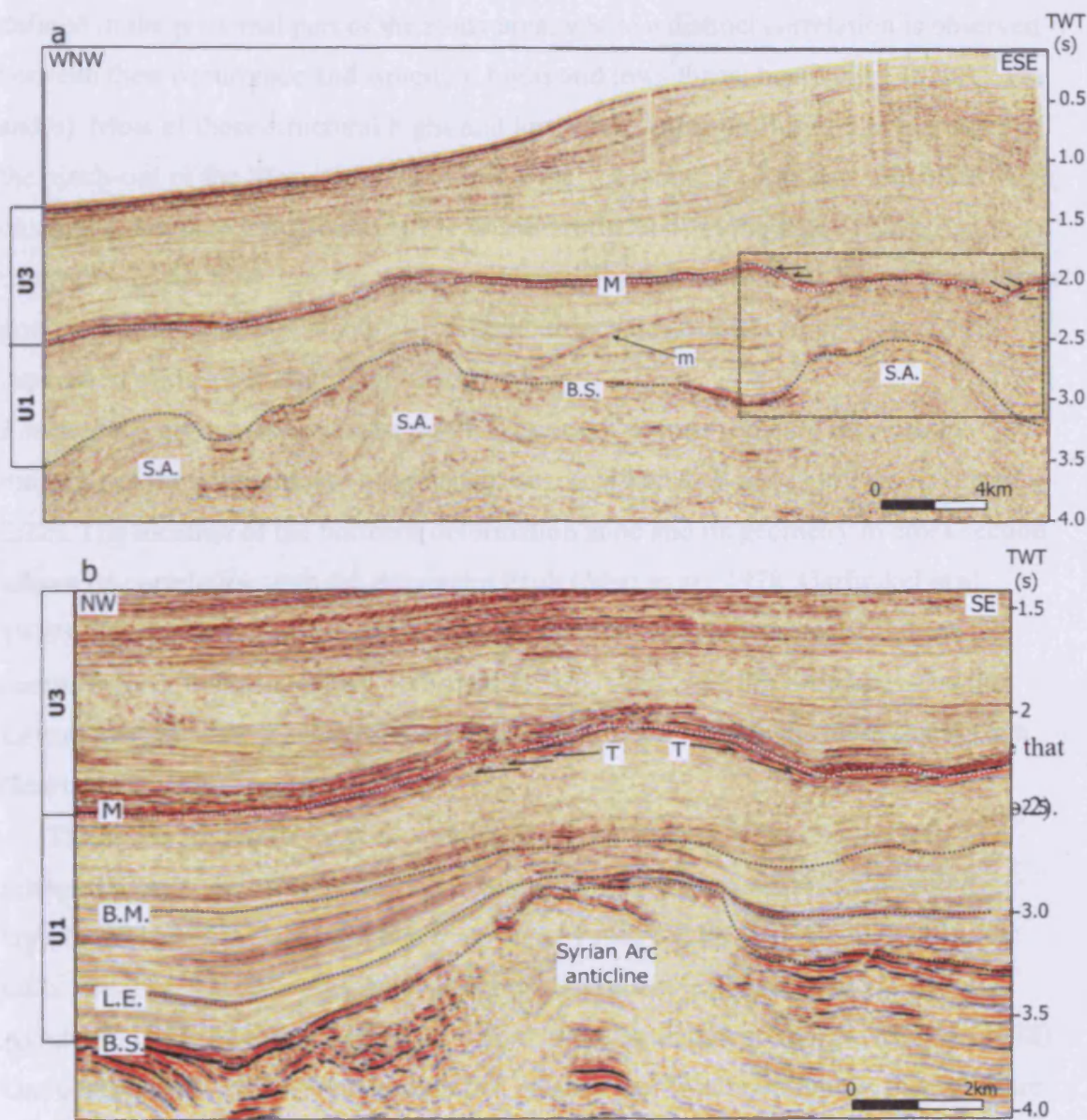


Figure 2.11 Seismic sections across the Levant margin (location in Fig. 2.7). (a) 2D seismic section showing the Syrian Arc anticlines (S.A.), mostly evident at the Base Senonian horizon (B.S.). The crests of the hinge of successive anticlines deepen westwards, and Horizon M is generally concordant with them. The box highlights an area of concave upward erosional relief on Horizon M, directly above a major anticline of the Syrian Arc. This geometry is associated with onlap (black arrows) of the reflections at the base of Unit 3. m: multiple, other acronyms explained in Fig. 2.2. (b) 3D seismic section (location in Fig. 2.7) showing the detailed stratigraphy and deformation above one of the Syrian arc anticlines. B.S.: Base Senonian Horizon; L.E.: Late Eocene Horizon; B.M.: Base Miocene Horizon (stratigraphy calibrated with well data). The Base Senonian Base Miocene seismic package clearly thins, onlaps and is upward against the Syrian Arc anticline, suggesting protracted activity of the structure in this time-span. The morphology of Horizon M still reflects the influence of the anticline, and is associated with low-angle truncation (T, black arrows) of the reflections at the top of Unit 1 against Horizon M.

On seismic cross sections, the crests of the hinge of successive anticlines appear to deepen progressively westwards (Figs. 2.11a). Consequently, these structures are best defined in the proximal part of the study area, where a distinct correlation is observed between their occurrence and structural highs and lows throughout Unit 1 (Figs. 2.11a and b). Most of these structural highs and lows are evident on Horizon M landward of the pinch-out of the Messinian evaporites (Figs. 2.11a and b). They are associated with onlap and downlap termination of the seismic reflections at the base of Unit 3 and truncation of the reflections at the top of Unit 1 (Figs. 2.11a and b). These observations point to the existence of a distinctly rugged surface pre-dating and influencing the deposition of the post-Unit 1 sediments.

Faults. Two northwest-southeast trending zones of deformation are revealed by mapping of the southern part of the study area (marked as P and G in Figs. 2.10 and 2.12). The location of the northern deformation zone and its geometry in cross section allows its correlation with the Palmahim Fault (Mart et al., 1978, Garfunkel et al., 1979). This has been interpreted as a strike-slip fault zone associated with both compressional and extensional deformation. This fault zone has been active on the Levant margin since the late Miocene and is possibly related to the Dead Sea system, (Mart et al., 1978).

The southern deformation zone is not as clearly imaged (Fig. 2.12), and its interpretation is therefore somewhat ambiguous. Its location suggests a possible correlation with the Gaza structure described by Neev & Ben-Avraham (1977). The Gaza structure has been previously interpreted as either a trough (Neev & Ben-Avraham, 1977) or a strike-slip fault linked to the Dead Sea system (Mart et al., 1978). Our observations do not support either of the previous interpretations of this structure. Our mapping shows that both the Palmahim Fault and the Gaza structure are closely related to the location of the Ashdod and El Arish-Afiq Canyons (Fig. 2.12), and consequently, to the embayments and salients of the Messinian evaporites (Fig. 2.10). Despite the uncertain timing and definition of these structures, this spatial correspondence suggests a causal connection among the Palmahim and Gaza structures and the salients in the marginal trend of the evaporites, through the control of long-lived faults on the location of the Ashdod and El Arish-Afiq Canyons and consequently, on the depositional loci of the Messinian evaporites.

2.6.2.4 Geomorphological features

Canyons. Confined areas of erosion and downcutting of Marfan II and the associated... at the top of Unit 1 have been observed in cross-section (e.g. Fig. 2.4) and are explained by the increased loading of detrital loads on the sub-structure map of Marfan II (Fig. 2.5). The incision is expressed in cross-section by a local... at the base of the Marfanian sequence, both in the field (Fig. 2.4) or in the general case (e.g. 2.6 and 2.7) of the study area. The incision defines a... structure, but is not an... (Fig. 2.4). In this... field

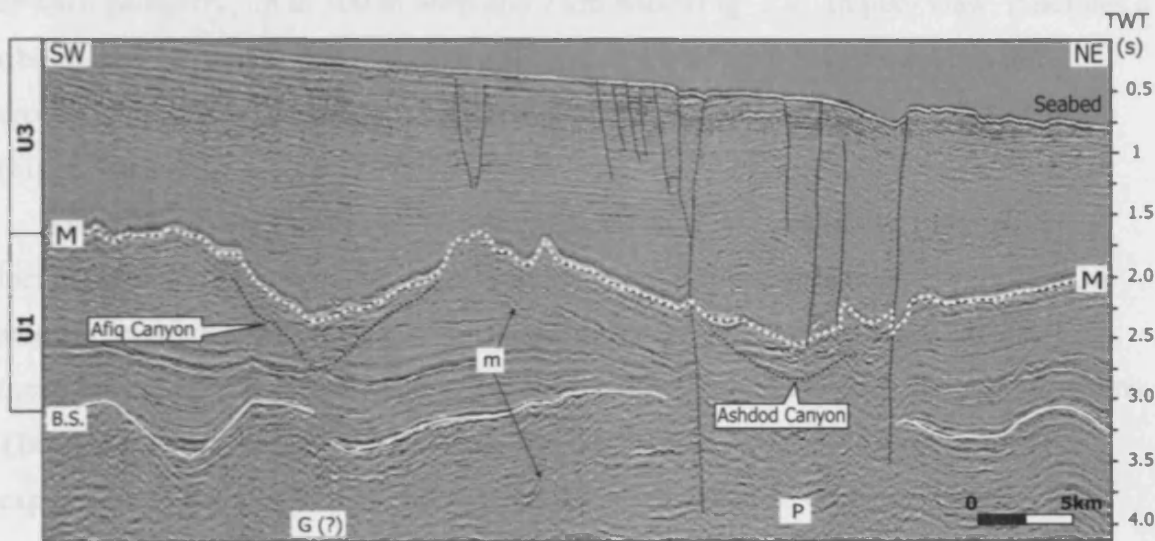


Figure 2.12 2D seismic section (location in Fig. 2.10) illustrating the cross-sectional geometry of the two zones of deformation in the southern part of the study area. The Palmahim fault zone (P) is imaged as two main vertical fractures marked by black dashed lines, nearby the Ashdod Canyon. These faults appear to displace the entire stratigraphic section from Unit 1 to Unit 3. The Gaza structure (G?) is tentatively correlated with a deformation zone displacing the Base Senonian horizon. This structure is mostly evident at the Syrian Arc anticline located below the Afiq Canyon. For explanation of the other acronyms see Figs. 2.2 and 2.11.

2.6.2.2 Geomorphological features

Canyons. Confined areas of incision and downcutting of Horizon N into the seismic reflections at the top of Unit 1 have been observed in cross section (e.g. Fig. 2.4) and are evidenced by the landward bending of contour lines on the time-structure map of Horizon N (Fig. 2.5a). The incision is expressed in cross section by erosional truncation at the base of the Messinian evaporites, both in the distal (Fig. 2.4) or in the proximal part (Figs. 2.6 and 2.13) of the study area. The incision defines a concave-upward geometry, up to 300 m deep and 2 km wide (Fig. 2.4). In plan view, it defines a ribbon-shaped pattern that is strongly aligned in a north-northwest direction and crosses almost continuously the southern part of the study area for more than 100 km (Fig. 2.10).

From the mapped geometry and morphology in cross section, we interpret the incisional features as canyons developed at the base of the Messinian evaporites. On seismic sections crossing the proximal part of the Levant margin (Figs. 2.8 and 2.13), these canyons occur directly above the axes of the Ashdod, El Arish and Afiq Canyons. Therefore, we interpret the canyons on the time-structure map of Horizon N as the expression of the Oligo-Miocene Ashdod, El Arish and Afiq Canyons at this stratigraphic level. The incisional pattern in the distal area represents the basinward prosecution of the thalwegs of the El Arish, Afiq, Ashdod Canyons (Fig. 2.10) and is traced on the basis of the landward bending of contour lines of the time-structure map of Horizon N (Fig. 2.5). Importantly, this indicates that the canyons at the base of the Messinian evaporites extend further basinward than the Oligo-Miocene submarine canyons, documenting active canyon erosion up to the distal part of study area at the stratigraphic level of Horizon N. No similar incisional features are observed internally in the evaporitic unit or at the top of the Messinian evaporites, pointing to a change of the erosional patterns in the later stages of the MSC.

Messinian scarps. The upslope part of Horizon M landward of the evaporite pinch-out presents an irregular erosional present-day topography (Fig. 2.14). This Messinian erosional surface is characterized by a series of well-defined slope breaks (MS1 to MS3 in Fig. 2.14), between a steeply sloping and a low angle surface. The most prominent of these features (MS1) is located in the eastern part of the seismic section displayed in Fig. 2.14. In this area, the gentle slope sector is defined by a surface dipping at an angle of approximately 2° and is associated with erosional truncation of

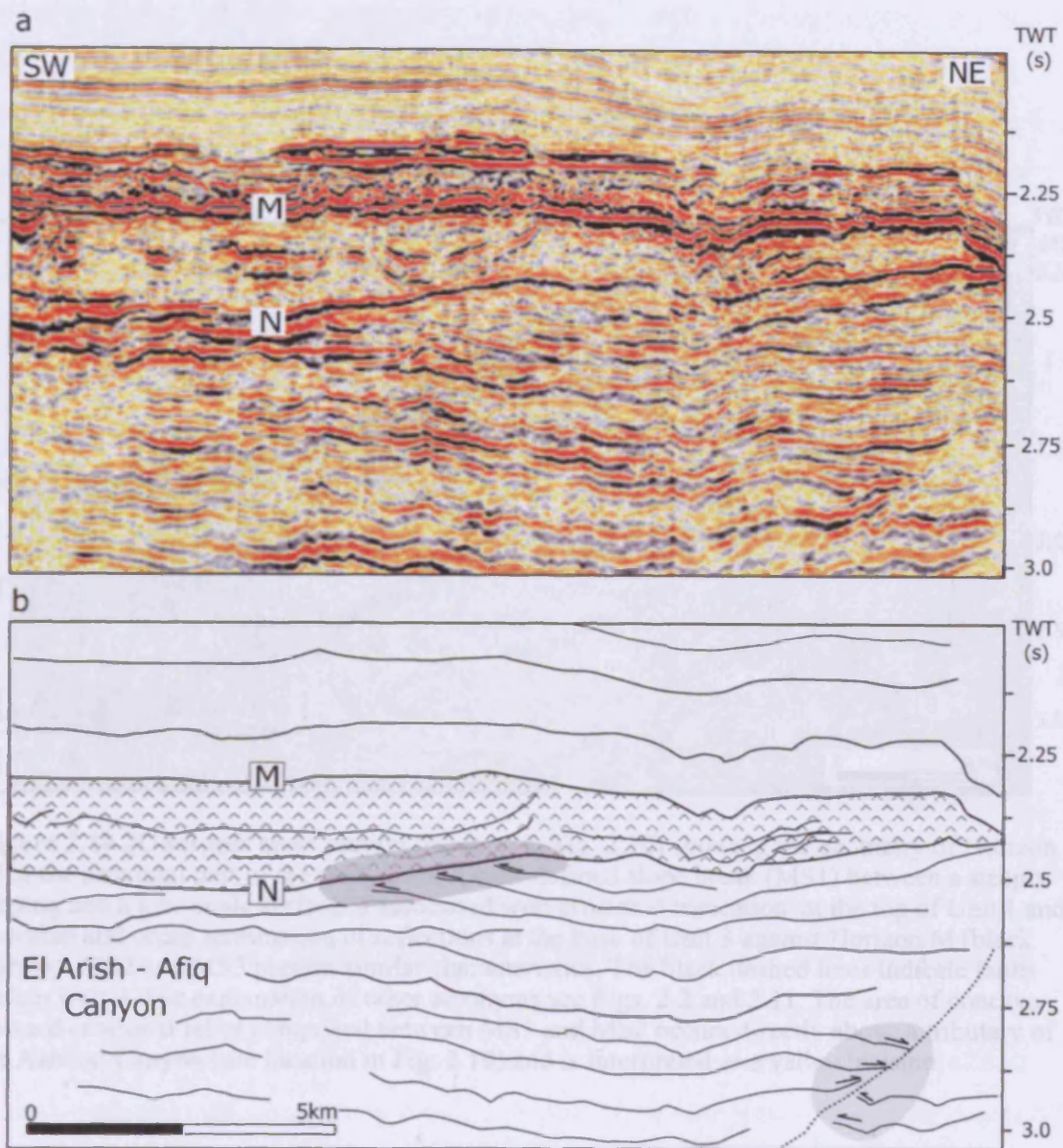


Figure 2.13 (a) 3D seismic section along the proximal part of the evaporitic system on the Levant margin, and (b) interpretation (location in Fig. 2.10). The black dashed line on the right side of the section shows the main incision of the El Arish - Afq Canyon, associated with erosional truncation pattern of the underlying seismic reflections. Erosional truncation is also observed on the reflections at the top of Unit 1 against Horizon N (shaded grey areas).

the 2-D seismic reflection within the upper part of Unit 1. This surface is overlapped by the overlying basal massive reflections of Unit 2 (Fig. 2.14). The steep slope sector is defined by a surface dipping at an angle of 3-10°.

A post-Miocene phase of folding and basement uplift of the Levant margin might have locally modified the original depositional angles. This is suggested by the coincidence of Horizon M with the folded 3-g-amp-like reflections at the base of Unit 2 (Fig. 2.11). The steeply sloping sector west of MS1 matches with the NW flank of the underlying Syrian Arc anticline (Fig. 2.14), suggesting a similar tectonic

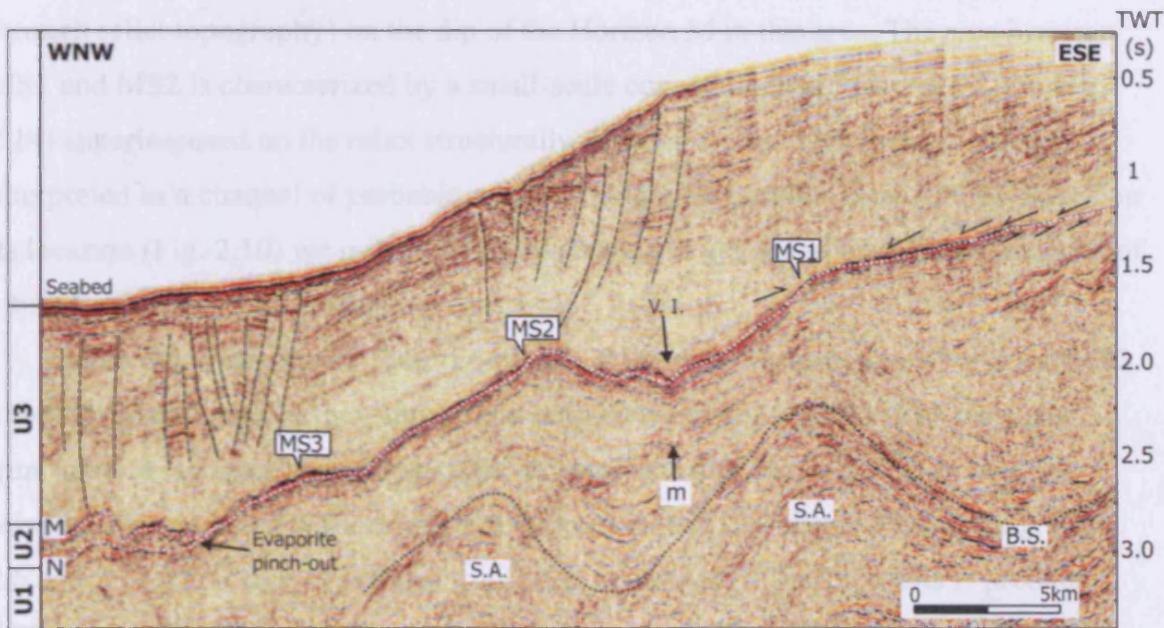


Figure 2.14 2D seismic cross section (location in Fig. 2.10) showing the geometry of Horizon M in the proximal part of the study area. A well-defined slope break (MS1) between a steeply sloping and a low-angle surface is associated with erosional truncation at the top of Unit 1 and downlap and onlap termination of reflections at the base of Unit 3 against Horizon M (black arrows). MS2 and MS3 present similar characteristics. The black dashed lines indicate faults within Unit 3. For explanation of other acronyms see Figs. 2.2 and 2.11. The area of concave upward erosional relief comprised between MS1 and MS2 occurs directly above a tributary of the Ashdod Canyon (see location in Fig. 2.10) and is interpreted as a valley incision.

the study area is an approximately constant depth. The slope breaks have been stepped across the regional dataset and they are oriented in a general northeast - southwest direction, following the tectonic lines of the Miocene structural surface (Fig. 2.10).

Based on the characteristics of the observed morphological features we interpret the steep sloping sectors as erosional scarps. The variable elevation of the slope breaks could indicate different erosional stages during the MSC. This could be explained by vertical tectonic movement occurring during the MSC. However, the large difference in elevation from interfluvial to overthrust scarps (>1000 m) far exceeds the expected

the underlying reflections within the upper part of Unit 1. This surface is downlapped by the overlying basal seismic reflections of Unit 3 (Fig. 2.14). The steep slope sector is defined by a surface dipping at an angle of 9-10°.

A post-Messinian phase of folding and basinward tilting of the Levant margin might have locally modified the original depositional angles. This is suggested by the concordance of Horizon M with the folded high-amplitude reflections at the base of Unit 2 (Fig. 2.11). The steeply sloping sector west of MS1 matches with the NW flank of the underlying Syrian Arc anticline (Fig. 2.14), suggesting a structural control (e.g. through relict topography) on the dip of the Horizon M in this area. The area between MS1 and MS2 is characterized by a small-scale concave-upward feature (V.I. in Fig. 2.14) superimposed on the relict structurally depressed area. This feature has been interpreted as a channel of probable subaerial origin by Ben-Gai et al. (2005). Based on its location (Fig. 2.10) we interpret that this feature is generated by localised incision of a tributary of the Ashdod Canyon.

Similar slope breaks are observed basinward from MS1, and named MS2 and MS3, although to some extent they appear less defined than MS1. Evidence of erosional truncation at Horizon M underneath these features is difficult to define on the 2D seismic sections and it is more clearly observed on the 3D seismic sections (e.g. Figs. 2.6 and 2.11). The lack of obvious truncation in parts of 2D seismic data is probably due to poorer vertical resolution of the 2D data compared to the 3D data, and to post-Messinian deformation. However, the abrupt changes in topographic gradient associated with MS1 to MS3 and the observed related erosional truncation are evidently restricted to the stratigraphic level of Horizon M (Fig. 2.14); therefore being interpreted as formed during the MSC. As observed on different seismic cross sections, each of the slope breaks exhibits a considerable lateral continuity and it occurs across the study area at an approximately constant depth. The slope breaks have been mapped across the seismic dataset and they are oriented in a general northeast - southwest direction, following the contour lines of the Messinian erosional surface (Fig. 2.10).

Based on the characteristics of the observed morphological features we interpret the steep sloping sectors as erosional scarps. The variable elevation of the slope breaks could indicate different erosional stages during the MSC. This could be explained by vertical tectonic movement occurring during the MSC. However, the large difference in elevation from innermost to outermost scarps (>1000 m) far exceeds the expected

values of differential subsidence and/or uplift of the Levant margin at that time (Tibor et al., 1992). Therefore we interpret that it is more plausible that the location of the scarps was controlled by changes in the base level of erosion, documenting repeated erosional phases on the Levant margin during the MSC.

Distal/proximal evaporite boundary. The trend of the boundary between distal and proximal evaporites is approximately northwest – southeast, therefore parallel to the regional trend of the structures of the Syrian Arc foldbelt and to the erosional scarps (Fig. 2.10). The difference between the present day and original boundary has been calculated where possible in the study area using the methodology displayed in Fig. 2.6b. The result is marked in the synoptic diagram with a black dotted line indicating the expected original position of the boundary, before post-depositional deformation (Fig. 2.10). The amount of post-Messinian evaporite deformation can be estimated analysing the marginal subcircular and elongated depressions at the top of Unit 2, landward of the proximal/distal evaporites boundary (Fig. 2.10). The location of these depressions suggests that the difference observed between the original and present day evaporite pinch-out is due to the same causal mechanism of the depressions, i.e. downdip migration or dissolution of the evaporites.

2.7 Discussion

2.7.1 Summary of the main observations

The key observations presented in the previous sections are summarized below:

- The Messinian evaporites on the Levant margin are seismically defined as a wedge up to 1.8 km thick in the basin, thinning eastward and extending landward into a major erosional surface.
- A system of canyons has been recognized at the base of the Messinian evaporites (Horizon N). They are up to 300 m deep and 2 km wide, and extend from the proximal to the distal part of the study area (more than 100 km basinward of the pinch-out of the Messinian evaporites). Importantly, these basal Messinian canyons developed directly above the mapped Oligo-Miocene El Arish, Afiq and Ashdod submarine canyons. Conversely, no evidence of similar canyon incision has been observed within or at the top of the Messinian evaporites.

- The time-thickness map of the Messinian evaporites reveals that their locus of pinch-out is regularly trending to the northeast - southwest, broadly parallel to the underlying compressional structures of the Syrian Arc foldbelt. Remarkably, a series of localized embayments in the isochron contours documents the thickening of the evaporites directly above the thalweg of the El Arish, Afīq and Ashdod Canyons.
- The Messinian erosional surface landward of the evaporite pinch-out (Horizon M) is morphologically characterized by a series of slope breaks, between a steeply sloping and a low angle surface, dipping basinward. The steeply sloping parts are associated with erosional truncation of the underlying seismic reflections, and are interpreted as scarps formed during the MSC.

The observation of these different morpho-structural elements poses two fundamental questions regarding the structural and depositional setting of the Messinian evaporites, i.e.: (1) what controlled the formation of the linear edge of the Messinian evaporites, and (2) what controlled the formation of the embayments in the distribution of the evaporites. The following discussion will attempt to answer these questions, in relation to the timing of canyon development and to the paleogeography of the basin.

2.7.2 Linear edge of evaporites

Three main controlling factors can be invoked to explain the linear morphology of the edge of the Messinian evaporitic basin in the study area: relict topography (e.g. pre-evaporitic shelf margin), tectonics and/or erosional or depositional processes inherent to the MSC. In the study area, the trend of the proximal/distal evaporite boundary is parallel to the direction and coincides with the location of the structural highs related to the Syrian Arc foldbelt (Fig. 2.10).

Previous studies have suggested that the structures of the Syrian Arc foldbelt played a significant role in controlling the pre-evaporitic structural setting of the Levant margin since the Late Cretaceous (Neev & Ben-Avraham, 1977). Our mapping confirms that Syrian Arc anticlines in Unit 1 controlled the geometry of the Oligo-Miocene clastic wedge, being active during its deposition. According to Druckman et al. (1995), the pre-evaporitic physiography of the Levant margin was characterized by a drowned Oligo-Miocene shelf edge nearly parallel to the present-day shelf edge and located up to 20 km inland from it. In the study area, we have no morphological

evidence so far of the position of the shelf edge immediately preceding the MSC. However, an approximate indication of the pre-evaporitic shelf location can be obtained from well data, which documents that the edge of the evaporites directly overlies the Oligo-Miocene slope sediments, therefore it is consistent with the paleogeography described by Druckman et al. (1995).

The most recent tectonic deformation observed in the study area suggests that thin-skinned gravitational tectonics accounts for the differences observed between original and present-day pinch-out of the Messinian evaporites in the proximal part of the evaporitic system (Fig. 2.6b). Preferential dissolution of the updip edge of the evaporites could also have contributed to the post-depositional deformation of the original pinch-out of the evaporites. A gravitational tectonic modification of the original depositional edges is ubiquitous amongst the world major evaporitic basins and the recognition of a similar structural response in the Levant margin is therefore expected. Previous authors have described the effects of this gravitational tectonic modification along the entire Israeli margin (Garfunkel & Almagor, 1987; Tibor & Ben-Avraham, 1992; Grandmann et al., 2005). Based on our data and on the comparison with nearby areas, we consider that gravitational tectonics and possibly dissolution-driven withdrawal shifted the position of the original evaporite pinch-out a few kilometres basinward of the original location, without modifying significantly the regional trend of the original evaporite pinch-out.

In conclusion, we suggest that the location of the Syrian Arc structures exerted controlled on the Oligo-Miocene physiography and subsequently on the distribution of the Messinian evaporites, providing accommodation for the evaporites and structurally controlling the linear edge of the evaporites through the relict topography of the Oligo-Miocene slope system basin.

2.7.3 Salients and embayments

The link between the salients and embayments of the Messinian evaporites and the location of the El Arish, Afiq and Ashdod Canyons, is clear evidence for the role of the canyons in controlling the architecture of the evaporitic system. The long-lived nature of these Oligo-Miocene submarine canyons has been recognized in previous studies (Druckman et al., 1995). A control by the canyons on evaporite deposition has been suggested for the Afiq Canyon (Neev, 1960; Druckman et al., 1995), but has not been

previously extended to the basinal part of the system, and its wider implications have not therefore been entirely appreciated. According to our observations, the embayments and salients observed in the marginal part of the study area could be explained with three different depositional architectures, as illustrated in the schematic diagram of Fig. 2.15:

1. Pre-evaporitic submarine canyon completely filled, successively re-excavated at the onset of the MSC (Fig. 2.15a).
2. Pre-evaporitic submarine canyon incompletely filled, and Messinian evaporites filling (completely or in part) the relict topography (Fig. 2.15b).
3. A combination of the two previous scenarios (Fig. 2.15c).

The canyons described at the base of the Messinian evaporites (Fig. 2.10) provide firm evidence that the Ashdod, El Arish and Afiq Canyons were actively eroding during the early stages of the MSC. Incision occurs only in the central part of the embayments defined in the isopach map of the Messinian evaporites (Figs. 2.7 and 2.13). Therefore the more likely explanation for the embayments and salients of the Messinian evaporites is that the evaporites fill a relict topographic depression, with incision occurring only in a limited and central part of it (Fig. 2.15c). In the more distal part of the study area, beyond the distal reaches of the Oligo-Miocene submarine canyons (Fig. 2.4), a different depositional architecture is envisaged, where incision at the base of the evaporites excavated unconfined Oligo-Miocene deep-water deposits (Fig. 2.15d). Based on this geometry, we propose that this incisional pattern at the base of the Messinian evaporites might represent an increased erosional activity of the canyons related to the sea-level lowering at the early stages of the MSC, documented in other areas of the Mediterranean basin (Barber, 1981; Riding et al., 1998; Lofi et al., 2005).

2.7.4 Implications for the MSC

The comparison of our study area with other Messinian evaporitic systems in the Mediterranean basin points to significant differences in the geometry of the evaporitic unit, and therefore possible substantial variations in the erosional and depositional processes occurring during the MSC. An important matter of debate in the entire Mediterranean basin is the correlation of the marginal erosional surface with the seismic reflectors defining the base (Horizon N) or the top (Horizon M) of the Messinian evaporites. Erosional processes at the base of the Messinian evaporites,

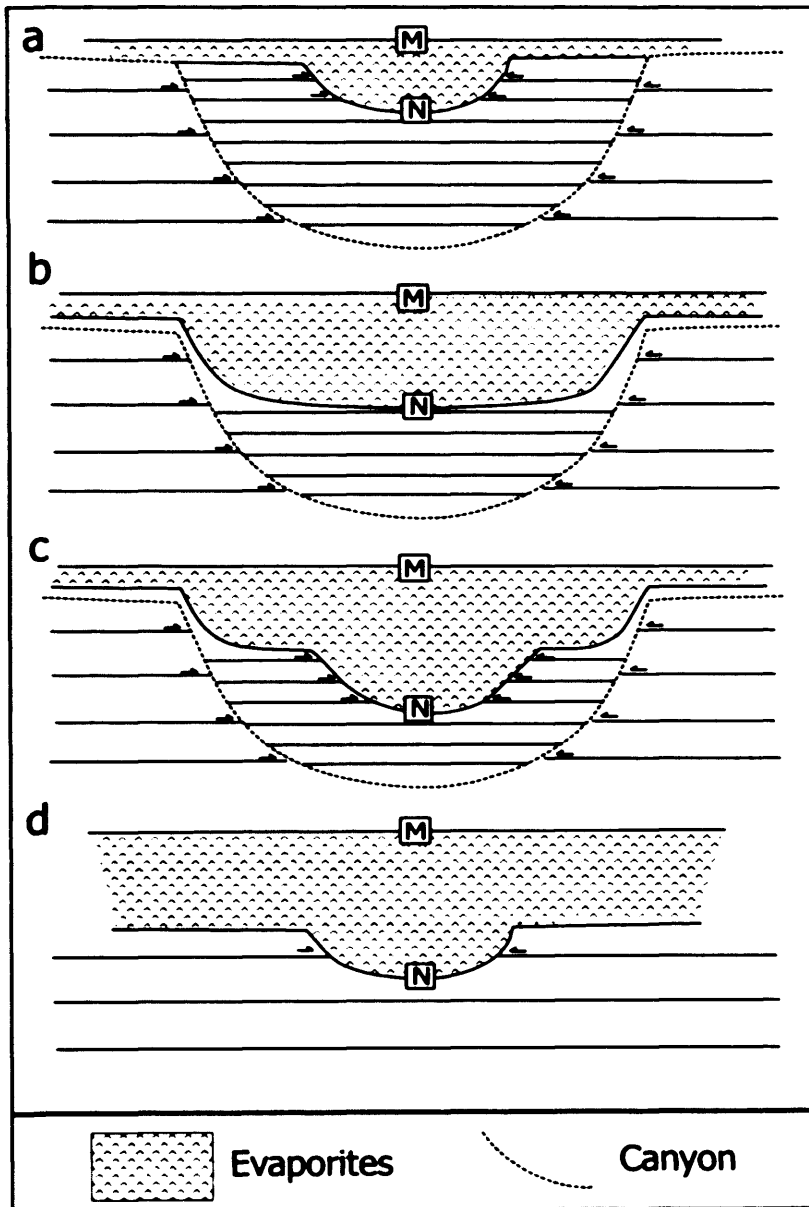


Figure 2.15 Schematic cartoon illustrating the possible geometries of the base of the Messinian evaporites (Horizon N) and modality of infill in relation with the underlying canyon system. (a) Pre-evaporitic submarine canyon completely filled, successively re-excavated at the onset of the MSC; (b) Pre-evaporitic submarine canyon incompletely filled, Messinian evaporite filling the relict topography; (c) A combination of the two previous scenarios, which is the most likely geometry for the deposits in the study area; (d) the distal scenario, with unconfined pre-evaporitic deep-basin sediments excavated by the canyons at Horizon N, at the basinward prosecution of the Oligo-Miocene submarine canyons.

associated with the development of regional unconformities, have been documented in many areas of the Mediterranean margins.

The erosional surface observed in the proximal part of the Messinian evaporitic system has been generally correlated to the base of the distal Messinian evaporites (e.g. Ryan, 1978; Guennoc et al., 2000) even if different erosional phases have been recognized within or at the top of the evaporites (e.g. Cita et al., 1978; Escutia & Maldonado, 1992). In the study area, the seismic-morphological analysis of the canyons and of the marginal Messinian scarps can be used to highlight and differentiate successive erosional phases. Clear indication of erosional activity linked to the canyons is observed in the early stages of the MSC. Conversely, the absence of incision in the late stages of the MSC reflects the reduced effect of the canyons as erosional focus, and could indicate the prevalence of an infill or bypass phase of the canyon during their deposition, following the basal erosion. The final expression of the canyon system in the Early Pliocene basin, after the end of the MSC, is dominated by an infill and bypass stage (Frey-Martinez et al., in press), i.e. sedimentation prevailed on the creation of accommodation. The canyon setting in the Levant margin bears similarities with the Messinian canyons in the Nile area (Rizzini et al., 1978; Barber, 1981). Conversely, it is strikingly different from other canyon systems described in the Western Mediterranean (e.g. Clauzon, 1982) where no direct evidence of pre-Messinian incision is described (Lofi et al., 2005). This interpretation could however be due to the paucity of record from the pre-MSC records, the base of the Messinian evaporites representing generally the acoustic basement.

Our mapping of a series of Messinian marginal scarps at discrete and constant elevations across the study area (Fig. 2.10) points significantly to the occurrence of distinct (and possibly rapid) base level changes during the MSC. The geometry of the Messinian scarps and of the adjacent gently sloping surfaces is similar to sea cliffs and shore platforms observed in shallow marine settings resulting from wave abrasion at the sea cliff base (Huggett, 2003). If this interpretation is correct, the gently sloping part of Horizon M must therefore correspond to a shore platform. In this case, the location of the hinge point between the scarp and shore platform could indicate the sea-level position during the different stages of the MSC. Analogue features have been described in the Nile Delta area as terraces parallel to the strike of the former Tortonian Nile delta (Barber, 1981). These features are interpreted as regressive terraces

indicating still-stand of base level and related to the northwest migration of the strandline during the fall of the Messinian sea level (Barber, 1981). A series of breaks of gradient have been also observed in longitudinal profiles of Messinian canyons in the Gulf of Lions in the Western Mediterranean (Lofi et al., 2005). These features are interpreted as related to successive sea-level falls leading to adjustment of river base level during the 'desiccation' phase of the MSC (Lofi et al., 2005).

Despite the uncertainty of the relative timing of the erosional events in the study area, the observation of these scarps and platforms on the Levant margin documents repeated phases of base level change during the MSC and provides an important paleogeographic boundary at the transition between subaerial and submarine erosional processes during the MSC. The direct evidence of protracted and multiple erosional events during the MSC suggest that Messinian erosional surface is likely to be of compound origin.

In conclusion, our data support the existence of common large-scale depositional processes in the Mediterranean margins during the MSC, but also advocate a variable modality and controls on the distribution of the Messinian evaporites. This variability could depend on the structural setting of the area analysed and possibly on the existence of a series of separate evaporitic sub-basins in the Western and Eastern Mediterranean, in which paleogeographic divides played an important role, as initially suggested by Montadert et al. (1978).

2.8 Summary and conclusions

The pre-evaporitic setting of the Levant margin is dominated by a series of structural highs related to anticlines of the Syrian Arc foldbelt. The development of these anticlines represented the main factor controlling the pre-evaporitic basin physiography and consequently, the differential accommodation space and the linear NE-SW directed edge of the Messinian evaporitic system. The influence of the anticlines is marked in the marginal area of the Levant Basin, while it is more subdued in the distal area, where the depocentres are mainly controlled by the regional post- rift subsidence pattern.

Our results document the importance of canyon systems for the understanding of the depositional and erosional processes active during the MSC, especially with regards to thickness variations of the proximal and distal part of the evaporitic wedge. In the

Levant area, the Oligo-Miocene submarine canyon systems (Afiq, El Arish and Ashdod Canyons) acted as preferential sites of erosion in the earliest stages of the MSC up to the Levant Basin and mainly as depocentres in the later stages of the MSC. This created the locally irregular geometry of the edge of the evaporites, characterized by major embayments and landward outliers of evaporites.

Additionally, our research provides evidence for the structural and architectural difference between the Levant area and the other Mediterranean margins during the development of the MSC. This refers in particular to the influence of inherited canyon patterns and to the internal stratigraphy of the evaporitic wedge. However, the main analogies observed in the depositional and erosional patterns mean that the study area in the Eastern Mediterranean can be used as an example in other Mediterranean areas where 3D seismic is not available yet and sub-salt imaging is limited. Further research is needed in order to understand the timing and the subaerial or submarine nature of the erosional surfaces observed at the top and the base of the Messinian evaporitic system.

Chapter Three: Clastic systems in the Messinian evaporites¹

3.1 Abstract

This study aimed at investigating evidence for the presence of clastic sediments at the base of the distal Messinian evaporites in the Levant region (Eastern Mediterranean). Seismic geomorphological analysis of 3D seismic data clearly reveals the occurrence of a well-imaged clastic body composed of two closely spaced channel-mouth lobe deposits, within the basal part of the Messinian evaporites. Comparable seismic facies observed at the same stratigraphic level elsewhere in the study area suggest the occurrence of additional clastic deposits and allows their correlation with a long-lived system of canyons (i.e. the El Arish and Afiq Canyons). Their seismic characteristics and the analogy with other coeval deposits in the Mediterranean Basin suggests a submarine (shallow or deep-water) depositional setting for the clastic bodies. Knowledge of the occurrence and distribution of these clastic deposits has considerable significance for the interpretation of the depositional environment of this basinwide evaporitic system.

¹ *Published as:*
C. Bertoni & J. A. Cartwright, Clastic depositional systems at the base of the Messinian (late Miocene) evaporitic series of the Eastern Mediterranean: Evidence from 3D seismic data. Submitted to the Special Publications, Geological Society of London, in press.

3.2 Introduction

The presence of clastic sediments within the Messinian (late Miocene) evaporites in the Mediterranean Basin represents an ongoing topic of debate since the discovery of this giant evaporitic system. Clastic evaporites interbedded with *in situ* gypsum, halite and anhydrite series have been recorded in outcrop in parts of the Mediterranean area (Ricci Lucchi, 1973; Schreiber et al., 1976; Vai & Ricci Lucchi, 1977; Roveri et al., 2001, 2003). Clastic deposits (mainly continental-derived) have also been observed on 2D seismic and well data on the margins of the Messinian evaporitic basin (Barber, 1981; Savoye & Piper, 1991; Lofi et al., 2005). Conversely, the occurrence of clastic sediments within the thick distal evaporitic series and their location within a subaerial or submarine depositional setting are not yet conclusively demonstrated (see e.g. Garfunkel & Almagor, 1987; Lofi et al., 2005).

Recently acquired high-quality 3D seismic data from the Levant region (Eastern Mediterranean, Fig. 3.1) permit the application of seismic geomorphology techniques (Posamentier, 2003) to the solution of this scientific problem. Detailed horizon mapping and areal analysis of seismic attributes (e.g. seismic amplitude) reveal the presence of a high-amplitude body within the lower part of the Messinian evaporites. The morphology and seismic character of this body allows its interpretation as composed of two channel-fed clastic lobes, similar in all aspects to other examples recorded worldwide (e.g. Weimer & Link, 1991; Collison, 1999). Comparable seismic facies observed at the same stratigraphic level in the study area suggest the occurrence of additional clastic bodies and allow their correlation with a long-lived system of canyons on the Levant continental margin (i.e. the El Arish and Afiq Canyons, Druckman et al., 1995).

The main aims of this study are to report the observation of clastic sedimentary bodies, to argue their origin as submarine or subaerial systems, and to discuss the implications of this discovery for the interpretation of clastic sediment fairways during the deposition of the Messinian evaporites. Ultimately, this study documents the predictive importance of 3D seismic analysis for future scientific investigations (e.g. ultra-deep drilling of the Messinian evaporites) aiming to understand the depositional environment of this giant evaporitic system.

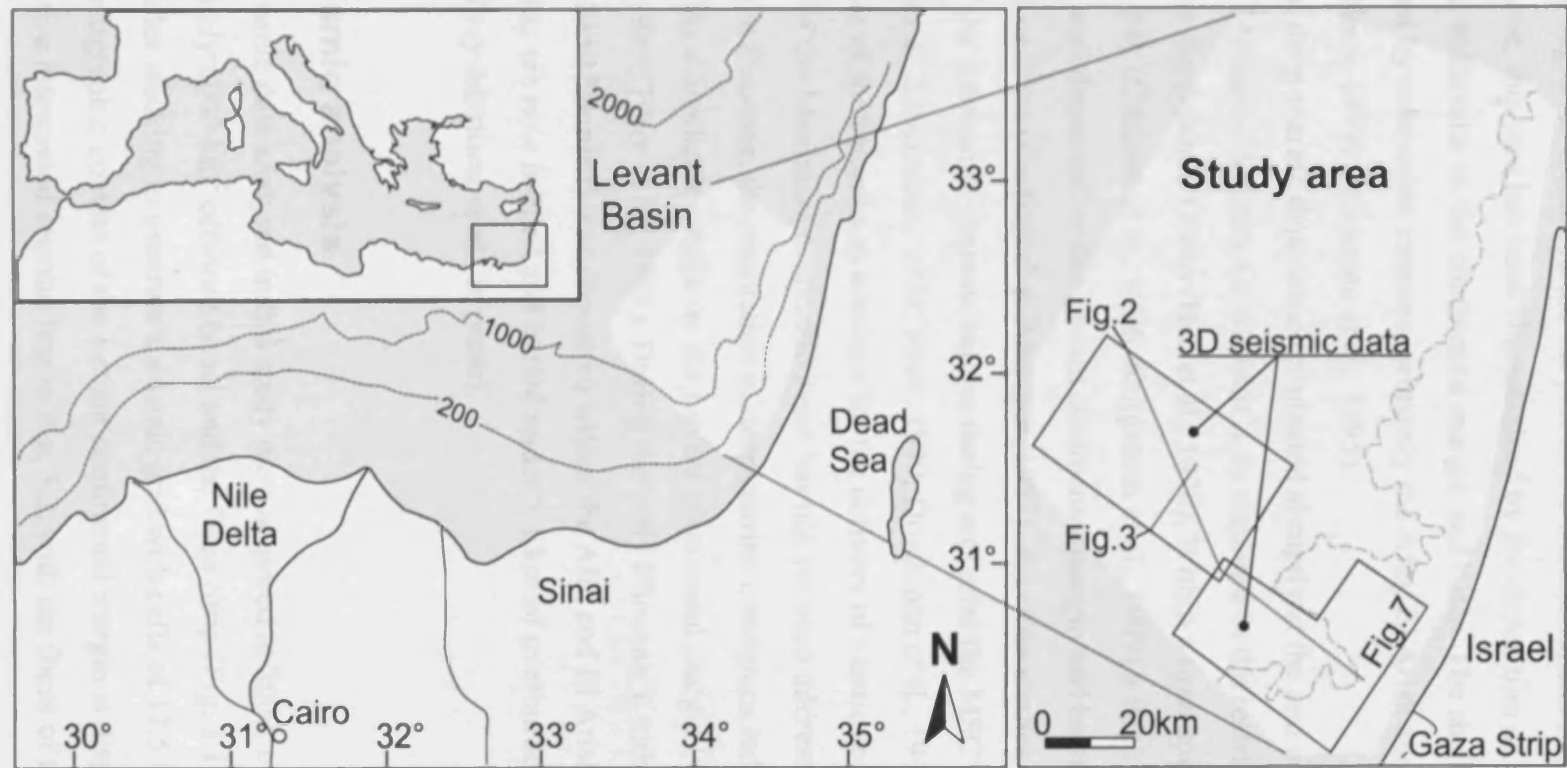


Figure 3.1 Location maps for the study area in the Eastern Mediterranean. The areas where 3D seismic data are available are indicated. The grey dashed line marks the locus of pinch-out of the buried Messinian evaporites (from Bertoni & Cartwright, in press).

3.3 Geological setting

The Levant region is located in the SE part of the Mediterranean Sea (Fig. 3.1). Since the Oligocene, this area has been characterized by the deposition of large volumes of siliciclastic sediments on the continental margin and basin. The shelf and slope areas were incised by submarine canyons, primarily the Afiq, El Arish and Ashdod Canyons (Fig. 3.1, Neev, 1979; Druckman et al., 1995).

Normal deep-marine deposition terminated abruptly at the end of the Miocene, during the Messinian Salinity Crisis (MSC), in response to the restriction of seawater supply from the Atlantic Ocean (Hsü et al., 1978). Within a time-span of significantly less than 1 My (Clauzon et al., 1996; Krijgsman et al., 1999) a thick wedge of evaporites was deposited on the Levant continental margin and basin, where it reaches a thickness of 2 km (Garfunkel & Almagor, 1987). Previous studies document the activity of the submarine canyons before, during and after the MSC in the study area (Buchbinder & Zilbermann, 1978; Neev, 1979; Druckman et al., 1995). However, the specific role of the canyons as conduits for the delivery of clastic sediments to the distal part of the Messinian evaporitic basin has not yet been addressed.

Since the Pliocene, the restoration of deep-marine conditions led to the rebuilding of the marine siliciclastic wedge on the Levant continental margin (Garfunkel & Almagor, 1985; Tibor et al., 1992). During the early Pliocene, a turbiditic basin floor fan (Yafo Sand Member) was deposited within the Afiq and El Arish submarine canyons, that are now infilled and buried under > 1 km of overburden (Druckman et al., 1995; Frey-Martinez et al., in press).

3.4 Seismic analysis

The 3D seismic data analysed in this study were acquired in 2000, over an area of approximately 6000 km² offshore Israel and the Gaza Strip (Fig. 3.1). These data were migrated after stacking to generate a seismic grid with cells of 12.5 by 12.5 m. The general stratigraphic context of the Levant continental margin is displayed with a representative interpreted seismic line in Fig. 3.2, with the focus of this paper being

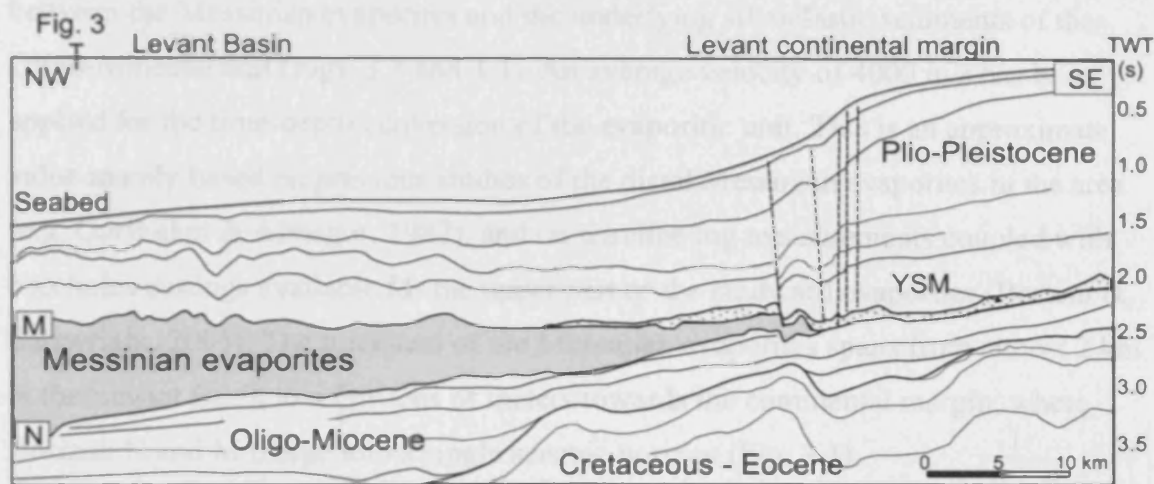


Figure 3.2 Schematic geo-seismic section showing the seismic-stratigraphic context of the study area in the Levant Basin and continental margin (see text for detailed explanation). N= Horizon N; M= Horizon M; YSM= Yafo Sand Member (indicated by the dotted fill pattern). The marginal faults in the Plio-Pleistocene unit are marked by subvertical dashed lines. The crossover point of Fig. 3.3 is also indicated. On the vertical scale, TWT is the two-way travel time expressed in seconds.

3.4.3 Detailed 3D seismic description of HAB1

The best-imaged high-amplitude body is HAB1. Its geometry in cross-section and in plan view is described in detail with reference to a series of seismic sections, time-structure maps and minimum amplitude window extractions (Figs. 3.5 to 3.12). On seismic sections, HAB1 is bounded at the top by horizon ME2, represented by a high-amplitude negative seismic reflection (Fig. 3.5). The zero-phase seismic polarity and

on the Messinian evaporites. The base and the top of this seismic unit are represented by respectively, Horizon N and M (Fig. 3.2), i.e. two distinct seismic events that are regionally correlatable across the Mediterranean Basin (Hsü et al., 1973). In the study area, Horizon M represents a high-amplitude positive seismic reflection generated by the acoustic impedance contrast between the deep-marine siliciclastic sediments of the Plio-Pleistocene unit and the underlying Messinian evaporites (Figs. 3.3 and 3.4). Horizon N represents a high-amplitude negative seismic reflection at the transition between the Messinian evaporites and the underlying siliciclastic sediments of the Oligo-Miocene unit (Figs. 3.3 and 3.4). An average velocity of 4000 m/s has been applied for the time-depth conversion of the evaporitic unit. This is an approximate value mainly based on previous studies of the distal Messinian evaporites in the area (e.g. Garfunkel & Almagor, 1987), and on wireline log measurements coupled with boreholes cuttings available for the upper part of the landward evaporites (Bertoni & Cartwright, 2005). The thickness of the Messinian evaporites spans from almost 2 km in the Levant Basin to a few tens of meters towards the continental margin, where Horizon N and M merge into a single seismic horizon (Fig. 3.4).

The distal Messinian evaporites are seismically composed of alternating transparent facies and continuous seismic reflections (Horizons ME20 to ME50 in Fig. 3.3). In the lower part of this unit, a series of high-amplitude seismic reflections are observed above Horizon N (Fig. 3.4). These reflections are correlatable laterally for up to 6 km (Figs. 3.5 and 3.6). The areal extent of these high-amplitude events is clearly imaged by computing the maximum seismic amplitudes over a 120 ms TWT (two-way travel time) window above Horizon N. The resulting image (Fig. 3.7) shows that they correlate with a series of km-scale high-amplitude bodies with a rather irregular and elongated ellipsoidal morphology. These bodies are located basinward of the pinch-out of the Messinian evaporites and fully confined within this unit (Fig. 3.7).

3.4.1 Detailed 3D seismic description of HAB1

The best-imaged high-amplitude body is HAB1. Its geometry in cross-section and in plan view is described in detail with reference to a series of seismic sections, time-structure maps and maximum amplitude window extractions (Figs. 3.8 to 3.12). On seismic sections, HAB1 is bounded at the top by Horizon ME2, represented by a high-amplitude negative seismic reflection (Fig. 3.8). The zero-phase seismic polarity and

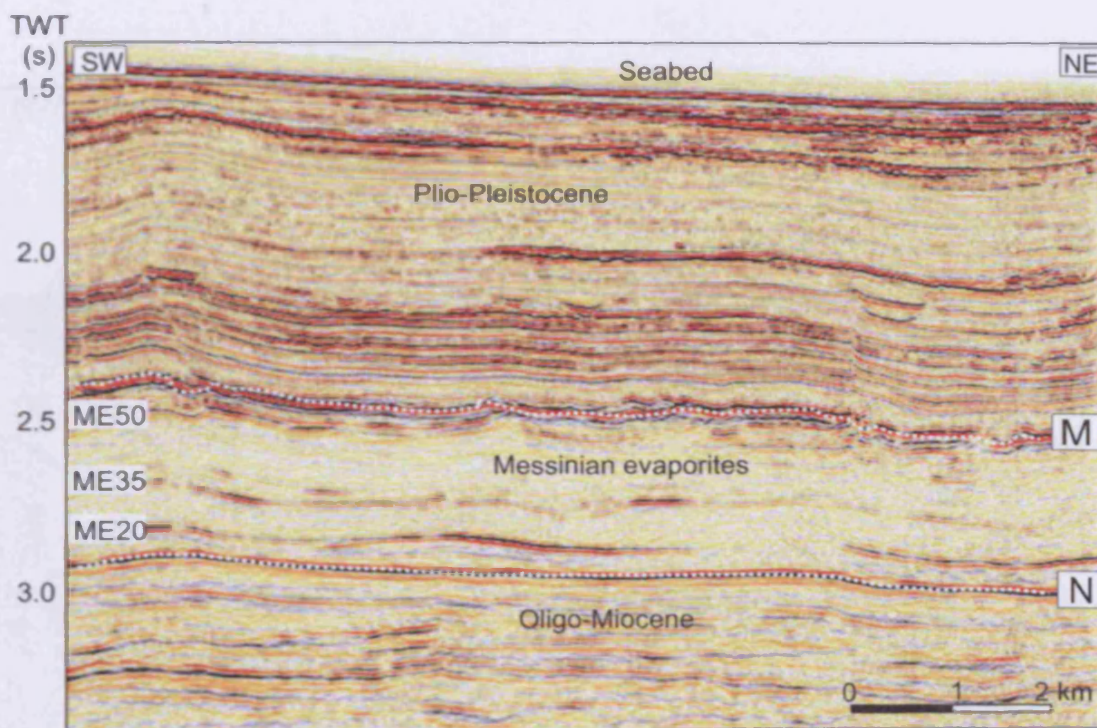


Figure 3.3 Seismic section crossing the study area in a NE-SW direction (location in Fig. 3.1). The stratigraphy of the distal part of the Messinian evaporites is displayed. In this area the Messinian evaporites are seismically composed of transparent facies alternating with medium to low amplitude seismic reflections (Horizon ME20 to ME50).

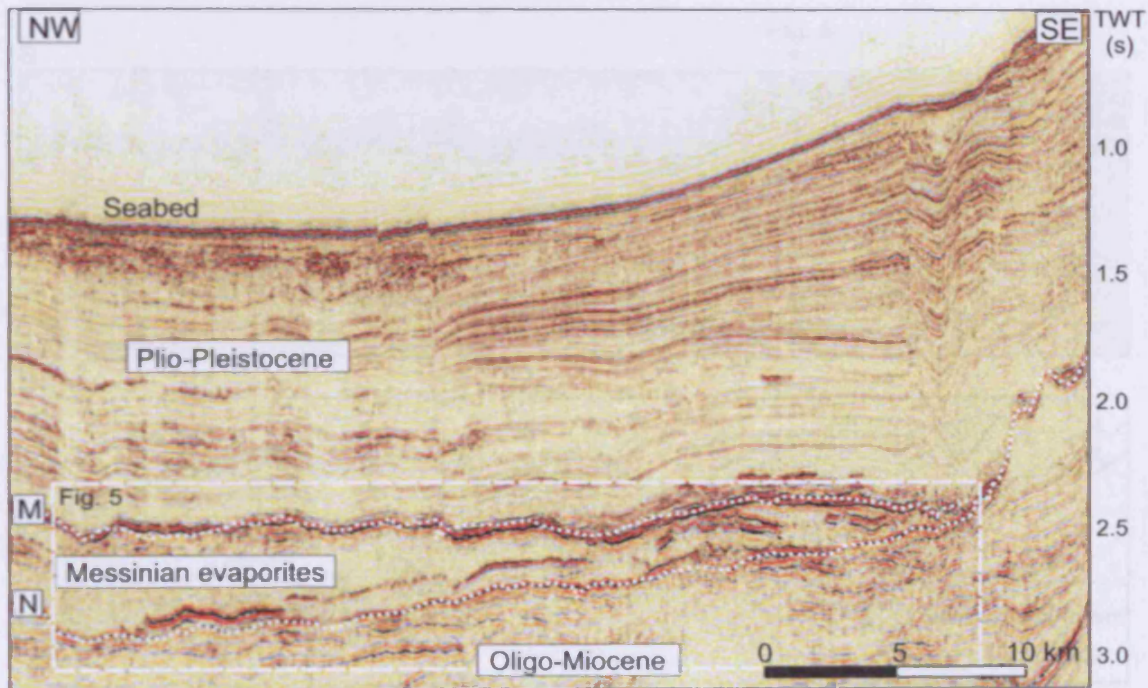


Figure 3.4 Seismic section crossing the study area in a NW-SE direction (see location in Fig. 3.7) displaying the stratigraphy of the Messinian evaporites from their proximal (SE) to their distal (NW) part. Note that the Messinian evaporites form in the study area a wedge from 1.8 km thick in the distal part to a few tens of meters towards the SE, where Horizon N and M merge into a single seismic horizon.

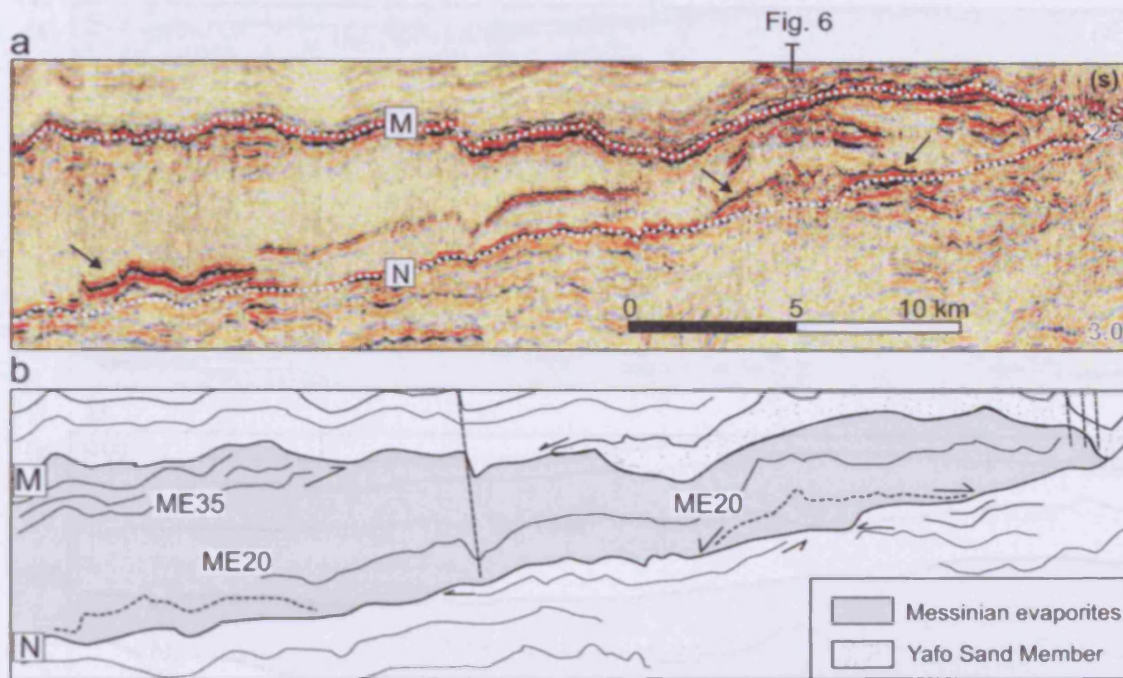


Figure 3.5 Seismic section crossing the study area in a NW-SE direction, and b) interpretation (see location in Fig. 3.7).

a) Close-up of the Messinian evaporites as displayed in the seismic section in Fig. 3.4. In the lower part of this unit, directly above Horizon N, the high-amplitude seismic reflections described in the text are indicated by the black arrows.

b) Line-drawing of the seismic section, with interpretation of faults and terminations of seismic reflections (indicated by black arrows).

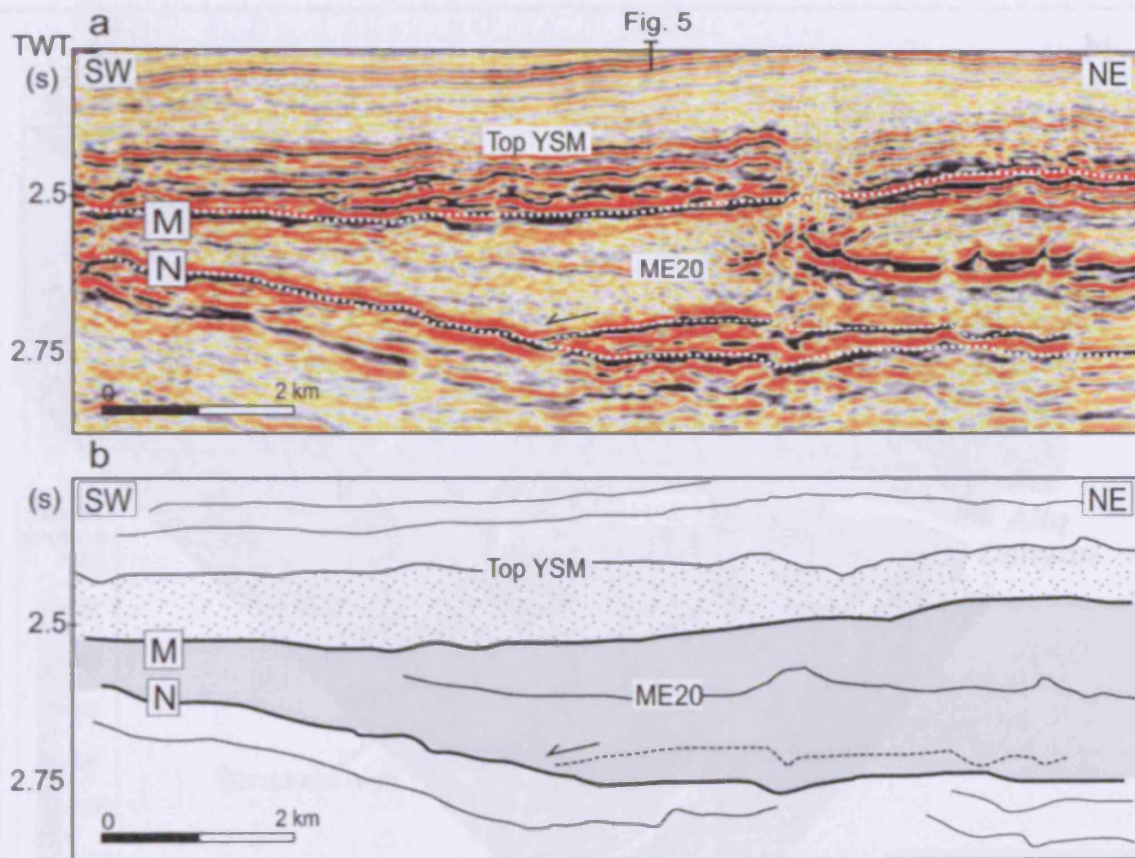


Figure 3.6 Seismic section crossing the study area in a NE-SW direction (see Figs. 3.5 and 3.7 for location).

a) Seismic cross-section with indication of the main seismic horizons and reflection terminations.

b) Line-drawing of the seismic section, with interpretation of faults and terminations of seismic reflections (indicated by black arrows) interpretation. In the lower part of this unit, the onlap termination of the high-amplitude seismic reflection against Horizon N (indicated by the black arrow) should be noted.

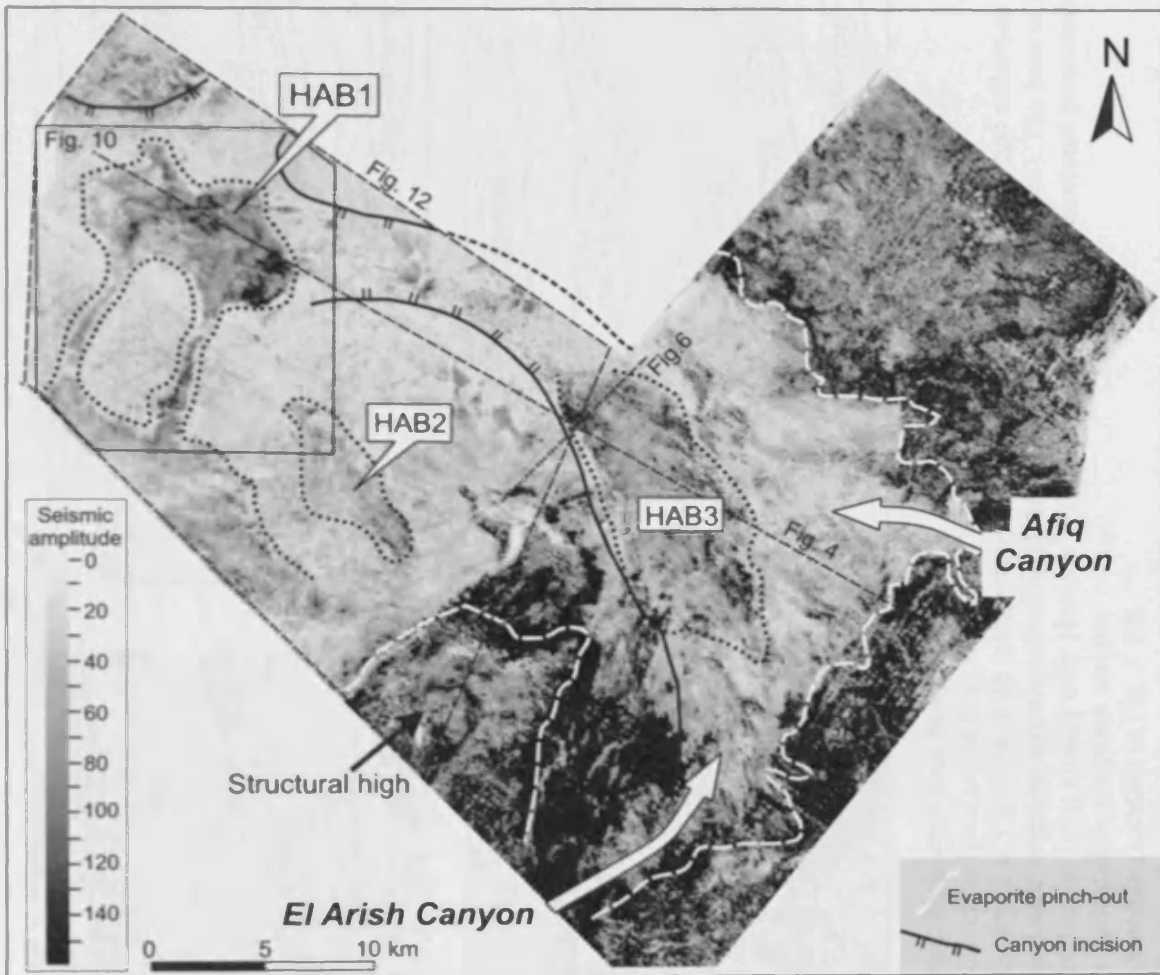


Figure 3.7 Maximum seismic amplitudes calculated over a 120 ms TWT (two-way travel time) window above Horizon N. The resulting image shows that the high-amplitude reflections shown on seismic sections in Figs. 3.4 to 3.6 correlate with a series of km-scale high-amplitude bodies (dark-grey coloured areas, marked with a white dotted line) named HAB1, HAB 2 and HAB 3. The bodies show an irregular and elongated ellipsoidal morphology. These bodies are located basinward of the pinch-out of the Messinian evaporites and thus fully confined within this unit.

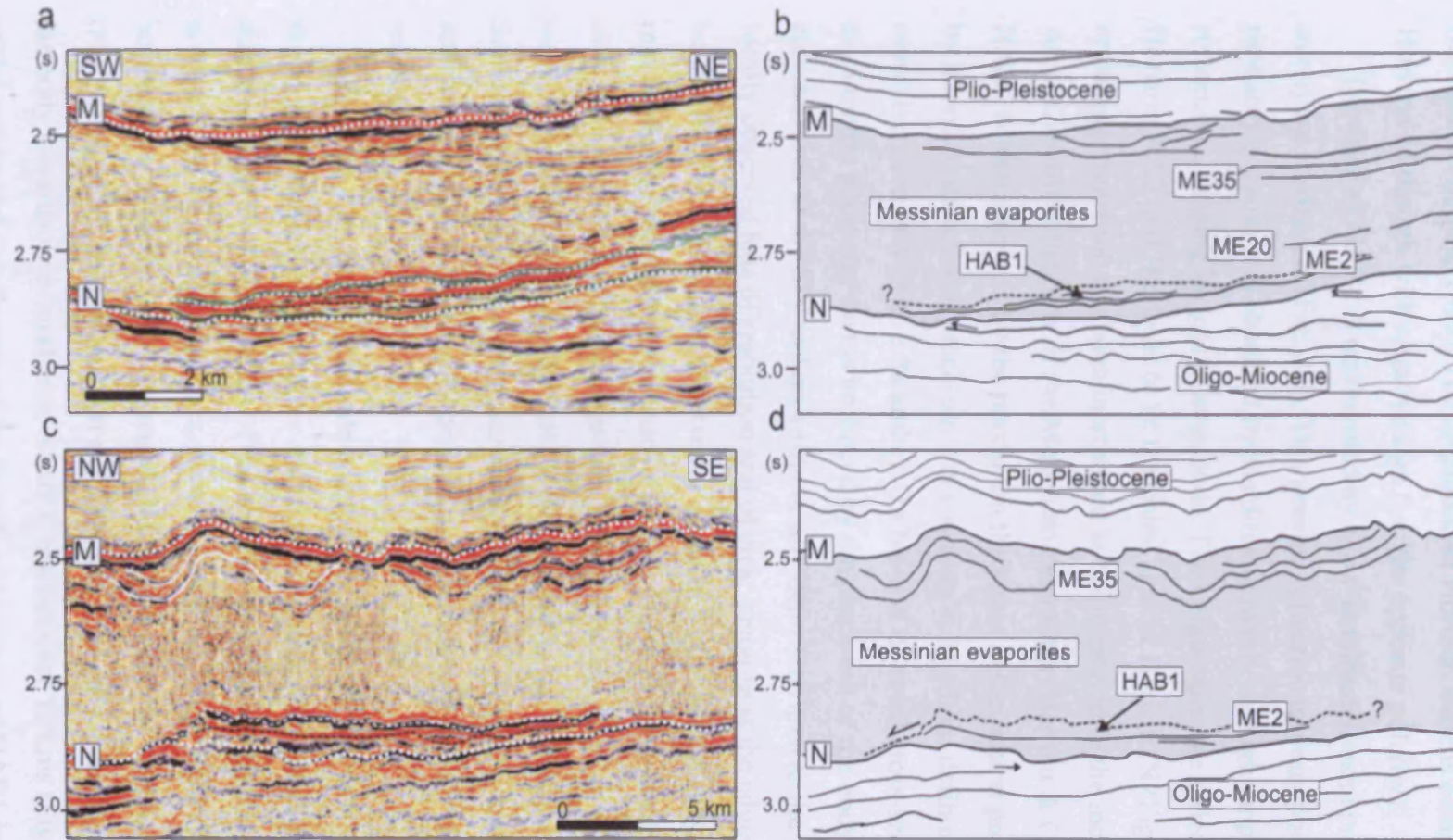


Figure 3.8 Seismic sections across the main high-amplitude body HAB1.

- a) Seismic section oriented in a NE-SW direction (location in Fig. 3.10).
 b) Line-drawing of the seismic section displayed in Fig. 3.8a, with interpretation of the main seismic horizons and reflection terminations. HAB1 is bounded at the top by a high-amplitude negative seismic reflection (Horizon ME2, white dashed line). The base of HAB1 is represented by a low-amplitude seismic reflection lying closely over Horizon N (black dashed line). The erosional truncation of the Oligo-Miocene reflections against Horizon N is indicated by the black arrows.
 c) Seismic section oriented in a NW-SE direction (location in Fig. 3.10).
 d) Line-drawing of the seismic section displayed in Fig. 3.8c, with interpretation of the main seismic horizons and reflection terminations.

negative amplitude character of Horizon ME2 has been assessed by comparison with flat spots observed at similar stratigraphic levels (Brown, 1999). This allows the definition of Horizon ME2 as a 'soft' seismic event generated by a decrease in acoustic impedance (Brown, 1999). The amplitude of Horizon ME2 is comparable to that of Horizon M though with negative sign (i.e. the opposite polarity).

The base of HAB1 is represented by a low-amplitude seismic reflection directly overlying Horizon N (Fig. 3.8). This seismic reflection appears poorly defined probably because it is obscured by the directly overlying high-amplitude seismic reflections, causing its loss in amplitude. The Oligo-Miocene reflections underlying Horizon ME2 and N appear to be truncated against Horizon N (Figs. 3.8a). This erosional truncation has been interpreted as being related to the incision of the Afq-EI Arish Canyon at the base of the Messinian evaporites (Bertoni & Cartwright, in press). HAB1 is characterized by the maximum thickness at the central parts of the body and by lateral bi-directional pinch-out and downlap at its edges, defining an overall mounded geometry (Fig. 3.8a and c). On NE-SW directed cross-sections HAB1 has an asymmetric geometry that is produced by the pinch-out of the body on a structurally elevated area to the SW and on a structurally depressed area to the NE (Fig. 3.9a). The locally observed loss of resolution and of clear imaging at the edges of the body could be due to overlapping and interference of the two opposite polarity wavelets represented by the top and the base of HAB1. These two reflections will be resolved only as long as their distance is greater than half the wavelength of the incident waveform, and this critical distance is defined as the tuning thickness (Badley, 1985). Some internal reflections are observed within HAB1 (Fig. 3.8a and c), although their internal geometry is not clearly defined because it is at the limits of vertical seismic resolution.

The areal maximum amplitude window extraction displayed in Fig. 10a clearly shows that HAB1 has an irregular-elliptic morphology elongated in a NW-SE direction. The maximum radius of the body is approximately 8.5 km and the minimum is 4 km (Fig. 3.10a), the total area covered being ca. 35 km². The thickness of HAB1 is best visualized on the isochron map computed between the base and top of this body (Fig. 3.10b). This map shows that the thickness gradually increases from the edges of the body towards its central area, where it reaches over 100 ms (Fig. 3.10b). A synopsis of the nature and distribution of the lateral terminations of HAB1 is also displayed on

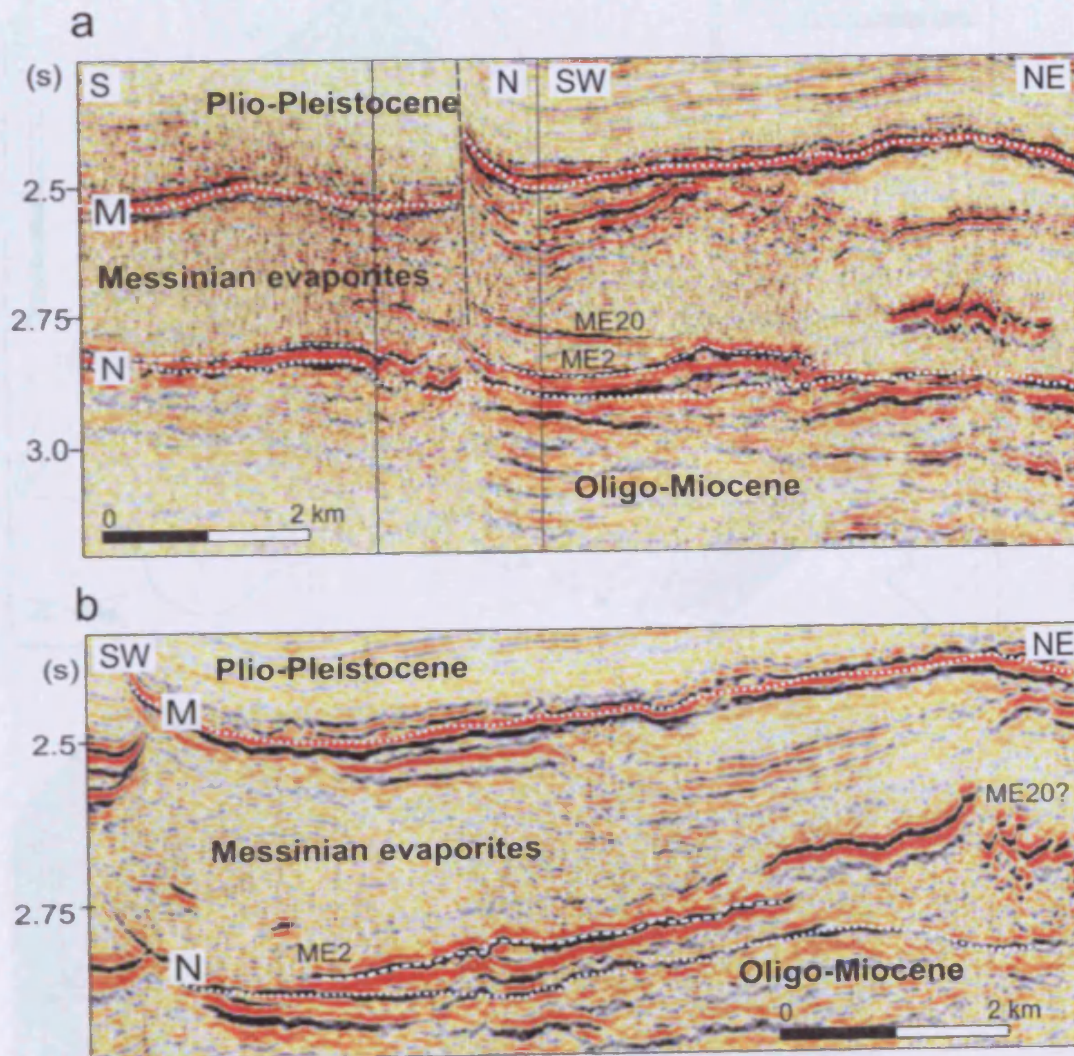


Figure 3.9 Seismic sections crossing the main high-amplitude body HAB1 (location in Fig. 3.10).

a) Seismic section crossing the body HAB1 in a S-N/SW-NE direction. In this section, HAB1 presents an asymmetric geometry that is produced by the pinch-out of the body on a structurally elevated area to the SW and on a structurally depressed area to the NE.

b) Seismic section crossing the body HAB1 in a NE-SW direction. On the north-eastern side of HAB1, Horizon ME2 is deformed by remobilization, hindering the interpretation of the nature of its original termination.

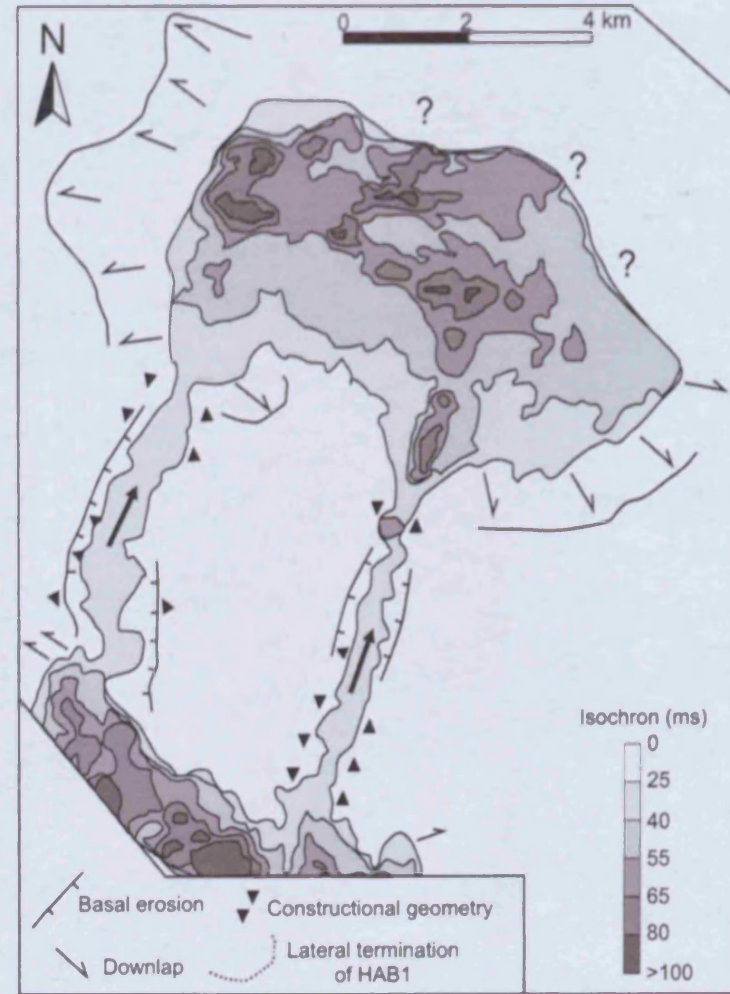


Figure 3.10 Morpho-structural maps of HAB1.

a) Close-up of Fig. 3.7, showing details of the morphology of HAB1 with a different colour display.

b) Isochron map calculated between the base and the top of HAB1. A synopsis of the nature and distribution of the lateral terminations of HAB1 is displayed in this map.

this figure (Fig. 3.10b). Horizon ME2 terminates laterally by downlap to the northwest (Figs. 3.8b and 3.10b). On the northeastern side of HAB1, Horizon ME2 is involved in remobilization caused by tectonic deformation (Fig. 3.9b), therefore we are unable to judge the nature of its original stratal termination and its possible correlation with the overlying reflections. On the eastern side, HAB1 appears to thin at its edge. However, the decrease in amplitude of Horizon ME2 in this area (e.g. Fig. 3.8a) prevents a definitive interpretation of this termination as a low-angle downlap of Horizon ME2 on the base of HAB1, or alternatively as an apparent downlap.

Two ribbon-shaped SE-NW oriented high-amplitude bodies are attached to the main part of HAB1, as clearly displayed in Fig. 10a. These features are approximately 0.5 km wide and 6 km long (Fig. 3.10a) and their thickness ranges from 20 to 50 ms (Fig. 3.10b). In cross-section, these bodies are subtle, convex-upward features (Figs. 3.11a and b). They appear as alternately confined and filling the underlying lows, or totally unconfined and showing a distinct constructional geometry (Fig. 3.11a), being laterally shifted as regards the location of the underlying structural depressions (Fig. 3.11b). Importantly, the isochron map in Fig. 10b defines the presence of two loci of increased thickness (up to > 100 ms) within the main part of HAB1, located immediately NE of the two ribbon-shaped bodies. These bodies are connected landward to a thicker high-amplitude body (up to 100 ms thick), located to the south of HAB1 (Fig. 3.10b). In cross-section (Fig. 3.11c) this body does not present a clear internal geometry and it is highly disrupted by a subsequent deformational phase, thus precluding a more detailed seismic analysis.

In order to define the complex relationship of HAB1 to the underlying basin physiography, we have overlain the amplitude map of Horizon ME2 to the 3D visualization of the time-structure map of Horizon N (Fig. 3.12). This visualization shows that the thicker body to the south of the ribbon-shaped features is located on a structurally elevated area (Fig. 3.12). The main ellipsoidal part of HAB1 is confined to a structurally depressed area to the NW, within the floor of the El Arish-Afiq Canyon (Fig. 3.12). Significantly for their interpretation, the ribbon-shaped features are positioned on a sloping part of the time-structure map of Horizon N that links the structurally elevated area to the SE to the depressed area to the NW (Fig. 3.12).

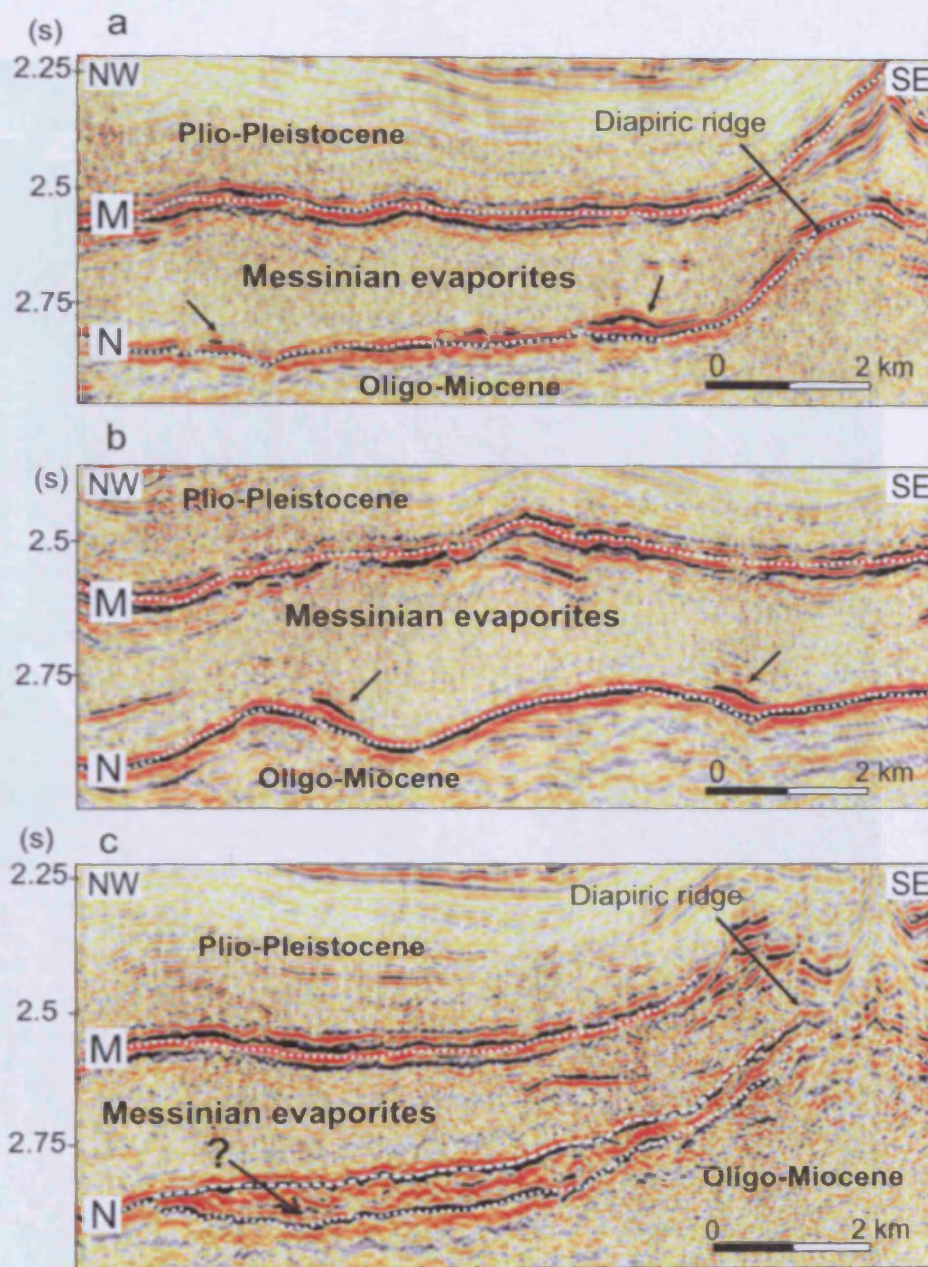


Figure 3.11 Seismic sections crossing HABI (location in Fig. 10a)

- a) Seismic section crossing in a NW-SE direction the two ribbon-shaped high-amplitude bodies attached to the main part of HABI. The bodies are subtle, convex-upward features and appear as alternately confined and filling in the underlying lows or totally unconfined and showing a distinct constructional geometry.
- b) Seismic section crossing the two ribbon-shaped bodies in a NW-SE direction. The bodies appear to be laterally shifted with regard to the location of the underlying structural depressions.
- c) Seismic section crossing the thicker high amplitude body located landward and to the south of the main part of HABI (location in Fig. 10a). In cross-section this body does not present a clear internal geometry because it is highly disrupted by a subsequent deformational phase.

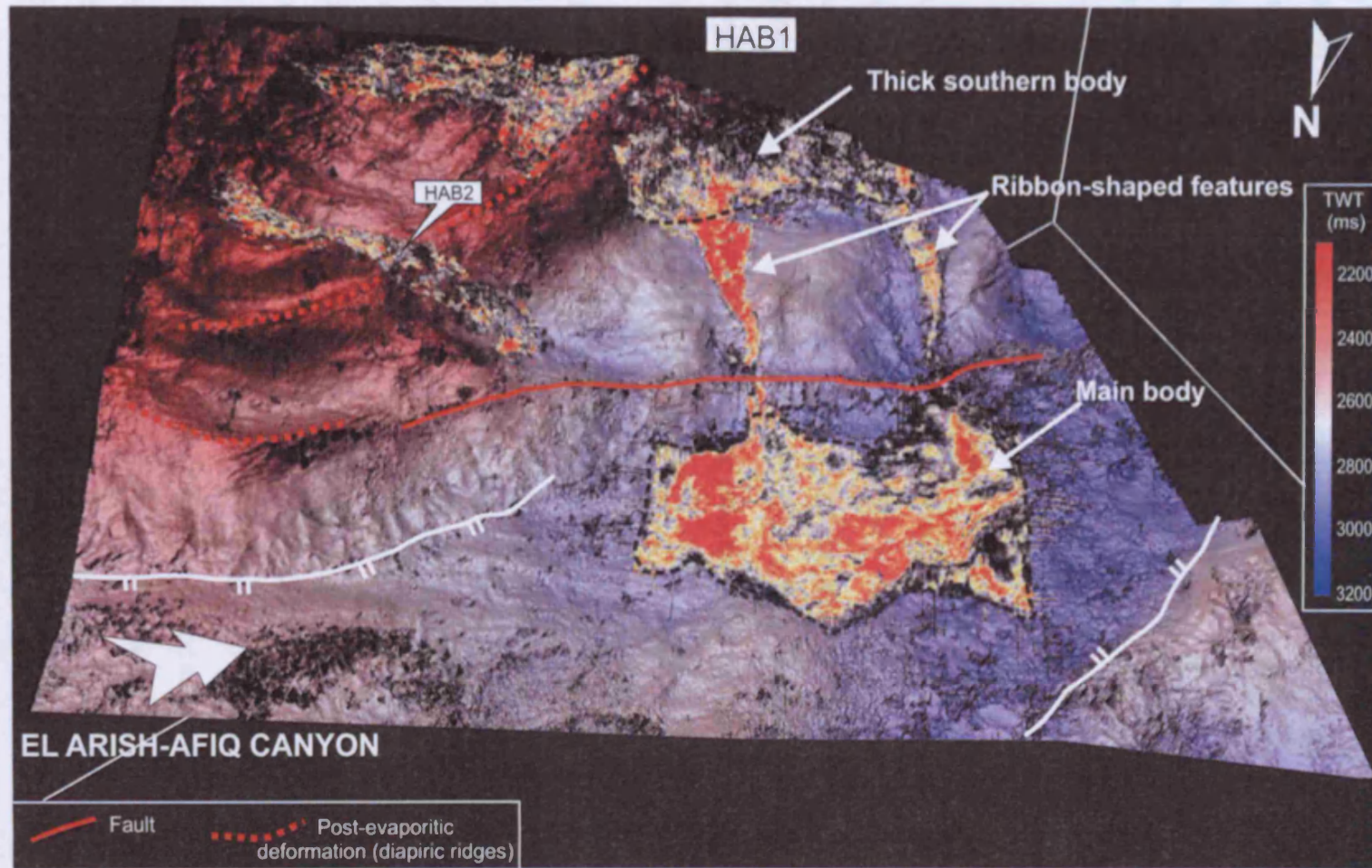


Figure 3.12 Three-dimensional perspective of HAB1 (as displayed in Fig. 3.10) draped over the time-structure map of Horizon N (location in Fig. 3.7). The maximum amplitude values are shown in red colour. This visualization illustrates the overall morphology and geometry of HAB1: the thicker body to the south of the ribbon-shaped features is located on a structurally elevated area and the main part of HAB1 is confined to a structurally depressed area to the NW, within the floor of the El Arish-Afiq Canyon. The ribbon-shaped features are positioned on a sloping part of the time-structure map of Horizon N that links the structurally elevated area to the SE to the depressed area to the NW. Fault and ridges indicated represent post-evaporitic deformational structures.

3.5 Interpretation

The most important features for the diagnosis of the high-amplitude body HAB1 are its lateral terminations, seismic character and shape. A key observation is that HAB1 presents an overall mounded geometry determined by lateral downlap and bi-directional pinch-out. Three main depositional bodies can be developed as mounded seismic features in evaporitic settings: halite pods (Taylor, 1998; Hodgson et al., 1992; Bishop et al., 1995), carbonate build-ups (Taylor, 1998) or clastic lobes (e.g. Mitchum, 1985). The simplest way to discriminate among these three possible interpretations is to assess the amplitude and polarity of the top of HAB1 in more detail.

The high-amplitude 'soft' seismic event defining the top of HAB1 is due the acoustic impedance contrast between the upper and lower units, and is a product of the different seismic velocities and densities of the two lithologies as juxtaposed at the boundary. The similarity in amplitude of Horizon ME2 to Horizon M and their opposite polarity (Fig. 3.8), would be consistent with Horizon ME2 representing a similar magnitude of acoustic impedance contrast, but with reverse relationship (evaporites overlying siliciclastic deposits).

In addition to the argument based on the acoustic character, perhaps the most significant characteristic for the diagnosis of the body is its morphology in plan view. HAB1 is composed of a main ellipsoidal part and of two attached ribbon-shaped bodies (Fig. 3.10a). This morphology is remarkably similar to channels feeding a downslope clastic body (Mitchum, 1985; Posamentier & Erskine, 1991; Weimer & Slatt, 2004). Conversely, the feeder channels would not be expected to develop in halite pods or carbonate build-ups. Based on the previous observations, we interpret HAB1 as a constructional clastic depositional body developed downstream of points where laterally confined flows from the feeder channels expand (e.g. Reading, 1999). The presence of the two feeder channels suggests a double-point source of the body from the SE (Fig. 3.10a). This interpretation is consistent with the presence of two depocentres immediately basinward of the two feeder channels (Fig. 3.10b). The two depocentres define a geometry analogous to clastic lobes generally observed at the termini of the feeder channels (Weimer & Slatt, 2004). The main part of the clastic

body can thus be described as composed of two closely spaced channel-mouth lobe deposits.

The main part of HAB1 overlies the floor of the El Arish-Afiq Canyon (Fig. 3.7). However, the location and direction of the feeder channels suggests that the source of sediment supply to the clastic body is lateral to the main canyon path (Fig. 3.7). The thicker body located to the south of the feeder channels (Fig. 3.10b) could represent the source, or a locus of accumulation of the clastic deposits in an intervening intra-slope basin. The clastic body appears as an overall constructional feature with only limited erosion observed at the base of the feeder channels and of the main body. The limited thickness of the body hinders the resolution of subtler depositional features such as channels within the lobes, and this precludes a detailed sequential seismic geomorphology analysis (Posamentier, 2003). The lack of clear lapout terminations and the uncertain correlation of Horizon ME2 to the north and east suggest that the clastic body could be much more extensive than mapped.

The other high-amplitude bodies observed in the study area (HAB2 and HAB3 in Fig. 3.7) occur at a stratigraphic position and show seismic characteristics comparable to HAB1 (Figs. 3.5 and 3.6). Although their morphology in plan view is less clearly defined than that of HAB1 (Fig. 3.7), we interpret them as clastic bodies by analogy with the interpretation of HAB1. HAB3 forms an elongated feature located at the intersection between the El Arish and Afiq Canyons (Fig. 3.7). Albeit no evidence of feeders is observed, the geographic position of this body suggests that the two canyons acted as the main conduits for the sediment supply. Clastic input from the El Arish - Afiq Canyon is registered in the study area from the Oligocene through the early Pliocene (Druckman et al., 1995; Frey-Martinez et al., 2005). No specific record in the literature exists for the clastic input during the deposition of the Messinian evaporites. We suggest that it is likely that such clastic supply continued even during the MSC, because the Levant continental margin was actively being eroded at this time (Gvirtzman & Buchbinder, 1978).

The seismic amplitude response of these clastic deposits is complex to interpret as it depends on the rock physics, thickness and fluids in the sediment (Weimer and Slatt, 2004). Therefore, further constraints on the lithology of the body (i.e. siliciclastic and/or evaporite or carbonate dominated) are not available simply considering the relative amplitude and polarity of the seismic reflections. Based on the pre-evaporitic

dominant siliciclastic setting of the area of interest and on the seismic geomorphological analysis here presented, we consider it more likely that the clastic deposits are dominantly represented by siliciclastic sediments. An evaporite clastic component could be possible if the reworked clastic sediments were derived from marginal evaporitic deposits. This could potentially occur considering the substantial diachroneity observed within the Messinian evaporites of different Mediterranean areas, with some marginal evaporitic deposits pre-dating the basinal evaporitic series (e.g. Rouchy, 1982; Butler et al., 1995; Clauzon et al., 1996; Riding et al., 1998).

We can give an estimate of the time-depth converted thickness of the body HAB1, based on a dominantly siliciclastic composition, and on the analogy with submarine siliciclastic fan deposits observed at similar depths in the study area, i.e. the Yafo Sand Member of early Pliocene age (unpublished well reports; Frey-Martinez et al., in press). The average seismic velocity obtained on wells for these deposits is 2000-2500 m/s which applied to HAB1 results in a thickness range of 100-125 m. The seismic velocity, and consequently, the thickness of the clastic body HAB1 would be significantly higher if the clastic deposit had instead an evaporitic component. Similarly, the data available do not allow us to determine with any certainty whether the evaporites enclosing or overlying the clastic bodies have a primary or clastic origin. Nonetheless, the analysis of the Messinian evaporites directly overlying the high amplitude bodies shows no evidence of any development of similar clastic bodies at higher stratigraphic levels, and the interbedding of clastic units therefore appears to be confined within the basal part of the evaporitic succession.

3.6 Discussion

3.6.1 Distribution of clastic sediments within the Messinian evaporites

Clastic sediments can constitute an important component of basinwide evaporites, as previously stressed in many studies (Schlager & Boltz, 1977; Schreiber, 1988; Martinez del Olmo, 1996; Kendall & Harwood, 1999; Peryt, 2000; Manzi et al., 2005). In the Western Mediterranean, a subject of current intense debate is whether a conspicuous part of the Messinian evaporitic unit has a clastic rather than evaporitic character (e.g. Lofi et al., 2005).

The clastic lobes described in this study are clearly located within the basal part of the distal Messinian evaporitic unit. Therefore, their occurrence implies that significant volumes of clastic sediments were supplied to the Levant Basin during the early stages of the deposition of the Messinian evaporitic unit. This is clearly shown by the stratigraphic position of the clastic bodies analysed above the erosional surface defining the base of the Messinian evaporites in this basin (i.e. Horizon N). The absence of similar clastic bodies within the overlying evaporites could be due to the fact that they deposited in different areas of the basin, or conversely, it could be linked to the subsequent inactivity of the fairways supplying the clastic sediments. Both hypotheses might be related to a variation in the base-level of erosion and clastic supply or to a change in the efficiency of the distributary system, and would be consistent with the high variability of depositional environments in evidence during the Messinian Salinity Crisis.

3.6.2 Depositional environment - submarine or subaerial?

The morphology and seismic character of clastic bodies are generally similar in either subaerial or submarine settings (Weimer & Link, 1991; Collison, 1999). In order to define the depositional environment of the clastic lobes composing HAB1, additional information must be taken into account, regarding any evidence for coeval subaerial exposure in the basin, and the position and geometry of the clastic bodies within the Messinian evaporites.

The physiography of the Levant continental margin during the MSC was characterized by structurally elevated areas landward of the pinch-out of the Messinian evaporites (Bertoni & Cartwright, in press). In these areas evidence of subaerial exposure is recorded as:

- A prominent erosional surface characterised by a dendritic drainage pattern (Gvirtzmann & Buchbinder, 1978, Mart & Ben Gai, 1982) comparable to the Messinian erosional surfaces described on the Ebro, Gulf of Lions and Nile continental margins (Ryan, 1978; Stampfli & Hocker, 1989; Guennoc et al., 2000; Frey-Martinez et al., 2004). These erosional surfaces closely resemble a badlands topography and are interpreted as subaerial (Ryan, 1978; Stampfli & Hocker, 1989; Frey-Martinez et al., 2004).

• A series of marginal scarps (Fig. 3.13, Bertoni & Cartwright, in press), that are analogous to the wavecut platforms and rejuvenation terraces observed in the nearby Nile delta (Barber, 1981). Importantly, the clastic deposits are located in an area basinward of the pinch-out of the Messinian evaporites, where such morphological evidence of subaerial exposure (badlands and/or terraces) is not observed (Figs. 3.7 and 3.13). Furthermore, the base of the Messinian evaporites directly beneath the clastic bodies shows evidence of erosion by a few confined incisional features related to the El Arish – Afiq Canyons (Figs. 3.7 and 3.13). This downslope change in the stream pattern from 'badlands' erosion to basinward focused incision would be consistent with a transition to a submarine environment.

Based on data compiled from previous studies, the clastic bodies HAB1, HAB2 and HAB3 appear to be located approximately at the same distance from the pinch-out of the Messinian evaporites (Fig. 3.13). However, the location of the channels feeding the body HAB1 appears to suggest that the source of sediment supply to this clastic body is lateral to the El Arish-Afiq Canyon (Fig. 3.13). Therefore, the basinward extension of the El Arish and Afiq Canyons appears to have acted as a bathymetrically depressed area attracting sediments from the south-west of the study area, externally to the El Arish and Afiq Canyons. The source of clastic supply could be either represented by a tributary of the El Arish Canyon, or by the Nile delta area, as suggested by the regional drainage pattern observed at the base of the Messinian evaporites (Fig. 3.13; Ryan, 1978). It is significant to note that during the Messinian lowstand, the Nile delta shifted extensively seawards (see e.g. Barber, 1981), thus approaching the area of the body HAB1. Consequently, this area would be located in close proximity of the Eonile and Eosahabi deltas, i.e. the two major sources of clastic material in the Eastern Mediterranean during the Messinian (Griffin, 2002). Based on these observations, the pre-Pliocene Nile delta system could be considered as a likely source of sediment supply for the clastic body HAB1.

A further indication of the depositional setting of the clastic body HAB1 arises from the analysis of its depositional geometry. It is noteworthy that the geometry of the feeders is mostly unconfined and convex upward i.e. mainly constructional, and this is generally regarded as typical of submarine rather than subaerial settings (Reading, 1996). The apparent effect of differential compaction in creating this geometry can be ruled out on account of the absence of incision or of downwarped reflections directly

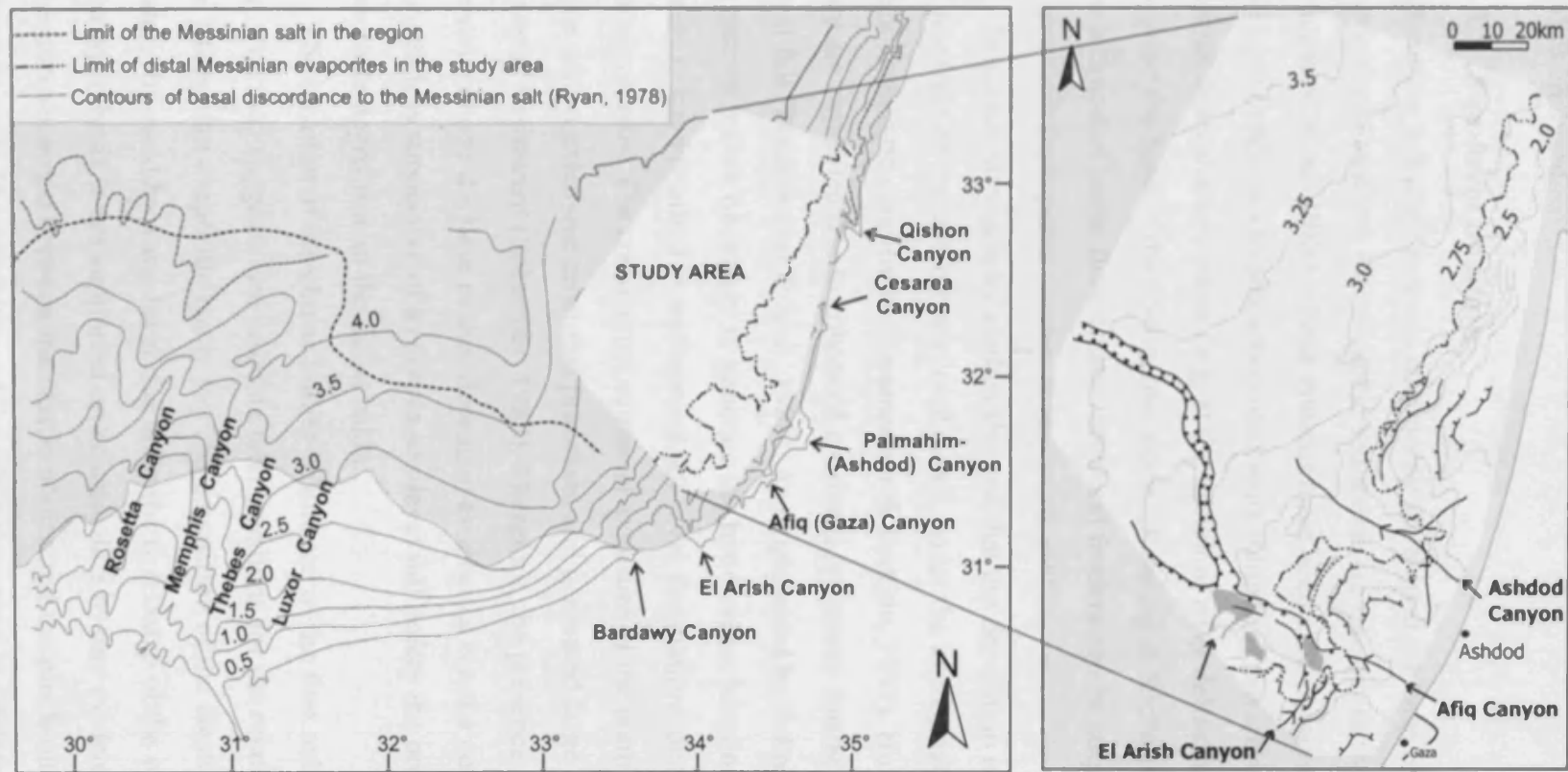


Figure 3.13 Map of the sector of the Eastern Mediterranean analysed, showing the regional setting of the basal discordance to the Messinian salt (and associated evaporite and clastic formations) and its marginal continuity with Horizon M (contour lines in seconds TWT; after Ryan, 1978). The landward limit of the Messinian salt in the region is also indicated (after Sage & Letouzey, 1990; Loncke, 2002; Bertoni & Cartwright in press). In the figure to the right, the distribution of the clastic sediments (in grey) is shown within the paleogeographic context of the base of the Messinian evaporites. Canyon incisions, erosional scarps and contour lines (in seconds TWT) of the base of the Messinian evaporites are after Bertoni & Cartwright (in press). The grey areas identify the location of the clastic deposits described in this study.

underneath the feeders. Based on these observations, we conclude that a submarine (shallow or deep-water) setting is more plausible than a subaerial setting for the clastic bodies analysed.

3.6.3 Sea-level position

Submarine turbiditic systems commonly develop at the base of slopes, within depositional systems where clastic sediments are transported via gravity-induced processes (Stow, 1986). These systems have been extensively studied mainly due to their importance as hydrocarbon reservoirs (Gluyas & Swarbrick, 2004). They can deposit from shallow-water (e.g. at the mouth of river deltas) to deep-water settings (beyond the base of the continental slope) (Reading & Richards, 1994). Furthermore, the location of basin-floor clastic lobes and feeders can be strongly influenced by active fault lineaments (Ratley & Hayward, 1993).

Sequence stratigraphy studies showed that the deposition of clastic lobes can occur at any tract of the relative sea-level curve, under the appropriate physiographic and sedimentologic conditions (Posamentier & Erskine, 1991). However, most commonly they are deposited due to enhanced erosional processes during intervals of relative sea level fall (Posamentier & Vail, 1988). As emphasized by Schreiber (1988) the cut-off in marine inflow necessary to generate the hypersaline Messinian evaporitic basin is likely to have resulted in widespread sea-level fluctuations during the Messinian Salinity Crisis. The consequent subaerial exposure of the continental margins would have driven extensive erosional processes and generated large quantities of reworked material basinward (Schreiber, 1988). Therefore, the presence of submarine clastic deposits above the base of the Messinian evaporites is not a conclusive proof but it is nonetheless supportive of a relative sea-level fall before the onset or at the beginning of evaporite deposition in the distal basin.

The location of the clastic bodies basinward of the first onlap of the evaporites (see e.g. Fig. 3.4) suggests two possible interpretations for the relative sea-level history of the Messinian evaporitic basin: (1) The deposition of the clastic bodies in shallow water, followed by a sea-level rise up to the first onlap of the evaporites. However, this first hypothesis is not supported on seismic data by any evidence of a subaerial exposure recorded between the clastic bodies and the pinch-out of the Messinian evaporites; (2) The deposition of the lobes occurring in a relatively deeper water

setting, with the sea level positioned not beyond the first onlap of the evaporites. The validity of either of these hypotheses needs to be tested by additional lithological and biostratigraphic constraints, and studies of basinal architecture of the evaporitic system. Sub-salt boreholes penetrating the clastic system are required in this key area of the Mediterranean Basin to confirm our seismic interpretation and consequently, to provide a full understanding of the processes acting at the initial stages of the Messinian Salinity Crisis.

3.7 Conclusions

- The analysis of 3D seismic data from the Levant Basin and continental margin has provided conclusive evidence of the presence of significant amounts of clastic sediments in the basal part of the distal Messinian evaporites in this area.
- Seismic geomorphology techniques revealed the presence of a remarkably well imaged clastic body at the base of the Messinian evaporites. This body is composed of two channels feeding two main downslope lobes. Comparable seismic facies observed at the same stratigraphic level suggest the occurrence of additional clastic bodies and allows their correlation with a long-lived system of canyons on the Levant continental margin.
- Based on the seismic geometry and the basin physiography during the deposition of the Messinian evaporites, we conclude that a submarine (shallow or deep-water) setting is more plausible than a subaerial setting for the clastic bodies analysed. Further studies and data are needed in order to define more accurately the water depth at which the clastic bodies deposited and consequently, the relative sea-level history in this part of the Messinian evaporitic basin.

Chapter Four: Unconformity at the top of the Messinian evaporites¹

4.1 Abstract

This study uses the integration of seismic (3D and 2D) and well data to produce a detailed seismic-stratigraphic analysis of the basinal Messinian (late Miocene) evaporites in the Levant region (Eastern Mediterranean). Mapping and sequential analysis of a series of intra-evaporitic horizons and of the packages bounded by them has been undertaken throughout the study area. The application of this methodology permitted the detection of a discordant relationship between the intra-evaporitic horizons and the top of the Messinian evaporites (Horizon M) and, subsequently, the definition of Horizon M as an erosional unconformity. Thus, this study provides the first clear evidence of the occurrence of widespread areal erosion at the top of the basinal Messinian evaporites in the Levant region.

Furthermore, the structural analysis of the deformed intra-evaporitic horizons has documented the occurrence of an early phase of evaporite deformation at the end of the Messinian, preceding the completion of the erosional truncation expressed at Horizon M. The most likely mechanism of deformation is considered to be differential loading associated with a prograding shelf wedge on the basinal evaporitic system. The direction of the intra-evaporitic compressional structures indicates that the deformation could have been initiated by the aggradation and progradation of the Nile delta and submarine fan during the final stages of the deposition of the Messinian evaporites.

¹ Submitted as:

C. Bertoni & J. A. Cartwright, Origin of the unconformity at the top of the basinwide late Miocene evaporites in the Eastern Mediterranean. Submitted to Basin Research.

4.2 Introduction

The late Miocene (Messinian) evaporitic series and erosional surfaces have been extensively investigated throughout the Mediterranean Basin, to unravel the events that led the so-called 'Messinian Salinity Crisis' (Ryan et al., 1973; Hsü et al., 1978). Nonetheless, the interpretation of the original depositional geometry of the basinal part of this evaporitic system is still uncertain in most of the Mediterranean regions, mainly due to limited availability of subsurface data (e.g. Hardie & Lowenstein, 2004). In this study, we use integrated seismic (3D and 2D) and well data to analyse the basinal Messinian evaporites in the Eastern Mediterranean. Specifically, we aim the origin of the surface defining the top of the Messinian evaporites, discussing its significance for the understanding of the processes acting during the last stages of the Messinian Salinity Crisis.

It is widely accepted that the deposition of the Messinian evaporites terminated at the end of the Messinian Salinity Crisis due to a basinwide marine transgression of early Pliocene age (Cita, 1975; Hsü et al., 1977; McKenzie, 1999). Alternative hypotheses suggest a gradual or a late Messinian refilling in some areas of the Mediterranean Basin (e.g. Riding et al., 1998; Krijgsman et al., 1999, 2001). Erosion at the top of the Messinian evaporites and in the late Messinian has been recorded in some marginal areas of the Mediterranean basin (Roveri et al., 2001; Lofi et al., 2005; Cornée et al., 2006). In the Levant-Nile region, a discordance can be observed between the nearly horizontal top of the evaporites and the underlying westward dipping intra-evaporitic reflections on the regional 2D seismic profiles published by Ryan (1978). The lack of detailed and continuous documentation from the available seismic data and one-dimensional well record has hindered the interpretation of the role of tectonic movements and/or sea-level changes in forming this discordant upper boundary.

This paper presents a study based on seismic and well data from the Levant Basin in the Eastern Mediterranean. This dataset allowed the definition and detailed mapping of the top of the Messinian evaporites (Horizon M) and of a series of intra-evaporitic seismic horizons. Horizon M is represented on a semi-regional scale by a broadly horizontal surface, deformed by short wavelength faults and folds, and concordant with the overlying Pliocene seismic reflections. The intra-evaporitic horizons dip to the NW

and are discordant to Horizon M. This discordant relation defines, in seismic stratigraphic terms, either a toplap or an erosional truncation surface (Mitchum et al., 1977). We interpret this discordant surface based on three fundamental parameters: (1) the distribution and geometry of the terminations of the intra-evaporitic horizons, (2) the relationship to their structural deformation and (3) the thickness variations of the intra-evaporitic packages. Moreover, the analysis of the timing and mechanism driving the intra-evaporitic deformation gives important clues for the understanding of the top evaporitic setting, and of early stages of salt tectonic deformation.

The main aim of this paper is to show that the top surface of the Messinian evaporites in the Levant Basin represents an unconformity due to a basinwide erosional event. This is in marked contrast to previous interpretations of this important boundary in this area. We use our results to discuss whether the observed regional erosional truncation surface was caused by a regression or transgression at the end of the Messinian Salinity Crisis. We ultimately intend to discuss the wider significance of the occurrence of erosional events during the deposition of the evaporites for the general debate on the depositional and structural setting of the Messinian evaporites in the Mediterranean Basin.

4.3 Geological background

The study area is located in the Levant Basin, and is delimited by the Nile cone to the southwest, by the Erathosthenes Seamount and Cyprus Trench to the northwest, and by the Dead Sea fault system to the east (Fig. 4.1). Since the Oligocene, the Levant area was configured as a shelf to basin siliciclastic system (Druckman et al., 1995; Buchbinder & Zilbermann, 1997). During the Oligo-Miocene the continental slope was incised by prominent submarine canyons (Druckman et al., 1995; Buchbinder & Zilbermann, 1997).

At the end of the Miocene, normal marine sedimentation was abruptly interrupted by the onset of the Messinian Salinity Crisis (MSC), an event recorded in the entire Mediterranean Basin (Ryan et al., 1973; Hsü et al., 1977, 1978). During this period, the progressive restriction of the gateways to the world oceans caused the partial isolation of the Mediterranean Basin, the widespread erosion of the continental margins, and the deposition of thick sequences of evaporites in the deep basinal areas (Hsü et al., 1977,

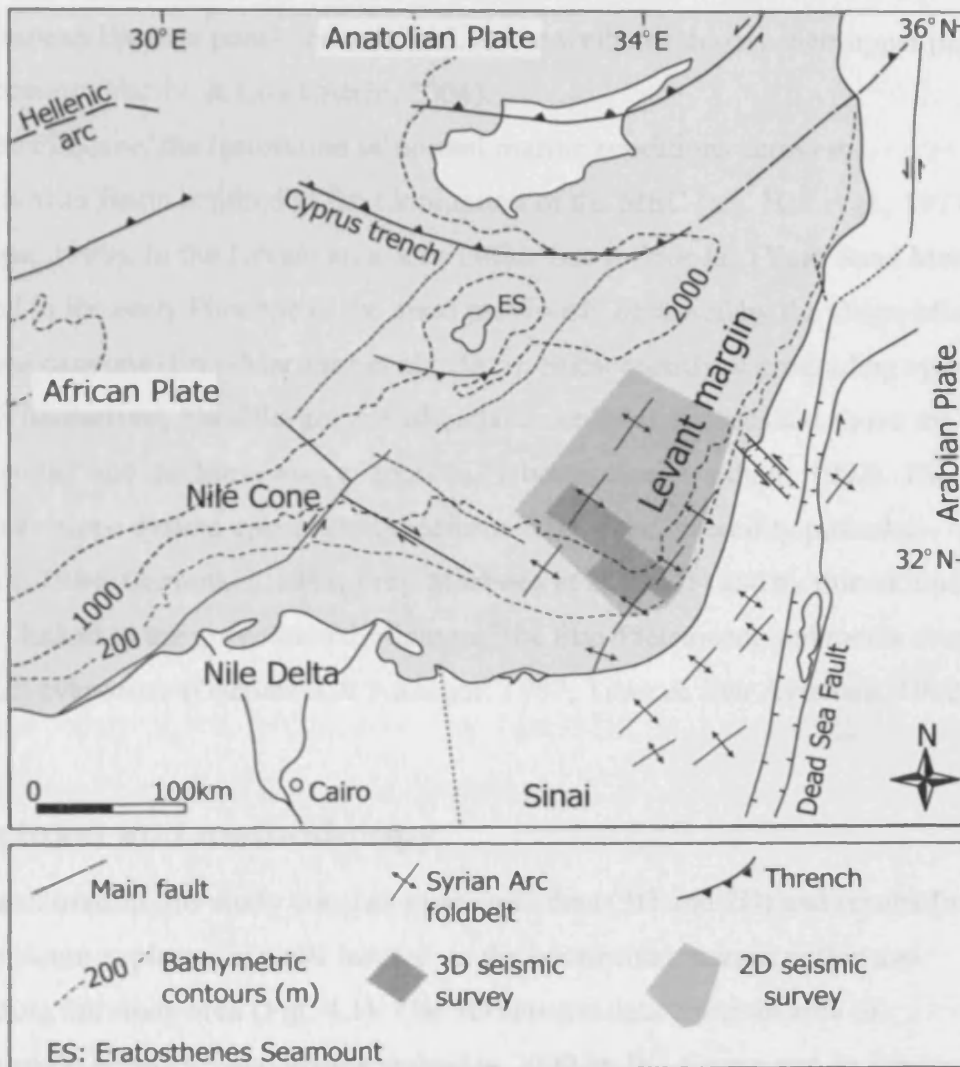


Figure 4.1 Location map showing the main structural elements of the Levant-Nile region (after Neev & Ben-Avraham, 1977; Tibor et al., 1992; Robertson, 1998; Abdel Aal et al., 2000; Vidal et al., 2000) with indication of the study area (2D and 3D seismic surveys).

1978; Cita & Ryan, 1978). The Levant area was characterised by the deposition of evaporites extending from beneath the present-day shelf (Neev, 1979; Cohen, 1988; Druckman et al., 1995) to the deep basin (Garfunkel & Almagor, 1987, Tibor & Ben Avraham, 1992). The evaporites observed on seismic data in this area are correlated to the Mavqim Formation recorded in wells on the shelf and on land (Cohen, 1988). So far, the knowledge of the depositional setting of the basinwide evaporites in the Mediterranean Basin is poorly constrained, as the wells reach only their upper part of the succession (Hardie & Lowenstein, 2004).

In the Pliocene, the restoration of normal marine conditions across the Mediterranean Basin resulted in the termination of the MSC (e.g. Hsü et al., 1977; McKenzie, 1999). In the Levant area, a turbiditic basin-floor fan (Yafo Sand Member) deposited in the early Pliocene in the areas previously occupied by the Oligo-Miocene submarine canyons (Frey-Martinez et al., 2005). Subsequently, a prograding system of mainly Nile-derived, Plio-Pleistocene siliciclastic sediments deposited above the Yafo Sand Member and the Messinian evaporites (Tibor & Ben-Avraham, 1992). The present day slope system appears to be deformed by slope instability processes (Almagor, 1984; Garfunkel, 1984; Frey-Martinez et al., 2005) and by thin-skinned tectonics linked to the gravitational gliding of the Plio-Pleistocene sediments above the Messinian evaporites (Garfunkel & Almagor, 1987; Tibor & Ben Avraham, 1992).

4.4 Dataset and methodology

The dataset used in this study consists of seismic data (3D and 2D) and results from nine petroleum exploration wells located on the continental margin within and surrounding the study area (Fig. 4.1). The 3D seismic data cover an area of approximately 6200 km² and were acquired in 2000 by BG-Group and its joint venture partners (Fig. 4.1). The seismic data is near zero phase with SEG normal polarity, i.e. an increase in impedance is represented by a positive amplitude. The 3D seismic dataset was migrated with a single pass 3D post-stack time migration. The seismic surveys were acquired with an in-line trace interval of 6.25 m and a line spacing of 25 m and a sampling interval of 4 ms. The final data for these two surveys were defined on a 12.5 by 12.5 m grid with 6400 bin cells per sq km after processing (unpublished survey reports).

The dominant frequency content of the data varies generally decreasing with depth, being approximately 50 Hz in the Pliocene to recent section. The vertical and lateral resolution for the Pliocene interval is estimated to be respectively 10 m and 40 m, using an average velocity value of 2000 m s^{-1} , as derived from velocity checkshot data (Frey-Martinez et al., in press). Within the Messinian evaporitic unit, the dominant frequency and velocity are considered to be 30 Hz and 4000 m s^{-1} , respectively. Therefore, the resulting vertical resolution is of approximately 35 m. It should be considered, however, that the vertical resolution can change significantly due to the high variability in the frequency content and seismic velocity within the evaporitic unit.

The 2D seismic data consist of a set of multichannel seismic profiles acquired in 1983 and migrated with a post-stack time migration. They cover approximately 6000 km and present a grid spacing of ca. $10 \times 10 \text{ km}$. The 2D seismic data were used in this study for regional correlation and mapping. A set of exploration wells complete the dataset of this study from which wireline logs and unpublished commercial stratigraphic reports, mainly based on cutting analyses were available. The well data were used for stratigraphic and lithological analysis, for correlation of the depositional units and for time-to-depth conversion.

4.5 Seismic stratigraphy of the Messinian evaporites

The Messinian evaporites constitute a clearly-defined seismic stratigraphic unit bounded below and above by the Oligo-Miocene and Plio-Pleistocene siliciclastic units, respectively (Fig. 4.2). The evaporites are bounded by two regionally continuous seismic horizons: Horizon N and Horizon M (Fig. 4.2). These horizons represent, respectively, the base (N) and the top (M) of the Messinian evaporites in the entire Mediterranean Basin (Ryan, 1973).

Horizon N is a high-amplitude seismic reflection generated by the negative acoustic impedance contrast between the Messinian evaporites and the underlying Oligo-Miocene marine clastic sediments (Fig. 4.3). The distal evaporitic series has not been drilled to its base within the study area, or elsewhere in the Mediterranean Basin. Therefore, Horizon N is defined only on the basis of the change in seismic attributes between the evaporitic unit and the underlying marine deep-water sediments. Horizon N has been mapped across the study area and its morphology has been analysed in

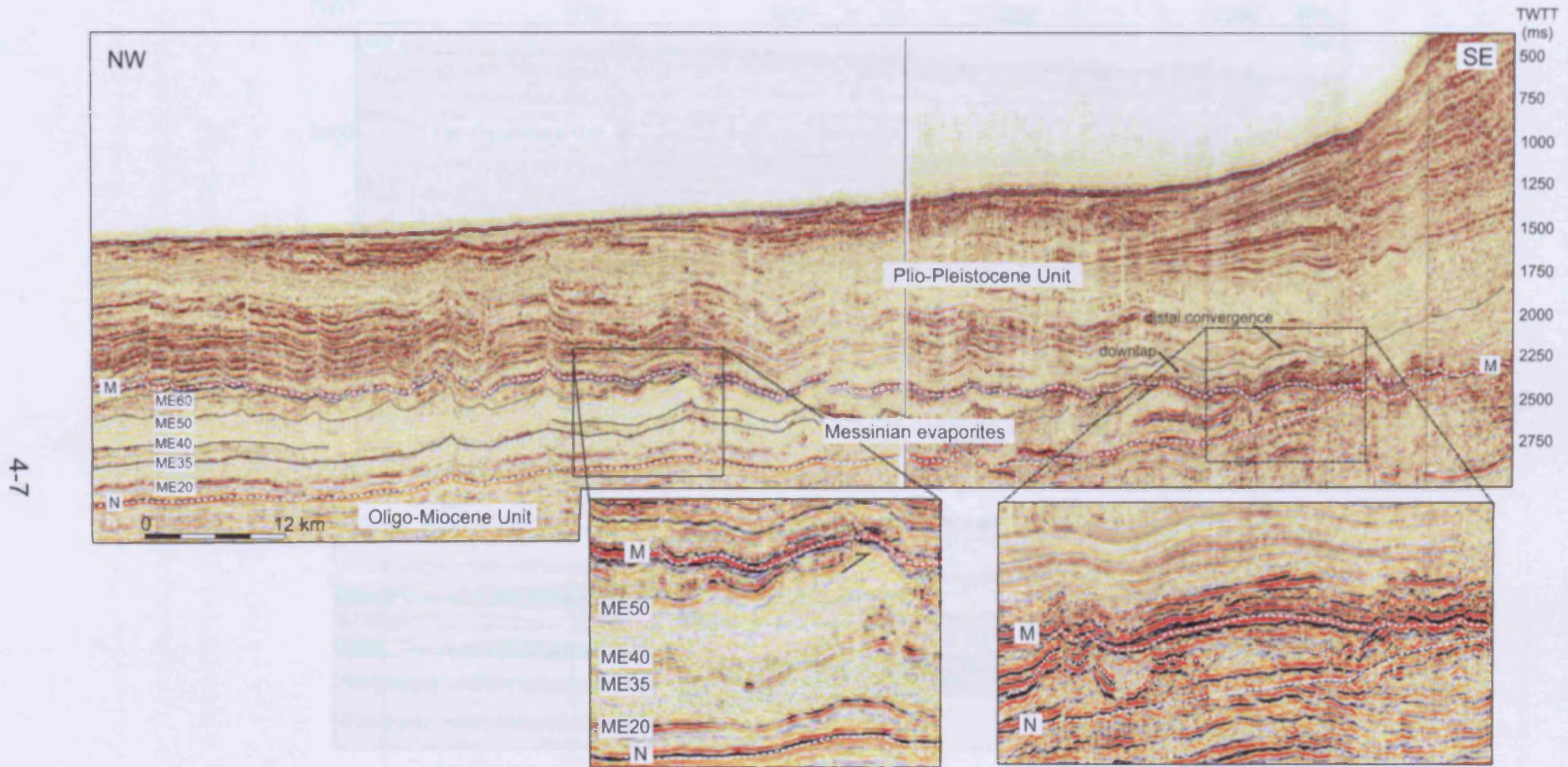


Figure 4.2 Seismic section crossing the three 3D seismic datasets in a NW-SE direction (location in Fig. 4.6), showing the seismic stratigraphic context of the Messinian evaporites. On the vertical scale, TWTT is the two-way travel time expressed in milliseconds. In this section, the structures deforming Horizon M and the overlying Plio-Pleistocene reflections should be noted. These folds and faults and the associated syn-kinematic growth of the seismic packages are caused by thin-skinned gravitational gliding of the clastic wedge, detached above or within the Messinian evaporites (see text for explanation). In the lower part of the figure, two close-ups of the seismic section highlight the updip terminations of Horizon ME20 and ME50, as indicated by the black arrows.

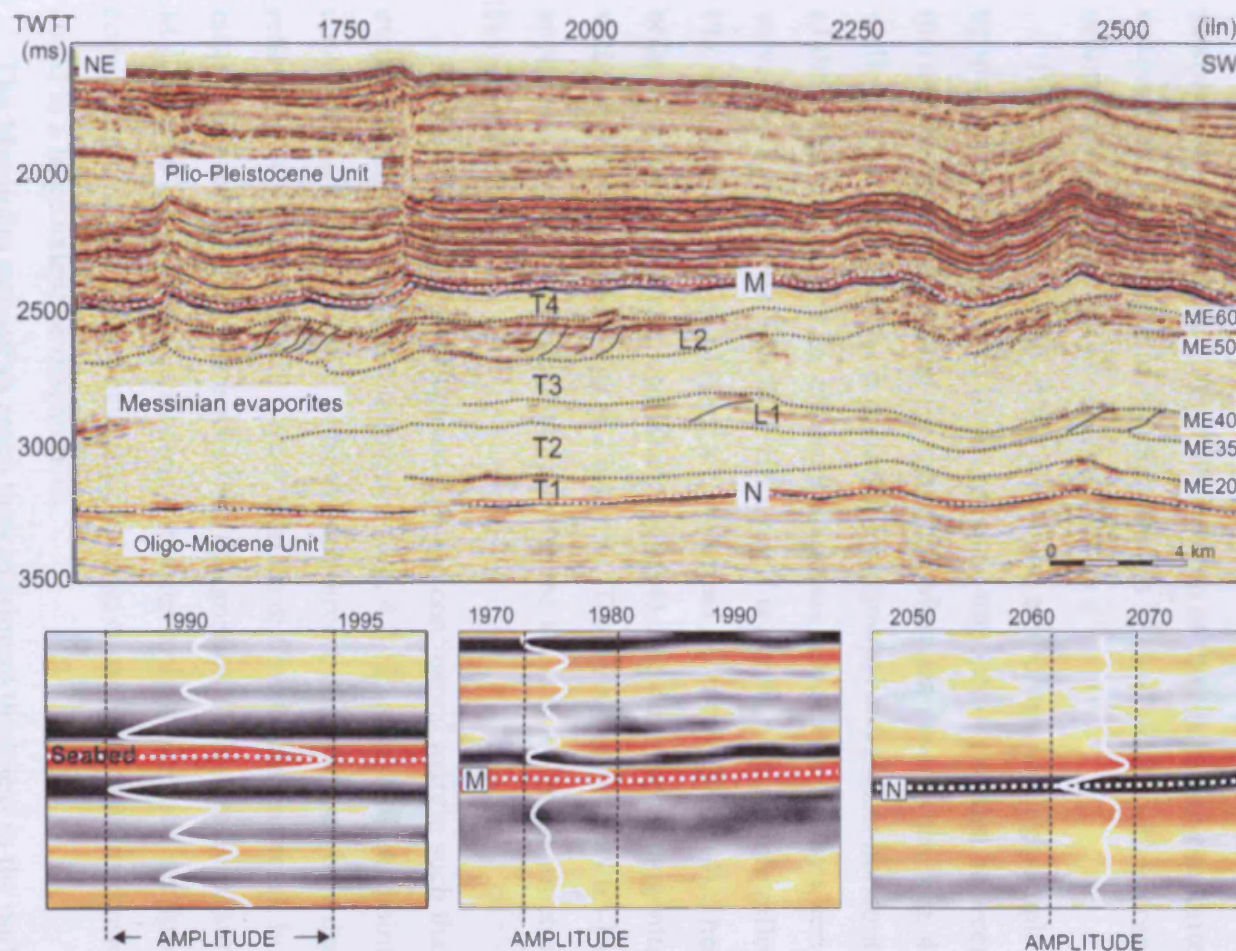


Figure 4.3 3D seismic section crossing the study area in a NE-SW direction (location in Fig. 4.6), showing the seismic stratigraphic context of the Messinian evaporites. On the vertical scale, TWTT is the two-way travel time expressed in milliseconds. T1 to T4 are the transparent seismic packages and L1 to L2 are the layered seismic packages defined in this study within the unit of the Messinian evaporites. In the lower part of the figure, three close-ups of the seismic section show the waveform response of a single wavelet (highlighted over the seismic volume) across the seabed, Horizon M and Horizon N. Note that the seabed and Horizon M produce a positive wavelet (the main peak deviates to the right).

detail in Bertoni & Cartwright (in press). This horizon is characterised by a regionally westward dipping surface, with a variable angle of $0.6 - 1^\circ$, as calculated on seismic sections perpendicular to its strike, taking Horizon M as the regional reference datum (Fig. 4.2). Horizon N is relatively undeformed, although it appears to be locally upwarped or downsagged (Fig. 4.3). These deflections represent an apparent deformational geometry caused by seismic pull-up or push-down, and results from the seismic velocity contrast at the deformed top of the Messinian evaporites, between the evaporites (average seismic velocity 4000 m s^{-1}) and the Plio-Pleistocene marine clastic sediments (average seismic velocity 2000 m s^{-1}).

Horizon M, i.e. the top of the Messinian evaporites, is a high-amplitude positive seismic reflection generated by the acoustic impedance contrast between the Pliocene marine clastic sediments and the top of the Messinian evaporites (Fig. 4.3; unpublished well reports). This horizon is regionally continuous and almost horizontal across most of the study area (Fig. 4.2), although it appears to be deformed by a series of short wavelength structures (Fig. 4.2). Horizon M is overlain by seismic reflections of the Plio-Pleistocene unit, displaying a clinoformal geometry (Fig. 4.4). These reflections onlap Horizon M in the marginal area (Fig. 4), and downlap or tangentially converge with it in the distal area (Figs. 4.2 and 4.4). The basal part of the Plio-Pleistocene unit appears to be deformed concordantly with the short-wavelength structures observed on Horizon M (Fig. 4.2).

Horizon N and M converge towards the continental margin such that the Messinian evaporites thin in a wedge-like manner (Fig. 4.2). Eastward of this point of convergence a single seismic horizon is observed, characterised by a distinct erosional relief (Fig. 4.4; Ben Gai et al., 2005; Bertoni & Cartwright, in press). Following the established nomenclature, we adopt the designation of this erosional surface as Horizon M (Ryan, 1973). However, this does not necessarily represent a stratigraphic correlation with the basinal evaporitic setting, considered that this erosional surface could to a large extent be diachronous.

The Messinian evaporites reach their maximum thickness in the northwestern part of the study area, where they are up to 850 m thick (equivalent to ca. 1700 m thick) (Fig. 4.2; Bertoni & Cartwright, in press). The evaporitic series is internally composed of an alternation of transparent and bedded/layered seismic facies (Figs. 4.2 and 4.3). The main intra-evaporitic seismic reflections composing the bedded facies are

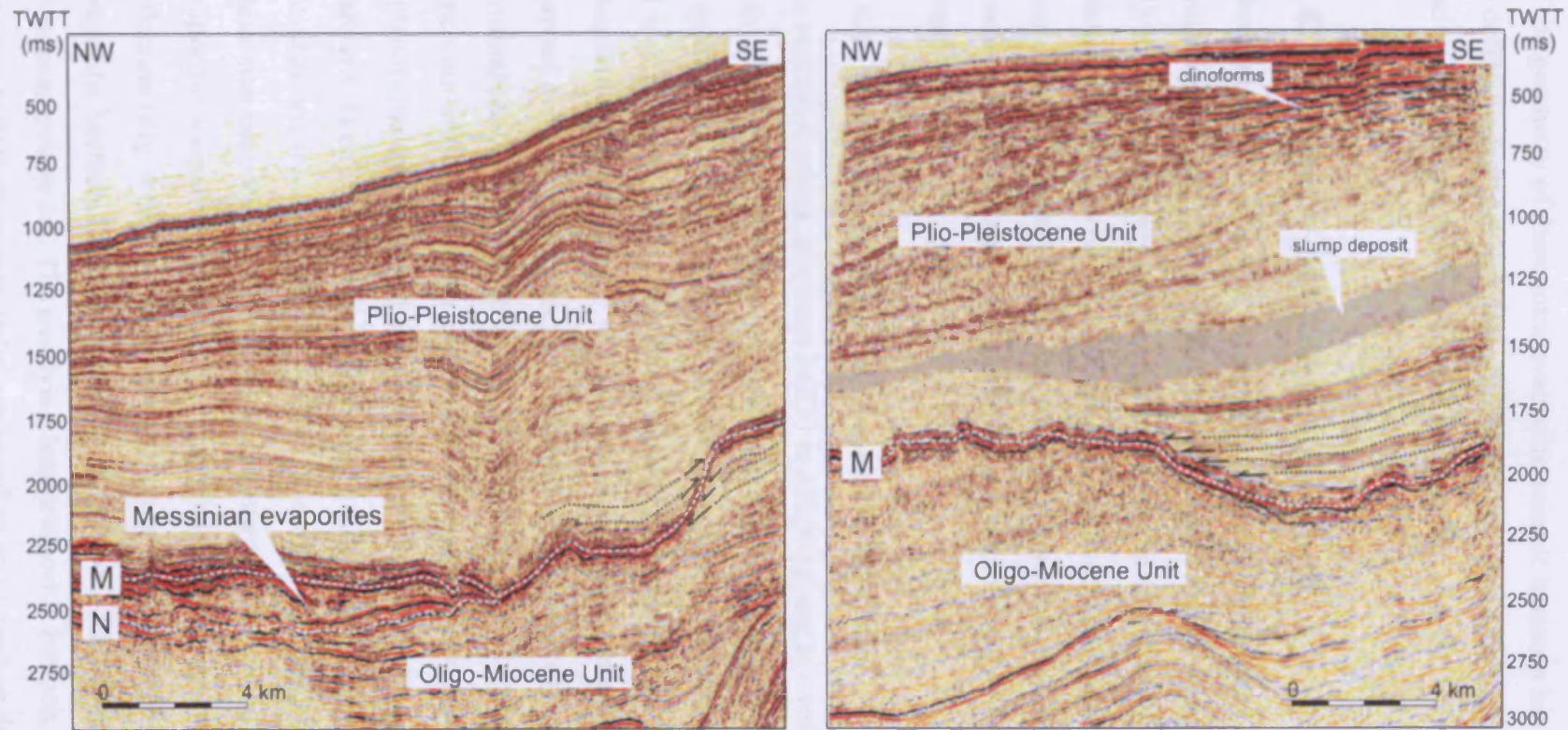


Figure 4.4 Seismic sections crossing the study area in a NW-SE direction (location in Fig.4.6). On the vertical scale, TWTT is the two-way travel time expressed in milliseconds. Note that Horizon M is overlain by the seismic reflections of the Plio-Pleistocene unit, which display a clinoformal geometry. These reflections overlap Horizon M in the marginal area to the SE (as indicated by black arrows), and downlap (as indicated by black arrows) or tangentially converge with it in the distal area to the NW. The occurrence of a prominent slump deposit within the Plio-Pleistocene Unit is highlighted with grey colour.

Horizons ME20, ME35, ME40, ME50, ME60 (Figs. 4.2 and 4.3). A detailed analysis of the geometry of these intra-evaporitic seismic horizons has been undertaken in order to define the tectonic and depositional context of the top of the Messinian evaporites, and this analysis is the focus of the next section.

4.6 Geometry of the evaporitic unit

Three main parameters are essential to recognize the original relationship of the intra-evaporitic horizons ME20 to ME60 to the top of the Messinian evaporites (Horizon M): their 3D geometry (i.e. dip and strike, updip and downdip terminations), the thickness and facies of the enclosed intra-evaporitic packages defined by them, and their overall structural deformation. These parameters have been examined in detail on a series of seismic cross-sections and time-structure maps of the base, top and intra-evaporitic horizons (Figs. 4.5 to 4.10).

4.6.1 Geometry of the intra-evaporitic horizons

On seismic sections, Horizons ME20 to ME60 appear as overall continuous seismic reflections, that dip to the west-northwest of $0.5 - 1^\circ$ (Fig. 4.2) and have a variable amplitude character. All the intra-evaporitic seismic horizons are discordant to Horizon M and terminate updip against it at a variable distance from the pinch-out of the Messinian evaporites (Figs. 4.2 and 4.5). The loci of updip terminations have been mapped across the study area as displayed in Fig. 4.6. Regionally, these updip terminations form a swathe with a NE-SW trend, broadly parallel to the present-day pinch-out of the Messinian evaporitic unit (Fig. 4.6). Locally, this trend shows embayments and salients that follow the location of the Afiq, El Arish and Ashdod Canyons, as described in Bertoni & Cartwright (in press) (Fig. 4.6). The updip terminations are not clearly defined and therefore not mappable in areas where the Messinian evaporites are extensively deformed, or where the continuity of the intra-evaporitic horizons is affected by a marked decrease in seismic amplitude of the reflection (Fig. 4.6). The updip termination of the stratigraphically lower intra-evaporitic horizon, i.e. Horizon ME20, is located 2-5 km from the pinch-out of the Messinian evaporites. The overlying intra-evaporitic horizon, i.e. Horizon ME35 to Horizon ME60, terminate updip westward, at an increasing distance from the pinch-out

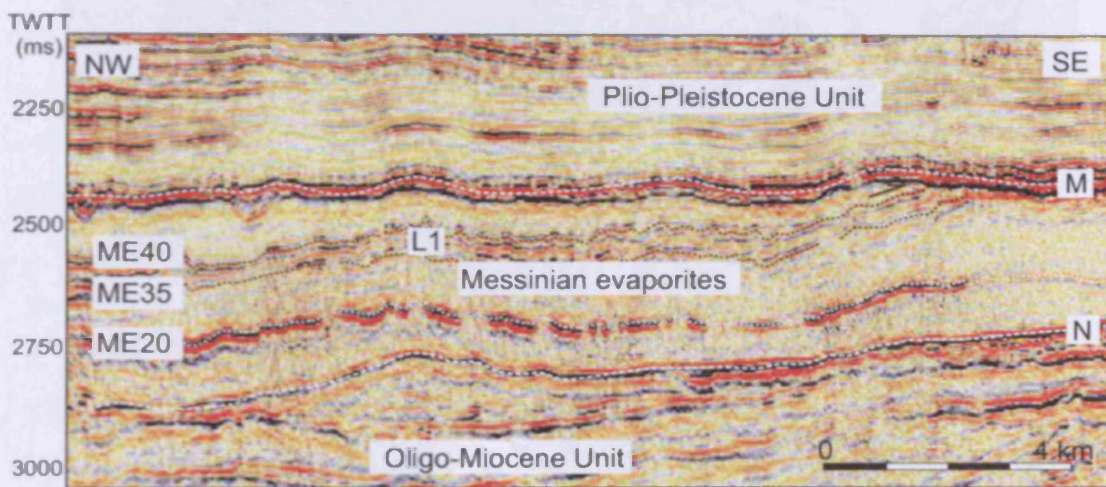


Figure 4.5 Seismic section crossing the Levant 3D seismic dataset in a NW-SE direction (location in Fig. 4.10) showing the geometrical relationship of the intra-evaporitic horizons ME20 to ME40 to the top of the Messinian evaporites (Horizon M). The discordance of the intra-evaporitic seismic horizons ME35 to ME40 with Horizon M should be noted. These horizons terminate updip against Horizon M basinwards (i.e. to the NW) of the pinch-out of the Messinian evaporites. On the vertical scale, TWTT is the two-way travel time expressed in milliseconds.

Figure 4.6 Table structure map of Levant M obtained in the 3D seismic dataset (contour interval 100 milliseconds TWTT), showing the regional distribution of the updip termination of the intra-evaporitic horizons ME20, ME35 and ME40 on the top of the Messinian evaporites. The updip termination of the Messinian evaporites is indicated by the black dashed line. The updip terminations are not clearly defined and their position is variable in areas where the Messinian evaporites are not continuous (e.g. marked by a shaded area in the figure). The updip termination of the Messinian evaporites is marked by a shaded area in the figure.

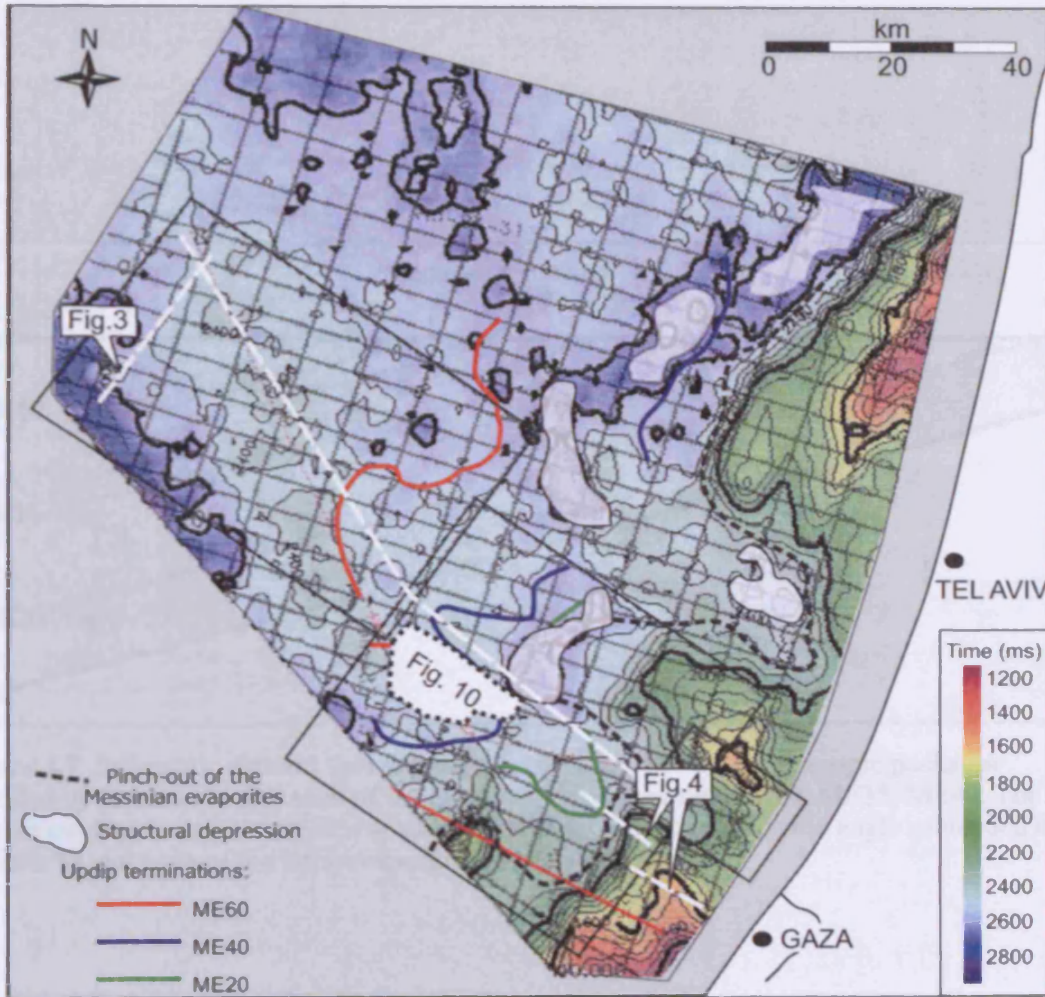


Figure 4.6 Time-structure map of Horizon M obtained in the 2D seismic dataset (colour bar expressed in milliseconds TWTT), showing the regional distribution of the up-dip termination of the intra-evaporitic horizons ME20, ME40 and ME60 on the top of the Messinian evaporites. The pinch-out of the Messinian evaporitic wedge is indicated by the black dashed line. The up-dip terminations are not clearly defined and therefore not mappable in areas where the Messinian evaporites are extensively deformed (e.g. located nearby structural depressions defined at the top of the Messinian evaporites, i.e. white shaded areas in the figure).

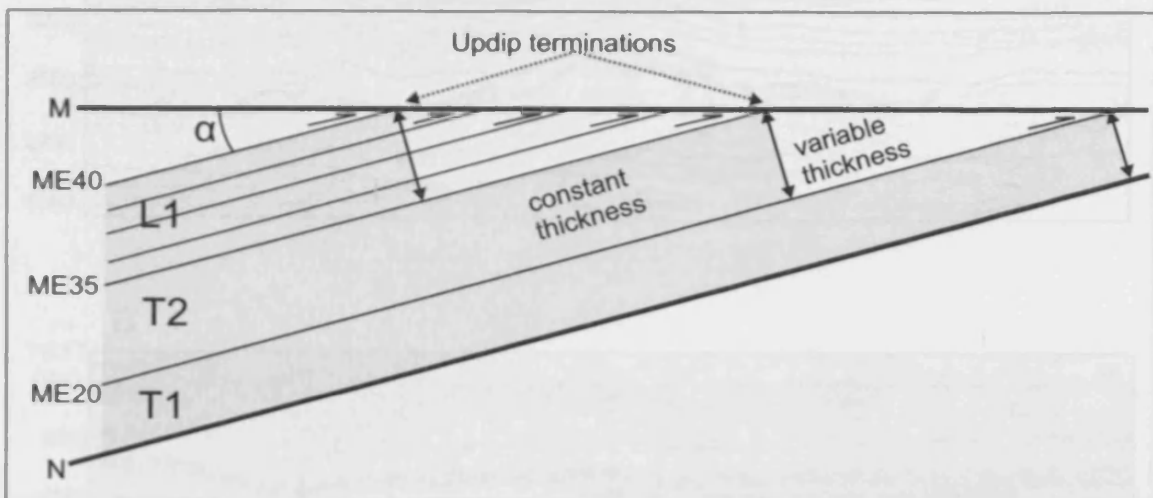


Figure 4.7 Schematic cartoon showing the thickness variations of the seismic packages bounded by Horizon M and each of the intra-evaporitic horizons ME20, ME35, ME40. The cartoon evidences how the thickness variation is strictly dependent on the angle subtended by Horizon M and each of the intra-evaporitic horizons (angle α).

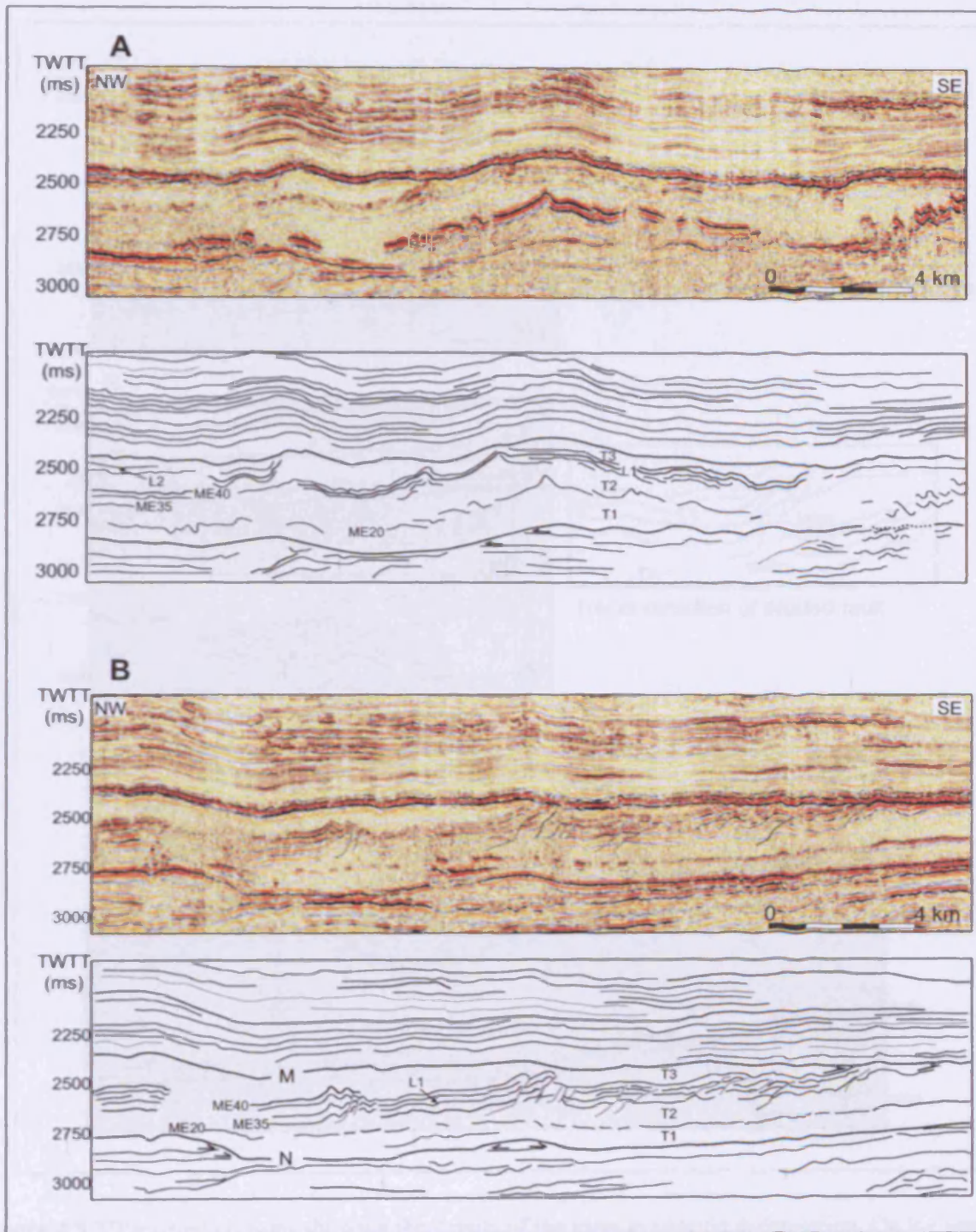


Figure 4.8 3D seismic sections crossing the study area in a NW-SE direction (location in Fig. 4.10), showing the general context of intra-evaporitic deformation.
 a) The top of the Messinian evaporites (Horizon M) is relatively unstructured in comparison with the intensely deformed intra-evaporitic horizons. T1 to T4 are the transparent seismic packages and L1 to L2 are the layered seismic packages defined in this study within the unit of the Messinian evaporites. The black arrows indicate truncation reflection terminations.
 b) Two types of structures deform the intra-evaporitic horizons: low amplitude weakly asymmetric folds, and thrust faults. The faults are marked with black dotted lines. The black arrows indicate truncated reflection termination.

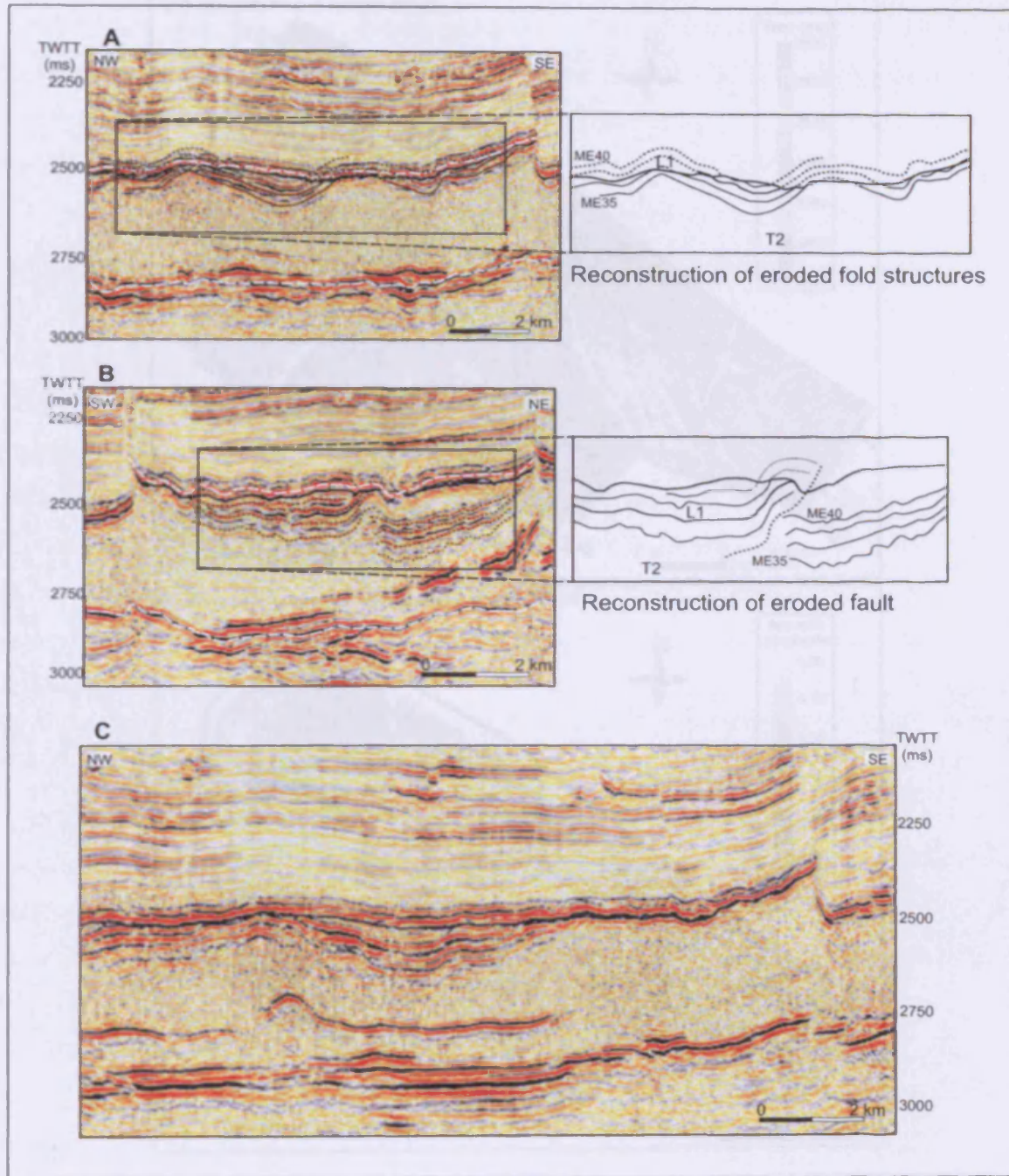


Figure 4.9 3D seismic sections showing the details of the intra-evaporitic deformation. On the vertical scale, TWTT is the two-way travel time expressed in milliseconds.

a) 3D seismic section crossing the study area in a NW-SE direction (location in Fig. 4.10), showing the folded structures deforming the intra-evaporitic layered package L1. In the right part of the figure, the hypothetical reconstruction of the eroded folds above Horizon M is indicated by the dotted lines.

b) 3D seismic section crossing the study area in a SW-NE direction (location in Fig. 4.10), showing one of the faulted structures deforming the intra-evaporitic layered package L1. In the right part of the figure, the hypothetical reconstruction of the eroded fault above Horizon M is indicated by the dotted lines.

c) 3D seismic section crossing the study area in a NW-SE direction (location in Fig. 4.10), showing the general context of the truncated folded structures deforming the intra-evaporitic layered package L1.

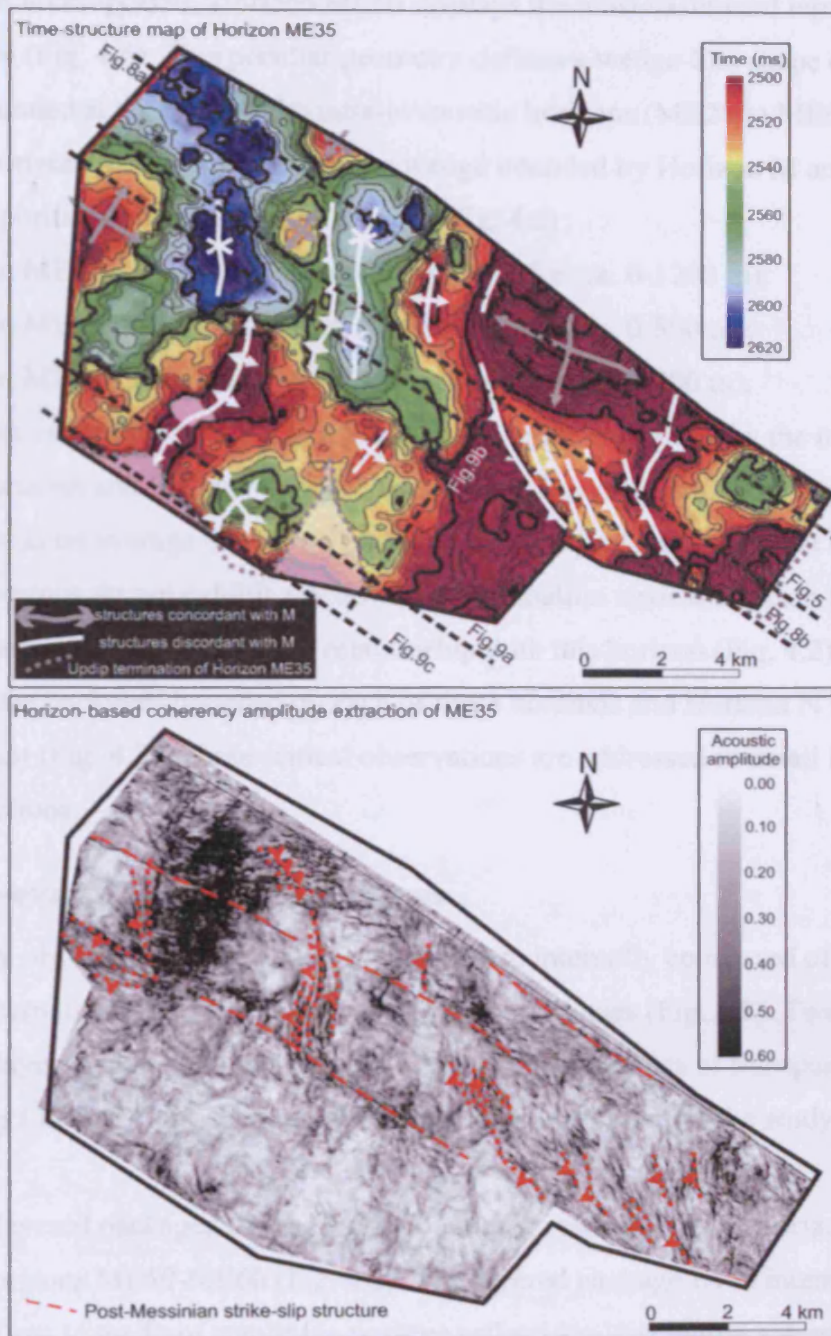


Figure 4.10 Maps showing the general structural deformation of Horizon ME40.

a) Time-structure map of Horizon ME35 obtained in the 3D seismic dataset (location in Fig. 4.6). The colour bar is expressed in milliseconds TWTT. The interpretation of the folds and faults deforming Horizon ME40 is shown. The discordant structures appear to be laterally persistent for many kilometres. In plan view, the direction of these faults and folds is consistent, and is dominantly oriented to the NW-SE and N-S, while the vergence of the thrust sequences is to the E or NE.

b) Horizon-based coherency amplitude extraction of Horizon ME35 (covering the same area as Fig. 4.10a), showing the detailed structural interpretation. The red dashed line indicates a superimposed strike-slip fault system post-dating the deposition of the Messinian evaporites. The area of Fig. 4.10a is marked with the black peripheral box for comparison.

of the Messinian evaporites. Horizon ME60 displays the most basinward termination in the study area (Fig. 4.6). This peculiar geometry defines a wedge-like shape of the packages bounded at the base by the intra-evaporitic horizons (ME20 to ME60) and at the top by Horizon M. The thickness of the wedge bounded by Horizon M and each of the intra-evaporitic horizons varies as follows (Fig. 4.2):

- Horizon ME20 - Horizon M: from 0 to 600 ms (i.e. ca. 0-1200 m);
- Horizon ME35 - Horizon M: from 0 to 400 ms (i.e. ca. 0-800 m);
- Horizon ME50 - Horizon M: from 0 to 250 ms (i.e. ca. 0-500 m).

This thickness variation is strictly dependent on the angle subtended by the intra-evaporitic horizons and Horizon M, as shown in the schematic cartoon in Fig. 4.7 (angle α), that is on average $0.5 - 1^\circ$. Conversely, it is important to note that the intra-evaporitic horizons do not exhibit any downdip termination against Horizon N, maintaining and exhibit a concordant relationship with this horizon (Fig. 4.2). The thickness of the packages bounded by each of these horizons and Horizon N is thus nearly constant (Fig. 4.2). These critical observations are addressed in detail in the following sections.

4.6.2 Intra-evaporitic seismic packages

As previously observed, the Messinian evaporites are internally composed of packages displaying alternatively layered and transparent seismic facies (Fig. 4.2). Two main packages of layered seismic facies (L1 and L2) and four packages of transparent seismic facies (T1 to T4) are distinguished in the most distal part of the study area (Fig. 3).

The two layered packages L1 and L2 are bounded, respectively, by horizons ME35-ME40 and horizons ME50-ME60 (Fig. 4.3). The layered package L1 is internally composed of low to medium amplitude positive reflections, displaying a dominant frequency of 30 Hz. The layered package L2 is internally composed of medium to high amplitude positive reflections, with a dominant frequency of 50 Hz. Seismic cross-sections show that, at a wide scale, these layered packages present an approximately constant thickness, varying from 80-100 ms (L2) to 100-120 ms (L1) (i.e. from ca. 160-200 m to 200-240 m) (Figs. 4.2 and 4.3). Their thickness decreases abruptly approaching the updip termination of the bounding horizons against Horizon M (Fig. 4.5). This thickness variation defines a marginal wedge-like geometry controlled by the

location of the updip termination of the upper and lower boundary of the layered packages (Fig. 4.7). The thickness of the packages L1 and L2 appears to be locally affected by deformation (Figs. 4.3 and 4.5). However, this deformation does not generally affect the overall continuity of the horizons across the study area.

The four transparent seismic packages T1 to T4 are bounded, as displayed in Fig. 4.3, respectively by Horizon N and M20 (T1), Horizon ME20 and ME35 (T2); Horizon ME40 and ME50 (T3), and Horizon ME50 and M (T4). The thickness of these seismic packages ranges between 100 ms (T1) and 250 ms (T3). The thickness is almost constant and displays its maximum variation in the region of the updip termination of the bounding horizons, similarly to the pattern observed for the layered packages L1 and L2 (Fig. 4.7). Conversely, at a local scale the transparent packages T1 to T4 show a more irregular thickening and thinning, particularly evident in the proximal part of the study area (Fig. 4.2). This pattern can be correlated with the occurrence of the deformational structures in the bounding layered packages and reflections (e.g. Fig. 4.3).

The composition of the transparent packages T1 to T4 can be inferred based on their seismic character and on their general stratigraphic context. Transparent seismic facies are typical of homogeneous, contorted, chaotic or steeply dipping geologic units (Mitchum et al., 1977). Reflection-free areas on seismic sections are commonly observed within large igneous masses, thick seismically homogeneous shales or sandstones, or salt bodies (Mitchum et al., 1977). Salt layers are identified within the Messinian evaporites in the Mediterranean Basin, based on the halokinetic structures and linked seismic artefacts (e.g. pull-up effect), and by the seismic facies characterised by a weak (low-amplitude) chaotic reflection zone (Montadert et al., 1978; Garfunkel and Almagor, 1987). In the study area, thick halite intervals are recorded in the marginal part of the Messinian evaporites (Bertoni & Cartwright, 2005). Based on these observations, we consider that the transparent seismic facies is mostly likely to indicate the presence of halite deposits within the Messinian evaporites.

Conversely, the composition of the layered packages L1 and L2 can be inferred based on their seismic character (in particular their lateral continuity), sedimentary patterns (seismic geomorphology) and on their general stratigraphic context. Importantly, the polarity of these reflections implies a positive acoustic impedance contrast for ME35 to ME60 (Fig. 4.3) and negative acoustic impedance contrast for

ME20 (Fig. 4.3), with respect to the enclosing halite facies. In evaporitic settings (e.g. Taylor, 1998), this type of seismic response generally indicates the juxtaposition of halite on anhydrite or limestone facies (positive) and on shale/marl facies (negative)(Nurmi, 1988). 3D mapping and attribute analysis of these horizons did not resolve any clear geomorphological pattern such as dendritic systems of channelised flow paths, supporting a putative clastic lithological interpretation. In contrast, the high lateral continuity of the reflection character is more indicative of chemical sedimentation processes (for the acoustically hard layers), or marly or muddy depositional systems (for the acoustically soft layers).

4.6.3 Structural deformation of the intra-evaporitic horizons

Detailed analysis and mapping of the intra-evaporitic horizons revealed that they locally display an intensely deformed geometry and are folded and faulted with a structural relief of the order of 100-200m (e.g. Fig. 4.2). The intra-evaporitic horizons are in some areas deformed concordantly with the structural deformation exhibited by both Horizon M and the lower part of the Plio-Pleistocene unit (Fig. 4.2). Localised thickness variation of the transparent intra-evaporitic packages T1 to T4 is also observed (e.g. Fig. 4.2). The strongly coupled deformation of the evaporites and the lowermost Plio-Pleistocene unit can be related to the well-documented development of thin-skinned gravitational tectonics detaching above or within the Messinian evaporites in the Levant area (Garfunkel & Almagor, 1987; Tibor & Ben-Avraham, 1992, Gradmann et al., 2005).

Importantly, however, in parts of the study area, the top of the Messinian evaporites (Horizon M) is relatively unstructured in comparison with the intensely deformed intra-evaporitic horizons. In particular, Horizon ME20 and the layered package L1 appear to be locally interrupted and deformed by a series of short-wavelength folds that are not expressed at Horizon M or within the overlying parallel Plio-Pleistocene reflections (Fig. 4.8). This geometry is especially evident in the central part of the study area, on Horizons ME35-ME40 (Fig. 4.9). 3D mapping shows that these folds are laterally persistent for many kilometres (Fig. 4.10).

Significantly, the regional dip of Horizon ME35 in this central area ranges between 4° and 12° degrees (depth converted using nearby well data)(e.g. Fig. 4.9). This angle is consistently steeper than the more general regional dip of Horizon ME35 in the less

deformed areas (i.e. $0.5 - 1^\circ$), and this clearly argues for post-depositional deformation of the horizons.

Two types of structures can be identified in this central area: low amplitude weakly asymmetric folds and thrust faults (Fig. 4.8b). The core of the folds is represented by the underlying transparent packages (T1 and T2, Fig. 4.9a and c). The fold axes plunge in a N-S/NNW-SSE direction, although doubly plunging anticlinal and synclinal structures are also observed (Fig. 4.10). The thrust faults have throws ranging from a few metres (e.g. Fig. 4.8b) to ca. 300 m (e.g. Fig. 4.9b). The fault plane dip ranges from 10° to 30° as a maximum value. The thrusts are linked to the asymmetric folds with the typical geometry of thrust propagation folds (Jamison, 1987, Mitra, 1990). In plan view, the direction of the faults and folds is consistent, and is dominantly oriented to the NW-SE and N-S (Fig. 4.10). The vergence of the thrust sequences is to the E or NE (Fig. 4.10). The structures are thus oblique to the NE-SW strike of the Levant continental margin.

The map presented in Fig. 4.10 contains folds that are either concordant or discordant to Horizon M. The origin of the discordant fold and thrust structures are discussed in more detail below.

4.7 Interpretation

4.7.1 *Intra-evaporitic deformation*

There are two distinct evolutionary pathways that can be invoked to explain the discordant fold and thrust structures developed within the intra-evaporitic horizons:

(1) the synchronous development of the deformational structures within a structural multilayer system with a detachment at Horizon M, or

(2) the deformational events occurred in a series of discrete and diachronous phases.

In order for (1) to apply, and for the discordant folds and thrusts to have formed synchronously with the remainder of the deforming evaporites (the concordant structures), it is necessary to invoke a multilayer system in which a series of detachment planes for the fold and thrust structures occurred both within the Plio-Pleistocene unit and the Messinian evaporites. In a multilayer combination, the widespread development of detachment layers generally reflects the control on the structural development that is imposed by the anisotropy and heterogeneity of the

stratigraphic column (Suppe, 1985). In the study area, the detachment planes would probably have localised along weak bedding planes located at the top (i.e. Horizon M) and within the evaporitic unit (e.g., intra-evaporitic horizons). In this situation, the faults at the L1 stratigraphic level would represent duplex thrust systems, coeval but detached from the overlying deformed Plio-Pleistocene unit. Horizon M would thus represent the upper detachment level as a roof thrust structure of the duplex system.

This interpretation is highly complex and takes no account of the previously described occurrence of an erosional truncation at Horizon M (Fig. 4.9a and b). This erosional truncation can most simply be interpreted to argue that these structures pre-date the formation of Horizon M. As a consequence, the most likely explanation for the difference observed in the structural deformation of Horizon M and the intra-evaporitic horizons is that the deformation of the intra- and post-evaporitic deposits occurred in a series of discrete and diachronous deformational phases commencing with a previously undocumented syn-evaporite deformational phase post-dating the deposition of Horizon ME40 and preceding the completion of the unconformity expressed at Horizon M. This much simpler evolution thus accounts for the development of concordant and discordant structures in the same general deformational province because it places their evolution in two discrete episodes, separated by the regional unconformity at Horizon M.

4.7.2 Origin of the top-evaporitic surface

The specific stratigraphic origin of the surface defining the top of the Messinian evaporites can be interpreted on the basis of stratal discontinuity observed on the seismic data. The discordant angular relationship recorded between the NW-dipping intra-evaporitic horizons (ME20 to ME60) and the nearly horizontal Horizon M is diagnostic of an unconformity *sensu* Mitchum et al. (1977). The updip termination of reflections against flat-lying overlying reflections can be related to two types of unconformity: a nondepositional unconformity or an erosional unconformity (Fig. 4.11, Brown & Fisher, 1980). In the case of a nondepositional unconformity, Horizon M would represent a toplap surface, formed mainly as a result of deposition bypass and with only limited erosion (Fig. 4.11a; Mitchum et al., 1977). Conversely, in the case of an erosional unconformity, Horizon M would represent a surface created by the

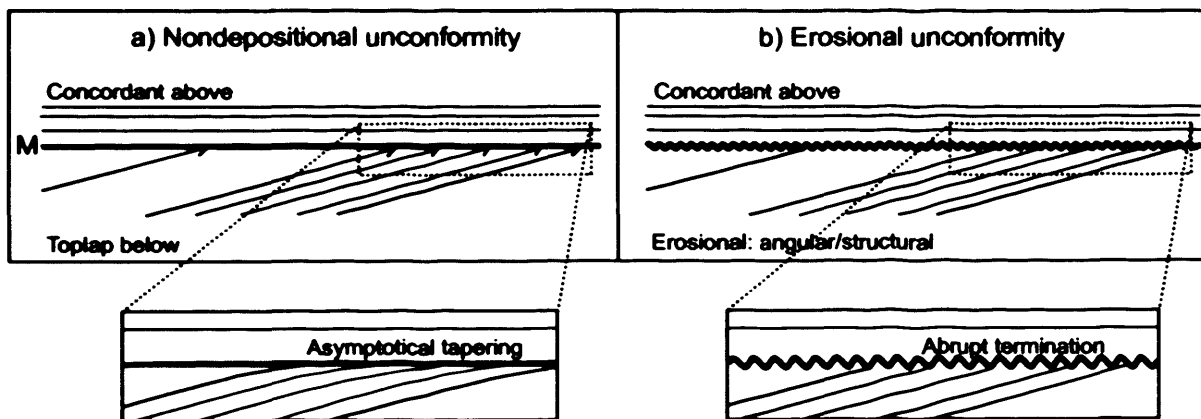


Figure 4.11 Schematic cartoon showing the two possible geometry of updip termination of reflections against flat-lying overlying reflections.

a) Geometry defining a nondepositional unconformity (Brown & Fisher, 1980).

b) Geometry defining an erosional unconformity (Brown & Fisher, 1980).

erosional truncation of the underlying intra-evaporitic horizons (Fig. 4.11b, Mitchum et al., 1977).

The distinction between these two cases can be drawn based on the geometry of the terminations of the intra-evaporitic horizons, and on the thickness variations of the seismic packages bounded by them. Previous authors have interpreted Horizon M in the study area as a toplap surface, based on the lack of evidence of erosional truncation (Gradmann et al., 2005). Toplap surfaces imply the development of a prograding clinoformal system and are generally characterised by underlying strata tapering and approaching asymptotically against the upper boundary (Fig. 4.11a, Mitchum et al., 1977). Conversely, in the truncated relation the strata tend to maintain parallelism as they terminate abruptly against the upper boundary (Fig. 4.11b, Mitchum et al., 1977). In the study area, the intra-evaporitic horizons display a rather abrupt termination against Horizon M. In addition, the absence of downdip termination or basinward convergent relationship of the intra-evaporitic horizons to Horizon N argues against the earlier development of a prograding clinoformal evaporitic system that would be the corollary to defining an updip toplap surface.

An additional aspect to take into account for the interpretation of the origin of the top evaporitic surface regards its extent. The discordant relationship between Horizon M and the intra-evaporitic horizons covers an area of approximately 10,000 km². Previous studies argued that toplap surfaces are rarely widespread on a regional or semi-regional scale (Cartwright et al., 1993). The development of a widespread toplap surface in the Levant area appears thus particularly unlikely, considering the evidence of repeated and consistent sea-level changes recorded during the deposition of the Messinian evaporites (Barber, 1981; Druckman et al., 1995).

Finally, probably the most convincing observation for the interpretation of Horizon M is the previously discussed evidence of erosional truncation of the deformed intra-Messinian reflections against Horizon M. Based on all the previous observations, we interpret Horizon M as an erosional unconformity. The location of the mapped updip terminations of the intra-evaporitic horizons provides an approximate indication of the minimum areal development of this erosional unconformity. The interpretation of Horizon M as an erosional truncation surface contrasts with its definition in previous studies as the correlative conformity of the proximal Messinian erosional surface (Ben Gai et al., 2005). In the study area, the onlap and downlap of the undeformed Pliocene

reflections on this erosional unconformity (Figs. 4.2 and 4.4) indicates clearly that the erosion occurred before the early Pliocene, and therefore precludes any origin of the erosional unconformity as being due to a tectonic movement during the Plio-Pleistocene.

4.8 Discussion

4.8.1 Depositional geometry of the Messinian evaporites

The interpretation of the original depositional geometry of the Messinian evaporites is still a subject of considerable debate in most areas of the Mediterranean Basin. Recent studies have indicated that no consensus exists, for example on the water depth at the time of deposition of the evaporites (Hardie & Lowenstein, 2004). Comprehensive models for the basinwide distribution and architecture of the Messinian evaporites, based on the geometry of seismic reflectors, have so far only been achieved for the Gulf of Lions continental margin, in the Western Mediterranean (Lofi et al., 2005). In the Nile-Levant region, the available depositional models focus on the marginal part of the evaporitic system, and on the link between the marginal clastic deposits and the evaporites (Barber, 1981; Loncke, 2002). The geometry of the Messinian evaporitic unit in the Levant area, however, is evidently different from these settings. The repetition of stratified and transparent seismic packages observed in the study area (e.g. Garfunkel & Almagor, 1987; Bertoni & Cartwright, 2005) appears to be restricted to this part of the Mediterranean Basin. In this context, the analysis of the top surface of the evaporites is a fundamental component for the interpretation of the overall geometry of this depositional system. In this section, we compare the observations made in this study with analogous worldwide evaporitic systems to discuss the possible original depositional architecture of the Messinian evaporites in the Levant area.

In the Levant region, the reconstruction of the original limits of the depositional bodies, is hindered by the erosion at the top of the Messinian evaporites which truncated a considerable part of the basin margin sequence. Nonetheless, some conjectures can be based on the preserved geometry of the evaporitic unit. Using standard seismic stratigraphic principles, the geometry of Horizons ME20 to ME60 could either have been originally composed by sigmoidal/oblique clinoforms, or instead by parallel/divergent onlap (Fig. 12; Mitchum et al., 1977). In order to

distinguish between these two possible geometries, it would be useful to compare them with analogous giant evaporitic systems, although nowhere else is there such a complete preservation of relatively undeformed basin margin evaporite sequences.

Evaporite systems on the scale of the Messinian have not been widely considered as being likely to be progradational. Some authors have suggested a progradational system was in place during deposition of the Upper Permian of Northern Europe (Schlager and Bolz, 1977; Strohmenger et al., 1996). This evaporitic system is composed of a narrow sulphate-dominated platform, characterised by the thickest bodies at the basin margin, thinning both towards the basin centre and the terrestrial hinterland (Schlager and Bolz, 1977). In contrast, however, in the Levant Basin, the absence of downlap termination of the intra-evaporitic horizons on Horizon N and their widespread parallelism rules out an original development of the Messinian evaporites as a clinoformal system (Fig. 4.12a).

Consequently, the most likely original architecture of the Messinian evaporites is considered to be parallel or divergent onlap (Fig. 4.12b and c). In the shelf area of the Levant margin, Cohen & Parchamovsky (1986) reported an onlapping configuration of the depositional bodies of the marginal Messinian evaporites in Israel (Cohen & Parchamovsky, 1986). An onlap geometry of the marginal Messinian evaporites is also in accordance with the depositional model developed for the coeval evaporites in the Western Mediterranean, where the Messinian evaporites form a series of transgressive bodies that onlap the eroded continental margin (Lofi et al., 2005).

The distinction between parallel and divergent onlap pattern (Fig. 4.12b and c) can be considered further on the basis of the analysis of the basinal setting of the study area. During the Messinian Salinity Crisis, relatively high density of the evaporitic minerals (mainly halite and anhydrite, average density 2.3 g/cc) replaced in the basin the normal deep-water sedimentation, and significant sea-level falls led to rapid water unloading and erosion on the margin. As a consequence, differential vertical movements between the continental margin and basin can be expected to have developed during the deposition of the Messinian evaporites. An evaporite load of 1.8 km (i.e. the maximum thickness recorded in the study area) is likely to have produced subsidence due to isostatic adjustment in excess of 1000 m (Allen & Allen, 1990; Schenk et al., 1994). This estimate suggests that a significant differential basinal syn-sedimentary subsidence and marginal uplift most probably occurred during the deposition of the Messinian

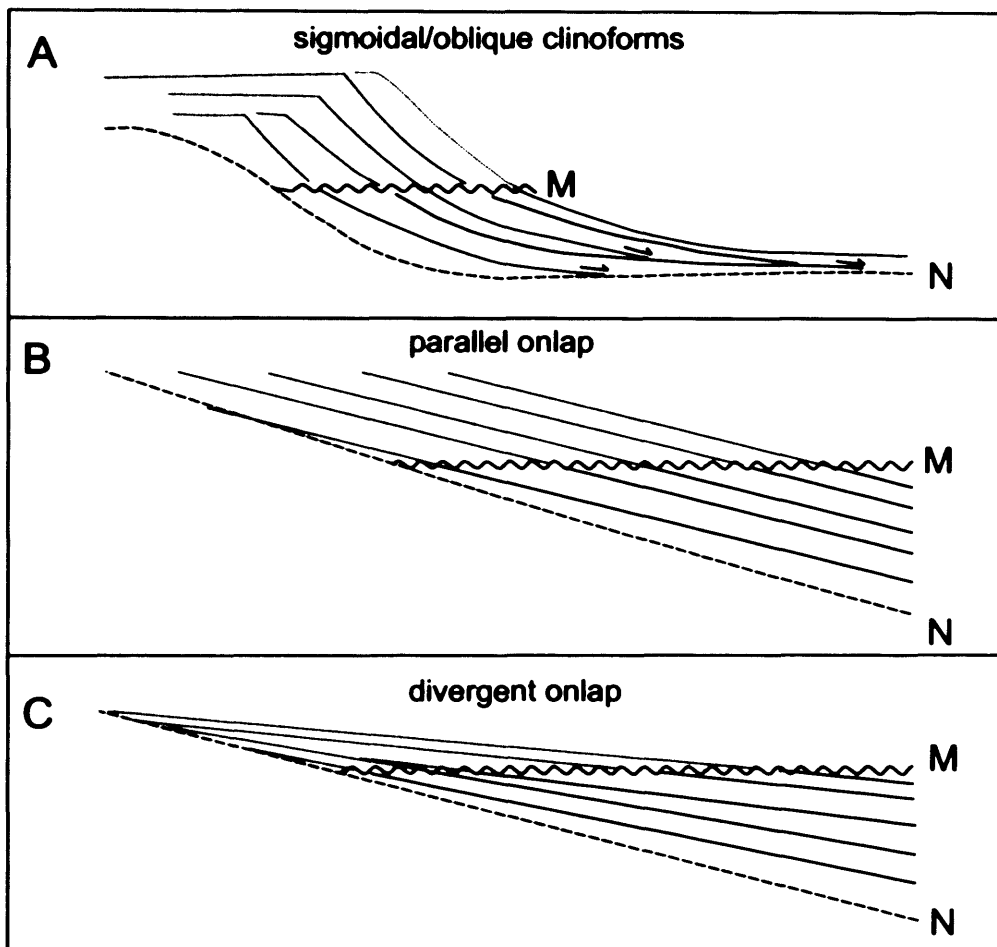


Figure 4.12 Schematic cartoon illustrating the possible original geometry of Horizons ME20- ME60 preceding the completion of the unconformity expressed at Horizon M. The dotted lines indicate the eroded part of the horizons while the continuous lines indicate the preserved part of the horizons. The arrows mark the expected termination patterns.

- a) Original geometry of horizons as sigmoidal/oblique clinoforms.
- b) Original geometry of horizons as parallel onlap.
- c) Original geometry of horizons as divergent onlap.

evaporites. The high depositional rate of the evaporitic deposits (1-100 m/ky, Schreiber & Hsü, 1980; Kendall & Harwood, 1996) suggests that the basinal tilt was matched by sedimentation. Thus, we consider it probable that a divergent onlap pattern configuration represented the original depositional geometry of the basinal evaporitic unit, before being removed by erosion (Fig. 4.12c).

4.8.2 Mechanism of structural deformation

An important issue arising from the structural interpretation of Horizon M and the intra-evaporitic horizons regards the mechanism driving for their deformation. In the Levant region, it is generally interpreted that salt tectonic deformation post-dates the deposition of the Messinian evaporitic unit, i.e. it is Pliocene or younger (Garfunkel & Almagor, 1987; Tibor & Ben-Avraham, 1992). However, our interpretation shows that in the study area the structural deformation of the intra-evaporitic horizons predates the formation of the erosional unconformity at the top of the Messinian evaporites, i.e. it occurred during the Messinian. Such an early onset of evaporite deformation rules out a genetic mechanism based on density contrast of the Plio-Pleistocene overburden, as it is common in many halokinetic settings (Jackson et al., 1995). In this section, we discuss the possible alternative mechanisms based on the analysis of the local stress field, on the comparison with nearby areas and with worldwide analogues (e.g. Clark, 1999; Mascle et al., 1999; Loncke, 2002). These mechanisms are: (1) the influence of deep structures and regional plate tectonics stress field; and (2) differential loading and subsidence due to shelf progradation into the basin over early evaporitic layers (Koyi, 1996; Ge et al., 1997).

The Levant region is situated in a tectonically complex area at the zone of interaction among the Anatolian, African and Arabian plates (Fig. 4.1; Badawy & Horvath, 1999; Vidal et al., 2000; Polonia et al., 2002). The formation of the NE-SW trending anticlines and synclines of the Syrian Arc fold belt in the Late Cretaceous (Fig. 4.1, Garfunkel, 1988; Eyal, 1996; Buchbinder & Zilberman, 1997) caused differential vertical movements and tilting in the shelf and basin of the Levant region (Fig. 4.1; Neev & Ben-Avraham, 1977; Tibor & Ben-Avraham, 1992; Buchbinder & Zilberman, 1997). The compressional movements continued until the end of the early Miocene or even the Pliocene (Tibor et al., 1992; Druckman et al., 1995; Eyal, 1996). During the Messinian local tilting and movement of the basement structures linked to

the Syrian Arc could have contributed a stress regime that triggered the downslope movement of the highly unstable evaporitic deposits. Nevertheless, the orientation of the intra-evaporitic folds and vergence of the thrust faults indicates a dominant compression direction from the WSW or SW (Fig. 4.10). This compressional stress field is not consistent with the regional stress field resulting from the Syrian Arc folding, that is thus unlikely to have directly driven the intra-evaporitic deformation.

Differential loading and subsidence due to shelf progradation into the basin over early evaporitic layers could have triggered basinward instability of the evaporitic deposits (Koyi, 1996; Ge et al., 1997). In the study area, the dominant compression direction from the SW is transverse to the Levant continental shelf. This indicates that progradation of the Levant shelf is unlikely to have driven the intra-evaporitic deformation. An important role in this process could have alternatively been played by the Nile continental margin. Previous studies record the development of an early Nile delta system coeval and laterally correlative to the Messinian evaporites (Barber, 1981; Griffin, 2002). Thus, the progressive aggradation and progradation of the Nile delta and submarine fan could have driven differential loading on the basinal evaporitic system. The Levant region is sufficiently close to the Nile delta area to be affected by these movements (Fig. 4.1; a radius of 100-150 km). The compression direction originated by the progradation of the Nile system from the SW is consistent with the stress field recorded in the study region. If this hypothesis is confirmed, our results would suggest that differential loading driven by progradation of the Nile was active in the Levant Basin at least since the final stages of the deposition of the Messinian evaporites.

4.8.3 Implications for the Messinian erosional events in the Mediterranean Basin

The interpretation of Horizon M as an erosional unconformity bears important insights on the understanding of the Messinian evaporitic system and consequently, on the processes acting in the area at the final stages of the Messinian Salinity Crisis. The development of widespread erosional surfaces is expected in such a rapidly changing environment, where sudden sea-level changes exposed previously submerged areas. Numerous erosional phases are documented across the Mediterranean Basin, before, during and after the deposition of the Messinian evaporites (Mauffret, 1976; Ryan & Cita, 1978; Escutia & Maldonado, 1992; Butler et al., 1995; Guennoc et al., 2000;

Cornée et al., 2006). In the area of the Gulf of Lion continental margin (Western Mediterranean) seismic data record only one significant basinwide erosional event at the base of the evaporites, overlapped by transgressive Messinian deposits (Guennoc et al., 2000; Lofi et al., 2005). Elsewhere in the Western Mediterranean, erosive channels developed at the top, within and at the base of the Messinian unit (Field & Gardner, 1991; Escutia & Maldonado, 1992), and erosional features have been recognised in wells (Ryan & Cita, 1978), suggesting the occurrence of multiple and compound erosional surfaces.

The erosion observed at the top of the Messinian evaporites could be either the product of subaerial exposure or submarine erosion. As pointed out by Schlager (1993), it is extremely difficult to unequivocally recognize subaerial exposure on seismic profiles; even if erosional truncation is observed, it need not be subaerial (Huuse & Clausen, 2001). It is widely accepted that the MSC terminated when normal deep-water marine conditions re-established in the Mediterranean Basin (the so-called 'reflooding' stage after the Crisis). Consequently, two main hypotheses can be advanced regarding the origin of this erosional surface: the first, that it results from a late lowstand during the end of the Messinian, or the second, that it represents the ravinement stage of the reflooding of the Levant Basin. A final regression at the end of evaporite deposition would be consistent with previous models developed in the study area (Druckman et al., 1995). However, a detailed examination of the post-Messinian deposits in terms of backstripping and subsidence analysis are required in order to answer this question, and this goes beyond the scope of this paper.

The prominent erosional truncation surface observed at the top of the Messinian evaporites in the study area represents a unique case in this panorama. This result, coupled with the observation of an erosional surface at the base of the Messinian evaporites (Bertoni & Cartwright, in press) documents the occurrence of at least two major erosional events, respectively during the first and last stages of the Messinian Salinity Crisis in the Levant region. The comparison of our study area with other areas of the Mediterranean Basin documents significant differences in the geometry of the Messinian evaporitic unit and possibly in the frequency of regional erosional events during the Messinian Salinity Crisis. This difference can be ascribed to the different local tectonic setting, or could instead suggest that the Eastern and Western

Mediterranean underwent a different evolution during the MSC, due to the structural configuration of the Mediterranean Basin at that time.

4.9 Conclusions

- This study records the first clear evidence of the occurrence of erosional truncation at the top of the basinal Messinian evaporites in the Levant region. The integration of seismic (3D and 2D) and well data allowed the detailed seismic-stratigraphic analysis of a series of intra-evaporitic horizons and of the packages bounded by them. This analysis permitted the detection of a discordant relationship between the intra-evaporitic horizons and Horizon M and, subsequently, the definition of top of the Messinian evaporites as an erosional unconformity.
- The preserved basinward geometry of the evaporitic unit and the comparison with worldwide analogues, point to divergent onlap as the expected original depositional geometry of the evaporitic system.
- The analysis of the structural deformation of the intra-evaporitic horizons has documented the occurrence of an early phase of evaporite deformation at the end of Messinian, and preceding the completion of the unconformity expressed at Horizon M.
- The most likely mechanism of deformation is considered to be differential loading associated with a prograding shelf wedge on the basinal evaporitic system. The direction of the intra-evaporitic compressional structures indicates that the deformation could have been initiated by the aggradation and progradation of the Nile delta and submarine fan, active in the Levant Basin at least since the final stages of the deposition of the Messinian evaporites.

Chapter Five: Dissolution structures in the Messinian evaporites¹

5.1 Abstract

Buried circular collapse structures above a tabular evaporitic body are recorded by recently-acquired 3D seismic data on the Levant Basin and continental margin, offshore Israel (Eastern Mediterranean). The structures formed during the Pliocene as buried Messinian (late Miocene) evaporites underwent extensive dissolution in a submarine, deep-water setting. 3D seismic analysis is used to describe the detailed morphology of the structures and the associated overburden, allowing the reconstruction of their origin and development.

It is proposed that evaporite dissolution led to the collapse of the weakly lithified overburden, and this deformed with a series of concentric extensional faults. From the structural analysis of the overburden, the estimated maximum duration of the dissolution event is 0.75 – 1 Ma. The mechanism proposed for the creation of the circular collapse structures is subjacent dissolution of the more soluble evaporites in the Messinian evaporites, due to focused vertical fluid flow at the base of the evaporitic series. Rapid release of overpressured fluids, as e.g. during an earthquake, is thought to have initiated the focused fluid flow, which impinged on the evaporitic seal to the point where dissolution occurred, creating the localized circular collapse structures in the overburden.

¹ *Published as:*

C. Bertoni & J. A. Cartwright (2005), 3D seismic analysis of circular evaporite dissolution structures, Eastern Mediterranean. Journal of the Geological Society of London, 162, 909-926.

5.2 Introduction

Evaporite dissolution is considered an important process in many evaporite-bearing basins worldwide (see e.g. Warren, 1999). Examples of evaporite dissolution have been described in the North Sea (Lohmann, 1972; Jenyon, 1983; Cartwright et al., 2001), Western Canada (Anderson & Knapp, 1993), Gulf of Mexico (Rezak et al., 1985; Hossack, 1995), US Permian Basin (Anderson & Kirkland, 1980) and West Africa (Hudec & Jackson, 2002). Evidence of dissolution is usually represented by discordant geometrical relationships of strata, hiatuses or the presence of residue breccias (Warren, 1999). In this paper, we provide clear morphological evidence for the occurrence of evaporite dissolution in the Levant Basin of the Eastern Mediterranean. 3D mapping of the late Miocene-Pliocene stratigraphic interval has revealed the presence of a series of kilometre-scale circular depressions. We interpret these structures as having formed during the Pliocene in response to the dissolution of buried Messinian evaporites within a fully submarine setting. The circular structures developed in a non-halokinetic setting, producing collapse and/or subsidence of the overlying deep-water sediments.

Circular depressions linked to evaporite dissolution have been widely documented in the previous literature (Sugiura & Kitcho, 1981; Davies, 1983; Kastens & Spiess, 1984; Clark et al., 1999). However, the lack of resolution in subsurface imaging has generally hampered their detailed morpho-structural analysis and therefore the precise mechanism by which they form is not clear. The exceptional imaging of the Messinian evaporite sequence and overburden on recently acquired 3D seismic data in the Levant Basin, however, provides a unique opportunity to investigate the processes that both drive evaporite dissolution and the deformational response to dissolution in this area.

The primary aim of this paper is to describe the morphology of evaporite dissolution structures in the study area and their associated structural setting. The structures are bounded by a series of extensional ring faults that exhibit similarities with salt withdrawal basins (Ge & Jackson, 1998; Maione, 2001), caldera collapse features (Branney, 1995; Cole et al., 2005) and impact craters (Stewart & Allen, 2002). The ring faults observed in the study area are extensional and exhibit a domino geometry, dipping towards the centre of the structure. The detailed analysis of the

deformation of the overburden is used in this paper as a tool to assess the timing of the dissolution process, i.e. its initiation, rate and termination.

The second aim of this study is to develop a model for the evolution of the localized dissolution structures, explaining how and when they formed, and what controls their distribution in the Levant Basin. Based on the detailed 3D seismic interpretation, we propose a mechanism for dissolution involving focused fluid expulsion from the thick basin fill succession beneath the evaporite sequence. This mechanism of subjacent dissolution may have occurred in other evaporite-bearing continental margins worldwide.

5.3 Regional framework

The Levant Basin and its continental margin are situated in the easternmost Mediterranean Sea, at the zone of interaction among the Anatolian, African and Arabian plates (Fig. 5.1, Vidal et al., 2000). This passive continental margin was formed due to rifting of the Tethys Ocean during the late Triassic to early Jurassic (Garfunkel & Derin, 1984). A carbonate platform setting dominated in the area during most of the Jurassic and Cretaceous (Bein & Gvirtzman, 1977; Druckman et al., 1995).

Commencing in the Late Cretaceous, the formation of the Syrian Arc fold belt created a series of NE-SW oriented compressional structures along the Levant continental margin (Fig. 5.1, Eyal, 1996, Buchbinder & Zilberman, 1997; Garfunkel, 1998). A system of submarine canyons developed on the slope during the Oligocene (Druckman et al., 1995). The most prominent of these are the Afiq (or Gaza-Beer Sheva), the El Arish and the Ashdod Canyons (Druckman et al., 1995; Buchbinder & Zilberman, 1997). During the Miocene the shelf was intermittently emergent, and the submarine canyons were extended to the shelf area through headward erosion (Buchbinder & Zilberman, 1997).

At the end of the Miocene, the connection between the Mediterranean Sea and the Atlantic Ocean became restricted, causing the onset of the Messinian Salinity Crisis (Hsü et al., 1978). The resulting sea-level fall led to a major erosional phase on the Mediterranean margins and to the deposition of a thick series of evaporites in the entire basin (Hsü et al., 1978). The Levant Basin records the lateral transition from the erosional unconformity to the evaporitic series (named the Mavqi'im Formation in

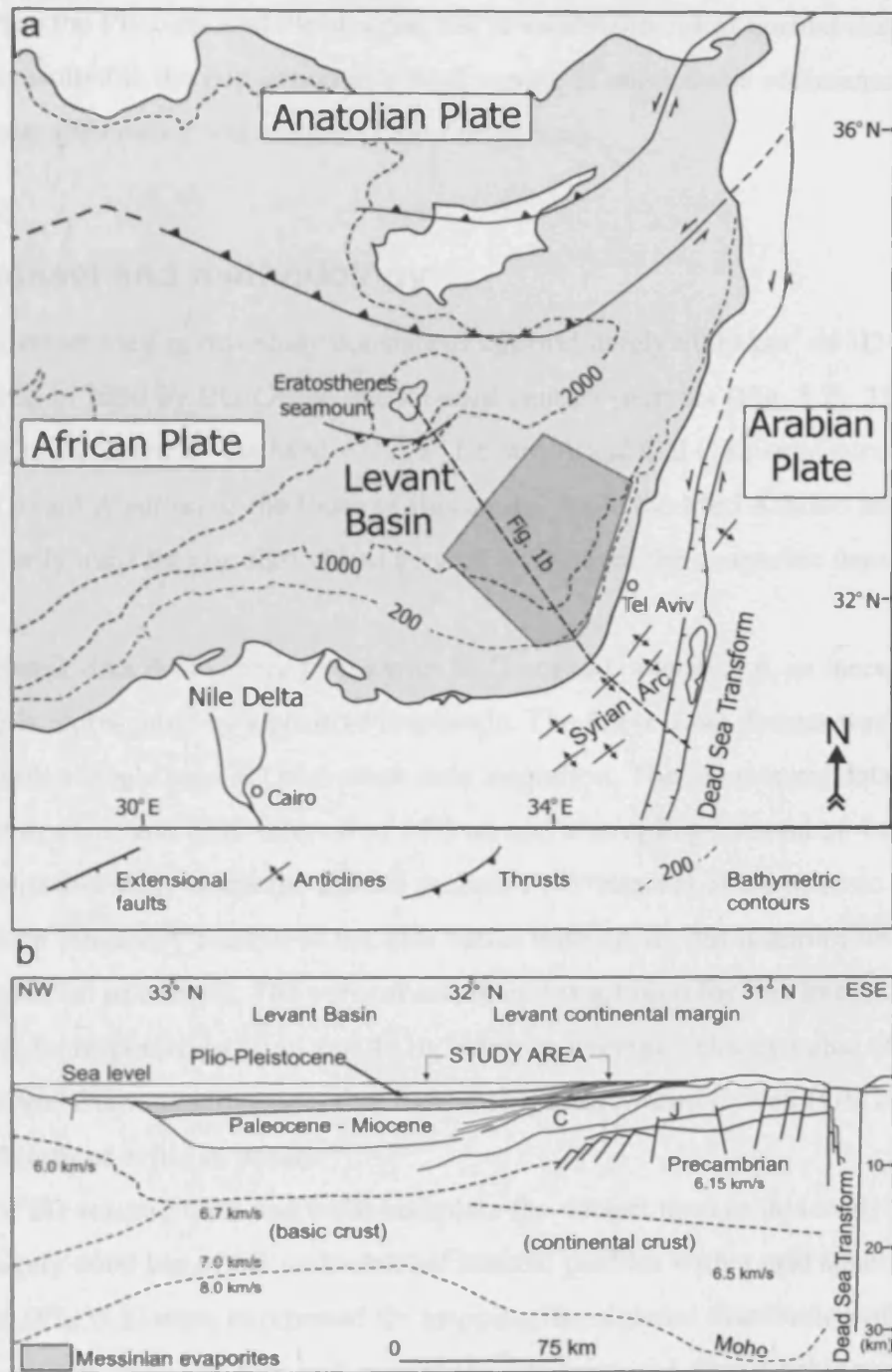


Figure 5.1 a) Schematic map of the Eastern Mediterranean, at the zone of interaction among the Anatolian, African and Arabian Plate. The main tectonic lineaments and the location of the Nile delta are indicated. The study area is highlighted by the dark grey box (3D and 2D seismic data). The contour lines represent the depth in metres of the Mediterranean seafloor. The position of the present day shelfbreak is approximately indicated by the 200 m contour line. Modified from Tibor et al. (1992); Robertson (1998); Vidal et al. (2000). b) Schematic regional cross-section through the Eastern Mediterranean basin (location shown in Fig. 5.1a; modified from Garfunkel 1998). C = Cretaceous; J = Jurassic.

Israel; e.g. Cohen, 1993) which is approximately 2 km thick in the deepest part of the basin. During the Pliocene and Pleistocene, the re-establishment of normal marine conditions resulted in the deposition of a thick wedge of siliciclastic sediments in the Levant Basin and continental margin (Yafo Formation).

5.4 Dataset and methodology

The main dataset used in this study consists of approximately 6000 km² of 3D seismic data acquired in 2000 by BG-Group and its joint venture partners (Fig. 5.2). The whole coverage is represented by the Med Ashdod, Levant A and Gal C seismic surveys (Fig. 5.2). The Levant A survey is the focus of this study, while the Med Ashdod and Gal C survey are only used for correlation and general analysis of the evaporitic depositional system.

The seismic data is near zero phase with SEG normal polarity, i.e. an increase in impedance is represented by a positive amplitude. The 3D seismic dataset was migrated with a single pass 3D post-stack time migration. The 3D seismic data consist of a grid with a line and CDP interval of 12.5 m, and a sampling interval of 4 ms. The main focus of this study spans the 2.5-3.5 second TWT interval of the seismic data. The dominant frequency content of the data varies with depth, but is approximately 50 Hz in the interval of interest. The vertical and lateral resolution for this interval is estimated to be respectively 10 m and 40 m, using an average velocity value of 2000 m/s, as derived from velocity checkshot data in the Gaza Marine-1 well (GM1 in Fig. 5.2; Frey-Martinez et al., in press).

A set of 2D seismic lines and wells complete the dataset used in this study. Approximately 6000 km of 2D multichannel seismic profiles with a grid spacing of ca. 10 x 10 km (Fig. 5.2) were interpreted for mapping the regional distribution of the depositional units. Wireline logs and unpublished commercial stratigraphic reports, mainly based on cutting analyses were available from nearby exploration wells (Fig. 5.2). The well data were used for stratigraphic and lithological analysis, for correlation of the depositional units and time to depth conversion.

The analysis of evaporite dissolution was undertaken focusing on the timing of deformation of the overburden to the circular structures. A series of parameters were measured in order to analyse the variation of the vertical relief (ΔZ) and the expansion

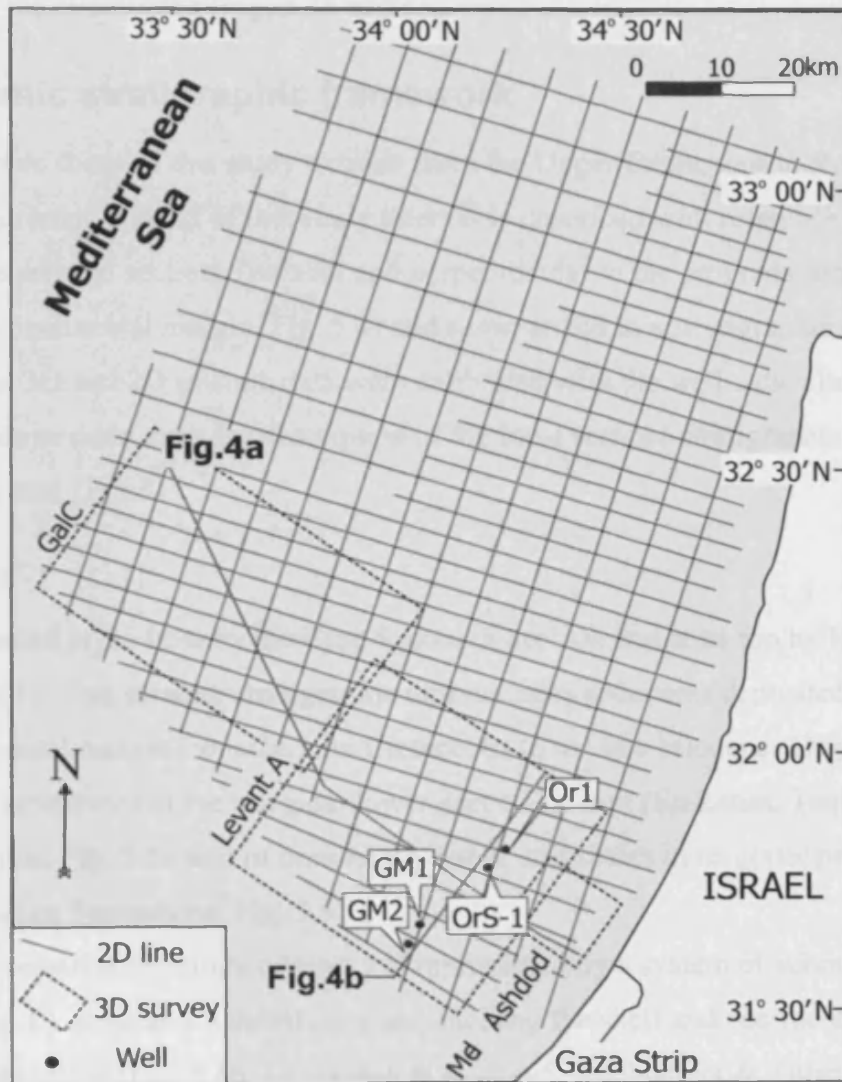


Figure 5.2 Map showing the details of the seismic surveys used in this study, together with the location of selected exploration wells. The 3D seismic surveys (Levant A, Gal C and Med Ashdod) are outlined by the dashed rectangles. The 2D seismic lines are outlined by the black dotted lines. The location of the seismic sections presented in Fig. 5.4 is also indicated.

index (E.I.) of the structure with depth (Fig. 5.3a). The E.I. is a parameter used to visualize the variation in thickness above syn-sedimentary structures, initially developed for growth faults (Thorsen, 1963). The same concept is here applied to circular structures that collapse or subside incrementally, and display syn-kinematic deposition of the overburden (Fig. 5.3b and c).

5.5 Seismic stratigraphic framework

The stratigraphic focus of this study extends from the Upper Cretaceous to Recent. The seismic-stratigraphic context of this study interval is described with reference to two representative seismic sections (parallel and perpendicular to the progradation direction of the Levant continental margin, Fig. 5.4) and summarized in a stratigraphic chart (Fig. 5.5). The 3D and 2D seismic data were calibrated with the well data, allowing the definition of three main units for description of the local seismic-stratigraphic context: Unit 1, Unit 2 and Unit 3.

5.5.1 Unit 1

Unit 1 is bounded at the base by the Base Senonian horizon and at its top by Horizon N (Fig. 5.4a and b). This seismic-stratigraphic unit includes sediments deposited on the Levant continental margin from the Late Cretaceous to the late Miocene. They are composed of limestones in the marginal lower part of the unit (En Zetim, Taqiye and Zora Formations, Fig. 5.5), and of dominantly marls and shales in its upper part (Bet Guvrin and Ziqim Formations, Fig. 5.5).

The most remarkable feature of Unit 1 is represented by a system of submarine canyons (Afiq, El Arish and Ashdod canyons) incising the shelf and continental margin in a SE-NW direction (Fig. 5.4b; Druckman et al., 1995; Buchbinder & Zilberman, 1997). The Afiq submarine canyon is the most prominent of these features (Fig. 5.4b). Its base is defined on seismic section by truncation of the underlying horizons (Fig. 5.4b). The canyon fill lacks detailed stratigraphic control, as none of the wells penetrate its maximum thickness in the canyon axis. However, some observations can be made based on the stratigraphic relationship with the wells located on the flanks of the canyon, integrated with previous work undertaken on the same canyon in the onshore region (Druckman et al., 1995). These observations suggest that the canyon fill sediments date back to the Oligocene, and unconformably overlie Lower Cretaceous to

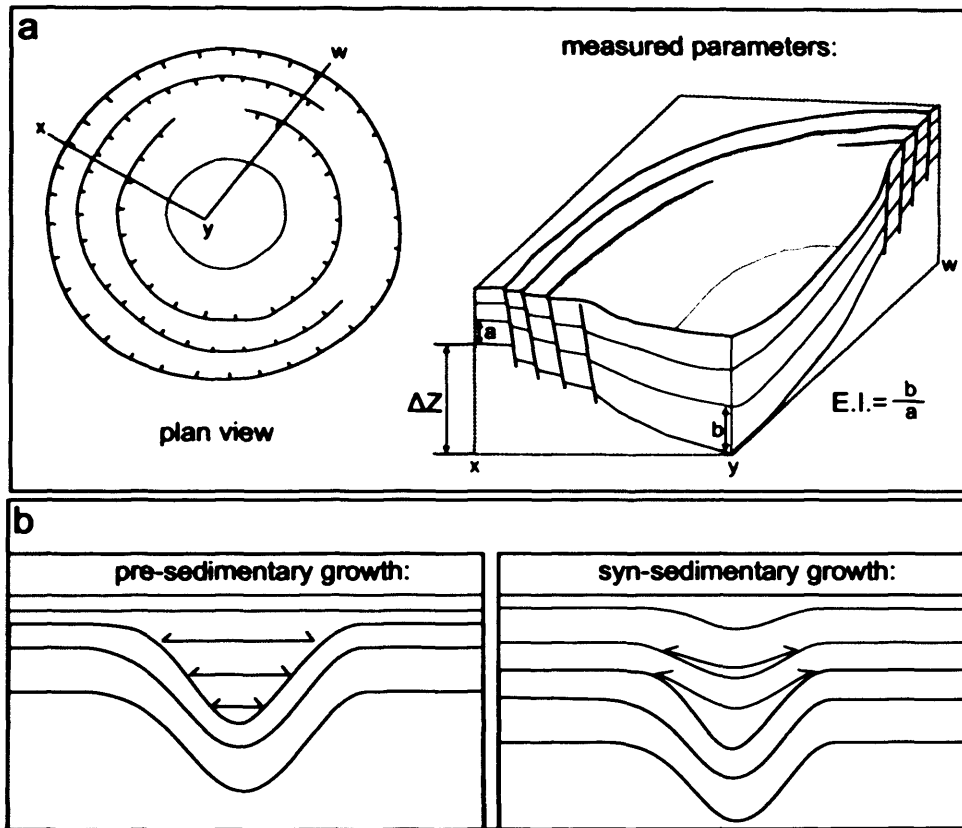


Figure 5.3 a) Idealised circular collapse depression showing the parameters measured for quantitative analysis of the dissolution structures studied in this paper (modified from Branney, 1995). The E.I. is defined by Thorsen (1963) as the ratio between the thickness of deposits downthrown (b , directly above the collapse structure) and the thickness upthrown (a , i.e. undisturbed sediments laterally bounding the collapse structure) measured on successive discrete stratigraphic intervals. The vertical relief (ΔZ) is measured on a selected stratigraphic horizon, as the difference in elevation between the centre and the rim of the collapse structure. b) Schematic representation of the expected geometry resulting from pre-sedimentary growth versus syn-sedimentary growth of the circular collapse structure. Note the difference between concentric parallel onlap in the first case, and concentric onlap coupled with divergent strata configuration and thickness variation in the second case.

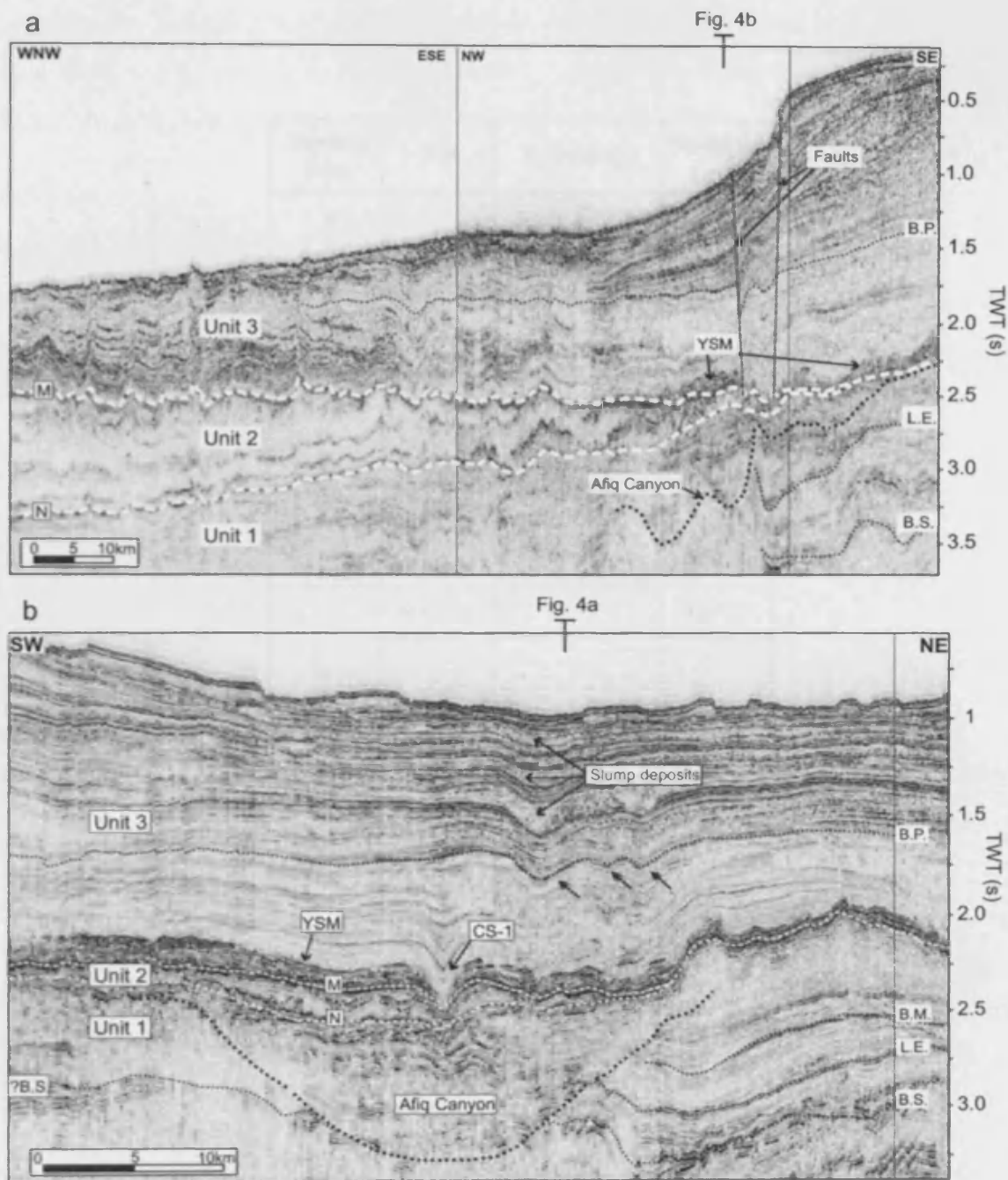


Figure 5.4 a) Composite seismic section across the Levant Basin and continental margin (see Fig. 5.2 for location). The three seismic-stratigraphic unit defined in this study (Unit 1, Unit 2 and Unit 3) are shown, together with the main interpreted horizons. Unit 2, the focus of this study, is represented by a thick wedge of evaporites pinching out towards the Levant continental margin. Marginal extensional faults within the Unit 3, detaching at Unit 2, are marked by dashed lines. The cross-over point of Figure 5.4b is indicated at the top and base of the section. YSM = Yafo Sand Member. B.S. = Base Senonian horizon; L.E. = Late Eocene horizon; M = Horizon M; N = Horizon N; B.P. = Base Pleistocene horizon. b) Seismic section along the direction of the Levant margin. Note the presence of the Oligo-Miocene Afiq submarine canyon, deeply incising within Unit 1. In Unit 3, interpretation of slump deposits is after Frey-Martinez et al. (2005). Localized downwarping of seismic reflections is observed within Unit 3 and highlighted by the black arrows. The cross-over point of Fig. 5.4a is indicated at the top and base of the section. CS-1 = circular structure CS-1; YSM = Yafo Sand Member.

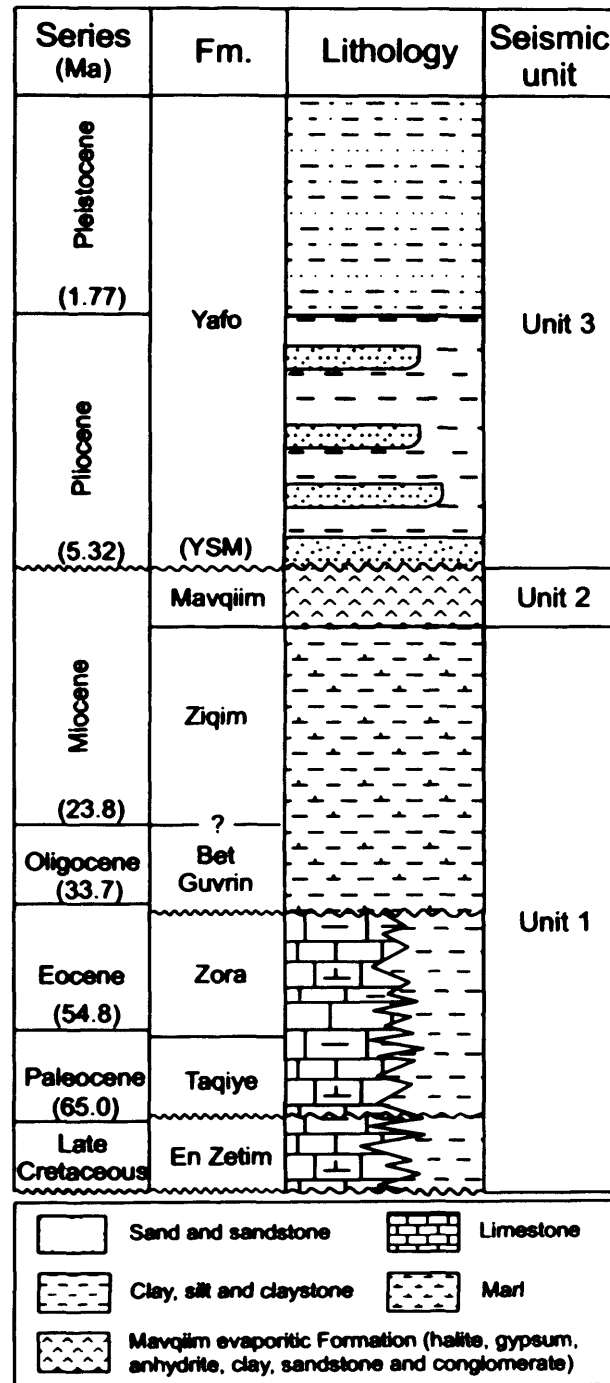


Figure 5.5 Stratigraphic chart showing the main formations observed in the study area (after Garfunkel & Almagor, 1987; Druckman et al., 1995), their age and the correlation with the seismic-stratigraphic units described in this paper. The lithological data are derived from unpublished stratigraphic well reports. Fm = Formation; YSM = Yafo Sand Member.

Upper Eocene deposits (Druckman et al., 1995). The lithology of the infill is represented by hemipelagic marls intercalated with debrites and fine- to medium-grained sandstone layers (Druckman et al., 1995).

5.5.2 Unit 2

This seismic-stratigraphic unit is bounded at the base by Horizon N and at the top by Horizon M. These horizons are regional seismic reflections, which represent the base (Horizon N) and the top (Horizon M) of the Messinian evaporites across the entire Mediterranean Basin (Hsü et al., 1973; Garfunkel & Almagor, 1987). Horizon N is represented in the study area by a strong negative seismic reflection (black event on the seismic sections) which exhibits a remarkable continuity (Fig. 5.4). This horizon is mainly conformable with the underlying reflections, showing only localized truncation in the marginal and basinal part of the study area.

Horizon M is a strong positive seismic reflection, highly continuous across the study area (Figs. 5.4a and b). The internal geometry of Unit 2 is characterized by the alternation of high and low amplitude seismic reflections with a transparent seismic facies (Fig. 5.4a). The thickness of Unit 2 varies from more than 1700 m towards the Levant Basin (Fig. 5.4a) to a few metres near the Levant continental margin, where eventually the Horizons N and M merge (Fig. 5.4a and b).

5.5.2.1 Well calibration of Unit 2

The stratigraphy of the Unit 2 is known only from stratigraphic reports that are mainly based on cutting analyses and petrophysical interpretation. However, there are only a limited number of full penetrations of the Messinian evaporites within the offshore Levant, with most of the wells either terminating within the upper part of the unit, or above it. The upper part of the Messinian evaporites is better calibrated, as where it has been cored (Fig. 5.6) it is found to consist of a layered evaporitic series that can be correlated to the Mavqiim Formation (Cohen, 1993; Druckman et al., 1995; Buchbinder & Zilberman, 1997). This part of Unit 2 in wells Gaza Marine-1, Gaza Marine-2, Or-1 and Or South-1 is composed of a thin layer of cryptocrystalline anhydrite passing upward to interbedded anhydrite and claystone, weakly calcareous, with traces of pyrite and chert (unpublished well reports). The lithologies within the near-basal part of the Messinian evaporites are inferred from well log data, and are

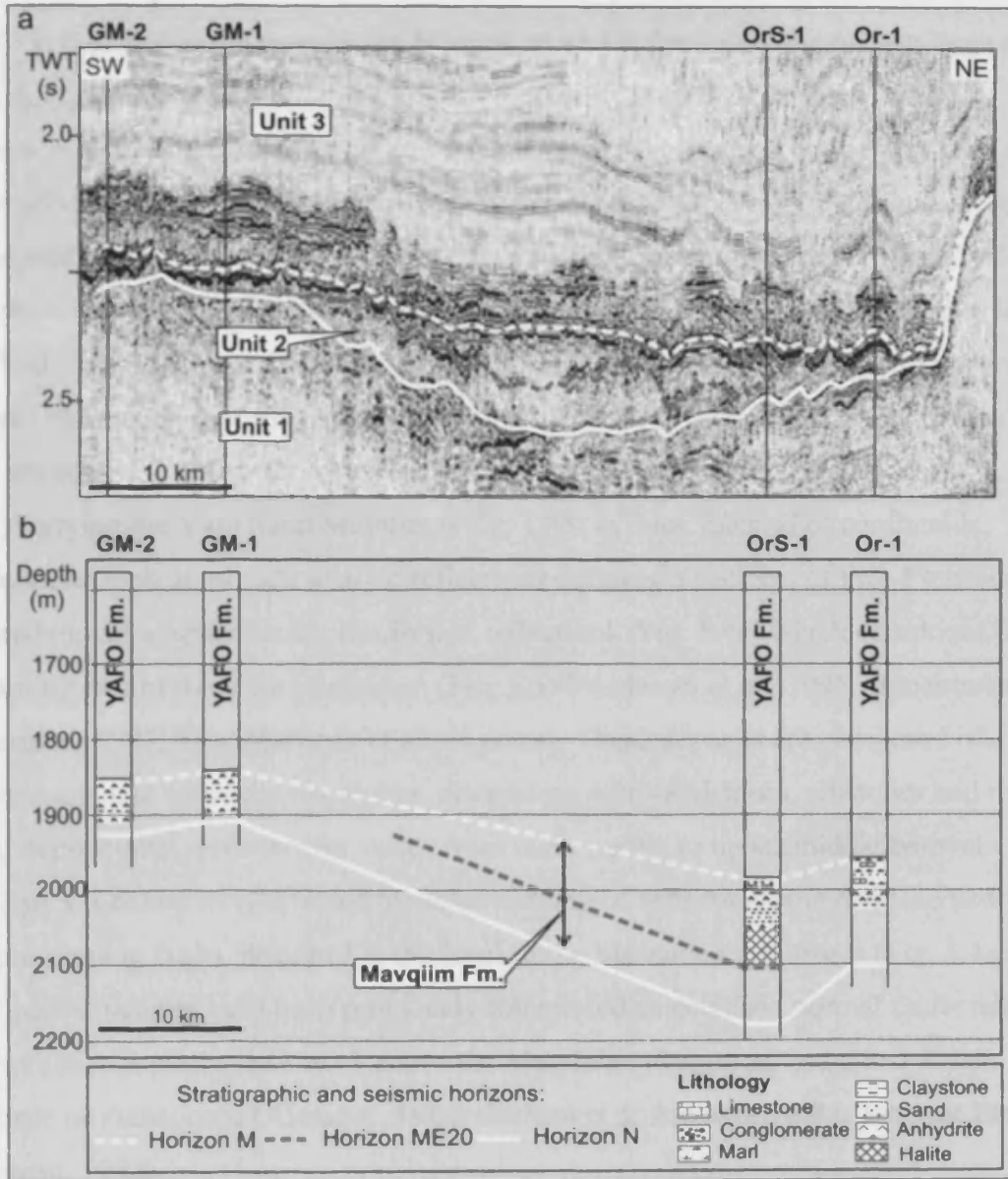


Figure 5.6 Correlation scheme of the Messinian evaporites in the Levant A seismic survey. a) Seismic section nearby the Levant margin, crossing the wells (location of wells in Fig. 5.2), and showing the seismic-stratigraphic units and the interpretation of the main seismic horizons. b) Schematic representation of the lithology and stratigraphic relationship of the Messinian evaporites as described in unpublished well reports. The main seismic horizons have been tied where possible to the lithological and stratigraphic units of the Mavqiim Formation.

composed of a thick halite interval, interbedded with a claystone/anhydrite layer that is a few metres in thickness (Fig. 5.6; unpublished well report).

5.5.3 Unit 3

Unit 3 is bounded at the base by the Horizon M and at the top by the present day seabed (Fig. 5.4). The basal part of Unit 3 is expressed as a 50 m thick package of high frequency, continuous high-amplitude seismic reflections that are restricted to the areas underlain by the Afiq and El-Arish canyons (Frey-Martinez et al., in press). According to the well data, this package consists of Lower Pliocene sandstone interbedded with claystone and marls, deposited in a basin floor turbiditic fan (Yafo Sand Member in Fig. 5.4b and 5.5; Frey-Martinez et al., in press). The El Arish and Afiq canyon have no seismic expression in the interval post-dating the Yafo Sand member and at present, they are buried features (Druckman et al., 1995; Frey-Martinez et al., in press).

Overlying the Yafo Sand Member is a c. 1700 m thick interval of continuous, moderate to high amplitude seismic reflections defining a package of Plio-Pleistocene progradational-aggradational clinoformal reflections (Fig. 5.4a) which comprises the remaining part of the Yafo Formation (Fig. 5.5; Druckman et al., 1995; Buchbinder & Zilberman, 1997; Frey-Martinez et al., in press). These deposits are composed of hemipelagic and turbiditic claystones, alternating with sandstones, siltstones and marls. Their depositional environment varies from outer neritic to upper/middle bathyal.

Unit 3 is extensively affected by downwarping of reflections and displacement by steeply-dipping faults, detached at the level of the Messinian evaporites (Fig. 5.4a and b). These structures have been previously interpreted as detached normal faults related to gravitational gliding of Unit 3 above the Messinian evaporites and dated as late Pliocene or Pleistocene (Almagor, 1984; Garfunkel & Almagor, 1987; Tibor & Ben Avraham, 1992).

5.6 Description of the circular structures

5.6.1 General features

Initial reconnaissance mapping of the study area using only the widely-spaced grid of 2D seismic profiles showed the top of the Messinian evaporites to exhibit a fairly featureless structure, with gentle dips and subtle topographic relief. However, more precise mapping of the top of the Messinian evaporites using the 12.5 m line spacing of

the 3D seismic data has led to the recognition of a series of localised depressions exhibiting a well-defined circular planform geometry. These structures (named progressively CS-1 to CS-10) are visible at the top of the Messinian evaporites and are evident on the time-structure map of Horizon M in the Levant A seismic survey (Fig. 5.7). They are situated a few hundred meters to a few kilometres basinward of the present day pinch-out of the Messinian evaporites (Fig. 5.7). The map shows the occurrence of the largest of the circular structures (CS-1) and a number of smaller structures (CS-2 to CS-10; Fig. 7). Their diameter varies from a few hundreds of metres (CS-2-9 and CS-10) to 1-2 km (CS-1 and CS-7). The occurrence of the circular structures is limited to the area outlined by the flanks of the Oligo-Miocene El Arish and Afiq submarine canyons (Fig. 5.7). One circular structure (CS-8) is located in a more basinward position, at c.10 km from the eastern margin of the Messinian evaporites (Fig. 5.7). This structure does not have a well-defined morphology on the time-structure map of Horizon M, but it is clearly circular on time-structure maps of the overlying horizons.

In cross section, the circular structures (Fig. 5.8 and 5.9) are bowl-shaped depressions with a gently concave upwards geometry. The stratal configuration of the deformed units is generally parallel stratified. However, some interbedded onlapping reflection-bound units are observed above the depressions (Fig. 5.8b and c). The depressions are rooted at the upper part of the Messinian evaporites (Fig. 5.8 and Fig. 5.9). The deformed stratigraphic interval lying above the depressions comprises the lower part of the Yafo Formation, from its base to the Upper Pliocene interval (Fig. 5.8b and c). This stratigraphic interval is defined as the overburden to the circular depressions. The largest of the circular depressions exhibits intense localised faulting of the overburden. Similar faulting may occur above the smaller circular depressions, but if so, is considered to be beneath seismic resolution. The thickness of the Messinian evaporites below the circular structures ranges from 150 m (Fig. 5.8) up to 800 m (Fig. 5.9).

Two other types of structures that relate to the deformation of the Messinian evaporites are evident on the map of Horizon M: a linear peripheral depression and marginal extensional faults (Fig. 5.7). Both the linear depression and the faults are detached at the level of the Messinian evaporites. The linear depression extends almost continuously along the locus of pinch-out of the Messinian evaporites and exhibits a

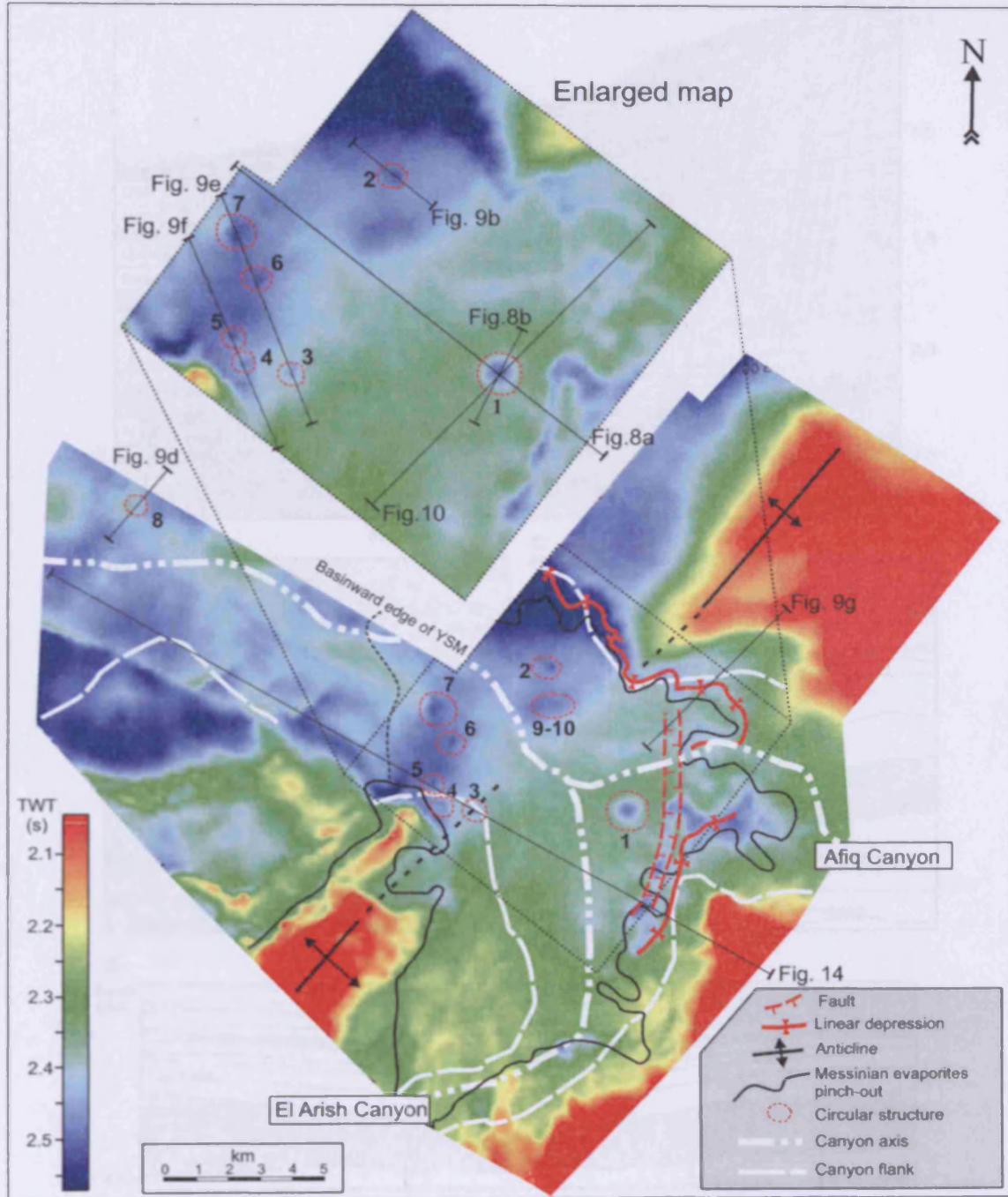


Figure 5.7 Time-structure map of Horizon M in the Levant A seismic survey. The zoom shows the distribution of the circular structures analyzed, named progressively CS-1 to CS-10. Note the presence of the linear depression and the extensional faults nearby the pinch-out of the Messinian evaporites. The main deep structures of the study area are represented by the anticlines (axes highlighted on the map) related to the Syrian Arc foldbelt system (Neev & Ben-Avraham, 1977, Tibor & Ben-Avraham, 1992). The location of the seismic sections displayed in Fig. 5.8, 5.9 and 5.13 is indicated.

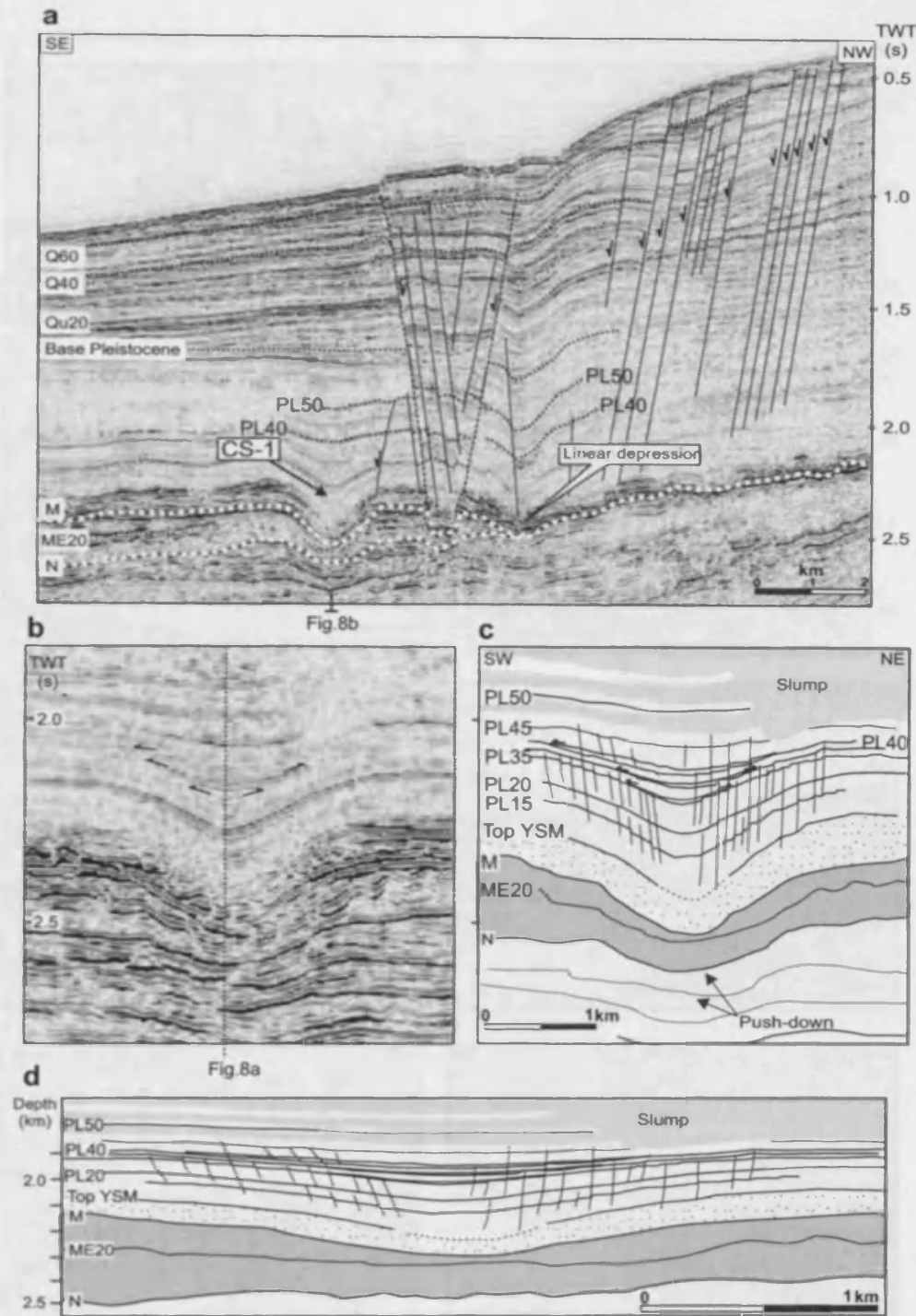


Figure 5.8 a) Seismic section perpendicular to the Levant margin, crossing the structure CS-1 through its centre (location in Fig. 5.6). The seismic package from the Base Pleistocene to Q60 shows thickness variation across the extensional faults, defining their phase of growth. b) Seismic section crossing CS-1 through its centre, and c) interpretation. The apparent downsag of Horizon N and the underlying seismic reflections below CS-1 is caused by a seismic 'push-down', due to the seismic velocity contrast between the Messinian evaporites (Unit 2) and the marine clastic sediments of Unit 3. This section shows the thickening of the stratigraphic package PL20-PL50 and onlap of reflections within the same interval above CS-1. Note the set of extensional and subvertical faults, steeply dipping toward the centre of CS-1 and deforming its overburden. YSM = Yafso Sand Member. d) 1:1 vertical to horizontal ratio of Fig. 5.8c.

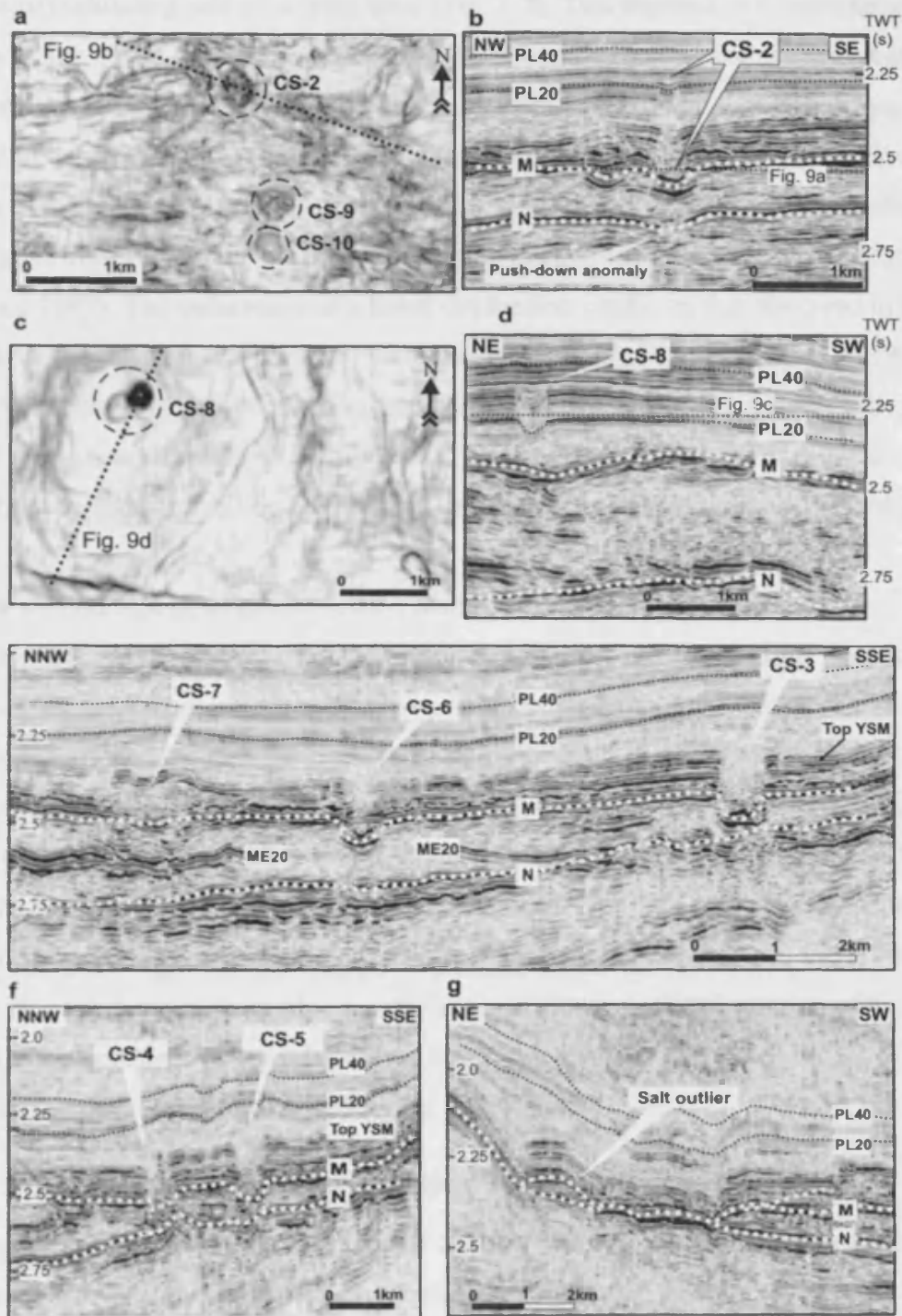


Figure 5.9 a) Variance time slice (2512 ms) showing the circular appearance of CS-2, CS-9 and CS-10 in plan view. The location of the seismic cross section of Fig. 5.9b is indicated. b) Seismic section across CS-2 (see Fig. 5.7 for location). A minor push-down effect is present at the Horizon N beneath CS-2. c) Variance time slice (2256 ms) showing the circular appearance of CS-8 in plan view. The location of the seismic cross section of Fig. 9d is indicated. d) Seismic section across CS-8 (see Fig. 5.7 for location). e) Seismic section across CS-3, CS-6 and CS-7 (see Fig. 5.7 for location). f) Seismic section across CS-4 and CS-5 (see Fig. 5.7 for location). M = Horizon M, N = Horizon N. g) Salt outlier located in the northern area of the pinch-out of the Messinian evaporites (see Fig. 5.7 for location).

straight to undulating pattern in plan view (Fig. 5.7). This depression is associated with downwarping of the overlying reflections (Fig. 5.7 and 5.8). This feature resembles peripheral sinks and rim synclines observed adjacent to salt diapirs, i.e. the depression created in the surface as a result of the flowage of the mobile layer into the positive feature (Trusheim, 1960). The same linear peripheral depression has been described at the edge of dissolving thick evaporitic beds, due to edge-inward meteoric dissolution (Warren, 1997). The occurrence of a linear depression similar to that observed in the study area has been recorded in the Eratosthenes Seamount (Major & Ryan, 1999) and in the Bannock Structure, Mediterranean Ridge (Von Huene, 1997), nearer to the study area. These linear depressions are filled with brines that are the result of dissolution of evaporites by fluids travelling up the flank of the structure (Von Huene, 1997; Major & Ryan, 1999).

The second type of evaporite-related features is represented by a system of extensional faults deforming Unit 3 at the eastern margin of the Messinian evaporites (Fig. 5.7 and 5.8). They are interpreted as growth faults based on sediment thickness variation from the hangingwall to the footwall of the fault (Fig. 5.8; Cartwright, 1992). These faults have been related to gravitational gliding of the Plio-Pleistocene sediments above the evaporite detachment level (Almagor, 1984; Garfunkel & Almagor, 1987; Tibor & Ben Avraham, 1992). They are analogous to the peripheral evaporite-related structures described in the North Sea (Jenyon, 1986; Coward & Stewart, 1995; Huuse, 1999). In some parts of the study area, the process of marginal deformation of the Messinian evaporites created salt outliers that are observed landward of the locus of pinch-out of the Messinian evaporites (Fig. 5.9g).

5.6.2 Circular structure CS-1: detailed 3D seismic interpretation

The most dramatic and best imaged of the circular depressions mapped within the study area is CS-1, as clearly seen on the time-structure map of Horizon M (Fig. 5.7). Because of the quality of the imaging, this structure is described in detail in the present section. CS-1 is a relatively isolated feature, situated 2 km west of the eastern pinch-out of the Messinian evaporites (Fig. 5.7).

5.6.2.1 Morphology

CS-1 exhibits a concave upward, U-shaped geometry at Horizon M, with a diameter of c. 2 km, as measured on cross section between its opposite external rims (Fig. 5.8). The

base of this structure is rooted in the upper part of the Messinian evaporites (Fig. 5.8). The overlying Pliocene reflections display a regular layer-cake stratigraphy of downwarped reflections defining a U-shaped depression (Fig. 5.8). The morphology of CS-1 is mostly evident on the 3D visualization of the time-structure map of Horizon PL20 (Fig. 5.10). Half of the circular depression is visible in this display as a sharply defined, nearly half-conical structure (Fig. 5.10).

5.6.2.2 Stratigraphic architecture

Seismic sections crossing CS-1 (Fig. 5.8) clearly show that this structure is associated with structural deformation of the overburden, which is represented by the horizons overlying CS-1 from Horizon M to PL60 (Fig. 5.8b and c). The base of the Messinian evaporites (Horizon N) exhibits an apparent sag beneath CS-1 (Fig. 5.8b and 5.10). This feature is interpreted as a negative seismic velocity anomaly (push-down, see Fig. 4 for explanation). Restored to its original depth, Horizon N appears undeformed beneath CS-1 (Fig. 5.8d).

Horizon M displays a partly chaotic geometry across CS-1 (Fig. 5.8a and b). The flanks of the depression are oversteepened, and exhibit a maximum dip of 10°-16°. The chaotic and oversteepened character of Horizon M in this area indicates collapse of the upper parts of the Messinian evaporites in the circular area defined by CS-1. This collapse is associated with a vertical negative relief of approximately 180 m, defined as the maximum downwards deflection below the regional datum.

Importantly, there is evidence of volume loss within the Messinian evaporites, in the area defined by CS-1, when compared to the original depositional thickness in nearby areas where there are no circular structures or signs of evaporite depletion (Fig. 5.8a). Due to the clearly defined conical morphology of the circular depression, it is possible to calculate the discrete loss of volume associated with CS-1 in the upper part of Unit 2 as c. 0.188 km³. There is evidence from the reflection configurations within the Messinian that volume loss was not uniform over the full vertical extent, but was restricted to the upper part of the Messinian evaporites (Fig. 5.8 and 5.10). As it appears in Figure 5.8d, the thickness of the seismic package comprised between Horizon N and ME20 is nearly constant while the package from ME20 to Horizon M thins considerably across CS-1. This observation argues strongly that this lower interval (Horizon N-ME20) was virtually unaffected by the depletion.

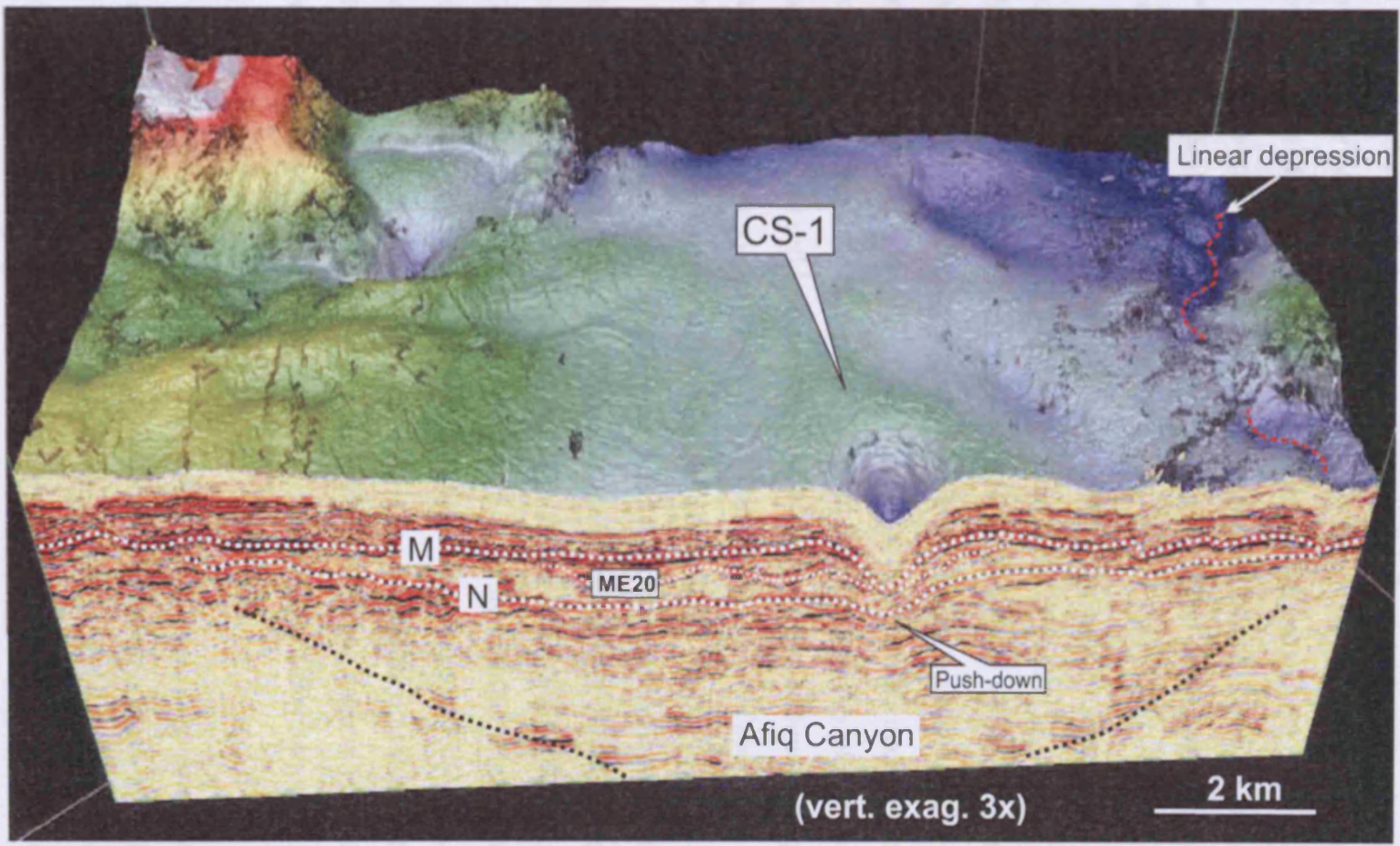


Figure 5.10 Three-dimensional visualization of the time-structure map of Horizon PL20, cutting at the top of a seismic section parallel to the Levant continental margin (see location in Fig. 5.7), and crossing the circular structure CS-1. Half of CS-1 is visualized on this map, showing the relationship with the underlying stratigraphy. In Unit 2 (Messinian evaporites) the interval between Horizon ME20 and Horizon M appears to thin-out toward the flanks of CS-1.

5.6.2.3 Structural analysis

The overburden to CS-1 displays a sequential deformation pattern that constrains the timing of the development of this structure. The overburden can be divided into three packages based on the geometry of the seismic reflections (Fig. 5.8b and c):

- The first package is bounded at the base by Horizon M and at the top by Horizon PL20. This package is composed of parallel-stratified downsagged reflections, with no considerable thickness variation across CS-1 (Fig. 5.8b and c).

- The second seismic package is bounded at the base by Horizon PL20 and at the top by Horizon PL50, and it is the key interval for structural analysis of the overburden deformation. This seismic package exhibits a convergent reflection configuration, coupled with localised but significant thickness variation above CS-1 (Fig. 5.8b and c). Importantly, in the interval PL35-PL45 there is evidence of concentric onlap against the internal rim of the depression (Fig. 5.8b and c). The geometry of this onlap relationship and the convergent reflection configuration suggest a syn-sedimentary growth of the structural depression (Cartwright, 1992) during deposition of sediments in the PL20-PL50 interval, as opposed to the infill of a pre-existing structure (Fig. 5.3b and c).

- The third seismic package is bounded at the base by Horizon PL50 and the top by the Base Pleistocene horizon. This package is composed of parallel reflections, which exhibit no downsag and thickness variation across CS-1 (Fig. 5.8b and c).

The transition from a parallel configuration in the overburden immediately overlying Horizon M to a convergent reflection configuration above indicates that the discrete and localized volume loss within the evaporites caused the downsag of the overburden (Horizon M-PL20) and led to the subsequent infill of the depression during the progressive development of its structural relief (PL20-PL50 interval).

5.6.2.4 Faults

The structural deformation of the overburden to CS-1 is associated with a series of high-angle normal faults exhibiting predominantly domino geometry (Fig. 5.8b and c). The faults dip inwards toward the downsagged part of CS-1, with throws ranging from 10 to 15 m and dips from 60° to nearly subvertical (Fig. 5.8d). The faulted interval occurs between Horizon M and PL50 (Fig. 5.8c), with a thickness of c. 500 m (Fig. 5.8d). The fault system is interpreted to consist of a set of small growth faults, because the faults must have affected the seabed at the time of their formation, as indicated by

the onlap and thickening pattern of the overburden in the PL20-PL50 package (Fig. 5.8c). The fault pattern in plan view is particularly well seen on the TWT- dip map of horizon PL20 (Fig. 5.11) where the faults exhibit a striking concentric pattern. Individual faults are approximately 500-1000 m long and traverse about 30 – 160° of arc around the collapse structure.

The faults are more numerous within a radius of 1 km from the centre of the structure (Fig. 5.11a and b). The planform geometry of the faults is comparable to 'ring faults' observed above collapse structures (e.g. karst, calderas, withdrawal basins; Branney, 1995; Stewart, 1999; Maione, 2001). The observations made on the set of faults above CS-1 suggest that they are the result of a horizontally radial extensional stress field, induced by the collapse of the circular depression.

5.6.2.5 Onset and timing

As documented above, the syn-sedimentary growth of the circular depression CS-1 has been stratigraphically tied to the seismic interval comprised between Horizons PL20 and PL50. The timing of formation of CS-1 has been quantitatively assessed by measuring two key parameters linked to the structural analysis of the overburden: the vertical relief (ΔZ) and expansion index (E.I.) (Fig. 5.3a). The values measured have subsequently been interpolated in diagrams where they are plotted against the depth of the point measured, and tied from wells to the chronostratigraphic chart (Fig. 5.12).

The ΔZ associated with CS-1 decreases progressively from Horizon M to PL65 (Fig. 5.12a-c). In the first part of the curve the vertical relief drops moderately, displaying very limited variation from 180 m to 160 m (Horizon M to PL20). Therefore the vertical relief in the Zanclean to the Lower Piacenzian interval is similar to the relief created by the collapse of the top of the Messinian evaporites. The value of the vertical relief drops rapidly from 160 to 50 m in the interval PL20-PL50, and is stratigraphically confined within the Piacenzian. This reduction mainly coincides with the convergent reflection configuration and onlap fill interval and hence the main phase of growth of the structure. The steepness of the curve then increases again reaching the zero value at Horizon PL65 (directly above the Base Pleistocene).

The E.I. diagrams (Fig. 5.12d-f) exhibit a general trend characterized by the main peaks well within the Piacenzian interval (horizons PL25 to PL50), where it reaches the value 2.1. The expansion index decreases both up and down section from the main

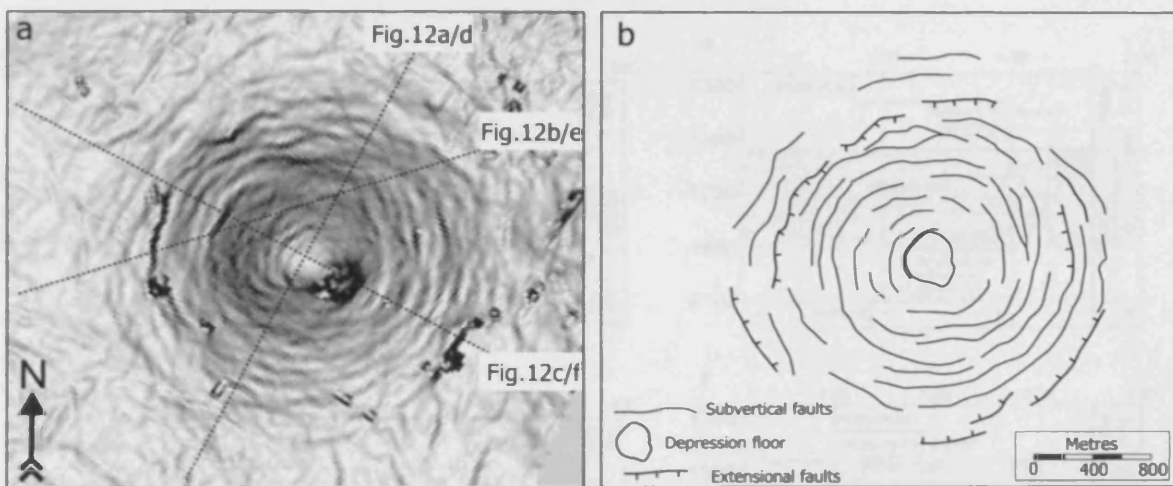


Figure 5.11 a) TWT-dip attribute map of Horizon PL20, and b) interpretation, showing the detailed morphology of this surface and the deformation associated with the circular structure CS-1. Note the pattern of concentric extensional and subvertical faults around CS-1. The dotted lines highlight the position of the seismic sections used for the measurements displayed in Fig. 5.12.

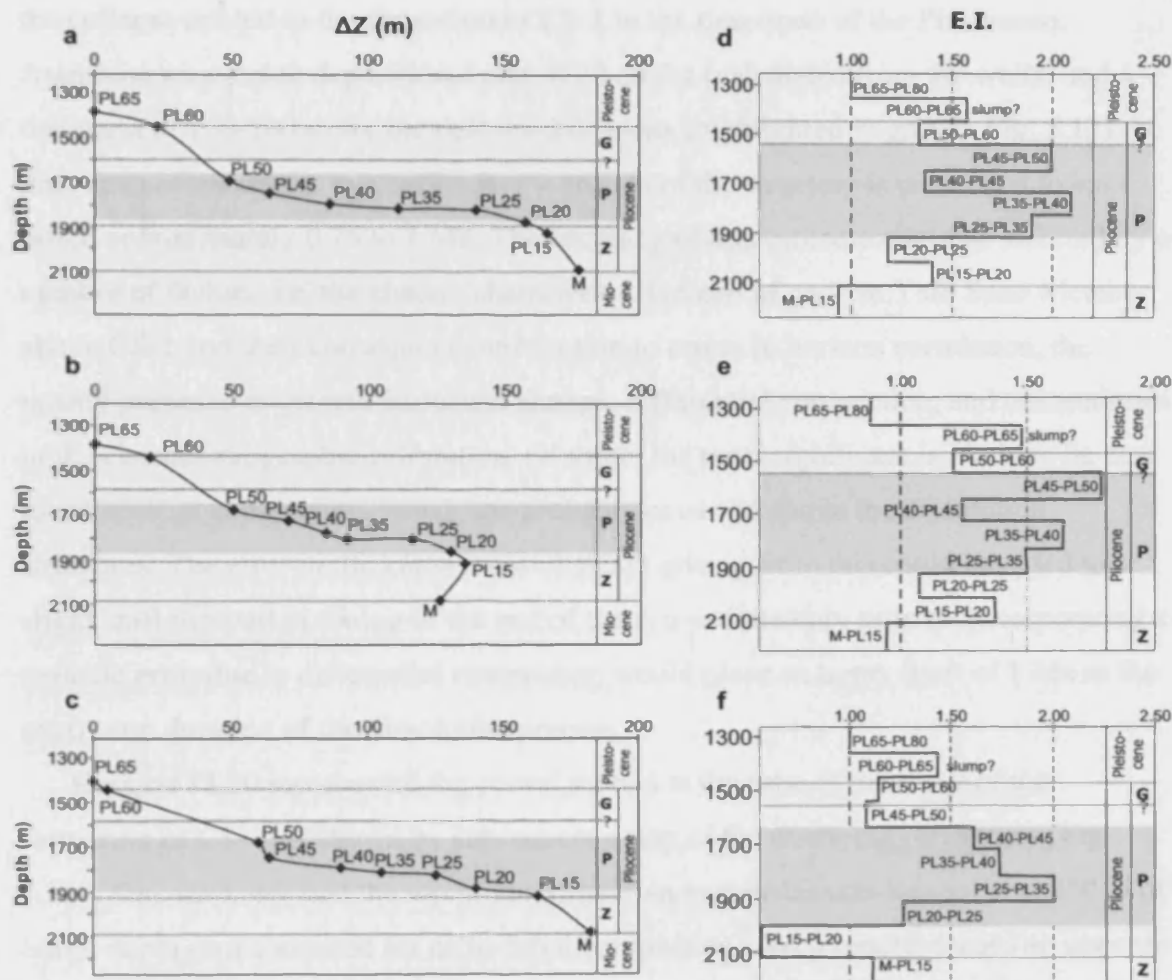


Figure 5.12 Diagrams showing the vertical relief (ΔZ) and expansion index (E.I.) measured and calculated on random seismic sections across CS-1 (see location of sections in Fig. 5.10). See Fig. 5.3a for explanation of the parameters. The reference horizon for the measurements is taken at the seabed that represents a horizontal surface above CS-1. ΔZ (Fig. 5.11a to c) and E.I. (Fig. 5.11d to f) are plotted (x axis) in the diagrams against the depth of the reference horizon (y axis, in meters), and against the stratigraphic chart. The grey areas highlight the maximum observed variation of the vertical relief (Figure 5.11a to c) and the maximum values of the expansion index (Figure 5.11d to f), which are interpreted as related to the time of maximum syn-sedimentary growth of CS-1.

peaks. Minor pulses of the E.I. (e.g. PL40-PL45 in Fig. 5.12d and e) could be explained by polyphase structuring of CS-1 within this interval.

The interpretation arising from these diagrams substantially constrains the onset of the collapse related to the formation of CS-1 in the time-span of the Piacenzian. Assuming an average depositional rate of 20 cm/ka (calculated from the wells) and a thickness of 150-200 m for the deformed deposits (highlighted in grey in Fig. 5.12) the time span of maximum syn-sedimentary growth of the structure is calculated to have lasted approximately 0.75 to 1 Ma. The accuracy of this estimate could be affected by a number of factors, i.e. the chaotic character of Horizon M and the Yafo Sand Member above CS-1 and their consequent contribution to errors in horizon correlation, the nearby presence of growth faults and slumps, differential compaction, and uncertainties in the chronostratigraphic calibration. Of these, the most significant is likely to be due to differential compaction, which has probably occurred above the dissolution structures. The error in thickness measurements arising from this could have led to a slight shift forward in timing of the end of the syn-sedimentary growth. Incorporating a realistic error due to differential compaction would place an upper limit of 1 Ma as the maximum duration of the dissolution process.

Horizon PL20 represented the coeval seabed at the time of the onset of the formation of CS-1, as shown by subsequent onlap of the overlying reflections (Fig. 5.8b). This indicates that the top of the Messinian evaporites was located at c. 250 m of burial depth (not corrected for differential compaction). Well reports record an upper to middle bathyal depositional environment of the Yafo Formation overlying the Messinian evaporites. Therefore it is concluded that the process responsible for the growth of the CS-1 structure was in a fully submarine environmental context.

Comparison of the timing of the development of CS-1 and other important structures on a more regional scale along the margin shows unequivocally that the collapse of CS-1 pre-dated the evolution of major gravity tectonic structures. Seismic sections perpendicular to the marginal extensional faults (Fig. 5.8a) show that although downwarping or displacement of the overburden above these structures are associated with thickness variation and onlap patterns similar to that observed in the overburden of CS-1, the timing of the growth interval is much later, within the Pleistocene (Fig. 5.8a).

5.6.3 Circular structure CS-2 to CS-10: detailed 3D seismic interpretation

On the time-structure map of Horizon M, a series of smaller circular depressions are identified and named CS-2 to CS-10 (Fig. 5.7). Their diameter ranges between 200 m and 1 km, and they are localized to a small area west of CS-1, close to the northern and southern locus of pinch-out of the Messinian Unit, or in a more basinward position.

The smaller circular structures are rooted within the upper part of the Messinian evaporites, where evidence of volume loss associated with the structures is observed (Fig. 5.9). However, the reduced size of the depressions precludes any accurate calculation of loss of volume in each case. The circular depressions exhibit the same general geometrical characteristics to those described for CS-1, i.e. the concave upward geometry and the disruption of Horizon M and of the overburden (Fig. 5.9). The negative structural relief above the structures ranges between 50 and 100 m as measured on Horizon M (Fig. 5.9a, e, f).

The deformed overburden to the circular structures appears to be more limited stratigraphically than the deformed overburden to CS-1. The vertical extent of the disrupted zone above CS-3 to CS-6 is confined to the Yafo Sand Member (Fig. 5.9e and f), while above CS-2 and CS-8 the disruption reaches the seismic reflections comprised between Horizon PL20 and PL40 (Fig. 5.9b and d).

The structural deformation of the overburden above the circular depressions shows variable characteristics, that are generally more difficult to analyse than in the case of CS-1. Thickness variation is observed above CS-2 and CS-8 in the PL20-PL40 stratigraphic interval (Fig. 5.9b and d). In this interval, onlap of seismic reflections is observed over CS-8, above Horizon PL20 (Fig. 5.9d). The overburden to CS-3, 4, 5 and 7 (Fig. 5.9e and f) exhibits a chaotic pattern and structural disruption within the Yafo Sand Member, while Horizon PL20 appears to be locally upwarped. No faulting is evident above any of these smaller circular structures. It seems likely, however, that owing to their limited size, faults may well be present but they may simply be too small to be imaged individually.

Despite the imaging problems associated with their smaller diameters, the timing of the onset of the smaller circular structures can be assessed by comparison with CS-1 using the same procedure applied in the case of CS-1. In general, the thickness variation of the overburden above all the circular depressions is confined to the interval between the Yafo Sand Member and Horizon PL40. The onlap observed above CS-8

(Fig. 5.9d) appears to constrain the time of formation of this particular circular structure well within the stratigraphic interval PL20-PL40. Therefore the smaller circular structures appear to have formed between the Zanclean and the Piacenzian (Horizon PL40). The growth interval of the smaller circular structures (Zanclean-Piacenzian) appears more extensive than that of CS-1 (Piacenzian). A discrepancy in the style of the structural deformation has also been observed between CS-1 and some of the smaller circular structures (e.g. the vertical sides of CS-3). These differences could be related to variation in degree of lithification of the overburden, causing it to collapse vertically (CS-3) rather than with more gentle downsagging (CS-1). However, it is equally likely that the discrepancies observed in timing of growth and in structural style could be due to imaging problems at the limits of seismic resolution, such that the real extent of deformation of the smaller circular structures is not correctly portrayed in the seismic data. Whatever the explanation for the minor differences, the overall growth period for all the circular structures overlaps to a high degree within the Pliocene, and this suggests a common mechanism for their origin.

5.7 Discussion

5.7.1 Observations and identification

A number of contrasting geological processes can produce circular structures ranging, from catastrophic gas expulsion to form pockmark craters, to meteorite impacts (Stewart, 1999). No general uniformity of process links this diversity of circular geological structures other than the action of the process is centred at a point (the centre of the circular feature). As discussed by Stewart (1999), the best approach to diagnose the origin of circular structures is to document their size, cross-sectional geometry and distribution with respect to the structural and stratigraphic context. The key characteristics of the circular structures observed in the study area are:

- the circular geometry in plan view, and negative (concave upward) relief, with their diameter ranging between 200 m and 2 km;
- the downwarped or partly chaotic overburden;
- the depletion of the underlying tabular Messinian evaporites;

- the concentric fault pattern and thereby dominantly radial extensional stress field centred on the axis of the depression.

Given the location of the collapse structures directly above a depleted evaporite unit, it is most plausible interpretation for the genesis of these structures is intrinsically linked to the loss of the evaporites from the region directly beneath the collapse structures. It is highly significant that on CS-1, the volume of missing evaporites is equivalent to the volume of the depression as measured at the Horizon PL20, implying a direct volumetric coupling between removal of evaporites and downwarping of the overburden.

Two mechanisms linked to deformation of evaporites can potentially generate circular structures, (1) evaporite withdrawal (Jackson & Vendeville, 1995), and (2) dissolution (Ge & Jackson, 1998). Withdrawal and flowage of mobile evaporites (most likely halite) involves a constant volume assumption, and therefore it should be expected that there would be positive salt structures of comparable excess volume above regional to match the depletion below regional (see e.g. Jackson and Talbot, 1986; Davison et al., 2000). The absence of any positive structural elements (as pillows or small diapirs) close to the depressions makes it difficult to accept salt withdrawal as a viable process for the genesis of the circular structures. Consequently, it is argued here that the only feasible mechanism for the formation of the circular depressions is the collapse of the overburden due to the *in situ* dissolution of the underlying Messinian evaporites.

The amount of fluid necessary to form the largest dissolution structure (CS-1) can be crudely estimated, assuming that dissolution of pure halite (NaCl) took place in fresh water solution. Using a solubility of NaCl in fresh water of 359 g/l (Davies, 1989), the volume of water required to dissolve 0.188 km³ of NaCl (i.e. the volume of CS-1) is calculated as 1.15 km³. Using a time-averaged dissolution rate, and based on the timing of 1 Ma for the growth period for CS-1, the minimum rate of evaporite dissolution can be estimated as 188 m³/a.

The interpretation of the circular depressions in the study area as dissolution structures is strengthened by the analogy with other described examples of circular collapse structures created by dissolution of evaporites on the seabed of the Eastern Mediterranean basin (Ross & Uchupi, 1973; Kastens & Spiess, 1984) and in the North Sea (Lohmann, 1972; Jenyon, 1983). Their circular pattern has generally been related

to their location at the top of underlying salt diapirs (Ross & Uchupi, 1973; Kastens & Spiess, 1984; Ge & Jackson, 1998; Cartwright et al., 2001). Despite the recognition that such structures occur in salt provinces, the mechanism of formation of circular dissolution structures above a tabular evaporitic body is poorly understood, and is therefore further discussed below.

5.7.2 Genesis

The mechanism invoked for the formation of the dissolution structures needs to account for the circular shape of the dissolution structures, their submarine context and the burial depth of the evaporites at the time of their formation. The key to understanding the mechanism lies in the analysis of the geological and hydrological framework of the basin, coupled with the timing of evaporite dissolution.

5.7.2.1 Mechanism of dissolution

Three main modes of dissolution of buried evaporites have been described in sedimentary basins (Johnson, 1997; Warren, 1997, 1999; Cartwright et al., 2001), according to the mechanism of migration of undersaturated fluid:

- (1) lateral dissolution;
- (2) superjacent dissolution;
- (3) subjacent dissolution.

(1) *Lateral dissolution* results from circulation of undersaturated fluids along the edges of the evaporite body. This process could have promoted linear dissolution along the evaporite pinch-out. However it cannot be invoked for the creation of the dissolution structures described here, due to their localised and circular geometry, and to their location at some distance from the edge of the evaporites.

(2) *Superjacent dissolution* results from circulation of relatively undersaturated fluids above the evaporites, from either an overlying aquifer or from fluids penetrating at the evaporites through structural pathways e.g. faults (Cartwright et al., 2001). In this area, the unit immediately overlying the evaporites is the Lower Pliocene Yafo Sand Member, which is a sand-dominated body. However, this permeable unit is strictly confined to the thalweg of the Afiq Canyon and sealed laterally, and is thus unlikely to have acted as an extensive aquifer. Moreover, at least one of the dissolution structures is located basinward of the most distal reaches of the Yafo Sand Member (Fig. 5.7) and could not therefore have been formed by fluids flowing along this potential aquifer.

The rest of the Yafo formation overlying the evaporites is dominantly composed of fine-grained siliciclastic sediments. Therefore this low permeability unit could not have acted as an extensive aquifer and it could not have provided the undersaturated fluids necessary for the dissolution of the Messinian evaporites. It could be argued that the marginal growth faults may have provided the pathways for penetration of undersaturated fluid at the top of the evaporites. However, syn-sedimentary growth of the faults is recorded only from the Lower-Middle Pleistocene (Fig. 5.8a), and therefore the timing of activity of the faults clearly post-dates the formation of the circular dissolution structures. Moreover, this mechanism of fault-related downward penetration of undersaturated fluid does not provide a simple explanation for the circular and localised geometry of the dissolution structures.

(3) *Subjacent dissolution* results from undersaturated fluids migrating along the base of the evaporites. Examples of this type of dissolution have been recorded in the North Sea (Cartwright et al., 2001) and Khorat Plateau in Thailand (Warren, 1997; El Tabakh et al., 1998). Evaporite beds are impermeable once buried to depths of few hundred metres, where they act as an aquiclude (Warren, 1997). In the study area, the thick evaporitic series could have acted as an efficient seal for upward migration of deep fluids in the clastic deposits of Unit 1, underlying the evaporites. It is therefore acceptable that relatively low salinity fluids within the pre-evaporitic sediments, migrating upward, could have promoted subjacent dissolution of the more soluble evaporites. Importantly, this mechanism could account for the circular and localized geometry of the dissolution structures, as explained further below.

The Levant Basin experienced considerable subsidence and sediment accumulation during the Pliocene (Tibor et al., 1992). It is probable that rapid burial of the pre-evaporitic units would render them prone to overpressuring, with the evaporitic series defining the top of the zone of overpressure even at shallow depths, because of the high sealing capacity of the evaporites (Warren, 1997). In support of this suggestion, evidence of focused vertical fluid flow processes related to overpressured pre-evaporitic sedimentary units such as mud volcanoes, diapirs, and seabed mounds have been described in the study area (Frey-Martinez et al., in press) and in the nearby deep Nile cone area (Loncke et al., 2004). Most significantly, a series of kilometer-scale conical mounds developed within the Yafo Sand Member has been attributed by Frey-Martinez et al., (in press) to highly focused vertical fluid flow along the axis of the Afiq

Canyon, providing evidence of sediment remobilization of the canyon fill and the Yafo Sand Member sediments. The striking similarity in the geometry and timing between the dissolution structures and the conical seabed mounds strongly supports the hypothesis of a common mechanism for their origin, driven by vertical and localized expulsion of fluids in the overpressured pre-evaporitic sediments. The location of the dissolution structures (Fig. 5.7) and of the mounds along the Oligo-Miocene depositional fairway of the Afiq Canyon (Frey-Martinez et al., in press) points to a pivotal role of the El-Arish and Afiq submarine canyons on the pathways and localisation of upward escaping pore fluids.

It is probable that where the Messinian evaporites were too thick to be pierced, the focused fluid flow partially dissolved and fractured the base of the evaporites, causing the fluids to penetrate into the upper parts of the evaporites. Based on these observations, we propose a model for the evolution of the circular dissolution structures in the study area, which is illustrated and explained in detail in Fig. 5.13.

Previously it has been argued that the depletion of evaporites to form the depressions above was focused mainly within the upper part of the Messinian evaporites. At first sight, this might be taken to suggest that suprajacent dissolution was a more likely model. However, in our view it is equally plausible that fracture conduits for the upwelling of undersaturated fluids ascending from below (Warren, 1999) could easily have preferentially dissolved the most soluble lithologies, located at the top of the layered evaporitic package. The fracture conduits would have been opened by the ascending high-pressure fluids, acting 'corrosively' on the lower part of the evaporite succession. This 'corrosive' action might then also explain the extraordinary circular planform of the dissolution structures themselves.

5.7.2.2 *Origin of fluid flow*

The origin of the fluids responsible for dissolution of the evaporites and creation of the circular structures can conceivably be attributed to three potential sources: (1) gypsum to anhydrite conversion, (2) sediment compaction, and (3) seismic pumping related to earthquakes on deep basement faults. The source of fluid supply needs to account for the timing, duration, salinity and most importantly, the circularity of the dissolution structures.

(1) Burial of gypsum results in its dehydration into anhydrite and this conversion releases fluids that are undersaturated in Na and Cl, and thus capable of dissolving

... (B) ... (C) ... (D) ...

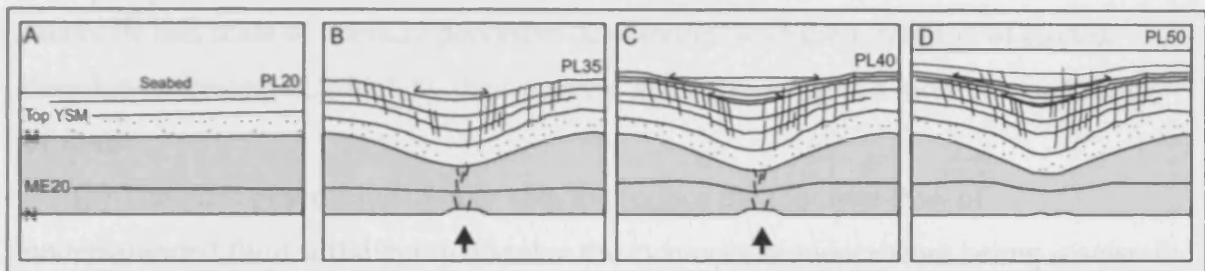


Figure 5.13 Schematic cartoon depicting the successive phases of formation of the circular dissolution structure CS-1. The dissolution process started in the early Piacenzian (B), when vertical focused fluid flow begun corroding the lower evaporitic unit and dissolving its upper and more soluble part, causing collapse of the overburden and successive onlap of sediments (B and C) at the coeval seabed. Note in this interval the formation of the concentric faults directly related to the collapse of the sediments above the depleted evaporitic unit. The process terminated by the late Piacenzian (D), with the deposition of Horizon PL50. N = Horizon N; M = Horizon M.

halite (Warren, 1991). This conversion could have occurred at the base or within the evaporitic unit in the study area. However, the temperature and pressure conditions required (Warren, 1991) were only reached within the Pleistocene, therefore much later than the formation of the circular structures. Gypsum to anhydrite conversion is therefore rejected as a possible mechanism for generation of the dissolving fluids.

(2) The second possible source of relatively undersaturated fluids is the compaction of the thick sedimentary sequences beneath the evaporites. Pore fluids expelled during compaction would most probably be undersaturated in composition (Magara, 1978). However, compaction of the pre-evaporitic sediments in the study area represents a gradual and areally widespread form of fluid expulsion, and it is therefore difficult to reconcile this scale of laterally pervasive dewatering with the formation of circular dissolution structures, which by their discrete geometry suggest a more focused supply of fluid.

(3) The third process potentially able to produce the requisite flow of undersaturated fluid sufficient to dissolve the evaporite sequence from below is seismic pumping related to earthquakes on deep basement faults. The tectonic framework of the study area shows clear evidence of the existence of deep-seated structures below the Messinian evaporites (Fig. 5.14). The principal structures are anticlines and faults linked to the Syrian Arc foldbelt (Fig. 5.14, Neev & Ben-Avraham, 1977; Garfunkel et al., 1979). The area is seismologically active at present and this level of activity could be expected to have occurred throughout much of the Neogene (Garfunkel & Almagor, 1985; Garfunkel, 1998; Vidal et al., 2000). Major earthquakes are well known to lead to expulsion of basinal fluids (Sibson et al., 1978), therefore the activity of deep-seated structures could have generated focused fluid flow by seismic pumping.

Although it could be argued that the deep-seated tectonic structures would most likely represent a linear fluid flow at depth, the flow could have become focused during its ascent. For example, previous workers have linked the occurrence of mud diapirs, mud volcanoes and slumps to earthquake activity in the southeastern Mediterranean region (Loncke et al., 2004; Frey-Martinez et al., in press).

Based on the arguments presented above, the most probable trigger mechanism for the initiation of the dissolution process is considered to be seismic activity. The circular dissolution structures are strikingly similar in shape, timing and location with mounded structures due to mud diapirism at this level of the Yafo Sand Member described just

5-34

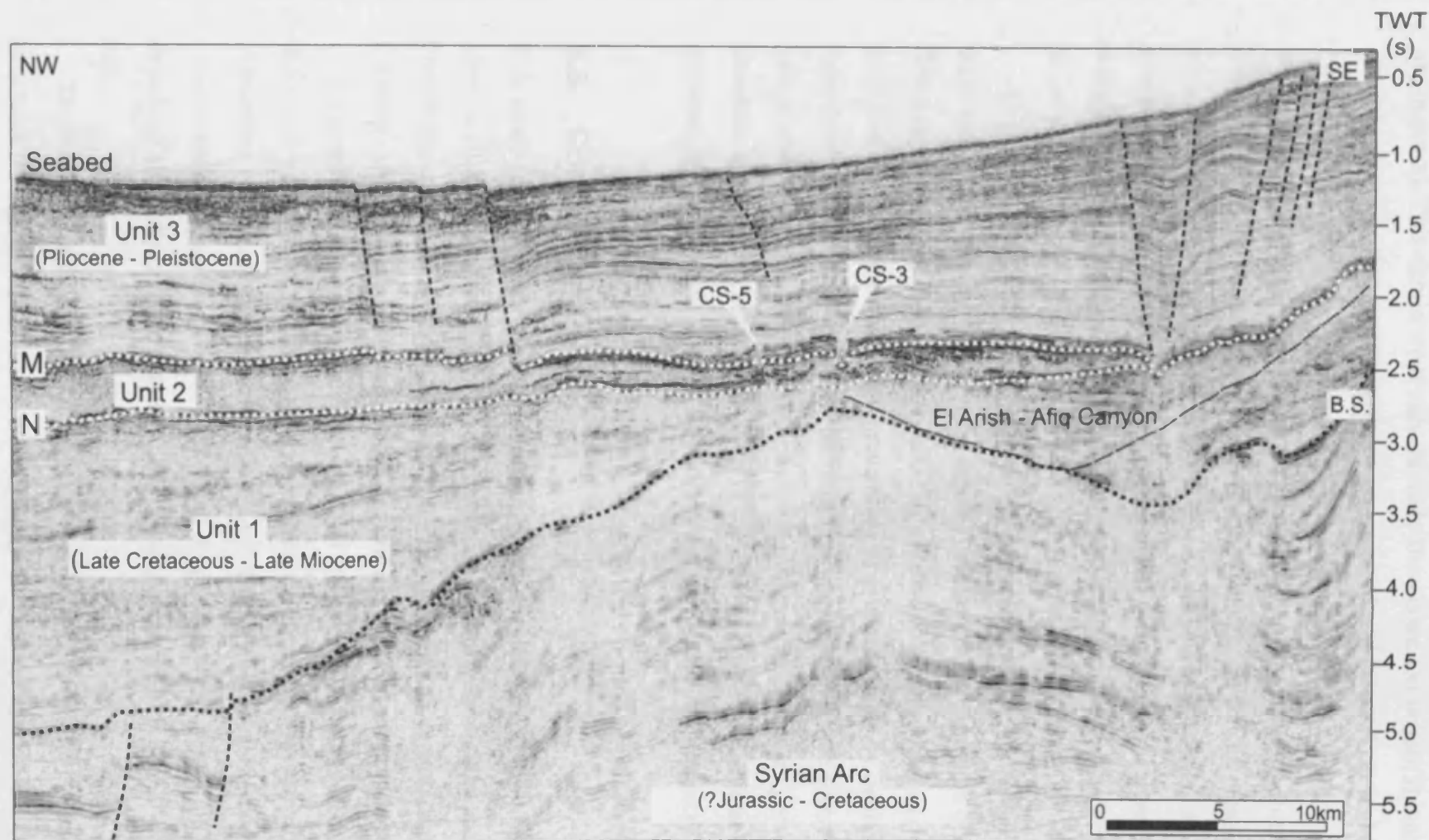


Figure 5.14 Seismic section crossing the Levant continental margin in a W-E direction, showing the deep structural setting of the study area (location of seismic section shown in Fig. 5.7). Note the relative position of the structure CS-3 above the Afq submarine canyon (dashed line) and the axis of the Syrian Arc anticline, and related fault system (dotted lines). B.S. = Base Senonian horizon; M = Horizon M; N = Horizon N. The interpretation of the faults post-dating the deposition of the Messinian evaporites, within Unit 3, is indicated with dotted lines.

50 km away, landward of the pinch-out of the Messinian evaporites (Frey-Martinez et al., in press). This similarity argues strongly for a common origin. It therefore seems entirely plausible that similar earthquake-triggered and focused vertical fluid flow could have impinged on the base of the evaporitic seal within the study area to the point where dissolution occurred with the resultant localized circular dissolution structures in the overburden. It is interesting to consider that were it not for the presence of the highly efficient seal of the Messinian evaporites, this form of vertical fluid expulsion might simply have resulted in mud diapirism or extrusion as is the case elsewhere within the region updip of the pinch-out of the Messinian evaporites (Frey-Martinez et al., in press).

The dissolution mechanism proposed in this paper may be applicable worldwide in other evaporite-bearing basins where similar conditions for expulsion of focused fluid flow are present (e.g. West Africa and Gulf of Mexico). Ultimately, as demonstrated here, such mechanism can lead to breaching of basinwide seals by depletion of considerable thicknesses of evaporites thus creating effective 'windows' for vertical hydrocarbon migration. An in-depth understanding of the processes presented here is therefore critical for a better evaluation of the efficiency of evaporitic seals, the presence of stratigraphic traps and pathways for the vertical migration of hydrocarbons.

5.8 Conclusions

This study records the occurrence of buried circular evaporite dissolution structures above a tabular evaporitic body in the Levant Basin, Eastern Mediterranean.

Dissolution occurred in buried evaporites and in a deep water setting during the Pliocene. The estimated maximum time of duration of the event is 0.75-1 Ma.

Evaporite dissolution led to the collapse of a weakly lithified overburden, which deformed with a series of extensional concentric faults. Other less conclusive indications of evaporite dissolution and evaporite-related deformation are observed close to the present margin of the Messinian evaporites; namely, salt outliers, faults detaching above the evaporite unit, and a linear depression along the evaporite pinch-out.

The mechanism of dissolution proposed for the creation of the circular collapse structures is subjacent dissolution of the more soluble evaporites in the Messinian

evaporites, due to focused vertical fluid flow at the base of the evaporitic series.

Instantaneous release of overpressured fluids, as e.g. during an earthquake, could have triggered and focused the fluid flow, which is thought to have impinged on the base of the evaporitic seal to the point where dissolution occurred with the resultant localized circular collapse structures in the overburden.

Chapter Six: Summary and discussion

6.1 Introduction

Chapters 2 to 5 have detailed the main results of this PhD research, being structured independently in specific topics on the depositional setting and the deformation of the Messinian evaporites in the Levant region. The main purpose of this chapter is to combine the information and the key results of the previous chapters in order to build an integrated evolutionary model for the Messinian evaporitic system in the region. This will be achieved by summarizing the main results of the previous chapters, and by discussing in chronological order the seismic characteristics of the different phases of evaporite deposition. The ultimate goal of this discussion is the identification of diagnostic features of relative sea-level changes. Finally, these results will be analysed in relation to their implications for the knowledge of the processes acting during the Messinian Salinity Crisis in the Mediterranean area.

6.2 Summary of results

6.2.1 Results on the controls for the architecture of the Messinian evaporites in the Levant region (Chapter 2)

- The pre-evaporitic setting of the Levant continental margin is dominated by a series of structural highs related to the anticlines of the Syrian Arc foldbelt. The development of these anticlines controlled the pre-evaporitic basin physiography and, consequently, the differential accommodation and the linear NE-SW directed edge of the Messinian evaporites. The influence of these anticlines is particularly marked in the marginal area of the Levant Basin, while it is more subdued in the distal area.
- A system of submarine canyons (Afiq, El Arish and Ashdod Canyons), developed on the Levant continental margin since the Oligo-Miocene, played a pivotal role in the depositional and erosional processes active in the study area during the MSC.
- These canyons acted as preferential sites of erosion in the earliest stages of the MSC up to the distal part of the Levant Basin. The recognition of confined

erosional truncation patterns in this research study allowed for the first time detailed mapping of the canyons at this stratigraphic level in the entire study area.

- The Afiq, El Arish and Ashdod Canyons acted as local depocentres for the distal evaporites in the later stages of the MSC. This is indicated by an evident increase in the thickness of the Messinian evaporites above the canyon axes. The thickness variation within the proximal and distal part of the evaporitic wedge is directly linked to the erosion of the canyons at the base of the evaporites, coupled with their subsequent infill. This originated the locally irregular geometry of the edge of the evaporites, characterized by major embayments and landward outliers.

6.2.2 Results from the analysis of clastic deposits at the base of the Messinian evaporitic system (Chapter 3)

- The 3D seismic geomorphological analysis of the lower part of the Messinian evaporites has revealed the presence of significant amounts of clastic deposits in their distal region.
- This research project has shown that the source of clastic supply to the evaporitic basin was directly linked to the Afiq and El Arish Canyons and possibly to the nearby Nile system.
- The seismic characteristics of the clastic deposits and the coeval basin physiography indicate that they deposited in a submarine (shallow or deep-water) setting.

6.2.3 Results on the central and upper part of the Messinian evaporites (Chapter 4)

- The detailed seismic-stratigraphic analysis of a series of intra-evaporitic horizons and of the packages bounded by them permitted in this study the detection of a discordant relationship between the intra-evaporitic horizons and the top of the Messinian evaporites (Horizon M) in the Levant region.
- Clear evidence of the occurrence of erosional truncation has been recorded in the study area at the top of the basinal Messinian evaporites based on the terminations of the intra-evaporitic horizons and Horizon M. This allows for the first time in the Levant region the definition of top of the Messinian evaporites as an erosional unconformity.

- Based on the preserved geometry of the seismic reflections, the expected original depositional geometry of the evaporitic system comprised divergent intra-evaporitic horizons onlapping the continental margin.
- The analysis of the structural deformation of the intra-evaporitic horizons has documented the occurrence of an early phase of evaporite deformation at the end of Messinian, and before the erosional event forming Horizon M.
- The most likely mechanism for this deformation is considered to be differential loading linked to a prograding shelf wedge on the basinal evaporitic system. The direction of the intra-evaporitic compressional structures indicates that the deformation could have been initiated by the outbuilding of the Nile delta and submarine fan, active in the Levant Basin at least since the final stages of the deposition of the Messinian evaporites.

6.2.4 Results on post-depositional evaporite deformation (Chapter 5)

- A series of buried circular collapse structures have been identified by 3D seismic mapping of the top of the Messinian evaporites and the overlying Pliocene overburden. The collapse structures formed in buried evaporites and in a deep water setting during the Pliocene, within a maximum time-span of 0.75-1 Ma.
- Evaporite dissolution is proposed as the mechanism of formation for the collapse structures. Subjacent dissolution is thought to have acted on the more soluble facies in the Messinian evaporites, leading to the collapse of a weakly lithified overburden, which deformed with a series of extensional concentric faults.
- The trigger of dissolution has been possibly linked to focused vertical flow of undersaturated fluids at the base of the evaporites.
- Other indications of evaporite dissolution and evaporite-related deformation are observed close to the present margin of the Messinian evaporites; namely, salt outliers, faults detaching above the evaporite unit, and a linear depression along the evaporite pinch-out.
- The linear depression and faults have been linked to the gravitational collapse of the Plio-Pleistocene clastic wedge, detaching at the top or within the Messinian evaporites. The marginal evaporite withdrawal is balanced in the distal area with the development of compressional/transpressional deformation at the toe of the continental slope.

- The analysis of the syn-sedimentary growth of marginal extensional faults document that this gravity-related deformation occurred in the study area since the late Pliocene/early Pleistocene, thus it post-dates the timing of formation of the dissolution structures.

6.3 Basinal evolution of the Messinian evaporitic system

In this section, a series of topics will be addressed and clarified in order to place the previously listed results in an evolutionary basinal context. The section is structured as follows:

- Observations on the architecture of the Levant margin (Section 6.3.1).
- Sea-level at the base of the Messinian evaporites (Section 6.3.2).
- Sea-level during the deposition of the Messinian evaporites (Section 6.3.3).
- Sea-level at the top of the Messinian evaporites (Section 6.3.4).
- Remarks on the formation of the marginal Messinian erosional surface (Section 6.3.5).
- Summary of relative sea-level changes during the MSC (Section 6.3.6).

6.3.1 Observations on the architecture of the Levant margin

The aim of this section is to evaluate the difference between the original and present-day architecture of the Levant margin, with particular regard to the Messinian evaporites. In respect to this, two main factors must be taken into account: 1) the effect of post-depositional deformation on evaporite architecture, and 2) the impact of seismic effects on evaporite stratigraphy, in particular linked to velocity distortion on the visualisation of the stratigraphic units analysed.

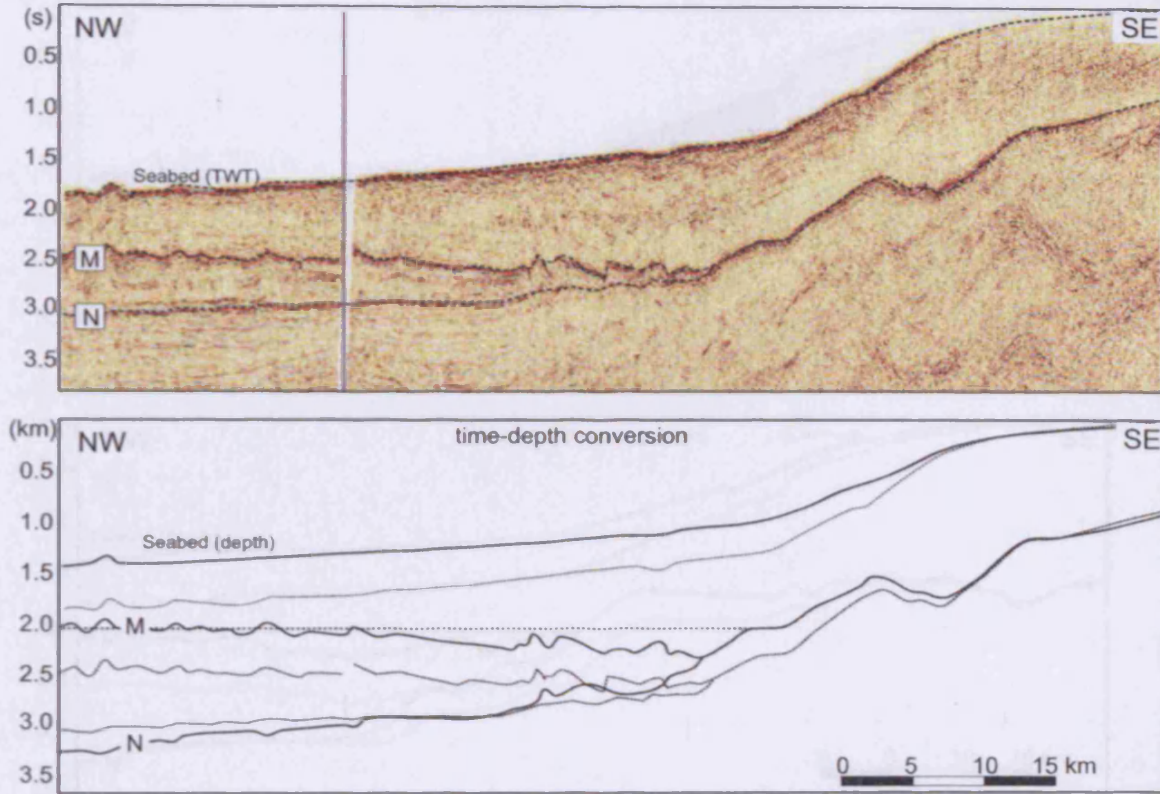
The effect of post-depositional deformation on the architecture of the Messinian evaporitic wedge has been analysed in this thesis, and widely discussed in previous studies of the Levant region. Chapter 5 has evidenced the presence of localized post-depositional deformation of the evaporitic unit, due to dissolution and withdrawal occurred during the Pliocene and Pleistocene. Numerous previous studies of the Levant margin have documented the regional extent of thin-skinned gravitational gliding of the Plio-Pleistocene clastic wedge. The related deformational structures detach at the top or within the Messinian evaporites (Garfunkel & Almagor, 1987; Tibor & Ben-Avraham,

1992; Gradmann et al., 2005). The deformation linked to dissolution, withdrawal and thin-skinned salt tectonics, however, appears to be localised, and its effect on the stratigraphy of the evaporites is limited and mainly focused in their marginal area (Chapters 2 and 5). Furthermore, the application of backstripping and subsidence analysis supported a similarity between the present-day and the original architecture of the Messinian evaporites (Tibor et al., 1992; Tibor & Ben-Avraham, 2005; Ben Gai et al., 2005). For the purposes of this PhD research, it is particularly significant to note that these previous studies confirm that the surface defining the top of the Messinian evaporites (Horizon M) presented originally an overall horizontal geometry, similar to the present-day setting (Tibor et al., 1992; Tibor & Ben-Avraham, 2005; Ben Gai et al., 2005).

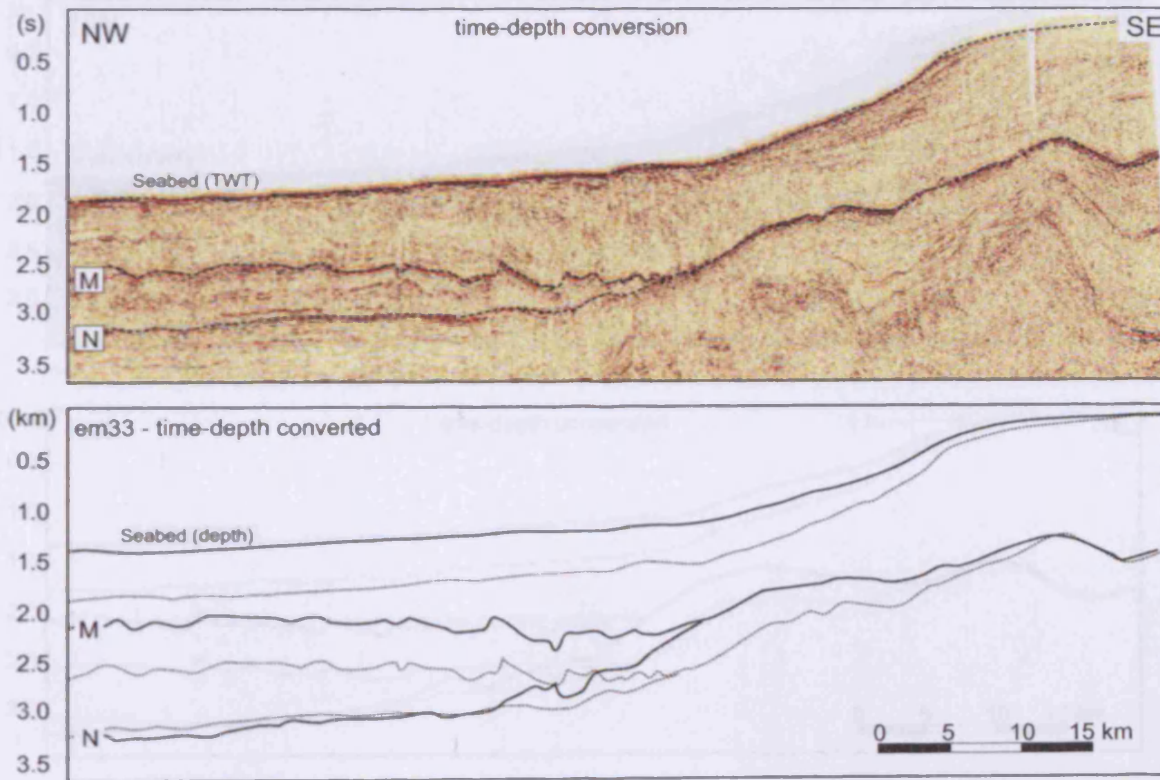
A further important factor to take into account for the interpretation of the original architecture of the Messinian evaporites is the impact of seismic velocity distortion on the visualisation of the stratigraphic units. The variation of thickness and facies of the formation crossed by the seismic waves with depth can cause considerable distortion in stacked time sections, compared with the actual depth and thickness relationship (Badley, 1985). These seismic effects must be appreciated in order to evaluate the authentic present-day architecture of the Messinian evaporitic wedge. The best way to appreciate these effects is to convert the time seismic sections to depth sections. Time-depth conversion is especially needed in order to support previous interpretation of regional morpho-structural features, angles and topographic elevations of the surfaces analysed. Consequently, in this section the time-depth conversion of a series of selected regional 2D seismic lines is undertaken. The procedure followed consists in applying a simple layer-cake model of seismic velocity distribution to the seismic units analysed. The time-depth conversion of the Messinian to recent interval has been undertaken on a series of seismic sections crossing the Levant continental margin in a NW-SE direction (Fig. 6.1). Additionally, the map of the time-depth converted Horizon M has been produced (Fig. 6.2). The following average seismic velocities have been used for the time-depth conversion:

- Water: 1.5 km/s
- Plio-Pleistocene deep-water clastic wedge: 2.0 km/s
- Messinian evaporites: 4 km/s

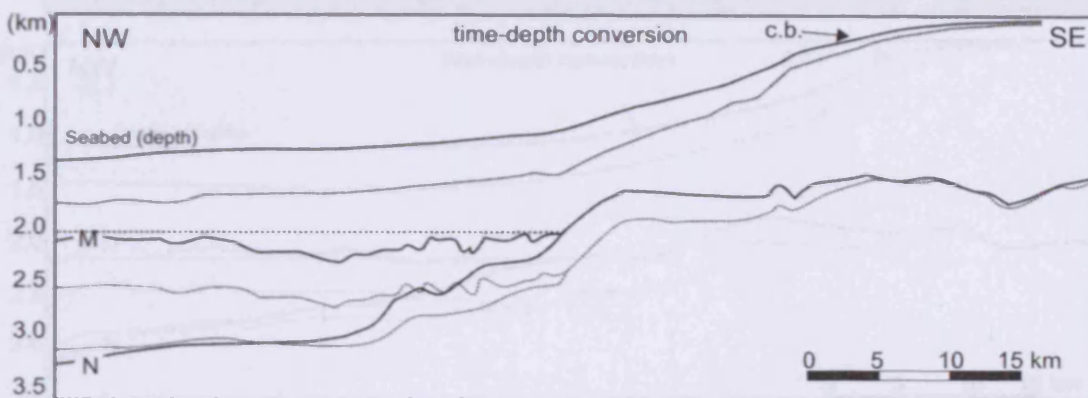
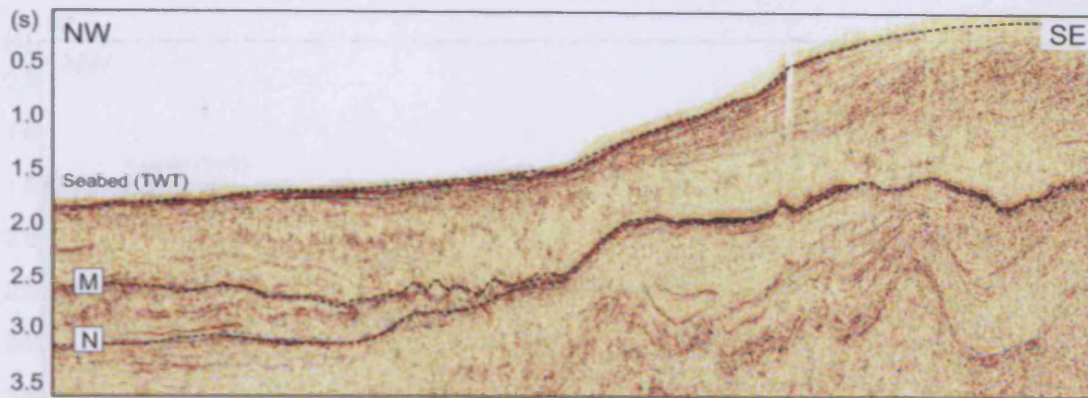
a



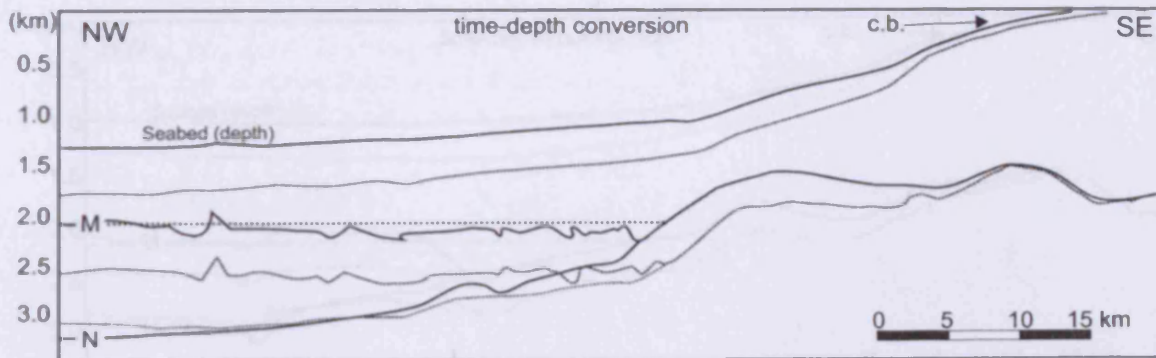
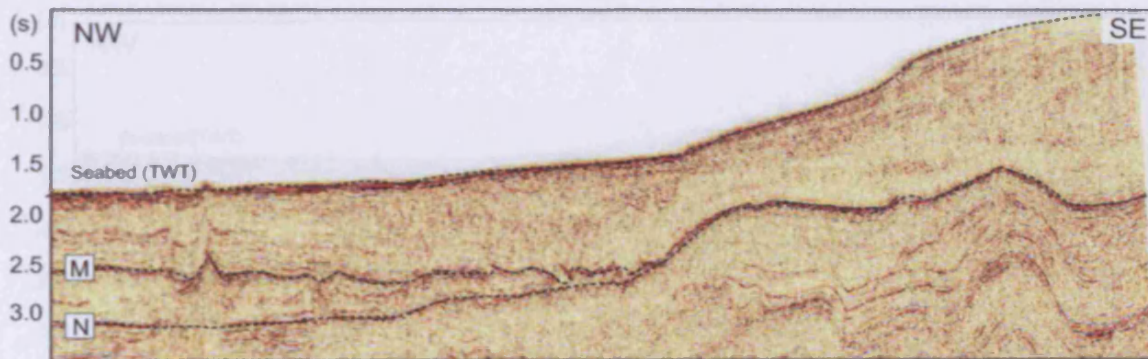
b

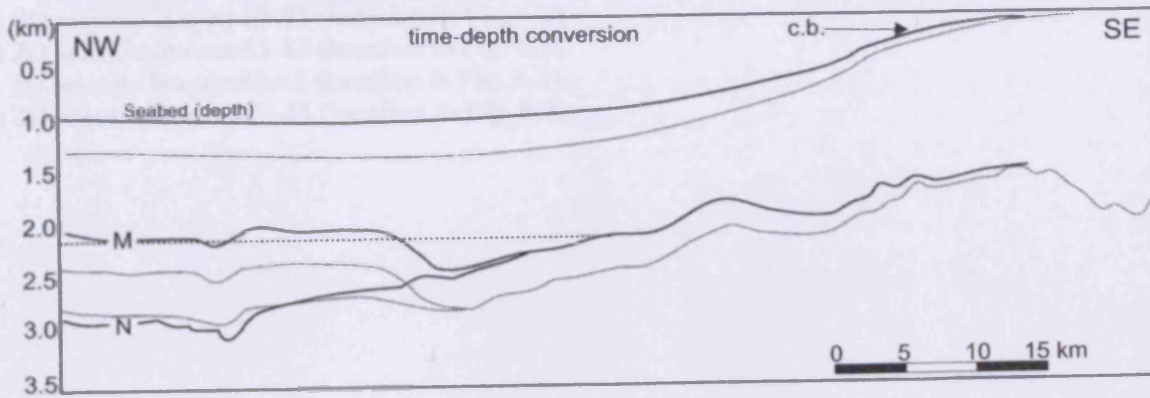
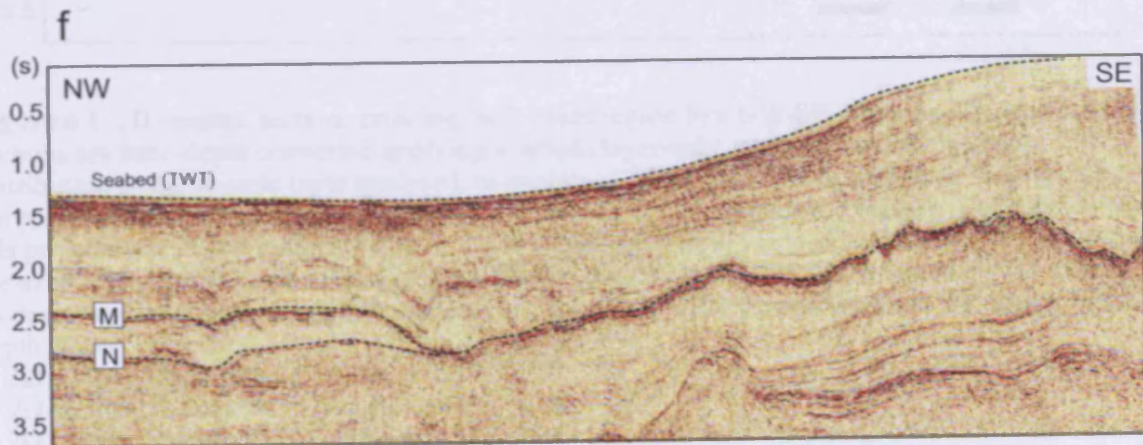
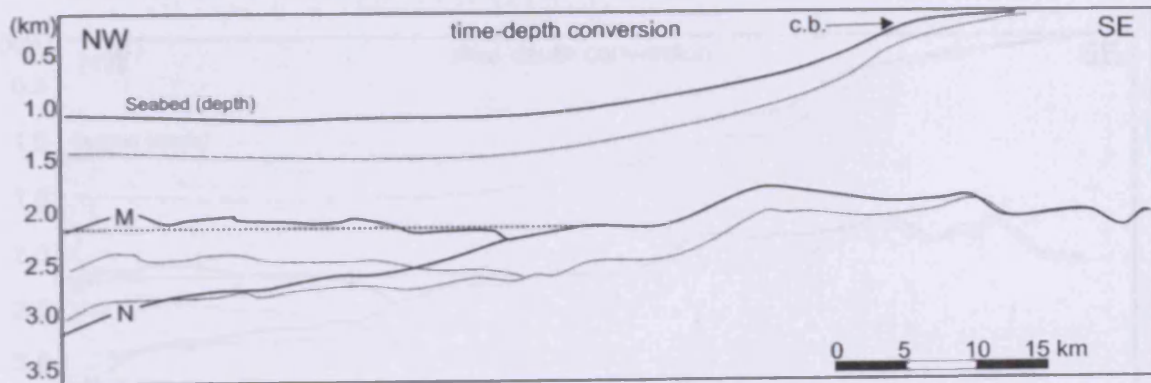
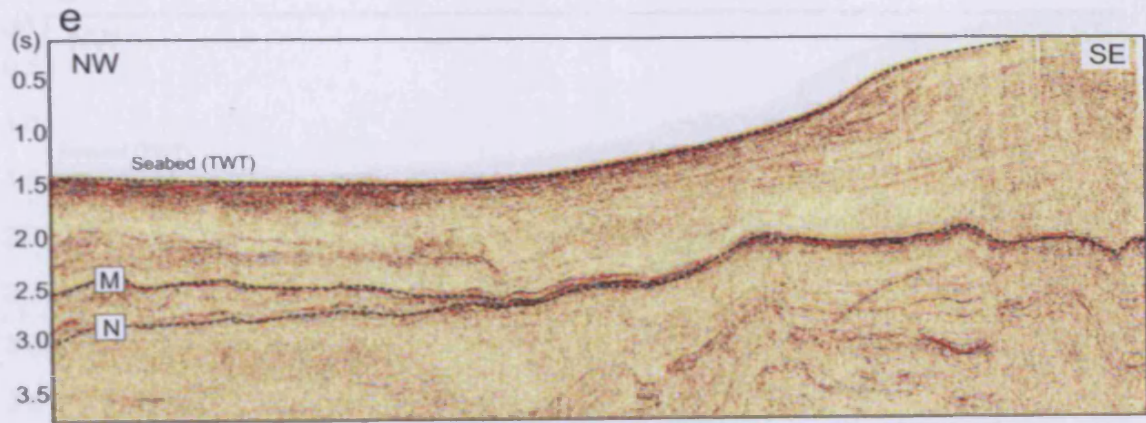


C



d





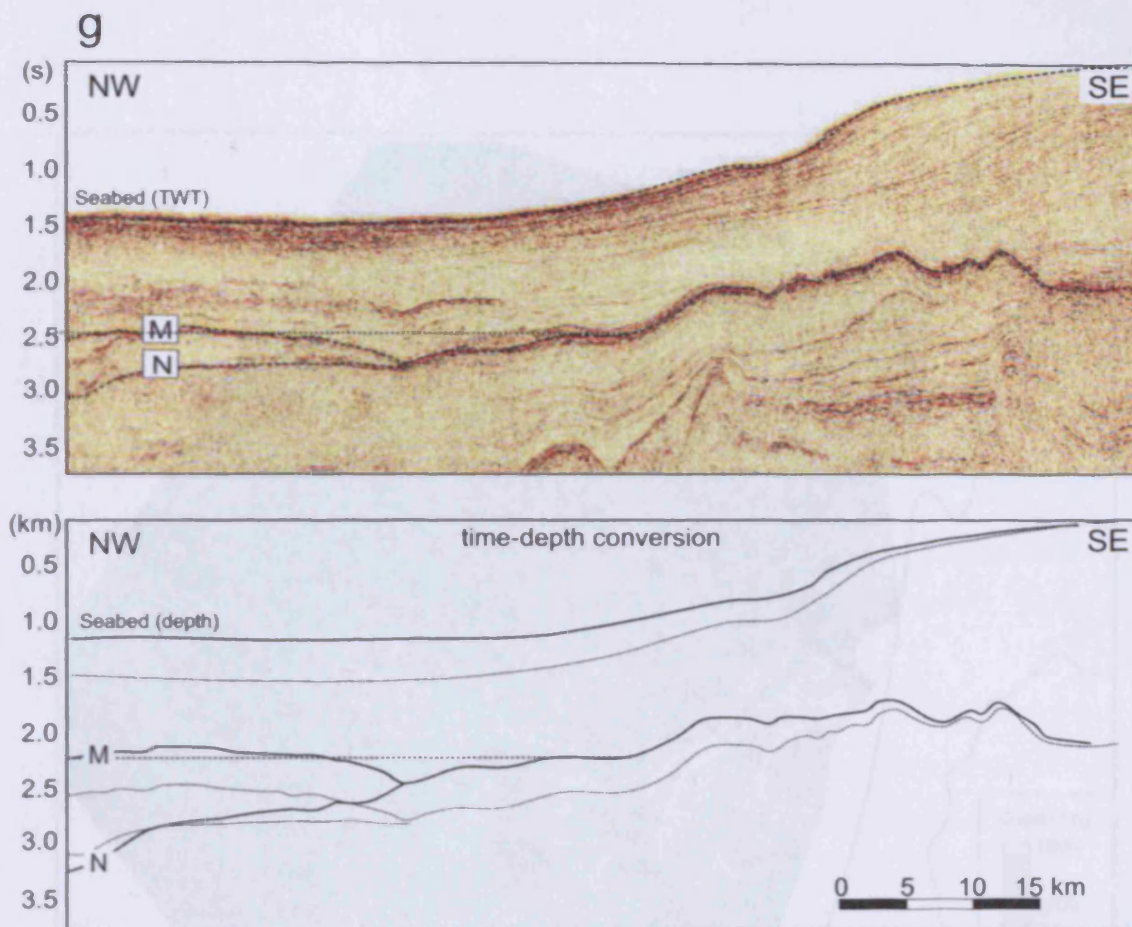


Figure 6.1 2D seismic sections crossing the Levant region in a NW-SE direction. The seismic sections are time-depth converted applying a simple layer-cake model of seismic velocity distribution to the seismic units analysed, as explained in the text. The black dotted line represents the projection of the regional top of the Messinian evaporites towards the margin. The coincidence of this projection with the marginal step in the erosional surface developed landward of the pinch-out of the evaporites should be noted in Fig. 6.1a, f and g. On the vertical scale, the numbers refer to seconds two-way travel time on the seismic sections, and to kilometres depth on the interpreted time-depth converted section.

- a) 2D seismic line em83-31 (location in Fig. 6.2).
- b) 2D seismic line em83-33 (location in Fig. 6.2).
- c) 2D seismic line em83-34 (location in Fig. 6.2).
- d) 2D seismic line em83-35 (location in Fig. 6.2).
- e) 2D seismic line em83-43 (location in Fig. 6.2).
- f) 2D seismic line em83-45 (location in Fig. 6.2).
- g) 2D seismic line em83-44 (location in Fig. 6.2).

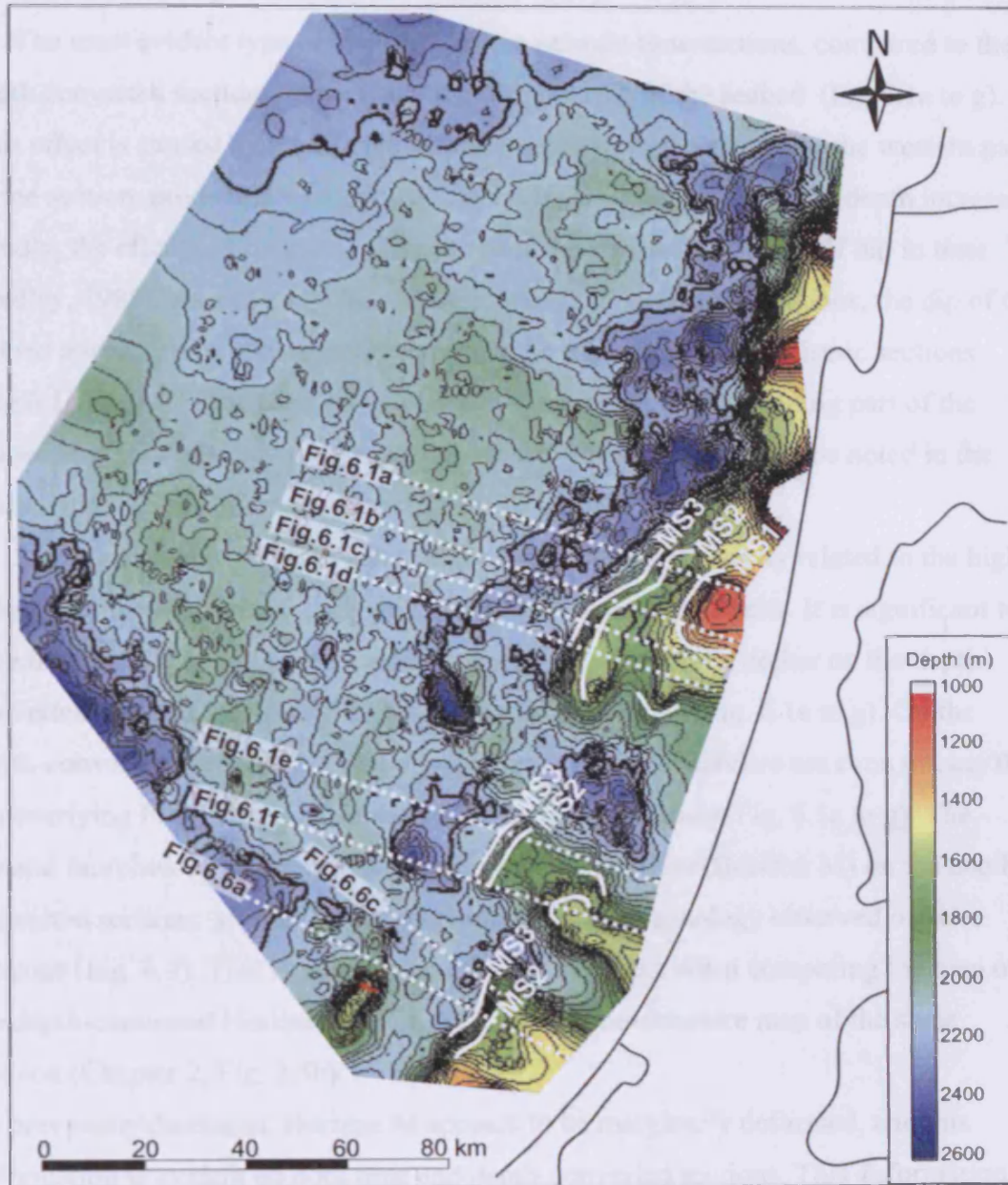


Figure 6.2 Map of the time-depth converted Horizon M in the 2D seismic survey area. The continuous white lines indicate the location of the marginal scarps MS1, 2 and 3 described in the text. The location of the seismic sections displayed in Fig. 6.1 and 6.7 is indicated by the white dotted lines.

These seismic velocities represent average values obtained by analysis of wells in the study area (Chapter 2, Section 2.4; see also Frey-Martinez et al. 2005) and based on previous studies (e.g. Garfunkel & Almagor, 1987).

The most evident type of distortion of the seismic time sections, compared to the depth converted sections, is probably the different dip of the seabed (Fig.6.1a to g). This effect is caused by the change in water depth from the eastern to the western part of the section, producing a velocity anomaly. In cases where the water depth increases rapidly, the effect can be great enough to produce a false impression of dip in time (Badley, 1985). As a consequence, on the time-depth converted sections, the dip of the seabed appears to be consistently lower than on the original time seismic sections (Fig.6.1a to g). This effect is particularly evident in the steeply sloping part of the seabed, and it is reflected on the morphological differences that can be noted in the underlying Messinian erosional surface (Horizon M).

A further seismic effect evident on the time sections is directly related to the high velocity of the evaporites, compared to the bounding seismic units. It is significant to note that the thickness of the evaporitic wedge is substantially higher on the depth-converted sections, compared to the original time sections (Fig. 6.1a to g). On the depth-converted sections it is visually apparent that the evaporites are even thicker than the overlying Plio-Pleistocene unit in their northwestern part (Fig. 6.1a to g). The general morphology of the top of the Messinian evaporites (Horizon M) on the depth converted sections appears to be comparable to the morphology observed on time sections (Fig. 6.1). This similarity is particularly evident when comparing the map of the depth-converted Horizon M (Fig. 6.2), to the time-structure map of the same horizon (Chapter 2, Fig. 2.5b).

As previously discussed, Horizon M appears to be marginally deformed, and this deformation is evident on both time and depth-converted sections. This deformation is focused at the pinch-out of the Messinian evaporites, where Horizon M is faulted and downwarped (Fig. 6.1). The projection of the regional top of the Messinian evaporites towards the margin is mostly coincident with a marginal step in the erosional surface developed landward of the pinch-out of the evaporites (Fig. 6.1a, e, f and g). By analogy with the procedure applied on the time sections, the original location of the pinch-out of the Messinian evaporites can be interpreted as explained in Chapter 2, Section 2.6.1. The original pinch-out of the Messinian evaporites can thus be

confidently traced largely following this marginal step (Fig. 6.1). The time-depth conversion thus provides an important reference value for the analysis of the evolution of the evaporite system, i.e. the present-day depth of the pinch-out of the Messinian evaporites. This reference value is nearly constant across the entire study area, being located at ca. 2000 – 2300 m below the present-day sea-level.

6.3.2 Sea-level at the base of the Messinian evaporites

In the previous chapters, a series of indications of the position of the sea-level at the base of the Messinian evaporites have been analysed. These indications refer in particular to erosional patterns and facies variations observed at this stratigraphic level. The main aim of this section is to evaluate the position of the sea-level at the base of the Messinian evaporites in relation to sea-level during the pre-evaporitic interval, by a synthesis of the observations from the previous chapters and comparing them with previous studies in the Levant region.

Chapter 2, Section 2.7.3 has documented an increase in the erosional activity of the Ashdod, El Arish and Afiq Canyons at the base of the Messinian evaporites. This erosional phase preceding or at the beginning of evaporite deposition has been interpreted as an indication of a sea-level fall occurring at the early stages of the MSC (Chapter 2, Section 2.7.3). The presence of erosion at this stratigraphic level confirms the results obtained in previous studies in the Levant region. These previous studies suggested that the onset of deposition of the evaporites of the Mavqiim Formation is associated with a regional drop of the sea-level (Buchbinder, 1993; Druckman et al., 1995).

A further indication of the occurrence of widespread erosional activity at the beginning of the MSC is provided in this PhD research by the detection of clastic depositional bodies in the basal part of the Messinian evaporites (Chapter 3). The guidelines for the interpretation of the clastic bodies previously obtained on the 3D seismic surveys can be applied in this section to identify clastic deposits throughout the entire 2D seismic survey area. The application of this methodology permitted the identification of the regional distribution of clastic deposits in the area, as displayed in Figs. 6.3 and 6.4. Furthermore, the location of these clastic bodies reinforces their direct link with the El Arish, Afiq, Ashdod and Cesarea canyons (Fig. 6.3). This finding ultimately confirms the regional extent of the erosional event at the base of the

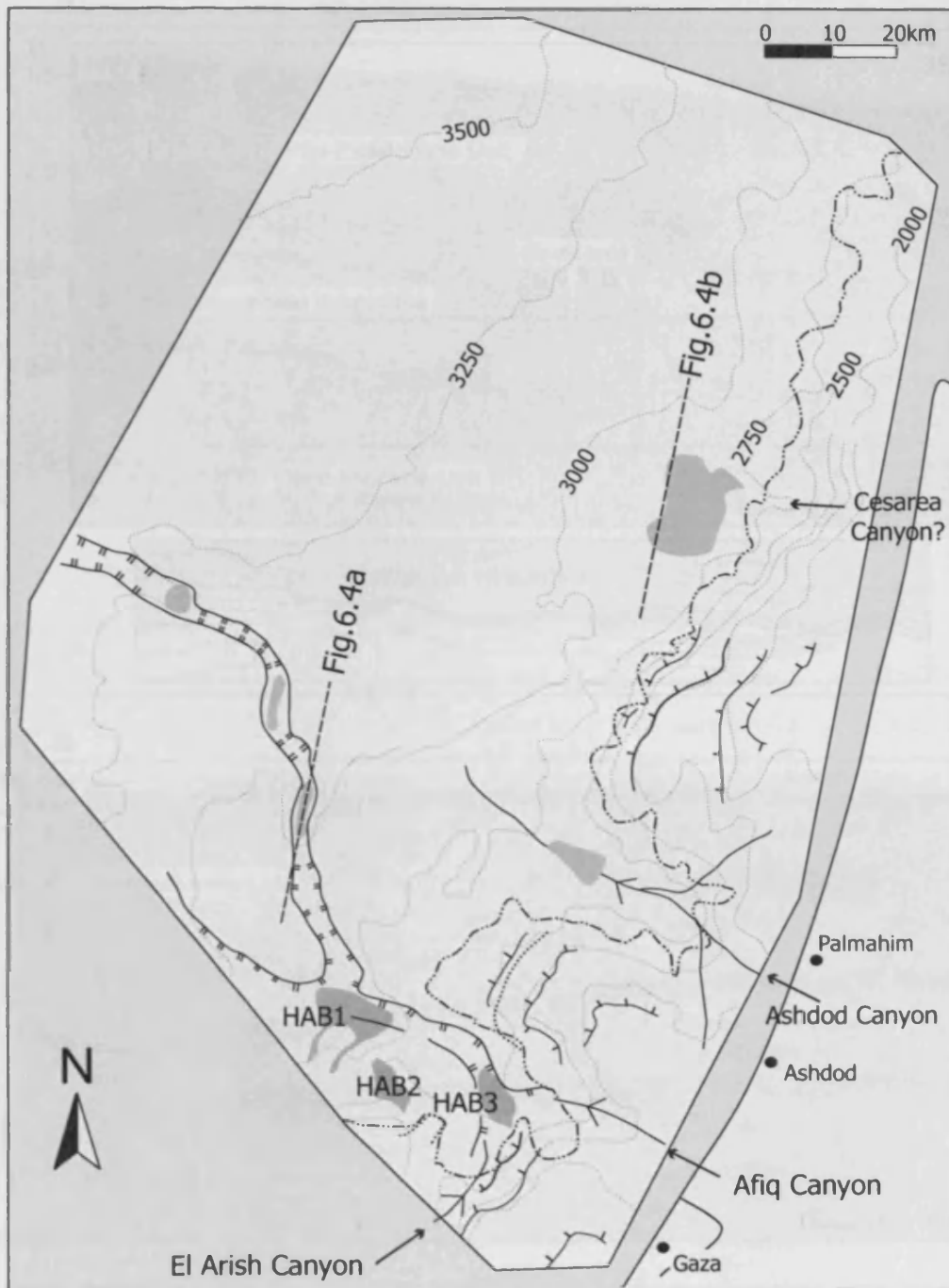


Figure 6.3 Synoptic diagram illustrating the distribution of clastic bodies (dark grey areas) throughout the study area. The location of the clastic bodies HAB1, 2 and 3 analysed in Chapter 3 is indicated. The map in the background shows the the main morphological and structural features overlain on the isochron lines of the base of the Messinian evaporites (Horizon N). For the explanation of the symbols, see Chapter 2, Fig. 2.10. The location of the seismic lines displayed in Fig. 6.4 is also indicated.

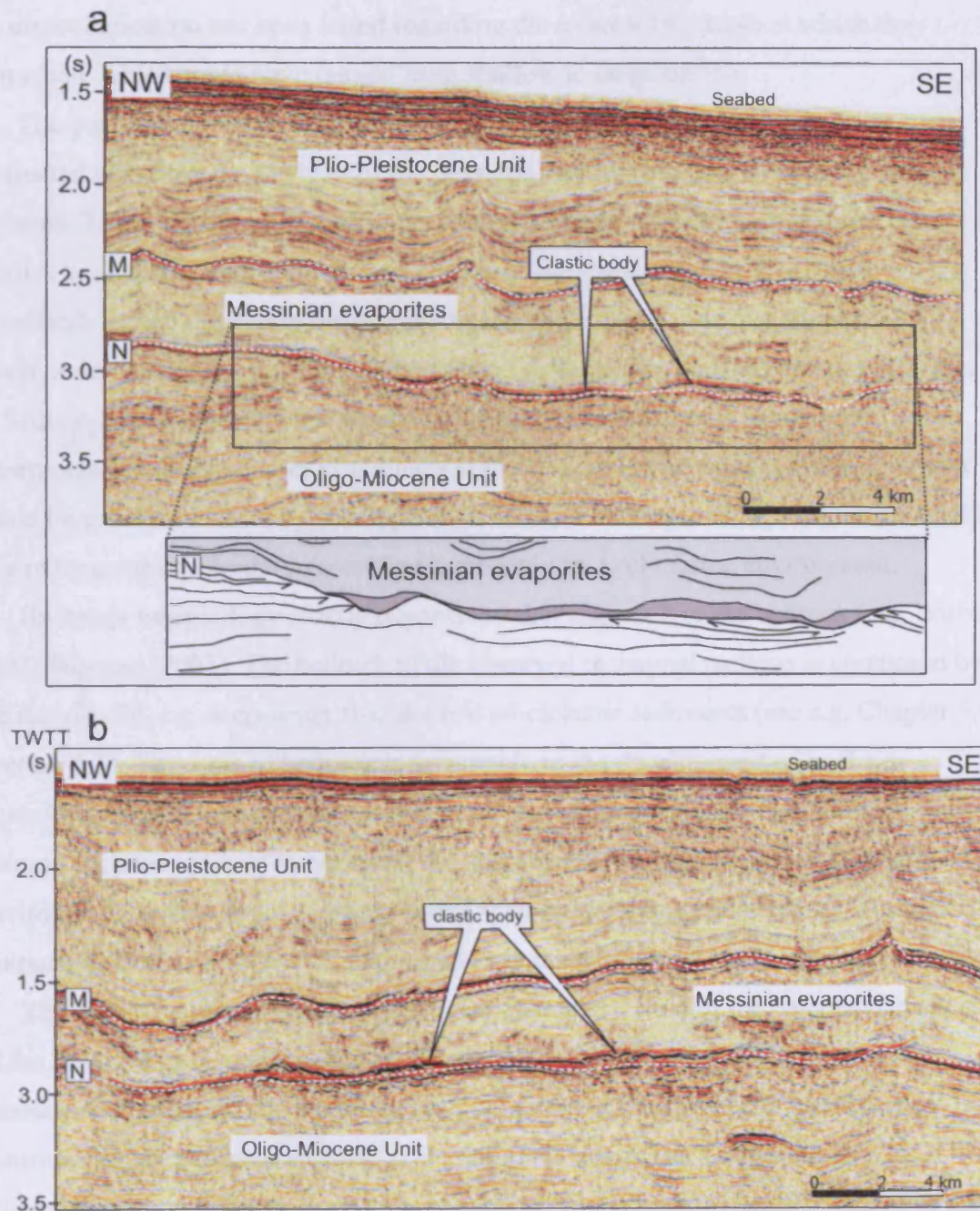


Figure 6.4 Seismic sections showing the distribution of clastic bodies at the base of the Messinian evaporites in the study area.

- a) 2D seismic section crossing the Levant region in a NW-SE direction (location in Fig. 6.3). The lower part of the figure displays a close-up of the seismic section, with the line-drawing and interpretation of the clastic body (dark grey colour) resting above the base of the Messinian evaporites (Horizon N). The black arrows mark the truncated termination of the pre-evaporitic reflection, directly related to the location of the Afîq-El Arish canyon flanks.
- b) 2D seismic section crossing the Levant region in a NW-SE direction (location in Fig. 6.3). The clastic body at the base of the Messinian evaporites is identified by the high-amplitude seismic event, by analogy with the procedure applied in Chapter 3.

Messinian evaporites. Although the clastic bodies have been interpreted as submarine, no direct indication has been found regarding the exact water depth at which they deposited, which could have ranged from shallow to deep marine.

The position of the sea-level at the base of the Messinian evaporites can be evaluated also from the analysis of the drainage and erosional patterns of the canyon systems. The comparison of the results obtained in this PhD research with previous studies has documented a downslope change in the stream pattern from areal ('badlands'-type) erosion in the marginal parts of the study area (e.g. Gvirtzmann & Buchbinder, 1978; Ryan, 1978; Barber, 1981) to basinward focused incision (Chapter 2, Section 2.6.3). This downslope change of the stream pattern is significant for the interpretation of the paleo-environments at the base of the Messinian evaporites, as it could be generated either by lithological differences in the pre-MSC substrate, or linked to a paleographic boundary separating a subaerial to a submarine environment.

Badlands morphology strictly depends on the resistance of the bedrock (e.g. Barber 1981; Huggett, 2003). The bedrock to the observed incisional patterns is composed by the canyon fill, i.e. deep-water fine-grained siliciclastic sediments (see e.g. Chapter 5, Section 5.5). This type of bedrock is favourable to the development of badlands. Therefore, the absence of areal erosion in the downslope region, and the change to focused incision is likely to represent the transition from a subaerial to a submarine environment. In this context, the erosional surface at the base of the distal Messinian evaporites (Horizon N) can be interpreted as entirely shaped by submarine processes.

These observations provide a significant characterization of the paleoenvironments of the basal Messinian evaporitic setting. Nonetheless, the landward extent of the submarine erosional surface remains uncertain, due to the absence of stratigraphic constraint on its presence/absence in the marginal area of the Levant region. The original transition between a subaerially exposed and submarine eroded surface at the base of the Messinian evaporites can have been potentially overprinted by subsequent erosional phases shaping the marginal Messinian erosional surface. Therefore, this lack of constraint hinders a precise estimate of the sea-level position at the base of the Messinian evaporites. As a consequence, future work based on additional data is needed in order to evaluate this factor and to produce an estimate of the sea-level drop that occurred at the onset of the deposition of the Messinian evaporites on the Levant margin and basin.

6.3.3 Sea-level during the deposition of the Messinian evaporites

The main aim of this section is to assess relative sea-level variations and basinal depth during the deposition of the Messinian evaporites. This will be attempted using the analysis of sea-level indicators and of basinal subsidence, derived from the results in the previous chapters and from previous studies in the Levant area.

In basinwide evaporitic settings, the location of the onlap termination of the evaporites can be generally taken as an indication of the shoreline facies, i.e. of sea-level position (see e.g. Warren, 1999). In the study area, the erosional truncation of the intra-evaporitic horizons (Chapter 4, Section 4.7.2) hinders the interpretation of their marginal terminations and of possible onlap patterns developed landward of this truncation. In Chapter 4, the probable original architecture of the evaporitic unit as been interpreted as composed of divergent onlapping packages, based on the geometry of the preserved horizons. This confirms previous studies based on drillholes in the Israel coastal plain, that indicate an onlap nature of the Mavqiim evaporites (Cohen & Parchamovsky, 1986). Moreover, this interpretation is supported by the similarity in the depositional geometry of the coeval evaporites of the Western Mediterranean area (e.g. Lofi et al., 2005). These results support the hypothesis that the location of the sea-level during the deposition of the evaporites was higher than present-day elevation of the truncation surface, i.e. Horizon M. Nonetheless, the exact location of the sea-level at this stratigraphic level still remains unknown.

A further attempt to estimate the depth of the Levant Basin at the time of evaporite deposition can be based on the analysis of the thickness of the Messinian evaporites. The deposition of this ca. 1.8 km-thick evaporitic wedge requires the existence of a significant space in the basin for their accommodation. Based on the data available, three main models can be hypothesized for the basinal setting of the Levant region during the deposition of the evaporites (Fig. 6.5). The first model (Fig. 6.5a) is based on the deposition of the distal part of the evaporites in a pre-existing very shallow sea (max. 200 m deep), with accommodation space created only by tectonic subsidence and sediment load. The second model (Fig. 6.5b) is based on the deposition of the distal evaporites in a pre-existing shallow ramp-setting sea. The third model (Fig. 6.5c)

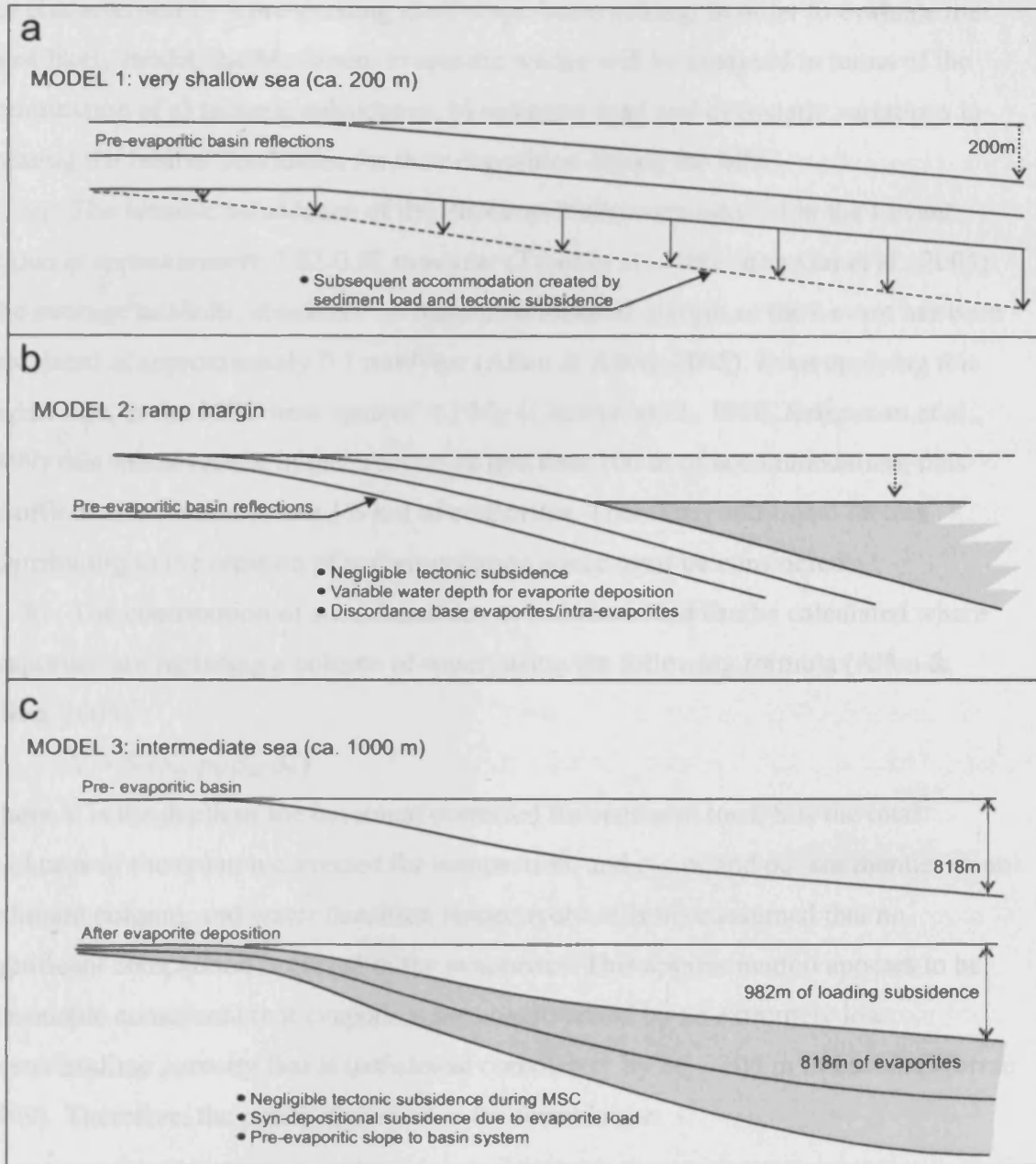


Figure 6.5 Basinal models proposed for the creation of the accommodation space necessary for the deposition of the ca. 1.8 km-thick Messinian evaporitic wedge in the Levant region.

- a) The first model implies the deposition of the distal part of the evaporites in a pre-existing very shallow sea (max. 200 deep), with accommodation space created only by tectonic subsidence and sediment load.
 - b) The second model implies the deposition of the distal evaporites in a pre-existing shallow ramp-setting sea.
 - c) The third model involves the deposition of the evaporitic wedge in an intermediate (ca. 1000m deep) sea characterised by a pre-existing shelf-slope-basin setting.
- The most likely basinal setting for the deposition of the Messinian evaporites is the third model (see discussion in the text).

involves the deposition of the evaporitic wedge in an intermediate (ca. 1000 m deep) sea characterised by a pre-existing shelf-slope-basin setting. In order to evaluate the most likely model, the Messinian evaporitic wedge will be analysed in terms of the combination of a) tectonic subsidence, b) sediment load and c) eustatic variations in creating the basinal conditions for their deposition during the MSC.

a) The tectonic subsidence of the Pliocene-Pleistocene interval in the Levant region is approximately 0.02-0.07 mm/year (Tibor et al., 1992; Ben-Gai et al., 2005). The average tectonic subsidence on mature continental margin as the Levant has been calculated at approximately 0.1 mm/year (Allen & Allen, 2005). Even applying this higher rate, in the MSC time span of < 1 My (Clauzon et al., 1996, Krijgsman et al., 1999) this would result in the creation of less than 100 m of accommodation, thus insufficient to accommodate 1.8 km of evaporites. Therefore, additional factors contributing to the creation of accommodation space must be considered.

b) The contribution of subsidence due to sediment load can be calculated where evaporites are replacing a column of water, using the following formula (Allen & Allen, 2005):

$$Y = S (\rho_m - \rho_b / \rho_m - \rho_w)$$

where Y is the depth of the basement corrected for sediment load, S is the total thickness of the column corrected for compaction, and ρ_m , ρ_b and ρ_w are mantle, mean sediment column, and water densities, respectively. It is here assumed that no significant compaction occurred in the evaporites. This approximation appears to be reasonable considering that evaporites are characterised by an extremely low intercrystalline porosity that is lost almost completely by 50 – 100 m of burial (Warren 1999). Therefore, the parameters used in the formula are:

ρ_m	ρ_b	ρ_w	S	Y
3.3 t/m ³	2.3 t/m ³	1.1 t/m ³	1.8 km	0.818 km

The result shows that a load of 1.8 km of evaporites is accommodated by an initial basinal depth of 0.818 km. Adding the previously calculated value of tectonic subsidence, a maximum basinal depth of 0.918 km is obtained. This demonstrates that the exceptionally high salt load combined with initial basinal depth had the potential to create a considerable part of the accommodation space necessary for the deposition of

the evaporitic wedge notwithstanding the limited duration of the MSC. The effects of evaporite load in the Levant Basin had previously been explored by Tibor & Ben-Avraham (2005). These authors document a deepening of the Levant shelf area (in the region of the Judea Mountains) of 400 m, due to evaporite loading in the basin. At the same time, the flexural response of the lithosphere to the removal of water load is thought to have an impact on the supply of eroded terrigenous sediments to the basin (Tibor & Ben-Avraham, 2005). In this context, the results of this PhD research further stress the importance of this factor in the creation of the accommodation for evaporite deposits in the marginal and basinal area of the Levant region.

The analysis of the pre-evaporitic geological setting provides important additional information about the depth of the basin immediately preceding the onset of evaporite deposition. As highlighted by Buchbinder et al. (1993), the marginal evaporites of the Mavqiiim Formation onlap detrital slope facies of the late Miocene Pattish reef complex, or the coeval open marine marlstones in the area of the Ashdod, Ashqelon and Barnea Canyons, beneath the present-day Israeli coastal plain. The evaporites rest, therefore, on relatively deep-water sediments (Buchbinder et al., 1993). Furthermore, the occurrence of Oligo-Miocene slope submarine canyons on the Levant continental margin documents the existence of a well-developed shelf-slope-basin siliciclastic system predating the deposition of the Messinian evaporites (Druckman et al., 1995). In conclusion, these observations and the previous results indicate the existence of a deep (>1000 m) basin setting preceding the onset of evaporite deposition (Tibor et al., 1992). The same setting is thought to be common to other coeval Mediterranean continental margins (e.g. Montadert et al., 1978).

c) Indications on the eustatic level and its variations during the sedimentation of the Messinian evaporites can be derived from the analysis of their depositional environment. The significant thickness of evaporites observed in the study area requires the basin brines to be repeatedly replenished with additional sea-water (Kendall & Harwood, 1996). As pointed out by Hodell et al. (1986) the great thickness of the Messinian salt in the Mediterranean Basin implies a communication between the Mediterranean and the global ocean throughout much of the MSC. Thus, a continuous inflow from the Atlantic in combination with blocked return has been proposed for the Messinian evaporitic basin in numerous studies (Hsü et al., 1977; Krijgsman et al., 1999; Meijer & Krijgsman, 2005). In the Messinian Main Salt Unit of the Western

Mediterranean, sedimentological evidence indicates many cycles of marine flooding and evaporite drawdown of water, followed by subaerial erosion (Hsü et al., 1977, 1978; Meijer & Krijgsman, 2005). In the Eastern Mediterranean, Cohen (1987) envisages a fully submarine origin for the Messinian evaporites subcropping underneath the Israeli coastal plain and shelf. In this PhD research, the results obtained in the previous chapters appear to indicate that the intra-evaporitic horizons and seismic packages are likely to represent transgressive-regressive cycles linked to allocyclic sea-level variations or autocyclic brine-level variations during the MSC. This pattern is analogous to cycles of brine and relative sea-level change observed in a number of recent and ancient evaporitic depositional provinces (Warren, 1999).

A direct constraint on the lithology characterising these transgressive-regressive facies, i.e. on the composition of these intra-evaporitic horizons is mainly based on their seismic response. The transparent seismic facies within the Messinian evaporitic unit has been interpreted as indicative of the presence of halite deposits (Chapter 4). Conversely, the intra-evaporitic horizons could indicate the juxtaposition of halite on anhydrite or limestone facies (positive seismic response) and on shale/marl facies (negative seismic response) (Nurmi, 1988). The spatial analysis of these horizons did not resolve any clear geomorphological pattern supporting a lithological interpretation. In contrast, the high lateral continuity of the reflection character is more indicative of chemical sedimentation processes (for the acoustically hard layers), or marly/muddy depositional systems (for the acoustically soft layers) (Chapter 4, Section 4.6.2).

Some constraint about the nature of the upper part of the Messinian evaporites has been provided by the marginal wells (Chapter 1, Fig. 1.9a). This part (few 10s of metres) of the evaporites is composed of a thin layer of anhydrite passing upward to interbedded anhydrite and weakly calcareous claystone, with traces of pyrite and chert (unpublished well reports). Based on cutting analysis, the depositional environment of this upper and marginal portion of the evaporites has been interpreted alternatively as continental (fluvial/lacustrine), sabkha and/or shallow marine, (unpublished well reports). Conversely, the lithologies within the near-basal part of the Messinian evaporites in this marginal area are inferred from well log data, and are composed of a thick halite interval, interbedded with a claystone–anhydrite layer that is a few metres in thickness (Chapter 5, Fig. 5.6; unpublished well report). These data provide insights on the depositional environments of the evaporites. Nonetheless, the data available do

not allow a detailed interpretation of facies juxtaposition, and of possible transgressive-regressive patterns within the basinal evaporitic system.

The variety of evidence for a deep-basinal pre-evaporitic setting collected in this section indicate that the first model hypothesised for the depositional setting of the evaporites, i.e. a pre-existing very shallow sea (Fig. 6.5a) can be ruled out. The second model proposed, i.e. the deposition of the evaporitic wedge in a pre-existing ramp-setting shallow sea (Fig. 6.5b) would require a high lateral variability of evaporite seismic facies. The lack of this variability, coupled with the nearly parallel geometrical relation between the base of the evaporites (Horizon N) and intra-evaporitic horizons, are used to reject this second model. Therefore, the most likely basinal setting for the deposition of the Messinian evaporites is the third model (Fig. 6.5c) i.e. deposition of the distal evaporitic wedge in a pre-existing shelf-slope-basin setting intermediate sea (ca. 1000 m deep). This result supports the pre-existence of a deep basin before the onset of the MSC, as observed in previous studies in the Levant region (Tibor et al. 1992; Buchbinder et al., 1993; Ben-Gai et al., 2005) and in most of the Mediterranean continental margins (Cita, 1973; Montadert et al., 1978). The result also confirms that the deposition of the Messinian evaporites in the Levant region occurred in a deep-basin, as it is indeed widely accepted for the evaporitic series throughout the Mediterranean Basin (e.g. Hsü et al., 1978; Warren, 1999).

Moreover, this study documents that sediment load rather than tectonic subsidence had a gradual and significant effect for the creation of accommodation space during evaporite deposition. For the general discussion on sea-level changes during the MSC, it is noteworthy that the absence of onlap terminations of the intra-evaporitic horizons within the evaporitic wedge confirms that the sea-level never dropped below the top of the Messinian evaporites during their deposition. This provides an important constraint on the bathymetry of the evaporitic basin during the MSC, and will be used in the following sections to build the evolutionary model for evaporite deposition in the Levant area.

6.3.4 Sea-level at the top of the Messinian evaporites

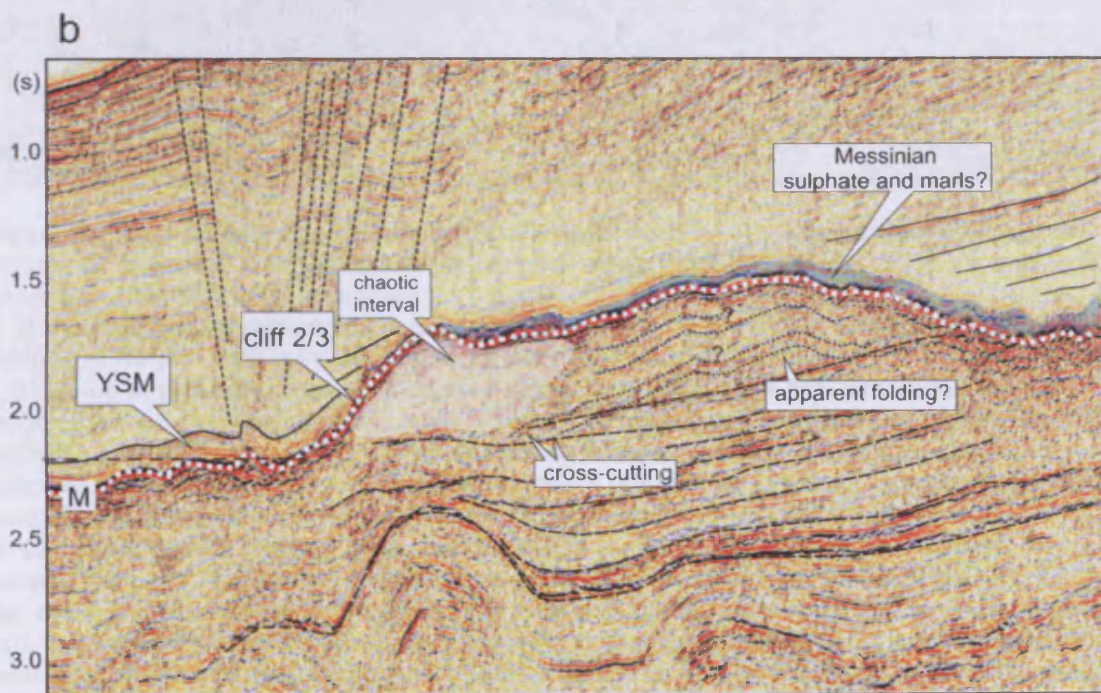
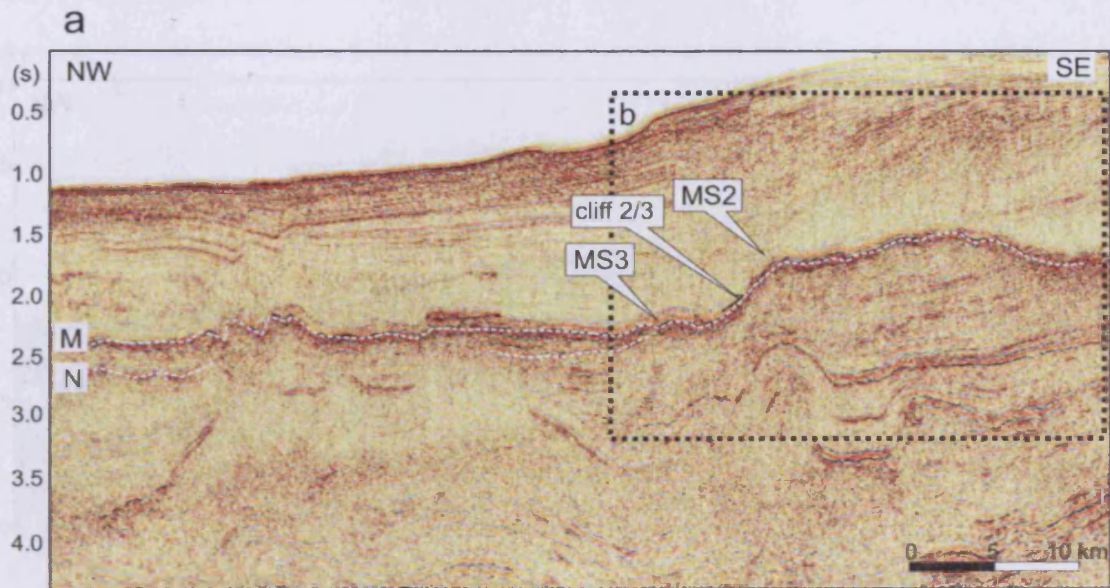
Chapter 4 has documented that, in the Levant region, the top of the distal Messinian evaporites represents an erosional unconformity. The analysis of the origin of this erosional unconformity can provide important insights for the identification of the sea-

level position at this stratigraphic level, and therefore it will be undertaken in this section.

As suggested in Chapter 4, Section 4.8.3, the top Messinian unconformity could either have been generated by subaerial or submarine erosion. A number of previous studies document the occurrence of a final regression of the sea-level at the end of evaporite deposition (e.g. Druckman et al., 1995; Clauzon et al., 1996; Krijgsman et al., 1999; Cornée et al., 2006). On the other hand, it is widely accepted that the MSC terminated when normal deep-water marine conditions were re-established in the Mediterranean Basin (Cita, 1975; Hsü et al., 1977; McKenzie, 1999). Consequently, the erosional event shaping the top of the Messinian evaporites could either have resulted from the late lowstand at the end of the Messinian, or as a ravinement surface linked to the refilling of the Mediterranean after the Salinity Crisis. The interpretation of the origin of this erosional surface is fundamental to determine the relative sea-level changes at the latest phases of the MSC in the Levant region. This section aims, thus, to evaluate if this surface is most likely to be subaerial or submarine in origin, and consequently, if the erosion was activated by a sea-level fall or rise.

Three main observations made in the previous chapters and sections are important for this interpretation:

- First, that erosional truncation covers a significant area of the Levant region (ca. 10,000 km², Chapter 4). The basinal horizontal geometry of this surface at the end of the Messinian is particularly remarkable, and has been evaluated in previous studies based on stratigraphic simulation programs (Ben-Gai et al., 2005). The occurrence of this horizontal base level of erosion documents an areal erosional phase that is typical of regression surfaces and conversely, difficult to achieve in a transgression or ravinement surface.
- Second, that the top of the Messinian evaporites correlates with the platform at the base of the lower marginal cliff observed in the study area (MS3 In Figs. 6.2 and 6.6). The platform has been interpreted as likely to represent a shoreline platform, and this argument will be further developed in Section 6.3.5;
- Finally, that fluvial, sabkha and brackish facies are recorded in the wells at the top of the evaporitic series (Section 6.3.3; unpublished well reports). The occurrence of a marine shallow-water and/or continental environment is in agreement with the fluvio-



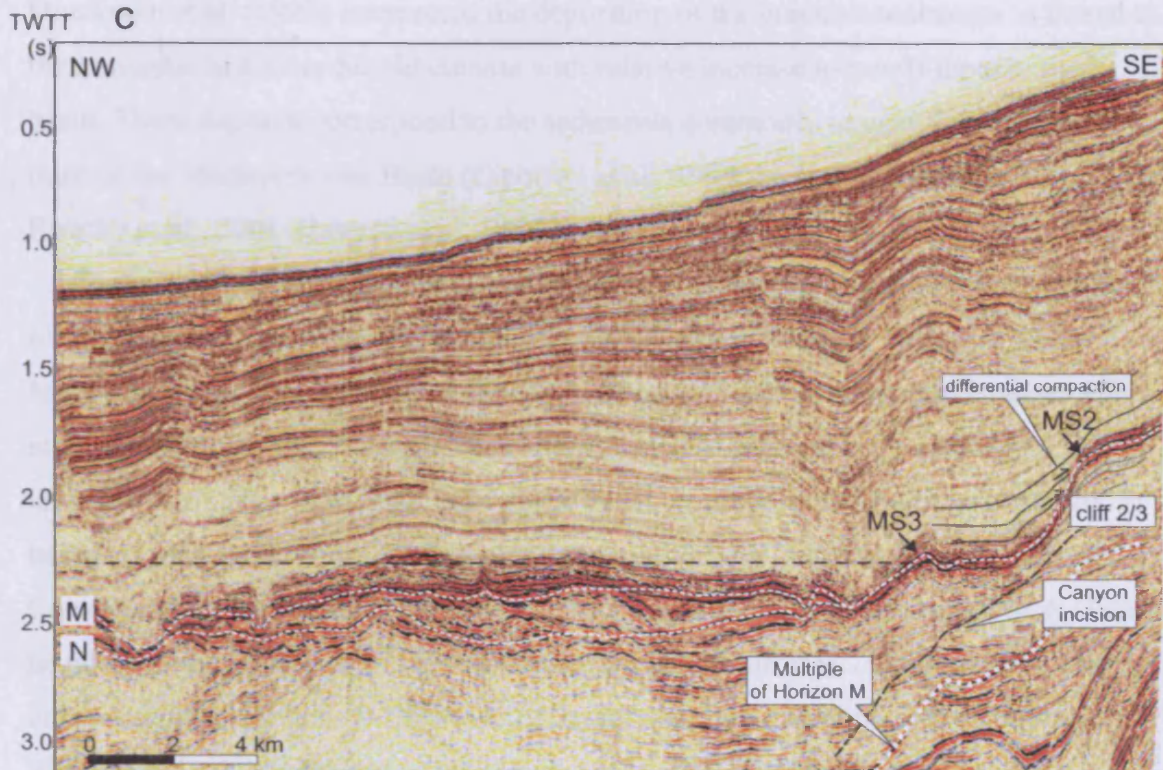


Figure 6.6 Seismic sections showing the details of the morphology and truncation of seismic reflections associated with the Messinian marginal scarps identified at Horizon M, eastward of the pinch-out of the Messinian evaporites.

a) 2D seismic section crossing the Levant margin in a NW-SE direction (location in Fig. 6.2). The location of the marginal scarp developed between MS2 and MS3 (cliff 2/3) is indicated.

b) Close-up of the seismic section displayed in Fig. 6.6a (location in Fig. 6.6a and in Fig. 6.2), showing the detailed seismic stratigraphic context of the marginal scarp developed between MS2 and MS3 (cliff 2/3). The interpretation of the main reflections, faults and seismic effects is indicated. The seismic package highlighted in blue is of unknown origin and it might correspond to marginal Messinian deposits, whose internal architecture is beyond seismic resolution.

c) 3D seismic section crossing the Levant margin in a NW-SE direction (location in Fig. 6.2). The onlap of the early Pliocene reflections on the scarp developed between MS2 and MS3 (cliff 2/3 of Fig. 6.6a) should be noted. It is significant to note also that the base of the cliff (MS3) is coincident with the projected top of the Messinian evaporites (horizontal black dashed line). The downward bending of the seismic reflections directly above MS2 is probably the product of post-depositional differential compaction of the Pliocene sediments above the morphological step defined at Horizon M.

lacustrine facies observed at the top of the Messinian evaporites in the lower slope and basin of the Levant region by Druckman et al. (1995). Similar coeval facies have been also recorded in the nearby Eratosthenes seamount region by Spezzaferri et al. (1998). Druckman et al. (1995) interpreted the deposition of the brackish sediments as linked to the transition to a more humid climate with relative increase in runoff input to the basin. These deposits correspond to the sediments commonly termed 'Lago-Mare' in most of the Mediterranean Basin (Cipollari et al., 1999; Iaccarino & Bossio, 1999; Rouchy et al., 2001; Bassetti et al., 2003).

Based on these geomorphological and paleoenvironmental observations, the most likely interpretation of the origin of the erosional unconformity at the top of the distal Messinian evaporites is subaerial exposure, developed during a regressive phase. This interpretation confirms the hypothesis that Horizon M represents the peak of the sea-level fall during the Messinian desiccation event, as proposed by Ben-Gai et al. (2005) based on two-dimensional stratigraphic simulation of the Levant continental margin. Consequently, the absolute elevation of this surface (i.e. -2000/-2300 s.l., Fig. 6.1) can be taken as the indication of the sea-level at the end of the MSC. Consequently, the intra-evaporitic horizons (ME20 to ME50) and their onlap terminations would have been eroded subaerially during the last stages of evaporite deposition. The reconstruction of the prosecution of the intra-evaporitic horizons landward of their truncation (Section 6.3.3; see also Chapter 4, Section 4.8.1) suggests that the sea-level during deposition of the evaporites, and preceding the final subaerial erosion, was located at a higher position. However, the absence of onlap terminations hinders the definition of the exact sea-level position at this stratigraphic level.

The identification of the top of the distal Messinian evaporites as the base-level preceding the Pliocene reflooding, permits the comparison with the basinal depth of the post-evaporitic interval. Consequently, the relative sea-level changes occurred from this stratigraphic level to the post-evaporitic setting can be evaluated. This can be estimated calculating the difference in elevation between the subaerial erosional surface at the top of the evaporites and the earliest Pliocene marine deposits overlying them. The earliest Pliocene sediments overlying the Messinian evaporites in the marginal part of the evaporitic wedge are represented by the basin-floor fan deposits of the Yafo Sand Member (Frey-Martinez et al., in press; unpublished well reports). The paleobathymetry of the Yafo Sand Member is considered in the range of 200-1000 m

(unpublished well reports). This is an important evidence as it gives a range of possible water depth for the Pliocene basin immediately after the end of evaporite deposition. Thus, the juxtaposition of the upper neritic to bathyal deposits of the Yafo Sand Member to the subaerially exposed top of the Messinian evaporites to suggests a relative sea-level rise of 200-1000 m in the Levant region during the early Pliocene. However, this should be considered as an approximate paleobathymetric indication, as further evidence is needed to support this interpretation. In particular, this interpretation needs to be supported by the analysis of the first phase of outbuilding of the Pliocene continental margin in the Levant region, an important physiographic indication that is not visualised in the study area.

6.3.5 Remarks on the formation of the marginal Messinian erosional surface

During the MSC, prominent Messinian erosional surfaces formed in most of the Mediterranean continental margins (Ryan & Cita, 1978). As pointed out in the previous chapters of this research study, the correlation of this marginal erosional surface with the distal evaporitic domain is complicated by the lack of a detailed stratigraphic constraint on this surface (Chapters 2 and 4). The aim of this section is to attempt a correlation between the marginal Messinian erosional surface and the distal evaporitic domain in the study area. This is done in order to obtain additional indications about relative sea-level variations during the MSC.

The marginal Messinian erosional surface has been interpreted in Eastern Mediterranean as generated by subaerial processes and distally correlated with the basal, pre-salt discordance (Horizon N) (Ross & Uchupi, 1977; Ryan, 1978; Barber, 1981; Mart & Ben Gai, 1982; Ben Gai et al., 2005). The identification of at least two base-levels of erosion in the study area during the MSC raises the question if the marginal erosional surface should be correlated to any of these basinward erosional events. The main indications of erosional phases are represented by the submarine incision at the base of the distal Messinian evaporites, and by the areal subaerial erosion at their top (see Sections 6.3.2 and 6.3.4). Additionally, it was discussed in this thesis that a series of marginal scarps developed on the marginal Messinian erosional surface possibly indicate different base-levels of erosion (Chapter 2, Section 2.6.4). These scarps bear similarities with sea-cliffs developed at the top of shore platforms,

thus they could indicate the position of the sea-level during the progression of the MSC. The details of the morphology and truncation of seismic reflections associated with the scarps are highlighted in Fig. 6.6. The onlap of early Pliocene reflections on the Messinian marginal scarps (Fig. 6.6) demonstrates that the relict scarps already existed at the end of the Messinian and are not related to salt withdrawal.

The formation and evolution of cliffs adjacent to shore abrasion platform is linked to basal erosion of the cliff, leading to progressive inland propagation of the cliff through retrogressive failure (Huggett, 2003). Consequently, the formation of the cliffs requires a period of constant base-level. Similar shore or wavecut platforms have been observed in the Nile delta area (Barber, 1981). These platforms are interpreted as rejuvenation terraces indicating constant lowering of base-level, with associated rapid falls and quiescent periods (Barber, 1981). The same concepts have been applied by Lofi et al. (2005) in the Gulf of Lions margin (Western Mediterranean), where the morphology of the Messinian erosional surface indicates a two-step sea-level fall during the MSC. In the Levant region, the most prominent and continuous cliff is developed between MS3 (2000-2250m depth) and MS2 (1750-1850m depth) (Figs. 6.2 and 6.6; see also Chapter 2). It is significant to note that this cliff is parallel to the pinch-out of the Messinian evaporites (Chapter 2, Fig. 2.10), and its base is coincident in most of the study area with the projected top of the Messinian evaporites (Fig. 6.1 and 6.6). This coincidence suggests that the cliff formed when the sea-level was located at the top of the Messinian evaporites, and consequently developed through retrogressive erosion at its base.

The interpretation of the top of the Messinian evaporites as the elevation of the sea-level points to a fully subaerial nature of the marginal erosional surface during the latest stages of the MSC. This erosion could explain the lack of significant or comparable thickness of evaporites landward of their present-day pinch-out. On the other hand, it is somewhat more complicated to relate the other scarps observed in the study area to a determined stage of the MSC, due to the lack of detailed chronological constraint in this marginal setting. By analogy with the nearby Nile delta (Barber, 1981) it could be speculated that these marginal cliffs were formed during occasional still-stands of sea-level, associated with the initial regression at the beginning of the MSC. Nonetheless, based on the data available, it is not possible to attempt a definitive

reconstruction of the sequential events leading to the formation of these scarps on the Levant margin.

6.3.6 Summary of relative sea-level changes during the MSC

In this section, the results obtained on the relative sea-level changes that occurred in the study area during the MSC are summarized, as displayed in a simplified evolutionary reconstruction (Fig. 6.7) and compared with estimates made in previous studies (Table 6.1). The main aspect of this reconstruction are listed as follows:

- Deep-water conditions existed in the Levant Basin before the onset of the MSC. This basin was characterized by a well-developed shelf-slope-basin siliciclastic system (Fig. 6.7a).

- The onset of the MSC was associated with a sea-level drop in the study region (Fig. 6.7b). The incision of the canyons indicate an erosional phase preceding the deposition of the distal Messinian evaporites. This initial fall is likely to have triggered the deposition of the clastic submarine deposits recorded in the basal part of the Messinian evaporites, basinward of their pinch-out. The source of clastic supply is most probably represented by the canyons and/or by the eroded subaerially exposed continental margin. The basinal extent of the subaerial exposure of the margin did not exceed the depth of the pinch-out of the distal evaporites. In previous studies, the estimated maximum sea-level fall linked with the MSC ranges between ca. 1000-2500 m (Table 6.1).

- The deposition of the distal Messinian evaporites took place in a fully submarine environment. The evaporites presented a divergent onlap geometry (Fig. 6.7c). This pattern of evaporite deposition could have been represented by a combination of transgressive, regressive and/or offlapping bodies depending on relative-sea-level changes in the basin. The final truncation of the onlap termination hinders the precise interpretation of the sea-level position, that must have been higher than the elevation of the top of the distal evaporitic wedge.

- The truncation surface at the top of the distal Messinian evaporites coincides with the final base-level at the end of the MSC (Fig. 6.7d). Brackish-shallow water and fluvial facies are recorded at this stratigraphic level (equivalent to the Mediterranean-wide Lago-Mare deposits), and the development of the marginal cliff and correlative platform MS3.

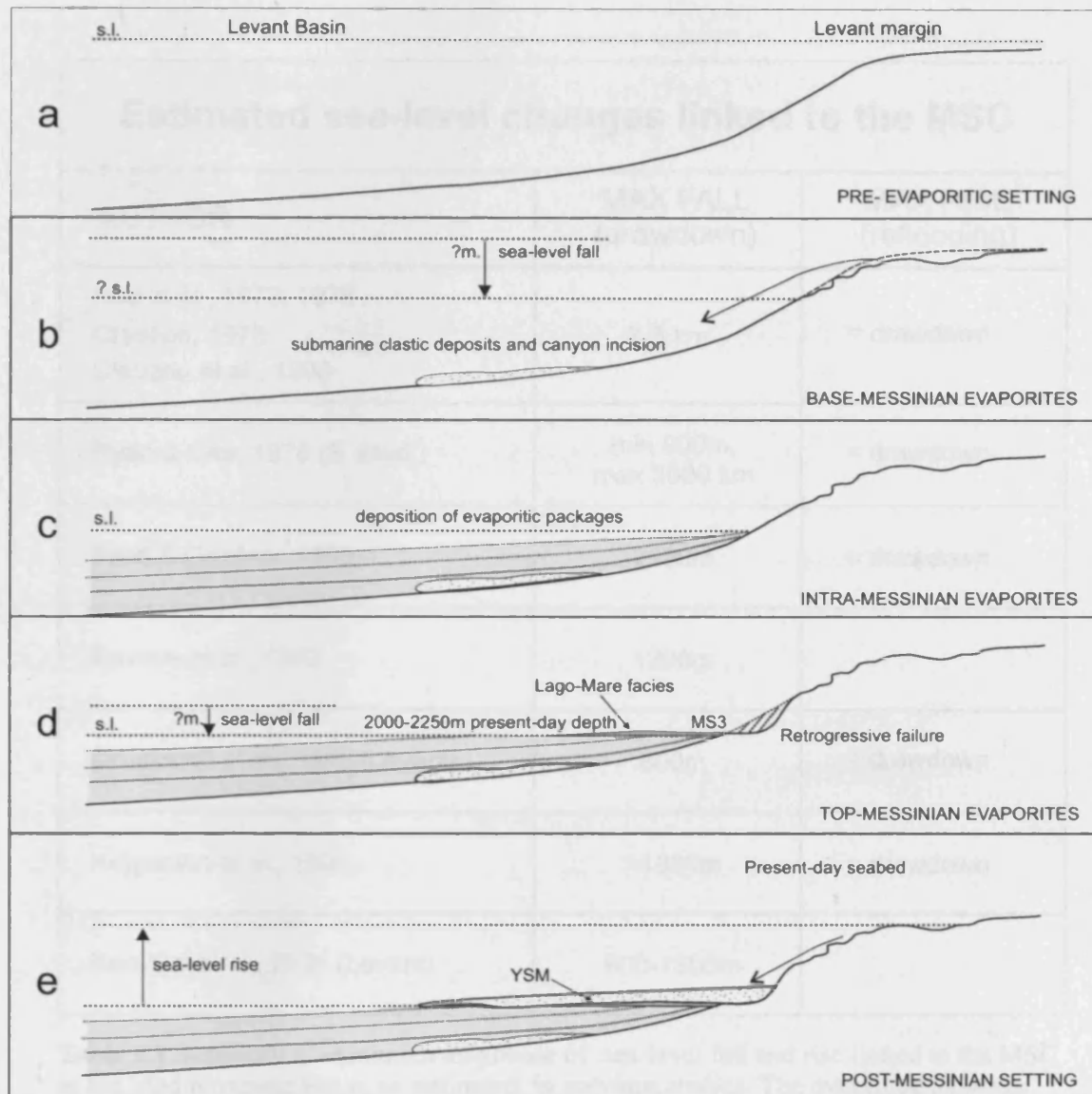


Figure 6.7 Cartoon showing a simplified evolutionary reconstruction of the relative sea-level changes and of the depositional and erosional processes occurred in the study area during the MSC (see detailed discussion in the text).

Estimated sea-level changes linked to the MSC		
AUTHOR	MAX FALL (drawdown)	MAX RISE (reflooding)
Hsu et al., 1973; 1978 Clauzon, 1978 Clauzon et al., 1996	2-3 km	= drawdown
Ryan & Cita, 1978 (E. Med.)	min 900m, max 3000 km	= drawdown
Field & Gardner, 1990	2500m	= drawdown
Savoie et al., 1993	1200m	
Druckman et al., 1995 (Levant)	800m	= drawdown
Krijgsman et al., 1999	>1000m	= drawdown
Ben-Gai et al., 2005 (Levant)	800-1300m	

Table 6.1 Summary of maximum amplitude of sea-level fall and rise linked to the MSC in the Mediterranean Basin, as estimated in previous studies. The overall equivalence between the drawdown and reflooding amplitudes should be noted.

- The end of the MSC in the study area is marked by the Pliocene sea-level rise, indicated by the deposition of a deep-water basin-floor fan (Yafo Sand Member, YSM) above the evaporites (Fig. 6.7e). In previous studies, the sea-level rise coinciding with the reflooding of the Mediterranean Basin is considered of similar amplitude to the drawdown during the Crisis (Table 6.1). In this study, approximate indications from wells suggest that this relative sea-level rise ranges from 200 to 1000 m. This value is comparable to the amplitudes obtained in previous studies in the Mediterranean area (Table 6.1).

6.4 Comparison with previous models and other evaporitic basins

The Messinian evaporitic basin represents one of the past ‘saline giants’ (Warren, 1999). It extends across some 2400 x 600 km and has evaporite fills up to more than 2 km (Kendall & Harwood, 1996). The absence of modern depositional analogues of similar scale, coupled with the scarcity of cores across the evaporites, has meant that determining the depositional conditions of these saline giants is highly contentious (Kendall & Harwood, 1996). In general, developing sequence-stratigraphic models for the evaporites is not straightforward mainly because they are highly dependent upon the hydrology of the basin. This is in its turn controlled by factors other than sea-level change (Kendall & Harwood, 1996). These observations reinforce the necessity of a comparison between the Messinian evaporites and other ancient saline giants in order to fully understand their depositional setting.

Figure 6.8 displays the distribution of the major ancient basinwide evaporitic systems in the world (Warren, 1999). The relatively deep-water conditions of the Messinian evaporites compared e.g. to modern sabkhas and salinas, means that a greater vertical and lateral continuity is expected in these deposits (Kendall & Harwood, 1996). In the study area, a widespread lateral continuity is supported by the presence of extensively traceable and correlatable intra-evaporitic seismic horizons. In some Mediterranean sub-basins, the continuity of the Messinian evaporitic deposits permits their detailed sequence analysis. This continuity, coupled with excellent outcrop exposures, explains why the gypsum evaporites of the marginal Messinian basins are amongst the most well-understood evaporite deposits in terms of sequence

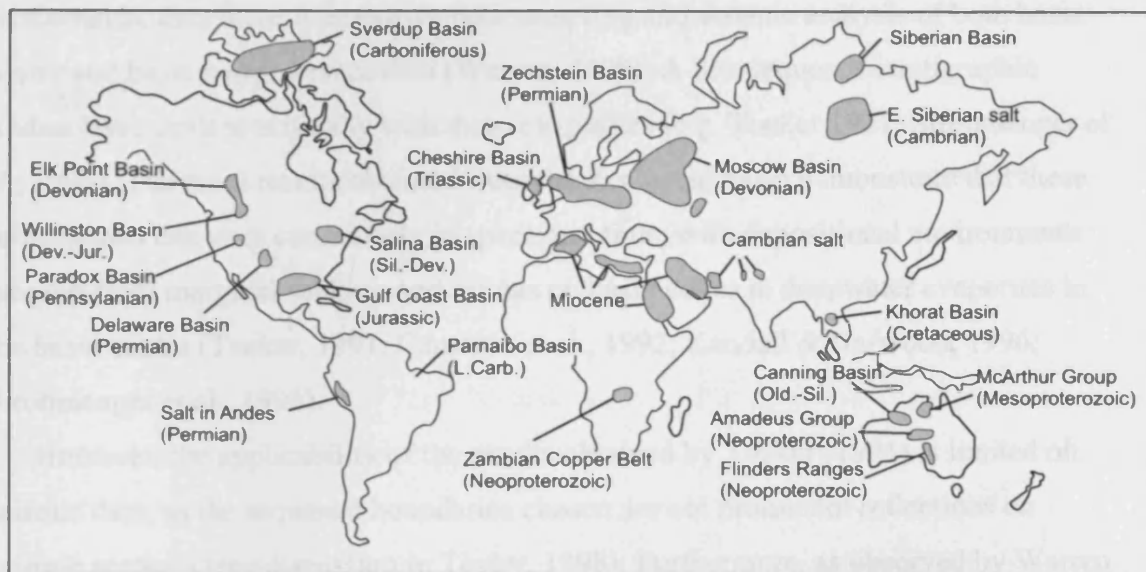


Figure 6.8 Map showing the location and age of some of the major basinwide evaporite deposits. The basins are drawn for visual clarity, not to exact scale (Warren, 1999).

analysis (Ricci Lucchi, 1973; Parea & Ricci Lucchi, 1972; Vai & Ricci Lucchi, 1977; Roveri et al., 2001; Manzi et al., 2005). Conversely, to date the only attempt to build a comprehensive model for the basinal Messinian evaporitic unit based on seismic data has been made in the Western Mediterranean area (Lofi et al., 2005).

Probably the best documented analogue of basinwide evaporites where high-resolution sequence analysis has been attempted are the anhydrite/halite evaporites of the Upper Permian Zechstein Basin in the North Sea (Fig. 6.8; Warren, 1999). In this evaporitic series, the entrained carbonates are onshore gas plays in Germany and the Netherlands, thus there is extensive core sampling and seismic analysis of both basin centre and basin margin evaporites (Warren, 1999). A few sequence stratigraphic studies have dealt specifically with these evaporites (e.g. Tucker 1991; Strohmenger et al., 1996). The main results obtained from the Zechstein basin demonstrate that these saline giants can vary enormously in space and time, with depositional environments ranging from marginal sabkhas and salinas on basin edges to deepwater evaporites in the basin centre (Tucker, 1991; Cameron et al., 1992; Kendall & Harwood, 1996; Strohmenger et al., 1996).

However, the applicability of the results obtained by Tucker (1991) is limited on seismic data, as the sequence boundaries chosen are not prominent reflections on seismic sections (see discussion in Taylor, 1998). Furthermore, as observed by Warren (1999), the stratigraphic interpretation of the Zechstein deposits is largely focused on the prospective carbonate intervals (e.g. Füchtbauer & Peryt, 1980; Strohmenger et al., 1996) and does not deal in any detail with the internal stratigraphy of the evaporite themselves. Significant differences are observed between the evaporite facies of the Zechstein and of the Messinian evaporites, the major probably being the scarce development of marginal carbonate platforms within the Messinian series (Schlager & Boltz, 1977). This difference could be linked to the dissimilar geodynamic setting and basinal topography of the two areas.

In the Messinian evaporites, onshore exposures and cores are available from the marginwards basins of Italy, where a number of seminal studies on both shallow and deep-water evaporite depositional environment were developed (Parea & Ricci Lucchi, 1972; Decima & Wezel, 1973; Schreiber et al., 1976; 1977). Conversely, there is little sampling and facies interpretation of the evaporites in the deeper parts of the Mediterranean Sea, where the sequences are thicker. Sampling is generally limited to

the upper few meters of the basinal evaporites (e.g. Friedman, 1973; Garrison et al., 1978; see discussion in Hardie & Lowenstein, 2004). In this context, the Nile-Levant region is particularly poorly known, due to the complete absence of scientific drilling in this area.

In the Eastern Mediterranean, Druckman et al. (1995) developed a model for the deposition of the Messinian evaporites in the Israel onshore and shelf area, based on well data coupled with a series of 2D seismic profiles. This model is focused on the analysis of the interaction of the Messinian evaporites with the Oligo-Miocene Afq submarine canyon (Druckman et al., 1995). The model does not take into account the development of significant thickness of halite-bearing deposits in the more distal areas of the Levant basin. An attempt to summarise the depositional environment of the evaporites in the Israeli area has also been made by Cohen (1988, 1993) based on well data. Nevertheless, this model is strongly focused on the subsurface of the Israeli shelf area and does not address the internal depositional geometry and composition of the thick distal wedge of evaporites.

The results obtained in this PhD research study confirm some of the aspects highlighted in these previous models. Firstly, the occurrence of two main sea-level falls, at the beginning and at the end of evaporite deposition, respectively, is recorded, in analogy with the model proposed by Druckman et al. (1995). These stages of sea-level fall are accompanied by erosion at the continental margin. Secondly, this study confirms the onlapping nature of the evaporites on the margin, as suggested by Cohen (1993). Finally, the results obtained can be confidently included in a model proposing the diachronous origin of the marginal and basinal evaporites, as suggested by Druckman et al. (1995). Conversely, some of the results of this research appear to contradict the previous studies. This refers, in particular, to the location of the pinch-out of the 'Lower evaporites' in Druckman et al. (1995) which does not appear to be consistent with the basinward location of the pinch-out of the Messinian evaporite in the study area. Additionally, the analogy between the two studies are strongly limited by the absence of occurrence of halite facies in the data analysed by Druckman et al. (1995).

From a more general perspective, a series of theoretical models have been developed for the deposition of the basinwide Messinian evaporites in the Mediterranean area (Chapter 1, Section 1.4.2). The results of this research suggest that

the two-step model by Clauzon et al. (1996) would be the most applicable to the Messinian evaporitic unit of the Levant area. The analogies observed regard the occurrence of a first sea-level fall at the onset of the MSC, and the final Messinian drawdown in the last stages of the MSC. It must be noted, however, that this model associates the apex of canyon erosional activity and the deposition of clastic fan with the last stages of the Salinity Crisis, while in the study region the accumulation of clastic deposits and focused canyon incision is mostly developed in the early stages of the MSC and of evaporite deposition.

In conclusion, this research provides evidence for the structural and architectural differences between the Levant area and the other Mediterranean margins during and after the Messinian Salinity Crisis. This refers in particular to the influence of pre-evaporitic canyon systems and to the internal stratigraphy of the evaporitic wedge in the Levant area. However, the many analogies observed in the depositional and erosional patterns mean that the study area can be used as an example for other areas of the Mediterranean basin where 3D seismic is not available yet and sub-salt imaging is limited.

6.5 Limitations and future research

The work presented in this thesis is a comprehensive study, based on seismic (2D and 3D) and well data, of the Messinian evaporites in the Levant region, covering their depositional setting and post-depositional deformation. By integrating different types of data, the evaporitic unit has been examined to a high level of accuracy that could not have been attained so far. Furthermore, this is one of the first studies to explore the application of 3D seismic data to the study of the Messinian evaporites, and the results strongly encourage further work in this direction.

Comparison and discussion of the pre, syn and post-evaporitic setting of the study area has allowed numerous aspects of their 3D architecture and evolution to be inferred. The conclusions presented here have also enhanced a deeper understanding of the causes, and processes acting during the Messinian Salinity Crisis in the Mediterranean Basin. Some of the results should be applicable worldwide to other saline giant systems. However, despite the advance in knowledge achieved throughout this research, some results and interpretations have been partially hindered by a series

of limitations. In this section, a review of such limitations and a series of research proposals to overcome them in the future are presented.

A significant limitation throughout this research has been the incomplete coverage of 3D seismic data of the study area. Accurate seismic mapping is necessary for determining the exact internal seismic stratigraphy of large-scale, basinwide systems such as the Messinian evaporites. Additionally, this is critical in order to implement the use of attribute-based interpretation techniques e.g. the seismic amplitude analysis that permitted the finding and interpretation of clastic depositional bodies within the evaporites. For these purposes, 3D seismic data is required over larger extensions of the study area, as 2D seismic datasets have inherent problems with the spatial aliasing of the imaged features.

Additionally, the limits of the resolution provided by the 3D seismic data (i.e. tens of meters) have precluded a more detailed analysis of the small-scale sedimentary and deformational patterns within the evaporites. This affected the interpretation of evaporite stratigraphy especially in the marginal parts of the basin, where their thickness is close to seismic resolution. Indeed, the seismic data used during this research project were processed and migrated to obtain the best imaging for the post-Messinian interval. This was due to the fact that the main exploration targets are located within the Pliocene section. As a result, imaging of the evaporite and pre-evaporite interval is limited. Nevertheless, the pre-evaporitic intervals are at a relatively immature stage of exploration. The increasing interest in the hydrocarbon prospectivity of these intervals will probably lead in the future to better techniques for the acquisition and migration of seismic data. This should allow an improved visualization of such intervals and hence, a more complete understanding of their depositional and structural context.

Data limitations have also precluded a higher degree of confidence when modelling the effects of subsidence and uplift due to evaporite load and water unload on continental margin and on the basin during the different stages of the MSC. This restricted the interpretation of their possible effects on the destabilization and erosion of the continental margin. Another interesting point concerned the interaction between evaporite deposition and vertical fluid flow and mud diapirism. This topic is still scarcely documented worldwide; in the case of the Messinian evaporites, so far only one study documented gas hydrate destabilization in pre-evaporitic marls ignited by the

MSC, based on outcrop data (Pierre et al., 2002). In order to attain a greater comprehension of all these aspects and their basinwide applications, an inclusive analysis of the effects of relative sea-level changes on vertical fluid and gas migration is needed. The integration of theoretical modelling approaches with further geophysical analysis is here considered as the best way of improving knowledge on the mechanisms controlling the interaction among evaporite deposition, sea-level changes, fluid and gas flow and migration at continental margins.

A final and important area where significant improvements can be made is in a more rigorous analysis of the well database. Additional and more detailed biostratigraphic and well log data through the evaporites are required to fully understand their stratigraphy and facies. The necessity of a more accurate well log database is especially patent when analysing the intra-evaporitic horizons. Due to lack of accurate borehole logs at these stratigraphic intervals, a more detailed examination of their genetic mechanism and therefore, of the paleoenvironmental context of the evaporite cycles in the basin has been prevented. This affected in particular the prediction of lithology and facies, not definitely resolvable only based on the seismic characteristics of the reflections. This, in turn, has limited a further understanding and discussion of the conditions (e.g. eustatic and climatic) under which the Messinian evaporites deposited.

The study area is a candidate of particular interest for future scientific drilling in the area, as advanced in recent international meetings (e.g. Corte Colloquium, 2004). The proposals aim not only to a better understanding of the depositional environment of the Messinian evaporites, but also to detailed structural analysis of the evaporites and climatic reconstructions. This type of inter-disciplinary research would represent a unique opportunity to enhance our understanding of many of the still poorly understood aspects of the Messinian Salinity Crisis in the Mediterranean Basin.

Chapter Seven: Conclusions

Seismic (3D and 2D) and well data have been used in this PhD research project to investigate the stratigraphic evolution, depositional systems and structural deformation of the Messinian evaporitic series in the Levant region. The investigations undertaken have produced detailed observations and deductions with regard to diverse aspects of the development of the Messinian Salinity Crisis in the study area, and more in general in the Eastern Mediterranean basin. Furthermore, insights of the impact of the evaporites on deformational processes and fluid flow migration at the Levant continental margin have been provided by this research. The results obtained should be of applicability to coeval evaporitic sub-basins across the Mediterranean and to other sedimentary basins worldwide. The primary conclusions for this PhD research study, and the specific conclusion that can be drawn for each of the previous chapters are summarised below.

7.1 General conclusions

- This study documents how 3D and 2D seismic analysis coupled with well analysis can help improve our knowledge of the processes acting during the Messinian Salinity Crisis (MSC) in the Eastern Mediterranean Basin.
- 3D seismic interpretation has proved to be a powerful tool when analysing the internal stratigraphy and deformational processes of the Messinian evaporites. The availability of a three-dimensional understanding of the resultant structures and their geological context has been critical to evaluate triggering mechanisms of deformation of the evaporites, and to infer their depositional environment.
- The Messinian evaporitic series is composed in the Levant region of a wedge up to ca. 1.8 km thick in the distal part of the basin, and of a proximal domain, where an erosional unconformity and possibly thin (sub-seismic resolution) evaporitic sediments deposited. The two areas are seismically separated by the locus of pinch-out of the distal evaporitic wedge, which has been mapped throughout the study area.

- The Messinian erosional surface is probably composite in age and in the environment of formation (i.e. submarine/subaerial).
- The base of the distal Messinian evaporites (Horizon N) is characterised by localised canyon incision, and this permitted its identification as an erosional surface. The incision of the canyons at this stratigraphic level has been linked to a sea-level fall at the beginning of the MSC.
- Clastic deposits have been discovered in the basal part of the Messinian evaporitic unit. Their presence supports the hypothesis of a sea-level fall associated with the initial stages of the MSC in the region.
- The deposition of Messinian clastic bodies and of the distal evaporites appears to have occurred mainly in a submarine environment.
- The top of the Messinian evaporites (Horizon M) represents an areal erosional surface which documents the subaerial exposure of a considerable part of the distal evaporites, and therefore a sea-level fall at the final stages of the MSC.
- The end of the MSC and evaporite deposition in the Levant region is marked by a sea-level rise, as indicated by the deposition of an early Pliocene basin-floor fan (Yafo Sand Member) and by the development clinofolds of Pliocene age.

7.2 Controls on the architecture of the Messinian evaporites

- The pre-evaporitic setting of the Levant continental margin is dominated by a series of structural highs related to the development of the Syrian Arc foldbelt. These anticlines controlled the pre-evaporitic basin physiography and, consequently, the differential accommodation and the linear NE-SW directed edge of the Messinian evaporites.
- The Afq, El Arish and Ashdod submarine canyons acted as preferential sites of erosion in the earliest stages of the MSC up to the distal part of the Levant Basin. The recognition of confined erosional truncation patterns in this research study allowed for the first time detailed mapping of the canyons at this stratigraphic level in the entire study area.
- The canyons acted as local depocentres for the distal evaporites in the later stages of the MSC. This is indicated by an evident increase in the thickness of the Messinian evaporites above the canyon axes. This originated the locally irregular

geometry of the edge of the evaporites, characterized by major embayments and landward outliers.

- The marginal embayments of the evaporites acted as a focus for post-evaporitic thin-skinned gravitational tectonics during the Plio-Pleistocene.

7.3 Clastic deposits at the base of the Messinian evaporites

- The presence of significant amounts of clastic deposits in the lower part of the Messinian evaporitic wedge was revealed by 3D seismic geomorphological analysis.
- The source of clastic supply to the evaporitic basin appears to be directly linked to the Afiq and El Arish Canyons on the Levant margin, and to the nearby Nile Delta system, to the southwest of the study area.
- The discovery of these clastic deposits documented the increased erosional and depositional activity of these clastic fairways at the initial stages of the MSC.
- The analysis of the seismic characteristics of the clastic deposits and of the coeval basin physiography suggested a submarine environment for the deposition of the clastic bodies.

7.4 Nature of the top of the Messinian evaporites

- The detailed seismic seismic-stratigraphic analysis of a series of intra-evaporitic horizons and of the packages bounded by them permitted the detection of a discordant relationship between the intra-evaporitic horizons and the top of the Messinian evaporites (Horizon M).
- The clear evidence of the erosional truncation of the intra-evaporitic horizons against Horizon M allowed for the first time in the Levant region the definition of top of the Messinian evaporites as an erosional unconformity.
- Based on the preserved geometry of the seismic reflections, the expected original depositional geometry of the evaporitic system is divergent onlap of the intra-evaporitic horizon on the continental margin.

7.5 Evaporite deformation: dissolution and salt tectonics

- This PhD research has documented the extensive occurrence of dissolution and salt tectonics deformation in the Messinian evaporites within the study area.
- The detailed structural analysis of the intra-evaporitic horizons has documented the occurrence of an early phase of evaporite deformation at the end of Messinian, before the erosional event forming Horizon M.
- The most likely mechanism of deformation is differential loading linked to a prograding shelf wedge on the basinal evaporitic system. The direction of the intra-evaporitic compressional structures indicates that the deformation could have been initiated by the outbuilding of the Nile delta and submarine fan, active in the Levant Basin at least since the final stages of the deposition of the Messinian evaporites.
- The occurrence of post-depositional evaporite dissolution is documented by the finding of a series of circular dissolution structures at the top of the Messinian evaporites. Dissolution occurred in the buried evaporites, in a deep-water setting, during the Pliocene.
- Dissolution is thought to have acted on the more soluble facies in the Messinian evaporites, leading to the collapse of a weakly lithified overburden, which deformed with a series of extensional concentric faults.
- The trigger of dissolution has been possibly linked to focused vertical flow of undersaturated fluids at the base of the evaporites.
- Other indications of evaporite dissolution and evaporite-related deformation are observed close to the present margin of the Messinian evaporites; namely, salt outliers, faults detaching above the evaporite unit, and a linear depression along the evaporite pinch-out.
- The linear depression and faults have been related to the gravitational collapse of the Plio-Pleistocene clastic wedge, detaching at the top or within the Messinian evaporites. The analysis of the syn-sedimentary growth of marginal extensional faults documented that this gravity-related deformation occurred in the study area since the late Pliocene.

REFERENCES

A

- Abdel Aal, A., El Barkooky, E., Gerrits, M., Meyer, H., Schwander, M. & Zaki, H., (2000) Tectonic evolution of the Eastern Mediterranean Basin and its significance for hydrocarbon prospectivity in the ultradeepwater of the Nile Delta. *The Leading Edge*, 19, 1086-1102.
- Allen, P.A. & Allen, J.R. (1990) Basin Analysis: principles and applications. Blackwell Scientific Publications, Oxford, 451 pp.
- Almagor G. & Garfunkel, Z. (1979) Submarine slumping in the continental margin of Israel and northern Sinai. *American Association of Petroleum Geologists Bulletin*, 63, 324-340.
- Almagor, G. (1984) Salt-controlled slumping on the Mediterranean slope of central Israel. *Marine Geophysical Research*, 6, 227-243.
- Anderson, R. Y. & Kirkland, D. W. (1980) Dissolution of salt deposits by brine density flow. *Geology*, 8, 66-69.
- Anderson, R. Y. & Knapp, R. (1993) An overview of some of the large scale mechanisms of salt dissolution in western Canada. *Geophysics*, 58, 9, 1375-1387.

B

- Badawy, A. & Horvath, F. (1999) The Sinai subplate and tectonic evolution of the northern Red Sea region. *Geodynamics*, 27, 433-450.
- Badley, M.E. (1985) Practical seismic interpretation. International Human Resources Development Corporation, Boston, 266 pp.
- Barber, P.M. (1981) Messinian subaerial erosion of the proto-Nile delta. *Marine Geology*, 44, 253-272.
- Bartov, Y. (1990) Geological photomap of Israel and adjacent areas, 1:750.000. Geological Survey of Israel.
- Bassetti, M.A., Miculan, P. & Ricci Lucchi, F. (2003) Ostracod faunas and brackish-water environments of the late Messinian Sapigno section (northern Apennines, Italy). *Paleogeography, Paleoclimatology, Paleoecology*, 198, 335-352.

- Bein, A. & Gvirtzman, G. (1977) A Mesozoic fossil edge of the Arabian plate along the Levant coastline and its bearing on the evolution of the Eastern Mediterranean. *In: D. Biju-Duval & L. Montadert (Eds.) Structural history of the Mediterranean Basins*. Editions Technip, Paris, 95-110.
- Ben Gai, Y., Ben-Avraham Z., Buchbinder, B. & Kendall C. G.St.C. (2005) Post-Messinian evolution of the Southeastern Levant Basin based on two-dimensional stratigraphic simulation. *Marine Geology*, 221, 359-379.
- Benson, R.H., Rakic-El Bied, K. & Bonaduce, G. (1991) An important current reversal (influx) in the Rifian Corridor (Morocco) at the Tortonian-Messinian boundary: the end of Tethys Ocean. *Paleoceanography*, 6, 164-192.
- Bertoni, C. & Cartwright, J.A. (2005). 3D seismic analysis of circular evaporite dissolution structures, Eastern Mediterranean. *Journal of the Geological Society of London*, 162, 909-926.
- Bertoni, C. & Cartwright, J.A. (in press). Controls on the basinwide architecture of Messinian evaporites on the Levant margin (Eastern Mediterranean). *Sedimentary Geology*.
- Birrel, S. & Courtier, J. (1999). Structural analysis of 3D seismic data, using the correlation attribute: a case study – Carboniferous of the Southern North Sea (UK). *In: A.J. Fleet & S.A.R. Boldy (Eds.) Petroleum Geology of Northwestern Europe: Proceedings of the 5th Conference*, 789-797.
- Bishop, D.J., Buchanan, P.G. & Bishop, C.J. (1995) Gravity-driven thin-skinned extension above Zechstein Group evaporites in the western central North Sea: an application of computer-aided section restoration techniques. *Marine and Petroleum Geology*, 12, 115- 135.
- Branney, M. J. (1995) Downsag and extension at calderas: new perspectives on collapse geometries from ice-melt, mining and volcanic subsidence. *Bulletin of Volcanology*, 57, 303-318.
- Brown, A. (1999). Interpretation of three-dimensional seismic data. *American Association of Petroleum Geologists Memoir*, 42, 514 pp.
- Brown, L.F. & Fisher, W.L. (1980) Seismic stratigraphic interpretation of depositional systems: examples from Brazil rift and pull-apart basins. *American Association of Petroleum Geologists Memoir*, 26, 213-248.

- Buchbinder, B. (1996a) Miocene carbonates of the Eastern Mediterranean, the Red Sea and the Mesopotamian Basin. *In: E. Franseen, M. Esteban, W. Ward and J-M. Rouchy (Eds.) Models for Carbonate Stratigraphy from Miocene reef complexes of the Mediterranean region.* Society of Economic Paleontologists and Mineralogists Concepts in Sedimentology and Paleontology, 5, 89-96.
- Buchbinder, B. (1996b) Middle and Upper Miocene reefs and carbonate platforms in Israel. *In: E. Franseen, M. Esteban, W. Ward and J-M. Rouchy (Eds.) Models for Carbonate Stratigraphy from Miocene reef complexes of the Mediterranean region.* Society of Economic Paleontologists and Mineralogists Concepts in Sedimentology and Paleontology, 5, 333-345.
- Buchbinder, B., Martinotti, G.M., Siman-Tov, R. & Zilberman, E. (1993) Temporal and spatial relationships in the Miocene reef carbonates in Israel. *Paleogeography, Paleoclimatology, Paleoecology*, 101, 97-116.
- Buchbinder, B. & Gvirtzman, G. (1976) The breakup of the Tethys Ocean into the Mediterranean Sea, the Red Sea and the Mesopotamian Basin: a sequence of fault movements and desiccation events (Abstract): First Congress of the Pacific Neogene Stratigraphy, Tokyo, 32-35.
- Buchbinder, B. & Zilberman, E. (1997) Sequence stratigraphy of Miocene-Pliocene carbonate-siliciclastic shelf deposits in the eastern Mediterranean Margin (Israel): effects of eustasy and tectonics. *Sedimentary Geology*, 112, 7-32.
- Butler, R.W.H., Lickorish, W.H., Grasso, M., Pedley, H.M. & Ramberti, L. (1995) Tectonics and sequence stratigraphy in Messinian basins, Sicily: Constraints on the initiation and termination of the Mediterranean salinity crisis. *Geological Society of America Bulletin*, 107, 425-439.

C

- Cameron, T.D.J., Crosby, A., Balson, P.S., Jeffery, D.H., Lott, G.K., Bulat, P.S. & Harrison, D.J. (1992) Upper Permian. UK Offshore regional report: The geology of the Southern North Sea. British Geological Survey, London, 43-54.
- Carnevale, G., Landini, W & Sarti, G. (2006) Mare versus Lago-Mare: marine fishes and the Mediterranean environment at the end of the Messinian Salinity Crisis. *Journal of the Geological Society of London*, 163, 75-80.

- Cartwright, J. A. (1992). The application of seismic stratigraphic methods in structural interpretation. *Joint association of petroleum exploration courses, Course Notes, Geological Society of London, 74 pp.*
- Cartwright, J. A., Stewart, S., & Clark, J. (2001) Salt dissolution and salt-related deformation of the Forth Approaches Basin, UK North Sea. *Marine and Petroleum Geology, 18, 757-778.*
- Cartwright, J.A., Haddock, R.C. & Pinheiro, L.M. (1993) The lateral extent of sequence boundaries. *Geological Society of London Special Publication, 71, 15-34.*
- Cipollari, P., Cosentino, D. & Gliozzi, E. (1999) Extension- and compression-related basins in central Italy during the Messinian Lago-Mare event. *Tectonophysics, 315, 163-185.*
- Cita, M.B. (1973) Mediterranean evaporites: paleontological evidences for a deep-basin desiccation model. *In: C.W. Drooger, (Ed.) Messinian events in the Mediterranean, 206-228.*
- Cita, M.B., Ryan, W. B. F. (Eds.) (1978) Messinian erosional surfaces in the Mediterranean. *Marine Geology, 27, 366 p.*
- Cita M.B., Wright, R.H., Ryan, W. B. F., Longinelli, A. (1978) Messinian paleoenvironments. *Initial Reports Deep Sea Drilling Project, 42 (1), U.S. Govt., Printing Office (Washington D.C.), 1003-1035.*
- Clark, J. (1999) Controls on Fulmar deposition, West Central Shelf, central North Sea. Unpublished PhD Thesis, University of London, 374 pp.
- Clark, J., Cartwright, J. A. & Stewart, S. (1999) Mesozoic dissolution tectonics on the West central Shelf, UK Central North Sea. *Marine and Petroleum Geology, 16, 283-300.*
- Clauzon, G. (1982) Le canyon messinien du Rhône: une preuve décisive du “desiccated deep-basin model” (Hsü, Cita et Ryan, 1973). *Bulletin Societe Géologique de France, 24, 597-610.*
- Clauzon, G., Suc, J-P., Gautier, F., Berger, A. & Loutre, M-F. (1996) Alternate interpretation of the Messinian salinity crisis: controversy resolved? *Geology, 24, 363-366.*
- Cohen, A. (1988). Stratification of the Messinian Evaporites in Israel. *Israel Journal of Earth Science, 37, 193-203.*

- Cohen, A. (1993) Halite-clay interplay in the Israeli Messinian. *Sedimentary Geology*, 86, 211-228.
- Cohen, A. & Parchamovsky, S. (1986) The Mavqi'im Formation of Israel – a series of overlapping evaporites of Messinian age. *Geological Survey of Israel Report*, 19/86, 31 pp.
- Cole, J. W., Milner, D. M. & Spinks, K. D. (2005) Calderas and caldera structures: a review. *Earth-Science Reviews*, 69, 1-26.
- Collison, J.D. (1999). Alluvial sediments. In: H.G. Reading, (Ed.) *Sedimentary environments: Processes, Facies and Stratigraphy*. Blackwell Scientific Publications, 37-82.
- Cornée, J-J., Ferrandini, M., Saint Martin, J.P., Münch, Ph., Moullade, M., Ribaud-Laurenti, A., Roger, S., Saint Martin, S. & Ferrandini, J. (2006) The late Messinian erosional surface and the subsequent reflooding in the Mediterranean: new insights from the Melilla-Nador basin (Morocco). *Paleogeography, Paleoclimatology, Paleoecology*, 230, 129-154.
- Coward, M. & Stewart, S. (1995) Salt-influenced structures in the Mesozoic-Tertiary cover of the southern North Sea, U.K. In: Jackson, M. P. A., Roberts, D. G. and Snelson, S. (eds.) *Salt tectonics: a global perspective*. American Association of Petroleum Geologists Memoir, 65, 229-250.

D

- Davies, P. B. (1983) Structural characteristics of a deep-seated dissolution-subsidence chimney in bedded salt. *Sixth International Symposium on Salt, Salt Institute*, Vol.1, 331-350.
- Davies, P. B. (1989) Assessing deep-seated dissolution-subsidence hazards at radioactive-waste repository sites in bedded salt. *Engineering Geology*, 27, 467-487.
- Davison, I., Alsop, I. G., Birch, P., Elders, C., Evans, N., Nicholson, H., Rorison, P. Wade, D., Woodward, J. & Young, M. (2000) Geometry and late-stage structural evolution of Central Graben salt diapirs, North Sea. *Marine and Petroleum Geology*, 17, 4, 499-522.

- Decima, A. & Wezel, F. (1973) Late Miocene evaporites of the Central Sicilian Basin, Italy. *Initial Reports of the Deep Sea Drilling Project* 13, U.S. Govt., Printing Office (Washington D.C.), 1234-1240.
- Dewey, J.F., Pitman III, W.C., Ryan, W.B.F., Bonin, J. (1973). Plate tectonics and the evolution of the Alpine system. *Geological Society of American Bulletin*, 84, 3137-3180.
- Druckman, Y., Buchbinder, B., Martinotti G. M., Siman Tov, R. & Aharon, P. (1995) The buried Afik Canyon (eastern Mediterranean, Israel): a case study of a Tertiary submarine canyon exposed in Late Messinian times. *Marine Geology*, 123, 167-185.
- Duggen, S., Hoernle, K., van der Bogaard, P., Rüpke, L & Morgan, J.P. (2003) Deep roots of the Messinian salinity crisis. *Nature*, 422, 602-606.

E

- El Tabakh, M., Schreiber, B.C., Utha-Aroon, C., Coshell, L. & Warren, J.K. (1998) Diagenetic origin of Basal Anhydrite in the Cretaceous Maha Sarakham salt: Khorat Plateau, NE Thailand. *Sedimentology*, 45, 579-594.
- Escutia, C., Maldonado, A. (1992) Paleogeographic implications of the Messinian surface in the Valencia trough, northwestern Mediterranean Sea. *Tectonophysics* 203, 263-284.
- Eyal, Y. (1996) Stress field fluctuations along the Dead Sea Rift since the Middle Miocene. *Tectonics*, 15, 157-170.

F

- Field, M.E. & Gardner, J.V. (1991) Valencia Gorge: possible refill channel for the western Mediterranean Sea. *Geology*, 19, 1129-1132.
- Frey-Martinez, J., Cartwright, J., & Hall, B. (2005) 3D seismic interpretation of slump complexes: examples from the continental margin of Israel. *Basin Research*, 17, 83-108.
- Frey-Martinez J., Cartwright J., Hall, B., Huuse, M. (in press) Clastic intrusion of deepwater sandstone reservoirs as a trap-forming process: examples from the Eastern Mediterranean. *American Association of Petroleum Geologists Memoir*.
- Frey-Martinez, J., Cartwright, J., Burgess, P.M. & Vicente Bravo, J.V. (2004) 3D seismic interpretation of the Messinian Unconformity in the Valencia Basin, Spain.

In: Davies, R.J., Cartwright, J., Stewart, S.A., Lappin, M. & Underhill, J.R. (Eds.) 3D Seismic technology: Application to exploration in sedimentary basins. Geological Society of London Memoir, 29, 91-100.

Friedman, G.M. (1973) Petrographic data and comments on the depositional environment of the marine sulfates and dolomites at sites 124, 132 and 134, western Mediterranean Sea. *Initial Reports of the Deep Sea Drilling Project, 13*, U.S. Govt., Printing Office (Washington D.C.), 695-708.

Füchtbauer, H. & Peryt, T. (1980) Introduction. *In: The Zechstein Basin (Ed. by H. Füchtbauer & T. Peryt),. E. Schweizerbart'sche Verlagsbuchhandlung, Stuttgart, 1-2.*

G

Gamboa, L.A. (2004) The South Atlantic Aptian evaporitic sequence in the deep water areas of the Santos Basin. 32nd International Geological Congress, Abstract Volume, pt. 1, abs. 85-3, p. 417.

Garfunkel, Z. (1984) Large-scale submarine rotational slumps and growth faults in the eastern Mediterranean. *Mar. Geol.*, 55, 305-324.

Garfunkel, Z. (1998) Constrains on the origin and history of the Eastern Mediterranean basin. *Tectonophysics*, 298, 5-35.

Garfunkel, Z. & Derin, B. (1984) Permian-Early Mesozoic tectonism and continental margin formation in Israel and its implications on the history of the Eastern Mediterranean. *In: J.E. Dixon & A.H.F. Robertson (Eds.) The geological evolution of the Eastern Mediterranean. Geological Society, London, Special Publications, 17, 187-201.*

Garfunkel, Z. & Almagor, G. (1985) Geology and structure of the continental margin off northern Israel and the adjacent part of the Levantine Basin. *Marine Geology*, 62, 105-131.

Garfunkel, Z. & Almagor, G. (1987) Active salt dome development in the Levant Basin, southeast Mediterranean. *In: I. Lerche & J. O'Brien (Eds.) Dynamical geology of salt and related structures. Academic Press, London, 263-300.*

Garfunkel, Z., Arad, A. & Almagor, G. (1979) The Palmahim disturbance and its regional setting. *Israeli Geological Survey Bulletin, 72, 56 pp.*

Garrison, R.E., Schreiber, B.C., Bernoulli, D., Fabricius, F.H., Kidd, R.B. & Melieres, F. (1978) Sedimentary petrology and structures of Messinian evaporitic sediments

- in the Mediterranean Sea. *Initial Reports of the Deep sea Drilling Project*, 42 (1), U.S. Govt., Printing Office (Washington D.C.), 571-612.
- Ge, H. & Jackson, M. P. A. (1998) Physical modelling of structures formed by salt withdrawal: Implications for deformation caused by salt dissolution. *American Association of Petroleum Geologists Bulletin*, 82, 2, 228-250.
- Ge, H., Jackson, M.P.A., Vendeville, B.C., Maler, M.O. & Handschy, J.W. (1997) Deformation of prograding wedges over a ductile layer – applications of physical models to geologic examples. *Gulf Coast Assoc. Geol. Soc. Trans.*, 47, 177-184.
- Giardini, D., Jimenez, M. J. & Grünthal, G. (Eds.) (2003) European-Mediterranean seismic hazard map. European Seismological Commission, <http://wija.ija.csis.es/gt/earthquakes>.
- Gluyas, J. & Swarbrick, R. (2004) *Petroleum Geoscience*. Blackwell Scientific Publications, Oxford, 359 pp.
- Gorini, C., Lofi, J., Duvail, C., Dos Reis, T., Guennoc, P., Lestrat, P. & Mauffret, A. (2005) The Late Messinian salinity crisis and the Late Miocene tectonism: Interactions and consequences on the physiography and post-rift evolution of the Gulf of Lions margin. *Marine and Petroleum Geology*, 22, 695-712.
- Gradmann, S., Hübscher, C., Ben-Avraham, Z., Gajewski, D. & Netzeband, G. (2005). Salt tectonics off northern Israel. *Marine and Petroleum Geology*, 22, 597-611.
- Griffin, D.L. (2002) Aridity and humidity: two aspects of the late Miocene climate of North Africa and the Mediterranean. *Palaeogeography, Palaeoclimatology, Palaeoecology*, 182, 65-91.
- Guennoc, P., Gorini, C. & Mauffret, A. (2000) Geological history of the Gulf of Lions: mapping the Oligocene-Aquitainian rift and Messinian surface. *Géologie de la France*, 3, 67-97.
- Gvirtzman, G. & Buchbinder, B. (1978) The late Tertiary of the coastal plain and continental shelf of Israel and its bearing on the history of the eastern Mediterranean. *Initial Reports of the Deep Sea Drilling Project*, 42 (2), U.S. Govt., Printing Office (Washington D.C.), 1195-1222.

H

- Hardie, L.A. & Lowenstein, T.K. (2004). Did the Mediterranean Sea dry out during the Miocene? A reassessment of the evaporite evidence from DSDP Legs 13 and 42A cores. *Journal of Sedimentary Research*, 74, 453-461.
- Hargreaves, R., Peach, D. et al. (2004) Hydrogeological map of the West Bank (1:250,000). Palestinian Water Authority and British Geological Survey.
- Hodell, D.A., Elmsstrom, K.M. & Kennett, J.P. (1986) Latest Miocene $\delta^{18}\text{O}$ changes, global ice volume, sea level and the 'Messinian salinity crisis'. *Nature*, 320, 411-414.
- Hodgson, N.A., Farnsworth, J. & Fraser, A. (1992) Salt-related tectonics, sedimentation and hydrocarbon plays in the Central Graben, North Sea, UKCS. In: R.F.P. Hardman (Ed.) *Exploration Britain: Geological insights for the next decade*. Geological Society of London Special Publications, 67, 31-63.
- Hossack, J. (1995) Geometrical rules of section balancing for salt structures. In: M. P. A. Jackson, D. G. Roberts, and S. Snelson (Eds.) *Salt tectonics: a global perspective*. *American Association of Petroleum Geologists Memoir*, 65, 29-40.
- Hsü, K. J., Cita M. B. & Ryan, W.B.F. (1973) The origin of the Messinian evaporites. *Initial Reports of the Deep Sea Drilling Project 13*, U.S. Govt., Printing Office (Washington D.C.), 1203-1231.
- Hsü K. J., Montadert, L., Bernoulli et al. (1977) History of the Messinian Salinity Crisis. *Nature*, 267, 399-403.
- Hsü, K. J., Montadert, L., Bernoulli, D., Cita M. B., Erikson A., Garrison R. E., Kidd, R. B., Melieres, F., Muller, C. & Wright R. H. (1978) *Initial Reports of the Deep sea Drilling Project*, 42 (1), U.S. Govt., Printing Office (Washington D.C.), 1249 pp.
- Hudec, M. R. & Jackson, M. P. A. (2002) Structural segmentation, inversion and salt tectonics on a passive margin: Evolution of the inner Kwanza Basin, Angola. *Geological Society of America Bulletin*, 114, 10, 1222-1244.
- Huggett, R. J., (2003) *Fundamentals of geomorphology*. Routledge, London, 386 pp.
- Huuse, M. (1999) Detailed morphology of the Top Chalk surface in the eastern Danish North Sea. *Petroleum Geoscience*, 5, 303-314.

Huuse, M. & Clausen, O.R. (2001) Morphology and origin of major Cenozoic sequence boundaries in the eastern North Sea Basin: top Eocene, near-top Oligocene and the mid-Miocene unconformity. *Basin Research*, 13, 17-41.

I

Iaccarino, S.M. & Bossio, A. (1999) Paleoenvironment of uppermost Messinian sequences in the western Mediterranean (sites 974, 975 and 978). In: Zahn, R., Comas, M.C. & Klaus (Eds.) *Proceedings of the Ocean Drilling Program, Scientific Results*, 161, College Station, TX, 529-541.

J

Jackson, M. P. A. & Talbot, C. J. (1986) External shapes, strain rates and dynamics of salt structures. *Geological Society of America Bulletin*, 97, 305-323.

Jackson, M. P. A. & Vendeville, B. (1995) Origin of minibasins by multidirectional extension above a spreading lobe of allochthonous salt. In: C.J. Travis, B.C. Vendeville, H. Harrison, *et al.* (Eds.) *GCSSEPM Foundation 16th Annual research conference: Salt, sediment & hydrocarbons*, 135.

Jackson, M.P.A., Roberts, D.G. & Snelson, S. (Eds.) (1995) Salt tectonics: a global perspective. *American Association of Petroleum Geologists Memoir*, 65, 447 pp.

Jamison, W.R. (1987) Geometric analysis of fold development in overthrust terranes. *Journal of Structural Geology*, 9, 207-219.

Jenyon, M. K. (1983) Seismic response to collapse structures in the Southern North Sea. *Marine and Petroleum Geology*, 1, 27-36.

Jenyon, M. K. (1986) Salt tectonics. London, Elsevier, 191pp.

Johnson, K. S. (1997) Evaporite karst in the United States. *Carbonates and Evaporites*, 12, 2-14.

K

Kastens, K. (1992) Did glacio-eustatic sea level drop trigger the Messinian salinity crisis? New evidence from Ocean Drilling Program Site 654 in the Tyrrhenian Sea. *Paleoceanography*, 7, 3, 333-356.

Kastens, K. A. & Spiess, F. N. (1984) Dissolution and collapse features on the Eastern Mediterranean Ridge. *Marine Geology*, 56, 181-193.

- Kearey, P., Brooks, M., Hill, I. (2002) An introduction to geophysical exploration. Third Edition. Blackwell Scientific Publications, Oxford, 262 pp.
- Kendall, A.C. & Harwood, G.M. (1996) Marine evaporites: arid shorelines and basins. *In: H. G. Reading (Ed.) Sedimentary environments: Processes, Facies and Stratigraphy*. 3rd edition, Blackwell Scientific Publications, Oxford, 281-324.
- Koyi, H. (1996) Salt flow by aggrading and prograding overburdens. *In: I. Alsop, D.J. Blundell & I. Davison (Eds.) Salt tectonics, Geological Society Special Publication*, 100, 243-258.
- Krijgsman, W., Hilgen, F.J., Raffi, I. & Sierro, F.J. (1999). Chronology, causes and progression of the Messinian salinity crisis. *Nature*, 400, 652-654.
- Krijgsman W., Fortuin, A.R., Hilgen, F.J. & Sierro, F.J. (2001) Astrochronology for the Messinian Sorbas basin (SE Spain) and orbital (precessional) forcing for evaporites cyclicity. *Sedimentary Geology*, 140, 43-60.

L

- Lofi, J., Rabineau, M., Gorini, C., Berne, S., Clauzon, G., De Clarens, P., Dos Reis, A. T., Mountain, G., Ryan, W.B.F. & Steckler, M.S. & Fouchet, C. (2003) Plio-Quaternary prograding clinoform wedges of the western Gulf of Lions continental margin (NW Mediterranean) after the Messinian Salinity Crisis. *Marine Geology*, 198, 289-317.
- Lofi, J., Gorini, C., Berne, S., Clauzon, G., Dos Reis, A. T., Ryan, W.B.F. & Steckler, M.S. (2005) Erosional processes and paleo-environmental changes in the western Gulf of Lions (SW France) during the Messinian Salinity Crisis. *Marine Geology* 217 (1-2), 1-30.
- Lohmann, H. (1972) Salt dissolution in subsurface of British North Sea as interpreted from seismograms. *American Association of Petroleum Geologists Bulletin*, 56, 3, 472-479.
- Loncke, L. (2002) Le delta profond du Nil: structure et évolution depuis le Messinien (Miocène Terminal). Thèse de Doctorat de l'Université P. et M. Curie, Paris 6, 230 pp.
- Loncke, L., Mascle J. & Fanil Scientific Parties (2004) Mud Volcanoes, gas chimneys, pockmarks and mounds in the Nile deep-sea fan (Eastern Mediterranean): geophysical evidences. *Marine and Petroleum Geology*, 21, 6, 669-689.

M

- Magara, K. (1978) *Compaction and Fluid Migration. Practical Petroleum Geology*, Elsevier, New York, 319 pp.
- Maione, S. J. (2001) Discovery of ring faults associated with salt withdrawal basins, Early Cretaceous age, in the East Texas Basin. *The Leading Edge*, August 2001, 818-829.
- Major, C. & Ryan, W. B. F. (1999) Eratosthenes seamount: record of late Miocene sea-level changes and facies related to the Messinian Salinity Crisis. *Memorie della Società Geologica Italiana*, 54, 47-59.
- Manzi, V., Lugli, S., Ricci Lucchi, F. & Roveri, M. (2005) Deep-water clastic evaporites deposition in the Messinian Adriatic foredeep (northern Apennines, Italy): did the Mediterranean ever dry out? *Sedimentology*, 52, 875-902.
- Mart, Y. (1982). Quaternary tectonic patterns along the continental margin of the southeastern Mediterranean. *Marine Geology*, 49, 327-344.
- Mart, Y. & Ben Gai, Mart, Y. (1982) Some depositional patterns at continental margin of southeastern Mediterranean Sea. *American Association of Petroleum Geologists Bulletin*, 66, 4, 460-470.
- Mart, Y., Eisin, B. & Folkman, Y. (1978) The Palmahim structure – a model of continuous tectonic activity since the Upper Miocene in the southeastern Mediterranean off Israel. *Earth and Planetary Sciences Letters*, 39, 328-334.
- Martinez del Olmo, W. (1996) Depositional sequences in the Gulf of Valencia Tertiary basin. In: P.F. Friend & C.J. Dabrio (Eds.) *Tertiary Basins of Spain: The stratigraphic record of crustal kinematics*. *World Regional Geology*, 6, 55-67.
- Masle, J., Benkhelil, J., Bellaiche, G., Zitter, S., Woodside, J., Loncke, L. & Prised Scientific Party (1999) Marine geologic evidence for a Levantine-Sinai plate, a new piece of the Mediterranean puzzle. *Geology*, 28 (9), 779-782.
- Mauffret, A. (1976) *Etude geodynamique de la marge des Iles Baléares*. Thèse de Doctorat de l'Université P. et M. Curie, Paris, 137 pp.
- McCulloch, M. T. & De Deckker, P. (1989) Sr isotope constraints on the Mediterranean environment at the end of the Messinian salinity crisis. *Nature*, 342, 62-65.

- McKenzie, J.A. (1999) From desert to deluge in the Mediterranean. *Nature*, 400, 613-614.
- McKenzie, J. & Sprovieri, R. (1990) Paleooceanographic conditions following the earliest flooding of the Tyrrhenian Sea. *Proceedings of the Ocean Drilling Program, Scientific Results*, 107, 405-414.
- Meijer, P.Th. & Krijgsman, W. (2005) A quantitative analysis of the desiccation and re-filling of the Mediterranean during the Messinian Salinity Crisis. *Earth and Planetary Sciences Letters*, 240, 510-520.
- Mitchum, R.M. (1985) Seismic stratigraphic recognition of submarine fans. In: Berg, O.R. & Woolverton D.G. (Eds.) *Seismic Stratigraphy II*. American Association of Petroleum Geologists Memoir, 39, 117-136.
- Mitchum, R.M. Jr., Vail, P.R. & Sangree, J.B. (1977) Seismic stratigraphy and global changes of sea-level part 6: seismic stratigraphic interpretation procedure. In: C.E. Payton (Ed.) *Seismic stratigraphy - applications to Hydrocarbon exploration*. American Association of Petroleum Geologists Memoir, 26, 117-134.
- Mitra, S. (1990) Fault-propagation folds: Geometry, kinematic evolution, and hydrocarbon traps. *American Association of Petroleum Geologists Bulletin*, 74, 921-945.
- Montadert, L., Letouzey, J., Mauffret, A. (1978) Messinian event: seismic evidence. *Initial Reports of the Deep sea Drilling Project*, 42 (1), U.S. Govt., Printing Office (Washington D.C.), 1037-1050.
- Müller, D.W. & Hsü, K.J. (1987) Event stratigraphy and paleoceanography in the Fortuna basin (Southeastern Spain): A scenario for the Messinian salinity crisis. *Paleoceanography*, 2, 679-696.
- Müller, D.W. & Mueller, P.A. (1991) Origin and age of the Mediterranean Messinian evaporites: implications from Sr isotopes. *Earth and Planetary Sciences Letters*, 107, 1-12.

N

- Neev, D. & Ben-Avraham, Z. (1977) The Levantine countries: the Israeli coastal region. In: Nairn, E. M. and Kaner, W. H. (Eds.) *The ocean basins and margins: The Eastern Mediterranean*. 355-377.

- Neev, D. (1960) A pre-Neogene erosional channel in the southern coastal plain of Israel. *Israeli Geological Survey Bulletin*, 25, 20 pp.
- Neev, D. (1979) Deep-water gypsum deposits as indicated by the Neogene geological history of the central coastal plain of Israel. *Sedimentary Geology*, 23, 127-136.
- Neev, D., Ben-Avraham, Z. (1977) The Levantine countries: the Israeli coastal region. In: Nairn, E.M. Kanes, W.H., (Eds.) *The ocean basins and margins*. Vol. 4A: The Eastern Mediterranean, Plenum Press, New York, United States, 355-377.
- Nesterhoff W.D. (1973) Mineralogy, petrography, distribution and origin of the Messinian evaporites. *Initial Reports of the Deep sea Drilling Project*, 13, 673-694.
- Nurmi, R.D. (1988) Geologic interpretation of well logs and seismic measurements in reservoirs associated with evaporites. In: *Evaporites and Hydrocarbons* (Ed. by B.C. Schreiber). New York, Columbia University Press, 405-459.

O

- Orszag-Sperber, F., Rouchy, J.M.& Elion, P. (1989) The sedimentary expression of regional tectonic events during the Miocene-Pliocene transition in the Southern Cyprus basins. *Geological Magazine*, 126 (3), 291-299.

P

- Parea, G.C. & Ricci Lucchi, F. (1972) Resedimented evaporites in the Periadriatic trough (Upper Miocene, Italy). *Israel Journal of Earth Sciences*, 21, 125-141.
- Peryt, T.M. (2000) Resedimentation of basin centre sulphate deposits: Middle Miocene Badenian of Carpatian Foredeep, Southern Poland. *Sedimentary Geology*, 134, 331-342.
- Pierre, C., Rouchy, J.-M. & Blanc-Valleron, M.-M. (2002) Gas hydrate dissociation in the Lorca Basin (SE Spain) during the Mediterranean Messinian salinity crisis. *Sedimentary Geology*, 147, 247-252.
- Polonia, A., Camerlenghi, A., Davey, F. & Storti, F. (2002) Accretion, structural style and syn-contractonal sedimentation in the Eastern Mediterranean Sea. *Marine Geology*, 186, 127-144.
- Posamentier, H.W. (2003) Seismic geomorphology; new tricks for an old dog. *Reservoir*, 30 (4), 18-19, 28, 30.

Posamentier, H.W. & Vail, P.R. (1988) Eustatic controls on clastic deposition II – Sequence and systems tract models. *In: C.K. Wilgus, B.S. Hastings, et al. (Eds.) Sea level change - an integrated approach*. Society of Economic Paleontologists and Mineralogists Special Publication, 42, 125-154.

Posamentier, H.W. & Erskine, R.D. (1991) Seismic expression and recognition of ancient submarine fans. *In: Weimer, P. & Link, M.H. (Eds.) Seismic facies and sedimentary processes of submarine fans and turbidite systems*. Frontiers in Sedimentary Geology, Springer-Verlag, New York, 197-222.

R

Rathey, R.P. & Hayward, A.B. (1993) Sequence stratigraphy of a failed rift system: the Middle Jurassic to Early Cretaceous basin evolution of the Central and Northern North Sea. *In: Parker, J.R. (Ed.) Petroleum Geology of Northwest Europe: Proceedings of the 4th Conference*. Geological Society of London, 215-250.

Reading H.G. & Richards M.T. (1994) The classification of deep-water siliciclastic depositional systems by grain size and feeder systems. *American Association of Petroleum Geologists Bulletin*, 78, 798-822.

Reading, H.G. (1996) *Sedimentary environments: Processes, Facies and Stratigraphy*. Blackwell Scientific Publications, Oxford, 688 pp.

Rezak, R., Bright, T. & McGrail, C. (1985) Reefs and banks of the northwestern Gulf of Mexico : their geological, biological and physical dynamics. Wiley and Sons, New York, NY, 259 pp.

Ricchi Lucchi F. (1973) Resedimented evaporites: Indicators of slope instability and deep basin conditions in Periadriatic Messinian. *In: Drooger C.W. (Ed.) Messinian events in the Mediterranean*. Amsterdam, North Holland, 136-144.

Rider, M. H. (1986) *Geological interpretation of well logs*. Whittles Publishing, 175 pp.

Riding, R., Braga, J.C., Martin, J.M., Sanchez Almazo, I.M. (1998) Mediterranean Salinity Crisis: constraints from a coeval marginal basin, Sorbas, southeastern Spain. *Marine Geology*, 146, 1-20.

Rizzini, A., Vezzani, F., Cococetta, V. & Milad, G. (1978) Stratigraphy and sedimentation of a Neogene-Quaternary section in the Nile Delta area (A.R.E.). *Marine Geology*, 27, 327-348.

- Robertson, A. H. F. (1998) Mesozoic-Tertiary evolution of the easternmost Mediterranean area: integration of marine and land evidence. *Proceedings of the Deep sea Drilling Project Scientific Results*, 160, U.S. Govt., Printing Office (Washington D.C.), 723-782.
- Ross, D. A. & Uchupi, E. (1973) Structure and sedimentary history of Southeastern Mediterranean Sea-Nile Cone Area. *American Association of Petroleum Geologists Bulletin*, 61, 6, 872-902.
- Rouchy, J. M. (1982) La genèse des évaporites messiniennes de Méditerranée. *Mémoires du Muséum National d'Histoire Naturelle, Paris*, 50, 267 pp.
- Rouchy, J.M., Pierre, C. & Sommer, F. (1995) Deep-water resedimentation of anhydrite and gypsum deposits in the Middle Miocene (Belayim Formation) of the Red Sea, Egypt. *Sedimentology*, 42, 267-282.
- Rouchy, J. M., Orszag-Sperber, F., Blanc-Valleron, M.M., Pierre, C., Riviere, M., Combourieu,-Nebout, N., Panayides, I. (2001) Paleoenvironmental changes at the Messinian-Pliocene boundary in the eastern Mediterranean: southern Cyprus basins. *Sedimentary Geology*, 145, 93-117.
- Rouchy, J. M., Pierre, C., Et-Touhami, M., Kerzazi, K., Caruso, A., Blanc-Valleron, M. (2003) Late Messinian to Early Pliocene paleoenvironmental changes in the Melilla Basin (NE Morocco) and their relation to Mediterranean evolution. *Sedimentary Geology*, 163, 1-27.
- Roveri M., Bassetti, M.A. & Ricci Lucchi, F. (2001) The Mediterranean Messinian Salinity Crisis: an Apennine foredeep perspective. *Sedimentary Geology*, 140, 201-214.
- Roveri, M., Manzi, V., Ricci Lucchi, F. & Rogledi, S. (2003) Sedimentary and tectonic evolution of the Vena del Gesso basin (Northern Apennines, Italy): Implications for the onset of the Messinian salinity crisis. *Geological Society of America Bulletin*, 115 (4), 387-405.
- Ryan, W.B.F. (1973) Geodynamic implications of the Messinian salinity crisis. In: C. W. Drooger (Ed.) *Messinian events in the Mediterranean*. North-Holland, Amsterdam, 26-38.
- Ryan, W.B.F. (1978). Messinian badlands on the southeastern margin of the Mediterranean Sea. *Marine Geology*, 27, 349-363.

- Ryan, W. B. F. & Cita, M.B. (1978) The nature and distribution of Messinian erosional surfaces – indicators of a several-kilometer-deep Mediterranean in the Miocene. *Marine Geology*, 27, 193-230.
- Ryan, W.B.F., Hsü, K.J., et al. (1973) (Eds.). *Initial Reports of the Deep sea Drilling Project*, 13, 1447 pp.

S

- Savoie, B. & Piper, D.J.W. (1991) The Messinian event on the margin of the Mediterranean Sea in the Nice area, southern France. *Marine Geology*, 97, 279-304.
- Savoie, B., Piper, D.J.W., Droz, L. (1993) Plio-Pleistocene evolution of the Var deep-sea fan off the French Riviera. *Marine and Petroleum Geology*, 10, 550-571.
- Schenk, P.E., von Bitter, P. & Matsumoto, R. (1994) Deep-basin/deep-water carbonate-evaporite deposition of a saline giant: Loch Macumber (Visean), Atlantic Canada. *Carbonates and Evaporites*, 9 (2), 187-210.
- Schlager, W. & Boltz, H. (1977) Clastic accumulation of sulphate evaporites in deep water. *Journal of Sedimentary Petrology*, 47/2, 600-609.
- Schlager, W. (1993) Accommodation and supply- a dual control on stratigraphic sequences. *Sedimentary Geology*, 86, 111-136.
- Schreiber, B.C. (1988) Subaqueous evaporite deposition. In: Schreiber, B.C. (Ed.) *Evaporites and Hydrocarbons*: New York, Columbia University Press, p. 182-255.
- Schreiber, B.C., Friedman, G.M., Decima, A. & Schreiber, E. (1976) Depositional environments of Upper Miocene (Messinian) evaporite deposits of the Sicilian Basin. *Sedimentology*, 23, 729-760.
- Selli, R. (1960) Il Messiniano Mayer-Eymar 1867. Proposta di un neostatotipo. *Giornale di Geologia*, S.2, 28, 1-34.
- Sibson, R. H., Moore, J. M. & Rankin, A. H. (1978) Seismic pumping: a hydrothermal fluid transport mechanism. *Journal of the Geological Society of London*, 131, 6, 653-659.
- Sneh, A., Y. Bartov & Rosensaft, M. (2000) Geological shaded-relief map of Israel and environments, The Geological Survey of Israel, Jerusalem.
- Spezzaferri, S., Cita, M.B. & McKenzie, J.A. (1998) The Miocene/Pliocene boundary in the eastern Mediterranean: results from sites 967 and 969. In: Robertson, A. H.

- F., Emeis, K.-C., Richter, C. et al. (Eds.) *Proceedings of the Deep sea Drilling Project Scientific Results*, 160, U.S. Govt., Printing Office (Washington D.C.), 9-28.
- Stampfli, G.M. & Höcker, C.F.W. (1989) Messinian paleorelief from a 3-D seismic survey in the Tarraco concession area (Spanish Mediterranean Sea). *Geologie Mijnbouw* 68, 201-211.
- Steininger, F. & Rögl, F. (1984) Paleogeography and palinspastic reconstruction of the Neogene of the Mediterranean and Paratethys. *In: Dixon, J.E., Robertson A.H.F. (Eds.) The geological evolution of the Eastern Mediterranean*. Geological Society of London, Special Publications, 17, 659-668.
- Stewart, S. A. (1999) Seismic interpretation of circular geological structures. *Petroleum Geoscience*, 5, 273-285.
- Stewart, S. A. & Allen, P. J. (2002) A 20-km-diameter multi-ringed impact structure in the North Sea. *Nature*, 418, 520-523.
- Stow, D.A.V. (1986) Deep clastic seas. *In: H. G. Reading, (Ed.) Sedimentary environments: Processes, Facies and Stratigraphy*. 3rd edition, Blackwell Scientific Publications, Oxford, 399-444.
- Strohmenger, C., Antonini, M., Jager, G., Rockenbauch, K. & Strauss, C. (1996) Zechstein 2 carbonate reservoir facies distribution in relation to Zechstein sequence stratigraphy (Upper Permian, Northwestern Germany): an integrated approach. *Bulletin Centre de Recherches Exploration – Production Elf Aquitaine*, 20 (1), 1-35.
- Sugiura, R. & Hitcho, C.A. (1981) Collapse structures in the Paradox Basin. *Rocky Mountain association of Geologists – 1981 Field Conference*, 33-45.
- Suppe, J. (1985) Principles of structural geology. Prentice Hall, Englewood Cliffs, NJ, 537 pp.

T

- Tay, P.L., Lonergan, L., Warner, M., Jones, K.A. & the IMERSE Working Group (1999) Seismic investigation of thick evaporite deposits on the central and inner unit of the Mediterranean Ridge accretionary complex. *Marine Geology*, 186, 167-194.

- Taylor, J. C. M. (1998) Upper Permian – Zechstein. In: Glennie, K.W. (Ed.) *Petroleum geology of the North Sea – Basic concepts and recent advances*, 4th Edition, Blackwell Scientific Publications, Oxford, 174-211.
- Thorsen, C. E. (1963) Age of growth faulting in Southeast Louisiana. *Transactions – Gulf Coast Association of Geological Societies*, 13, 103-110.
- Tibor G. & Ben-Avraham Z. (1992) Late Tertiary sedimentary facies and structure of the Levant continental margin off central Israel. *Marine Geology*, 105, 253-273.
- Tibor, G. & Ben-Avraham, Z. (2005) Late Tertiary paleodepth reconstruction of the Levant margin off Israel. *Marine Geology*, 221, 331-347
- Tibor, G., Ben-Avraham, Z., Steckler, M. & Fligelman, H. (1992) Late Tertiary subsidence history of the Southern Levant Margin, Eastern Mediterranean Sea, and its implications to the understanding of the Messinian event. *Journal of Geophysical Research*, 97, B12, 17,593-17,614.
- Trusheim, F. (1960) Mechanism of salt migration in northern Germany. *American Association of Petroleum Geologists Bulletin*, 44, 1519-1540.
- Tucker, M.E. (1991) Sequence stratigraphy of carbonate-evaporite basins: models and applications to the Upper Permian (Zechstein) of northeast England and adjoining North Sea. *Journal of the Geological Society of London*, 148, 1019-1036.

V

- Vai, G.B. & Ricci Lucchi, F. (1977) Algal crusts allochthonous and clastic gypsum in a cannibalistic evaporite basin: A case history from the Messinian of the Northern Apennines. *Sedimentology* 24, 211-244.
- Vidal, N., Alvarez-Marron, J. & Klaeschen, D. (2000) Internal configuration of the Levantine Basin from seismic reflection data (eastern Mediterranean). *Earth and Planetary Science Letters*, 180, 77-89.
- Von Huene, R. (1997) Mediterranean Ridge structure: results from IMERSE. *EOS*, 78, 155.

W

- Warny, S.A., Bart, P.J. & Suc, J.P. (2003) Timing and progression of climatic, tectonic and glacioeustatic influences on the Messinian Salinity Crisis. *Palaeogeography, Palaeoclimatology, Palaeoecology*, 202, 59-66.

- Warren, J. K. (1991) Sulfate dominated sea-marginal and platform evaporative settings: sabkha and salinas, mudflat and salterns. *In: J. L. Melvin (Ed.) Evaporites, petroleum and mineral resources. Developments in Sedimentology*, 50, 69-180.
- Warren, J. K. (1997) Evaporites, brines and base metals: fluids, flow and 'the evaporite that was'. *Australian Journal of Earth Sciences*, 44, 149-183.
- Warren, J. K. (1999) *Evaporites: Their evolution and economics*. Blackwell Scientific Publications, Oxford, 438 pp.
- Weimer, P. & Link, M.H. (1991) Seismic facies and sedimentary processes of submarine fans and turbidite systems. *Frontiers in Sedimentary Geology*, Springer-Verlag, New York, 447 pp.
- Weimer, P. & Slatt, R.M. (2004) Deepwater reservoir elements. *In: Petroleum systems of deepwater settings. Distinguished Instructor Series* (sponsored by SEG and EAGE), 7, 6-1.

Z

- Zhang, J. & Scott, D.B. (1996) Integrated stratigraphy and paleoceanography of the Messinian (latest Miocene) across the North Atlantic Ocean. *Marine Micropaleontology*, 29, 1-36.

